MULTIFUNCTIONAL CHEMICAL CROSS-LINKERS FOR QUANTIFYING AND VISUALIZING INTRACELLULAR PROCESSES

A Dissertation

Presented to the Faculty of the Graduate School

of Cornell University

In Partial Fulfillment of the Requirements for the Degree of

Doctor of Philosophy

by

Michelle Rachel Sorkin

August 2019

MULTIFUNCTIONAL CHEMICAL CROSS-LINKERS FOR QUANTIFYING AND VISUALIZING INTRACELLULAR PROCESSES

Michelle Rachel Sorkin, Ph. D.

Cornell University 2019

Chemical cross-linkers have proven valuable for a diversity of biological applications such as protein enrichment, nanoparticle surface functionalization, and conjugate-based drug delivery. Two valuable subclasses of cross-linkers include cleavable and heteromultifunctional linkers. The introduction of cleavage sites within a linker is important for drug delivery applications, as it enables programmable and spatiotemporal release of tethered molecules or therapeutic cargo. Heteromultifunctional linkers that allow the orthogonal attachment of multiple biomolecules or chemical moieties are important for the synthesis of heterovalent ligands and molecular probes. Due to synthetic limitations, a vast majority of cleavable linkers have been limited to a single cleavage site. Traditional approaches for synthesizing heteromultifunctional linkers are limited to three functional groups and lack the functional diversity to allow for orthogonal cleavage via nonenzymatic cues. Further, approaches that utilize natural amino acids and peptidyl scaffolds are sensitive to proteolysis in the biological environment.

An emerging paradigm in polymer chemistry is the synthesis of sequence-defined polymers. Oligothioetheramides (oligoTEAs), a subset of sequence-defined polymers, have recently been reported by our research group. The oligoTEA synthesis approach utilizes an orthogonally reactive *N*-allylacrylamide monomer, which can undergo alternating photoinitiated thiol-ene “click” reactions and phosphine-catalyzed

thiol-Michael additions. Aside from their facile synthesis, oligoTEAs have several benefits including the incorporation of a diverse panel of pendant and backbone functionalities. Furthermore, oligoTEAs are stable to proteolytic degradation and as such are stable in the biological environment. We have leveraged the iterative nature of oligoTEA synthesis to address many of the limitations of heteromultifunctional cross-linker synthesis.

Herein, I will describe the development of oligoTEAs as a platform for synthesizing cleavable heteromultifunctional cross-linkers. We have taken this class of cross-linkers and applied it towards quantifying the intracellular processing of stimuli-responsive drug carriers. In combination with a kinetic model, we have extracted the rate constant for intracellular disulfide bond degradation in the HER2 receptor endocytic pathway. In collaboration with the Paszek group, we have also used our synthesis platform to design probes to visualize the glycocalyx via expansion microscopy. These probes selectively modify metabolically-labelled cell surface glycans via bioorthogonal “click” chemistry. Taken together, these works highlight the utility of oligoTEAs as a platform to design heteromultifunctional cross-linkers for a range of biological applications.

Biographical Sketch

I was born on August 11, 1992 in Springfield, Massachusetts. I grew up in the suburb of Longmeadow, Massachusetts. I consider myself very fortunate to have grown up in Longmeadow, where the public schools are filled with incredible educators.

In August 2010, I started my undergraduate degree at the University of Pennsylvania. I originally sought a degree in biomedical engineering but soon realized my passion for chemistry (and the full extent of my squeamishness). After 1 semester, I switched to chemical and biomolecular engineer as my major. At the end of my sophomore year, I began working as an undergraduate research assistant in the lab of Professor Robert R. Riggleman under the supervision of my graduate mentor, Amit Shavit. In the Riggleman lab, I applied molecular modeling approaches to characterize polymers and glassy materials. During my junior and senior year summers, I interned at the pharmaceutical companies, Bristol-Myers Squibb and Merck. At these internships, I studied different methods to formulate poorly soluble drugs.

After graduating from Penn in 2014, I started pursuing my PhD in chemical and biomolecular engineering at Cornell University. My interest in polymers and drug delivery led me to join the Alabi Lab at Cornell. During my PhD, I have developed methods to synthesize cleavable, heteromultifunctional cross-linkers. I have applied these cross-linkers to study the intracellular processing of antibody-based therapeutics, as described herein.

After completion of my PhD degree, I will be moving to the San Francisco bay area with my partner and former lab mate, Joshua Walker, and our 2 adorable dogs, Dumpling and Bowie. I will be working as a senior scientist at Berkeley Lights developing reagents and assays for the BLI platform.

This document is dedicated to all the family, friends, co-workers, and teachers that have supported me in all my academic and personal pursuits

Acknowledgements

First and foremost, I would like to acknowledge my advisor, Professor Christopher Alabi. I appreciate everything you have taught me, particularly in regards to chemical synthesis and experimental rigor. I appreciate the independence that you gave me which allowed me to grow as a researcher and enjoy a lot of "secret synthesis."

I would like to acknowledge my committee members, Professor David Putnam and Professor Susan Daniel. I appreciate all the feedback you have given me. Thank you for believing in me as a researcher and for helping me improve my presentation voice!

I would like to thank Sam and Nancy Fleming for financial support. It was an honor to be named a Fleming Scholar in 2016.

I am so grateful to the members of the Alabi lab for making the past 5 years productive and incredibly fun. Thank you for supporting my creativity and for making me laugh so loudly I was heard down the hall. I wanted to give special thanks to Dana Thornlow, one of the OG conjugation experts in Alabi lab, for research help and for listening to countless rants. I also wanted to thank Tina Artim for always providing a silver lining and for doing a lot of crafting with me. I would like to acknowledge Meghan O'Leary for being one of my favorite people in the world and a stellar lab mate.

Additionally, I would like to thank the undergraduate researchers that have contributed to this work, Daniel DeCorla, Alexia Marquez, Nicole Torosian, Sneha Kabaria, and Francis Ledesma. Words cannot express how grateful I am to Nicole for all the experiments she has done and for sticking with me until the end even though I know she had so many other things she would rather be doing her final semester than purifying antibodies.

I would like to thank the teachers at LHS, in particular Robert O'Connell, Jennifer Faulkner, Jonathan Matusko, and Robert Weir, for inspiring me and believing in me. I really would not have made it this far without everything you taught me and your support.

I would like to thank my family for their love and for supporting my desire to be in school for 22 years. Thank you for letting me follow my dreams, for being there for me whenever I needed you, and for being my biggest cheerleaders.

Last but not least, I would like to thank my partner, Joshua Walker. I cannot imagine what my PhD experience would have been like without you, and I cannot imagine my life without you. You are my soulmate, and I am so excited to start our new life together on the west coast.

Table of Contents

List of Abbreviations

ADC	Antibody-drug Conjugate
BBS	Borate Buffered Saline
$CDCl_3$	Deuterated Chloroform
CuAAC	Copper-catalyzed Azide-Alkyne Cycloaddition
DBCO	Dibenzocyclooctyne
DCM	Dichloromethane
DMEM	Dulbecco's Modified Eagle Media
DMF	Dimethylformamide
DMPA	2,2-Dimethoxy-2-phenylacetophenone
DMSO	Dimethyl Sulfoxide
DNP	2,4-dinitrophenol
DOL	Degree of Labelling
DOX	Doxorubicin
DTT	Dithiothreitol
EDC	1-Ethyl-3-(3-dimethylaminopropyl)carbodiimide
EDTA	Ethylenediaminetetraacetic Acid
EtOAc	Ethyl Acetate
Et_3N	Triethylamine
ExM	Expansion Microscopy
FBS	Fetal Bovine Serum
FRET	Förster Resonance Energy Transfer
GSH	Glutathione
NHS	N-hydroxy Succinimide
HIC	Hydrophobic Interaction Chromatography
LC-MS	Liquid Chromatography-Mass Spectrometry
MALDI-MS	Matrix Assisted Laster Desorption Ionization-Mass Spectrometry
MeOH	Methanol
MMAE	Monomethyl Auristatin E
MTGase	Microbial Transglutaminase
NMR	Nuclear Magnetic Resonance
oligoTEA	Oligothioetheramide
OPSS	Ortho-pyridyl Disulfide
PBS	Phosphate Buffered Saline
PEG	Polyethylene Glycol
PNGase F	Peptide:N-glycosidase F
RP-HPLC	Reverse Phase-High Performance Liquid Chromatography
SDS-PAGE	Sodium Dodecyl Sulfate-Polyacrylamide Gel Electrophoresis
SPAAC	Strain-Promoted Azide-Alkyne Cycloaddition
TFA	Trifluoroacetic Acid
THF	Tetrahydrofuran

List of Figures

List of Tables

Chapter 1 – INTRODUCTION

1.1. CLEAVABLE AND HETEROMULTIFUNCTIONAL CROSS-LINKERS

Chemical cross-linkers have proven valuable for a diversity of biological applications such as protein enrichment,[1,2] nanoparticle surface functionalization,[3,4] and conjugate-based drug delivery.[5] Two valuable subclasses of cross-linkers include cleavable and heteromultifunctional linkers.[6-9] First, the introduction of cleavage sites within a linker is important for drug delivery applications, as it enables programmable and spatiotemporal release of tethered molecules or therapeutic cargo. Second, heteromultifunctional linkers that allow the orthogonal attachment of multiple biomolecules or chemical moieties are important for the synthesis of molecular probes and heterovalent ligands.[10] Together, the ability to incorporate orthogonal cleavage sites within a heteromultifunctional linker enables selective and specific release of multiple biomolecules. This capability can lead to the engineering of targeted biological probes that can serve as response elements to multiple orthogonal inputs as well as therapeutic modalities that can be selectively released in response to different biological cues.

Due to synthetic limitations, a vast majority of cleavable linkers have been limited to a single cleavage site.[8] Traditionally, heteromultifunctional linkers have been synthesized utilizing substituted aromatic derivatives,[11,12] natural and nonnatural amino acids,[13,14] and peptidyl scaffolds.[10,15,16] Aromatic and amino acid-based linkers are built from a central chemical core. Therefore, the number of reactive sites present on the core building block and steric constraints dictate the final number of functional groups (typically limited to heterotrifunctional). Although feasible, this approach is labor intensive and involves multiple protection and deprotection steps. Alternatively, peptide-based scaffolds are built linearly using traditional solid-phase peptide synthesis

techniques.[17] This approach has the potential to yield multifunctional linkers with more than three orthogonal attachment sites. However, the peptide backbone is sensitive to proteolysis in the biological environment. Furthermore, the peptide backbone lacks the functional diversity to allow for orthogonal cleavage via other nonenzymatic cues. Thus, it would be advantageous to develop a method for synthesizing sequence-defined, proteolytically stable cross-linkers.

1.2. CLEAVABLE BONDS IN DRUG DELIVERY

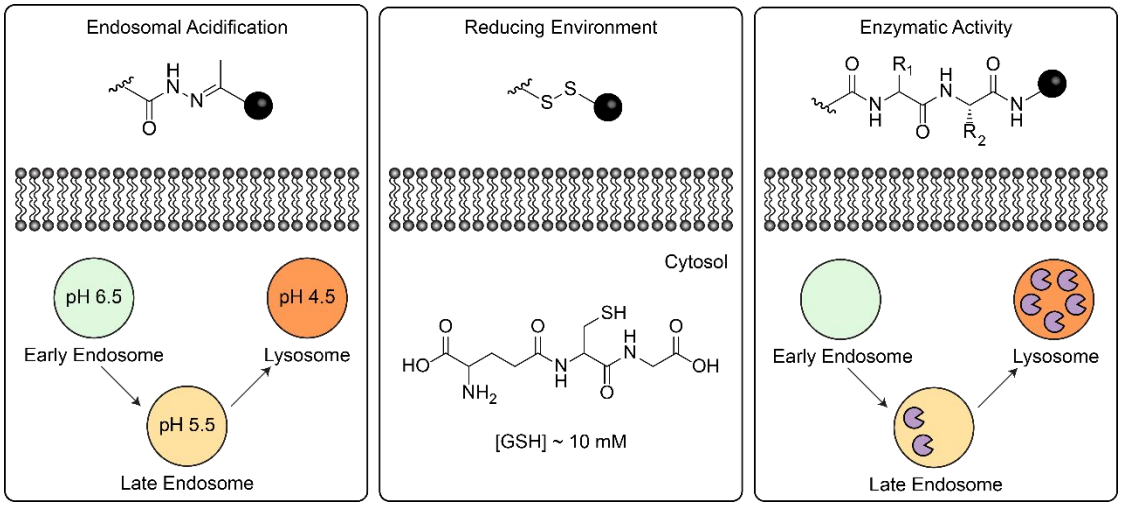

Figure 1.1. Types of intracellular stimuli that have been harnessed for drug delivery and their associated cleavable chemistries.

Cleavable bonds have long been an attractive intracellular switch for nanoparticle and conjugate-based drug delivery systems.[18,18-20] A wide variety of cleavable linkers have been designed to respond to three key intracellular stimuli: pH change, reducing environments, and enzymatic activity (Figure 1.1). Acid-labile linkers, such as hydrazones and esters, dissociate within acidified endocytic vesicles. Disulfide bonds are known to undergo intracellular reduction and cleavage to give free thiols. Peptide linkers, such as valine-citrulline and phenylalanine-citrulline, are cleaved and hydrolyzed by lysosomal enzymes. Drug payloads have been conjugated to

nanoparticles through acid-labile ester[21] and hydrazone[22] linkages as well as reduction-sensitive disulfide bonds.[23] A variety of cleavable chemistries have been explored for use in ADCs including hydrazone, disulfide, and dipeptide bonds.[24]

Hydrazone linkers are stable at neutral pH, but undergo dissociation in a mildly acidic medium.[25,25,26,26] This type of pH responsive bond cleavage favors acidic environments, such as those present in endosomes (pH 5.5-6.2) and lysosomes (pH 4.5-5), and hence has been exploited for controlled drug release. Hydrazones have been used to create several polymer-drug conjugates as prodrugs for controlled release and targeted delivery. In addition, hydrazone linkages have been incorporated into a variety of polymers used to formulate nanoparticle drug carriers for pH sensitive drug release.[27,28,28] Prodrugs incorporating pH-responsive hydrazone bonds have been shown to be rapidly cleaved in the endocytic compartment with appreciable cleavage after 1 hour of residence time.[29] Hydrazone linkers were employed in the first class of ADCs developed. In the first ADC approved in the U.S., Mylotarg, an acid-labile hydrazone linker was used to attach a calicheamicin drug to a humanized anti-CD33 monoclonal antibody. However, in post-approval studies, this ADC was found to possess a higher rate of toxicity than chemotherapy alone and was consequently withdrawn from the market. This type of cleavable chemistry has since been associated with nonspecific drug release, as further evidenced by other hydrazine-containing ADCs that have failed in Phase I clinical trials.[24,30] As such, researchers have moved towards the use of more stable cleavage chemistries such as disulfide and dipeptide linkers.

The disulfide bond is stable at physiological pH and in mildly oxidizing conditions such as those present in the bloodstream.[5,5,31,32,32] Intracellular concentrations of the reducing agent glutathione are 2-3 orders of magnitude higher

than in extracellular fluids. Hence, disulfide bonds remain stable within circulation, but can be cleaved rapidly in the reducing intracellular environment. Disulfide bonds have been shown to cleave with a half-life of 6 hours.[33] Furthermore, the intracellular glutathione concentration is much higher in cancer cells than in normal cells, which has been exploited for anticancer drug delivery systems. For example, disulfide-linked nanoparticles have recently been synthesized for the delivery of the drug paclitaxel into cancer cells.[34] This system has been shown to enhance the anti-cancer efficacy of paclitaxel. Another example of a nanoparticle-based system is a recently developed nanoparticle conjugate in which the antimitotic agent monomethyl auristatin E (MMAE) is conjugated through disulfide bonds that can be reduced by the high intracellular concentration of glutathione (GSH) found within tumor cells.[35] A reduction-sensitive disulfide linker has been employed in the ADC IGMN 779 which is currently in clinical trials.[36]

Dipeptide linkers have sought to leverage proteolytic specificity to achieve high stability in circulation.[37,38] Dipeptide-based linkers have been shown to cleave by specific lysosomal proteases, such as the ubiquitous cysteine protease cathepsin B.[37,37,38,38] Cathepsin B has considerably diminished activity extracellularly because it is inactive at physiological pH and is inhibited by serum protease inhibitors.[39] The dipeptide linkers, valine-citrulline and phenylalanine-citrulline, have high stability in serum but are rapidly degraded by cathepsin B within the lysosomes of target cells (half-life of approximately 15 hours).[40] As such, due to the inherently greater systemic stability over chemically cleavable linkers, there is heightened interest in the use of dipeptide linkers for drug release.[39,39,41] One of the few antibody-drug conjugates on the market, Brentuximab Vedotin, employs a valine-citrulline linker for efficient release of MMAE inside target cells.[42,42] This ADC has proven effective for the treatment of

Hodgkin and non-Hodgkin lymphoma. Recently, in June 2019, another ADC incorporating a valine-citrulline-MMAE linker was approved by the FDA. This ADC, polatuzumab vedotin, is used for the treatment of diffuse large B-cell lymphoma.[43] Studies have measured cleavage kinetics in well-plate assays using isolated cathepsin B and/or rat/animal lysosomal lysate. However, bond cleavage kinetics monitored in solution are not representative of intracellular activity. Some new methods have also used peptides to assemble specific substrates with folic acid but these are not general to other pathways.

1.3. MONITORING INTRACELLULAR BOND CLEAVAGE

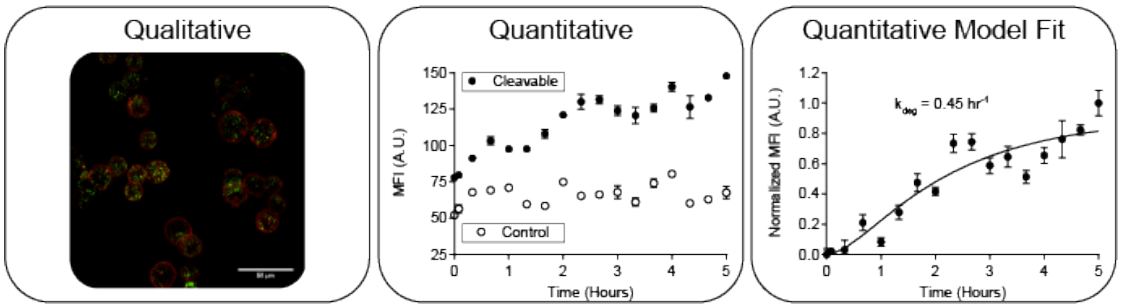

Figure 1.2. Typles of studies used to monitor intracellular bond cleavage.

Due to the growing use of cleavable chemistries within the realm of drug delivery, numerous researchers have examined intracellular bond cleavage. Many studies have used a fluorophore as proxy for a drug payload in order to use fluorescence as a read-out of bond cleavage. There have also been studies that exploit radiolabeling or mass spectrometry as detection methods. Depending on the methods and information obtained, these studies of intracellular bond cleavage can be classified into 3 main categories: qualitative, quantitative, and quantitative with theoretical model.

Qualitative Studies of Intracellular Bond Cleavage

Qualitative studies involve visualization of bond cleavage without any quantification. These studies generally involve confocal laser scanning microscopy as a method to visualize intracellular localization of molecules within intact cells. Guo et al. developed a pH-sensitive polymeric micelle conjugated to the chemotherapeutic drug doxorubicin (DOX).[44] The micelle was targeted to the folate receptor, which is found to be highly expressed on cancer cells relative to healthy cells, using folic acid as the substrate. Drug release was mediated via hydrolysis of a hydrazone linkage to DOX. Doxorubicin is a fluorescent molecule that has been found to be quenched ("off") when covalently linked to folic acid. Thus, when DOX is released intracellularly its fluorescence turns "on" and it can be visualized. This type of system is attractive in that it combines fluorescent and cytotoxic modalities that can be monitored intracellularly, however, it cannot be translated to many other systems as most drugs do not possess the same fluorescent activation. In this particular study, cells were incubated for 2 hours with the polymeric micelle and DOX release was visualized relative to a noncleavable control. A bright field image was used to confirm that the drug was released inside of the cell, and co-localization with Lysotracker was used to confirm localization within acidic vesicles as expected. The images generated visually indicated drug release but were not converted to numerical fluorescence values to compare to the noncleavable control. Quantification would be essential to prove that the cleavage was specific to the hydrazone bond.

Quantitative Measurements of Intracellular Bond Cleavage

Several studies have quantified intracellular bond cleavage using fluorescence-based methods such as confocal microscopy and flow cytometry. Comparable to the aforementioned study by Guo et al.,[44] Santra et al. developed a folate-targeting prodrug

with activatable fluorescence and cytotoxicity.[45] The probe was composed of folic acid, a cleavable disulfide linker, and the drug doxorubicin. Thus, in folate-receptor expressing cells the probe would become fluorescent and cytotoxic. Activation of the prodrug was monitored by flow cytometry and fluorescence microscopy. In addition to this system not being translatable to most other drugs, there is a complication from coupling fluorescence activation and drug release. Fluorescence emission was shown to be enhanced over 12 hours but then decreased due to induction of apoptosis in cells due to drug release. Nonetheless, this study did quantitatively demonstrate that fluorescence increased over 12 hours in comparison to a noncleavable control which exhibited constant fluorescence over this period.

Yang et al. also evaluated bond reduction in the folate pathway using fluorescence.[33] However, in this system, bond cleavage released a fluorophore as opposed to a drug molecule. As such, fluorescence would increase over time until all fluorophore was released. The conjugate used in this work was comprised of folic acid, a hydrophilic peptide spacer, and two Förster resonance energy transfer (FRET)-active fluorophores. FRET is a physical phenomenon that relies on the distance-dependent transfer of energy from a donor fluorophore to an acceptor fluorophore. In this study, the acceptor fluorophore was attached to the disulfide bond so that FRET would be lost upon disulfide reduction. Flow cytometry was used to analyze the FRET signal as a function of incubation time and bond cleavage was quantified by the ratio of reduced to intact FRET reporters. This study provided a time-course of intracellular disulfide cleavage. However, the synthetic scheme used for this study is limited because it is restricted to targeting only the folate receptor, and the peptide linker backbone is susceptible to proteolytic degradation.

Recently researchers at Genentech developed a FRET probe to enable simultaneous tracking of both antibody and payload in an antibody-drug conjugate.[40] The probe was composed of a dipeptide linker conjugated to the FRET pair of fluorophores, fluorescein and TAMRA, as well as the highly potent microtubule inhibitor DM1. This system was used to visualize payload release *in vitro* and *in vivo*. However, the kinetics of bond cleavage was not quantified. Further, the peptide-based scaffold is not amenable to studying other bond types due to its proteolytic sensitivity.

In addition to fluorescence-based approaches for studying intracellular bond cleavage, researchers have also used the method of radiolabeling. Radiolabeling is a technique that can be used to track a molecule by replacing specific atoms within the molecule by their isotope. Feener et al. synthesized a probe composed of poly-D-lysine, a disulfide bond, and a radiolabeled analog of methotrexate.46 Cleavage of this probe would result in the release of a molecule that could be easily measured via trichloroacetic acid-soluble radioactivity. In their experiment, cells were pulsed with the probe and then incubated for varying amounts of time to allow for intracellular disulfide bond reduction. The cells were then solubilized with Triton-X and precipitated with trichloroacetic acid. The total acid-soluble radioactivity was counted as a measure of disulfide bond reduction over time. Although this method is quantitative, it is not ideal as it requires safe handling and disposal of radioactive materials. This method also cannot be carried out on intact cells, as the cells need to be solubilized to measure radioactivity.

Quantitative Measurements of Intracellular Bond Cleavage with a Theoretical Model

It would be ideal to take quantitative measurements of intracellular bond cleavage further by fitting them to a model for intracellular processing and determining

rate parameters. Maass et al. developed a model to describe the cellular processing rates of an antibody conjugate composed of emtansine (DM1) nonspecifically conjugated to lysine residues via a noncleavable linker.[47] Previously developed models described the pharmacokinetics and pharmacodynamics of this ADC at an organism or tissue-specific level rather than at the cellular level.[48,49] Maass et al. sought to focus on the cellular level to attain rate parameters that could be used to enable the more rational design of antibody-drug conjugates. Their model tracks various species that are involved in the processing of the ADC including free surface receptors, ADC-receptor complexes, internalized intact ADCs, and degraded ADCs. Further, they report generalizable methods to determine rate constants including association, dissociation, net internalization, degradation, and efflux. Other important parameters include cell growth rate and receptor density. The degradation rate constant within this context refers to the degradation of the antibody itself, which is measured by lysing cells at various time points after incubation with the conjugate and running protein on a gel to determine the amount that is still intact.

While many ADCs rely on non-specific degradation, the majority of FDA-approved ADCs incorporate specific cleavage chemistries for drug release. As such, it would be ideal to develop a method to quantify the intracellular degradation rate of stimuli-responsive bonds. Based on the advantages and disadvantages of previously developed systems, it would be ideal for this new method to work on intact, live cells and be fluorescence-based to enable visualization of intracellular processing. In addition to specific cleavage chemistry, the identity of the target endocytic pathway is important as it affects binding affinity (i.e. association and dissociation rate constants), internalization rate, and cell growth rate.

1.4. ENDOCYTIC PATHWAYS

The endocytic pathway is made up of distinct membrane compartments which internalize molecules and surface proteins from the plasma membrane[50,51]. Receptor internalization can occur through clathrin-mediated or caveolae-mediated endocytosis.[52] Internalized molecules are then delivered to and sorted within early endosomes. Then, molecules are either recycled to the cell surface or targeted for lysosomal degradation. The extent to which internalized cargo is recycled or degraded is a fundamental property of each internalization pathway. A known, well-studied target that is clathrin-mediated with a high rate of recycling is the transferrin receptor.

The transferrin receptor (CD71/TfR) is a transmembrane glycoprotein found as a homodimer on the surface of cells that serves as the major transport route of iron via the endogenous transferrin protein.[53,54] Bound transferrin is internalized via clathrin-coated pits and trafficked through mildly acidic early endosomes and recycling endosomes. When iron-bound transferrin protein (holo-transferrin) is bound to its receptor in medium of pH less than 5, iron dissociates from the protein.[55] In this state, apo-transferrin stays bound to its receptor. When the pH of the medium is raised to 7, apo-transferrin is rapidly dissociated from its receptor ($t_{1/2}$ of 7 seconds at 37 °C). In cells such as HepG2 cells, surface-bound transferrin is rapidly internalized ($t_{1/2}$ of 3.5 min) and apotransferrin is rapidly recycled back to the surface ($t_{1/2}$ of 5 min). The binding affinity of transferrin is on the order of 10 nM.

The transferrin receptor has been found to be expressed at a higher level (up to 100 fold higher) in rapidly dividing cells such as tumor cells.[56,57] For example, the transferrin receptor density in HeLa cells is on order of 10^6 molecules per cell. Due to this heightened expression level, the transferrin receptor has been used for delivery of drugs, proteins, and therapeutic genes into cancer cells. Notable examples include the

use of transferrin-targeted nanoparticles to deliver siRNA to cancer cells in three patients with metastatic melanoma. Successful delivery resulted in selective downregulation of the RRM2 protein in the three patients.[58,58] The CD71 targeting strategy has also been exploited by SynerGene to create SGT-53, a biodegradable antiCD71-scFV targeted liposomal nanoparticle (scL) that targets tumor cells for the delivery of p53 tumor suppressor. Early data from phase I clinical trials show that the particles were well tolerated along with promising signs of anticancer activity.[59,59]These two clinical examples, along with numerous non-human primate studies validate the use of CD71 as a transport route for the efficient delivery of degradable therapeutics.

HER2 (human epidermal growth factor receptor 2) is a membrane tyrosine kinase which has been found to be overexpressed on 20-30% of breast cancer cells and is associated with poor prognosis.[60-62] The HER2 receptor density in SK-BR-3 cells is on order of 10^6 molecules per cell. Several monoclonal antibodies to HER2 have been developed and have shown antitumor properties *in vivo*. Trastuzumab is a humanized monoclonal antibody against the HER2 receptor.[63] Trastuzumab has been used alone as a therapeutic (known by the trade name Herceptin) as well as in the FDA approved antibody-drug conjugates, Kadcyla and POLIVY. The HER2 receptor has been shown to recycle back to the cell surface during receptor-mediated uptake of trastuzumab in SK-BR-3 cells ($t_{1/2}$ of recycling of 5 min). The binding affinity of trastuzumab to the HER2 receptor is very strong (K_D = 120 pM).

To understand and quantify the intracellular processing of stimuli-responsive drug delivery systems, there are various parameters that must be taken into account. The type of cleavable chemistry used affects the rate of drug release; hydrazone and disulfide bonds cleave on the order of hours and dipeptide bonds cleave on the order of days. In addition to bond type, intracellular processing rates depend on the endocytic

pathway studied. The nature of the receptor affects binding affinity of the ligand and internalization rate. Cell type is also important as it affects receptor density and growth rate. By developing a system to quantify bond cleavage intracellularly and coupling it with a kinetic model of intracellular processing, bond degradation rate constants can be quantified. These parameters can be used to improve the design of future stimuli-responsive drug systems.

Chapter 1 – REFERENCES

1.Nury, C. *et al.* A novel bio-orthogonal cross-linker for improved protein/protein interaction analysis. *Analytical …* **87,** 1853–1860 (2015).

2.Kluger, R. & Alagic, A. Chemical cross-linking and protein-protein interactions-a review with illustrative protocols. *Bioorganic chemistry* **32,** 451–472 (2004).

3.Christie, R. J., Anderson, D. J. & Grainger, D. W. Comparison of hydrazone heterobifunctional cross-linking agents for reversible conjugation of thiol-containing chemistry. *Bioconjugate Chemistry* **21,** 1779–1787 (2010).

4.Casi, G. & Neri, D. Antibody-drug conjugates: basic concepts, examples and future perspectives. *J Control Release* **161,** 422–428 (2012).

5.Lee, M. H. *et al.* Disulfide-cleavage-triggered chemosensors and their biological applications. *Chemical Reviews* **113,** 5071–5109 (2013).

6.Kendziora, D. M., Ahmed, I. & Fruk, L. Multifunctional linker for orthogonal decoration of gold nanoparticles with DNA and protein. *RSC Advances* **4,** 17980 (2014).

7.Thomas, J. D., Hofer, T., Rader, C. & Burke, T. R. Application of a trifunctional reactive linker for the construction of antibody-drug hybrid conjugates. *bioorganic & medicinal chemistry letters* **18,** 5785–5788 (2008).

8.Leriche, G., Chisholm, L. & Wagner, A. Cleavable linkers in chemical biology. *Bioorganic & medicinal chemistry* **20,** 571–582 (2011).

9.Yang, Y. & Verhelst, S. H. L. Cleavable trifunctional biotin reagents for protein labelling, capture and release. *Chem Commun (Camb)* **49,** 5366–5368 (2013).

10.Clavé, G. *et al.* A novel heterotrifunctional peptide-based cross-linking reagent for facile access to bioconjugates. Applications to peptide fluorescent labelling and immobilisation. *Organic & Biomolecular Chemistry* **6,** 3065–3078 (2008).

11.Chevalier, A., Hardouin, J., Renard, P.-Y. & Romieu, A. Universal dark quencher

based on ‘clicked’ spectrally distinct azo dyes. *Organic Letters* **15,** 6082–6085 (2013).

12.Viault, G. *et al.* The first ‘ready-to-use’ benzene-based heterotrifunctional cross-linker for multiple bioconjugation. *Organic & Biomolecular Chemistry* **11,** 2693–2705 (2013).

13.Frei, A. P. *et al.* Direct identification of ligand-receptor interactions on living cells and tissues. *Nat Biotechnol* **30,** 997–1001 (2012).

14.Beal, D. M. *et al.* Click-enabled heterotrifunctional template for sequential bioconjugations. *Organic & Biomolecular Chemistry* **10,** 548–554 (2011).

15.Lee, M.-R., Jung, D.-W., Williams, D. & Shin, I. Efficient solid-phase synthesis of trifunctional probes and their application to the detection of carbohydrate-binding proteins. *Organic Letters* **7,** 5477–5480 (2005).

16.Maurer, A., Zeyher, C., Amin, B. & Kalbacher, H. A periodate-cleavable linker for functional proteomics under slightly acidic conditions: application for the analysis of intracellular aspartic proteases. *J Proteome Res* **12,** 199–207 (2012).

17.Merrifield, R. B. Solid Phase Peptide Synthesis. I. The Synthesis of a Tetrapeptide. *Journal of the American Chemical Society* **85,** 2149 (1963).

18.D'Souza, A. J. M. & Topp, E. M. Release from polymeric prodrugs: linkages and their degradation. *J Pharm Sci* **93,** 1962–1979 (2004).

19.Leriche, G., Chisholm, L. & Wagner, A. Cleavable linkers in chemical biology. doi:10.1016/j.bmc.2011.07.048

20.Böhme, D. & Beck-Sickinger, A. G. Drug delivery and release systems for targeted tumor therapy. doi:10.1002/psc.2753

21.Davis, M. E. Design and development of IT-101, a cyclodextrin-containing polymer conjugate of camptothecin. *Advanced Drug Delivery Reviews* **61,** 1189–1192 (2009).

22.Liao, J. *et al.* Tumor-targeting and pH-responsive nanoparticles from hyaluronic acid

for the enhanced delivery of doxorubicin. *Int J Biol Macromol* **113,** 737–747 (2018).

23.Hong, R. *et al.* Glutathione-mediated delivery and release using monolayer protected nanoparticle carriers. *Journal of the American Chemical Society* **128,** 1078–1079 (2006).

24.Beck, A., Goetsch, L., Dumontet, C. & Corvaïa, N. Strategies and challenges for the next generation of antibody-drug conjugates. *Nature Reviews Drug Discovery* **16,** 315–337 (2017).

25.Binauld, S. & Stenzel, M. H. Acid-degradable polymers for drug delivery: a decade of innovation. *Chem Commun (Camb)* **49,** 2082–2102 (2013).

26.Lu, J., Jiang, F., Lu, A. & Zhang, G. Linkers Having a Crucial Role in Antibody-Drug Conjugates. *International journal of molecular sciences* **17,** 561 (2016).

27.Kratz, F. *et al.* Transferrin conjugates of doxorubicin: Synthesis, characterization, cellular uptake, and in vitro efficacy. *J Pharm Sci* **87,** 338 (1998).

28.Du, J.-Z., Du, X.-J., Mao, C.-Q. & Wang, J. Tailor-made dual pH-sensitive polymer-doxorubicin nanoparticles for efficient anticancer drug delivery. *Journal of the American Chemical Society* **133,** 17560–17563 (2011).

29.Li, S.-Y. *et al.* A pH-responsive prodrug for real-time drug release monitoring and targeted cancer therapy. *Chem Commun (Camb)* **50,** 11852–11855 (2014).

30.Jackson, D. & Stover, D. Using the Lessons Learned From the Clinic to Improve the Preclinical Development of Antibody Drug Conjugates. *Pharm Res* **32,** 3458–3469 (2014).

31.Cheng, R. *et al.* Glutathione-responsive nano-vehicles as a promising platform for targeted intracellular drug and gene delivery. doi:10.1016/j.jconrel.2011.01.030

32.Saito, G., Swanson, J. A. & Lee, K.-D. Drug delivery strategy utilizing conjugation via reversible disulfide linkages: role and site of cellular reducing activities. *Advanced*

Drug Delivery Reviews **55,** 199 (2003).

33.Yang, J., Chen, H., Vlahov, I. R., Cheng, J.-X. & Low, P. S. Evaluation of disulfide reduction during receptor-mediated endocytosis by using FRET imaging. *Proc Natl Acad Sci USA* **103,** 13872–13877 (2006).

34.Pan, A. *et al.* Disulfide-crosslinked nanomicelles confer cancer-specific drug delivery and improve efficacy of paclitaxel in bladder cancer. *Nanotechnology* **27,** 425103 (2016).

35.Qi, R. *et al.* Nanoparticle conjugates of a highly potent toxin enhance safety and circumvent platinum resistance in ovarian cancer. *Nat Commun* **8,** 2166 (2017).

36.Kovtun, Y. *et al.* IMGN779, a Novel CD33-Targeting Antibody-Drug Conjugate with DNA-Alkylating Activity, Exhibits Potent Antitumor Activity in Models of AML. *… Cancer Therapeutics* **17,** 1271–1279 (2018).

37.Dubowchik, G. M. *et al.* Cathepsin B-Labile Dipeptide Linkers for Lysosomal Release of Doxorubicin from Internalizing Immunoconjugates: Model Studies of Enzymatic Drug Release and Antigen-Specific In Vitro Anticancer Activity. *Bioconjugate Chemistry* **13,** 855 (2002).

38.Tian, R. *et al.* An intracellularly activatable, fluorogenic probe for cancer imaging. *Organic & Biomolecular Chemistry* **12,** 5365–5374 (2014).

39.Zhong, Y.-J., Shao, L.-H. & Li, Y. Cathepsin B-cleavable doxorubicin prodrugs for targeted cancer therapy (Review). *… journal of oncology* **42,** 373–383 (2012).

40.Lee, B.-C. *et al.* FRET Reagent Reveals the Intracellular Processing of Peptide-Linked Antibody-Drug Conjugates. *Bioconjugate Chemistry* **29,** 2468–2477 (2018).

41.Wu, A. M. & Senter, P. D. Arming antibodies: prospects and challenges for immunoconjugates. *Nat Biotechnol* **23,** 1137–1146 (2005).

42.Senter, P. D. & Sievers, E. L. The discovery and development of brentuximab

vedotin for use in relapsed Hodgkin lymphoma and systemic anaplastic large cell lymphoma. *Nat Biotechnol* **30,** 631–637 (2012).

43.Tilly, H. *et al.* Polatuzumab vedotin in combination with immunochemotherapy in patients with previously untreated diffuse large B-cell lymphoma: an open-label, non-randomised, phase 1b-2 study. *Lancet Oncol* **20,** 998–1010 (2019).

44.Guo, X., Shi, C., Wang, J., Di, S. & Zhou, S. pH-triggered intracellular release from actively targeting polymer micelles. *Biomaterials* **34,** 4544–4554 (2013).

45.Santra, S., Kaittanis, C., Santiesteban, O. J. & Perez, J. M. Cell-specific, activatable, and theranostic prodrug for dual-targeted cancer imaging and therapy. *Journal of the American Chemical Society* **133,** 16680–16688 (2011).

46.Feener, E. P., Shen, W. C. & Ryser, H. J. Cleavage of disulfide bonds in endocytosed macromolecules. A processing not associated with lysosomes or endosomes. *Journal of Biological Chemistry* **265,** 18780–18785 (1990).

47.Maass, K. F., Kulkarni, C., Betts, A. M. & Wittrup, K. D. Determination of Cellular Processing Rates for a Trastuzumab-Maytansinoid Antibody-Drug Conjugate (ADC) Highlights Key Parameters for ADC Design. *The AAPS Journal* **18,** 635–646 (2016).

48.Erickson, H. K. *et al.* The effect of different linkers on target cell catabolism and pharmacokinetics/pharmacodynamics of trastuzumab maytansinoid conjugates. … *Cancer Therapeutics* **11,** 1133–1142 (2012).

49.Wada, R. *et al.* Mechanistic pharmacokinetic/pharmacodynamic modeling of in vivo tumor uptake, catabolism, and tumor response of trastuzumab maytansinoid conjugates. *Cancer Chemother Pharmacol* **74,** 969–980 (2014).

50.Wileman, T., Harding, C. & Stahl, P. Receptor-mediated endocytosis. *Biochem J* **232,** 1–14 (1985).

51.Gruenberg, J. The endocytic pathway: a mosaic of domains. *Nat Rev Mol Cell Biol*

2, 721–730 (2001).

52.Maxfield, F. R. & McGraw, T. E. Endocytic recycling. *Nat Rev Mol Cell Biol* **5,** 121–132 (2004).

53.Qian, Z. M., Li, H., Sun, H. & Ho, K. Targeted drug delivery via the transferrin receptor-mediated endocytosis pathway. *Pharmacol Rev* **54,** 561–587 (2002).

54.Ciechanover, A., Schwartz, A. L., Dautry-Varsat, A. & Lodish, H. F. Kinetics of internalization and recycling of transferrin and the transferrin receptor in a human hepatoma cell line. Effect of lysosomotropic agents. *Journal of Biological Chemistry* **258,** 9681–9689 (1983).

55.Ciechanover, A., Schwartz, A. L., Dautry-Varsat, A. & Lodish, H. F. Kinetics of internalization and recycling of transferrin and the transferrin receptor in a human hepatoma cell line. Effect of lysosomotropic agents. *Journal of Biological Chemistry* **258,** 9681–9689 (1983).

56.Daniels, T. R., Delgado, T., Helguera, G. & Penichet, M. L. The transferrin receptor part II: targeted delivery of therapeutic agents into cancer cells. *Clin Immunol* **121,** 159–176 (2006).

57.Tortorella, S. & Karagiannis, T. C. Transferrin receptor-mediated endocytosis: a useful target for cancer therapy. *J Membr Biol* **247,** 291–307 (2014).

58.Davis, M. E. *et al.* Evidence of RNAi in humans from systemically administered siRNA via targeted nanoparticles. *Nature* **464,** 1067–1070 (2010).

59.Camp, E. R. *et al.* Transferrin receptor targeting nanomedicine delivering wild-type p53 gene sensitizes pancreatic cancer to gemcitabine therapy. *Cancer gene … **20,*** 222–228 (2013).

60.Arteaga, C. L. *et al.* Treatment of HER2-positive breast cancer: current status and future perspectives. *Nat Rev Clin Oncol* **9,** 16–32 (2011).

61.Mitri, Z., Constantine, T. & O'Regan, R. The HER2 Receptor in Breast Cancer: Pathophysiology, Clinical Use, and New Advances in Therapy. *Chemother Res Pract* **2012,** 743193 (2012).

62.Bertelsen, V. & Stang, E. The Mysterious Ways of ErbB2/HER2 Trafficking. *Membranes (Basel)* **4,** 424–446 (2014).

63.Gemmete, J. J. & Mukherji, S. K. Trastuzumab (herceptin). *AJNR Am J Neuroradiol* **32,** 1373–1374 (2011).

Chapter 2 – VERSATILE PLATFORM FOR THE SYNTHESIS OF ORTHOGONALLY CLEAVABLE HETEROMULTIFUNCTIONAL CROSS-LINKERS

Reprinted (adapted) with permission from Sorkin, M. R., Walker, J. A., Brown, J. S. & Alabi, C. A. Versatile Platform for the Synthesis of Orthogonally Cleavable Heteromultifunctional Cross-Linkers. Bioconjugate Chemistry ***28,*** *907–912 (2017).*

2.1. INTRODUCTION

An emerging paradigm in polymer chemistry is the synthesis of sequence-defined polymers. Oligothioetheramides (oligoTEAs), a subset of sequence-defined polymers, have recently been reported by our research group.[1,2] The oligoTEA synthesis approach utilizes an orthogonally reactive *N*-allylacrylamide monomer, which can undergo alternating photoinitiated thiol-ene “click” reactions and phosphine-catalyzed thiol-Michael additions. OligoTEAs are built off a fluorous tag liquid support, which enables incorporation of monomers using rapid solution-phase reaction kinetics and stepwise fluorous purification throughout synthesis. The fluorous purification handle can readily be removed post-synthesis by acid-catalyzed BOC deprotection to yield a terminal primary amine. The oligoTEA synthetic methodology has been used to assemble sequence-defined oligomers with a wide variety of composition and length.[1-3] Aside from their facile synthesis, oligoTEAs have several benefits including the incorporation of a diverse panel of pendant and backbone functionalities. Furthermore, oligoTEAs are stable to proteolytic degradation and as such are stable in the biological environment.[4]

2.2. RESULTS AND DISCUSSION

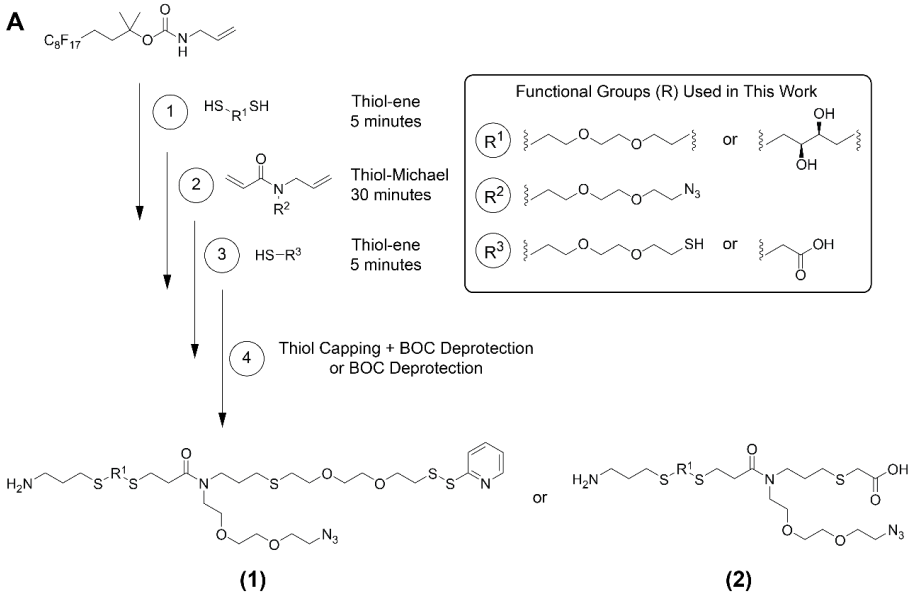

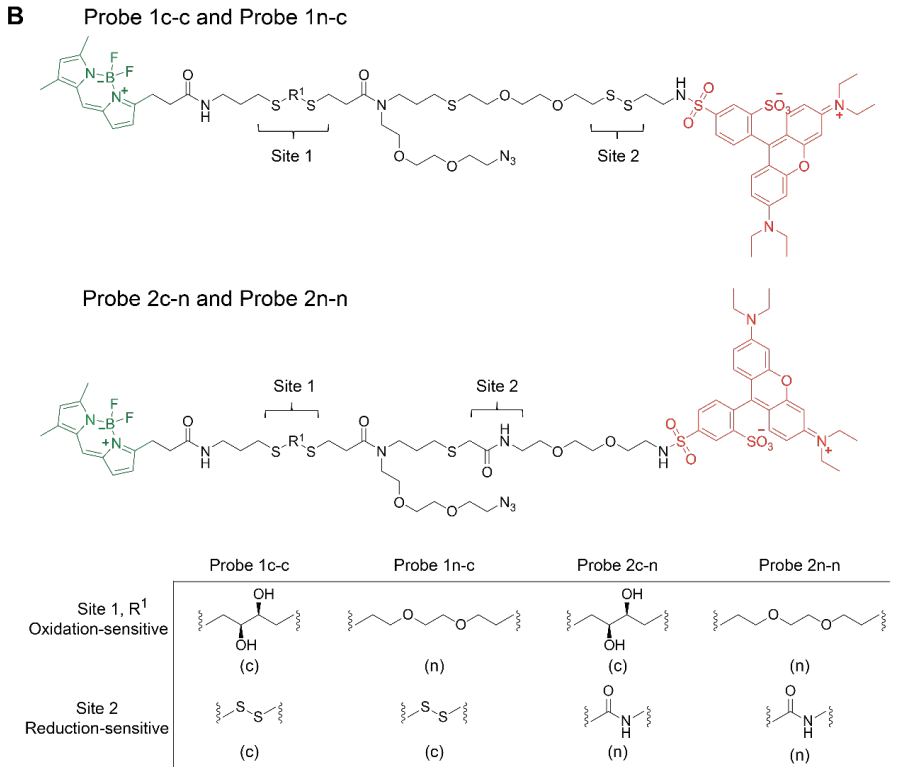

Figure 2.1. Synthesis of probes. A) OligoTEA synthesis. Steps: 1) Thiol-ene reaction 2) Thiol-Michael addition 3) Thiol-ene reaction 4) Thiol capping reaction + Boc deprotection or Boc deprotection B) Structures of fluorophore-conjugated oligoTEA probes, denoted as Probe 1c-c, Probe 1n-c, Probe 2c-n and Probe 2n-n.

Herein we report the design and synthesis of four heterotrifunctional oligoTEA-based chemical crosslinkers containing up to two orthogonal internal cleavage sites (Scheme 1). To the best of our knowledge, this represents the first reported synthesis of a heterotrifunctional crosslinker containing two orthogonal internal cleavage sites. First, fluorous BOC-protected allylamine was reacted with either L-dithiothreitol (L-DTT) or (2,2')-ethylenedioxydiethanethiol via a photoinitiated thiol-ene reaction (Scheme 1A, 1). Next, each product was reacted with an *N*-allylacrylamide azide monomer through a phosphine-catalyzed Michael addition (Scheme 1A, 2). The products of the Michael addition were then reacted in a second thiol-ene reaction with either (2,2')-ethylenedioxydiethanethiol or mercaptoacetic acid (Scheme 1A, 3). OligoTEAs containing (2,2')-ethylenedioxydiethanethiol were further reacted with 2,2'-dipyridyl disulfide as a capping group via thiol-disulfide exchange prior to cleavage from the fluorous support to give the class of compounds **1**. The oligoTEA products capped with mercaptoacetic acid were cleaved off the fluorous tag via acid treatment to give the class of compounds **2.** Fluorous purification was carried out between each step as previously described[1,1] to remove excess reagents. The final oligomers were purified via reverse-phase high-performance liquid chromatography (RP-HPLC)

To demonstrate their utility as multifunctional probes, the resulting heterotrifunctional oligoTEAs were conjugated to the Förster resonance energy transfer (FRET) pair, BODIPY and rhodamine (Figure 2.1). Purification via RP-HPLC was carried out after each fluorophore conjugation step. Cleavable site 1 is comprised of a *cis*-1,2-diol that is susceptible to oxidative cleavage by sodium periodate ($NaIO_4$). Cleavable site 2 is comprised of a disulfide bond that is susceptible to reductive cleavage by dithiothreitol (DTT). The four synthesized oligoTEA probes (Scheme 1B) will henceforth be referred to as 1c-c, 1n-c, 2n-c and 2n-n, where c and n represent

cleavable and non-cleavable bonds respectively (e.g. 1n-c = compound **1** with a noncleavable ethyleneoxide linkage and a cleavable disulfide bond). Relative RP-HPLC elution times for all four probes are shown in Figure 2.2A. The probes were then characterized by liquid chromatography-mass spectrometry (LC-MS) (Figure 2.2B). The loss of a fluorine atom is often observed in the mass spectrum of BODIPY.

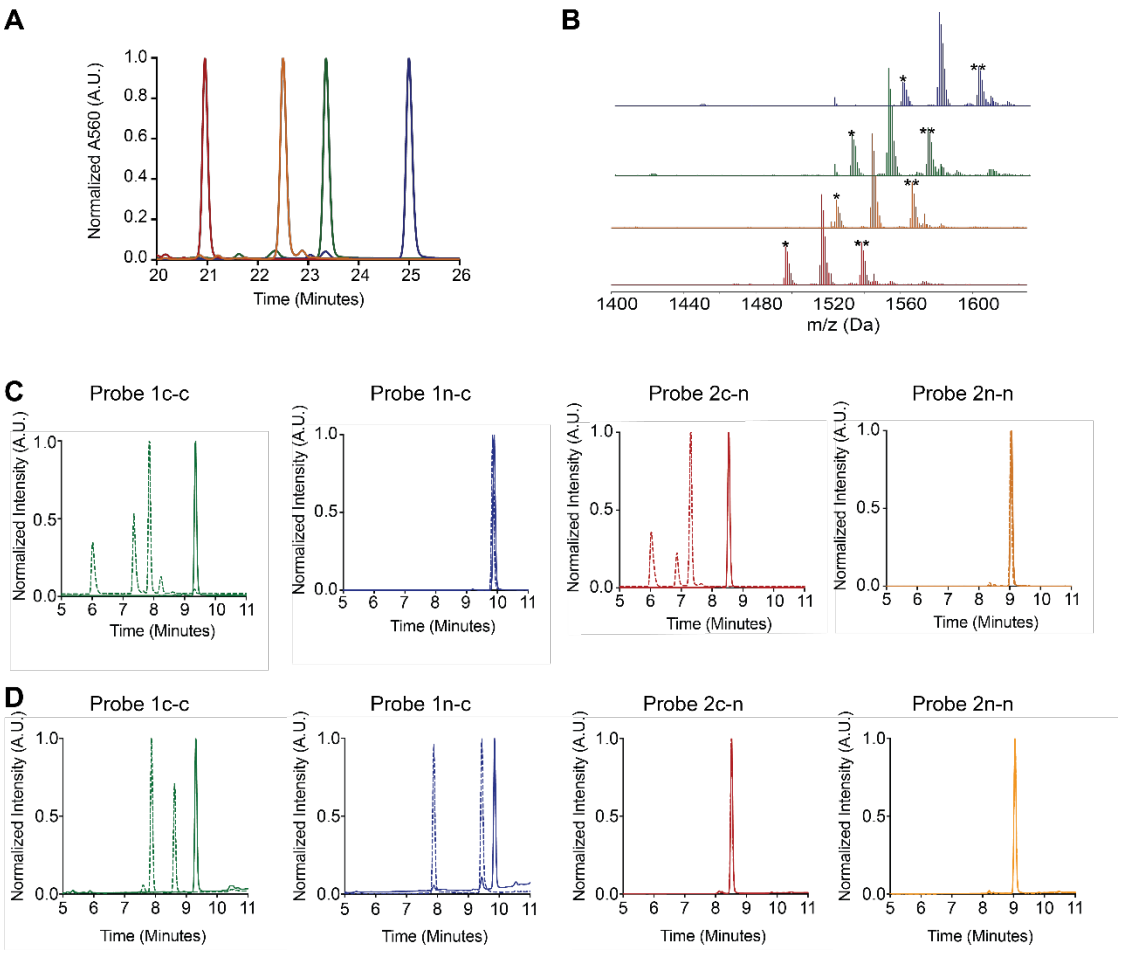

Figure 2.2. Characterization of probes. A) RP-HPLC traces of probes 1c-c (green), 1n-c (blue), 2c-n (red) and 2n-n (orange). B) LC-MS of probes. Ionization pattern of probes: $[M-F]^+$ (*), $[M+H]^+$ (most prominent), $[M+Na]^+$ (**). Probe 1c-c (green) m/z calculated: 1551.54, observed: 1551.50 $[M+H]^+$; Probe 1n-c (blue) m/z calculated: 1579.57, observed: 1579.49 $[M+H]^+$; Probe 2c-n (red) m/z calculated: 1516.58, observed: 1516.49 $[M+H]^+$; Probe 2n-n (orange) m/z calculated: 1544.62, observed: 1544.50 $[M+H]^+$. C) LC-MS SIM of probes treated with $NaIO_4$ (--- dashed line) and without $NaIO_4$ (- solid line). D) LC-MS SIM of probes treated with DTT (--- dashed line) and without DTT (- solid line).

Chemical cleavage of the probes was demonstrated by LC-MS using selected-ion monitoring (SIM) for the expected fragments after incubating the probes with $NaIO_4$ or DTT at room temperature for one hour (Figure 2.2C and Figure 2.2D). Upon treatment with $NaIO_4$, the oxidation-sensitive probes (1c-c and 2c-n) were cleaved to give multiple fragments. Sodium periodate, in addition to cleaving *cis*-1,2-diols to give aldehydes and hydrates, can oxidize thioethers such as those present in the oligoTEA backbone. Addition of $NaIO_4$ to Probe 1c-c gave a fragment at 6 minutes corresponding to the oxidized BODIPY hydrate (*m/z* calculated: 422.17, observed: 422.20 $[M+O+H_2O-F]^+$). In addition, we also observed two fragments between 7-8 minutes (single oxidation at each thioether or double oxidation at one thioether) corresponding to the doubly oxidized rhodamine aldehydes (1174.35 observed: 1174.30 $[M+2O+H]^+$). Similarly, addition of $NaIO_4$ to Probe 2c-n gave three fragments. The first fragment at ~6 minutes corresponds to the oxidized BODIPY hydrate (*m/z* calculated: 422.17 observed: 422.20 $[M+O+H_2O-F]^+$). The next two fragments appearing between 6.5-7.5 minutes correspond to the doubly oxidized rhodamine aldehydes (*m/z* calculated: 1139.39 observed: 1139.40 $[M+2O+H]^+$). Probes 1n-c and 2n-n show no cleavage after $NaIO_4$ treatment. Upon treatment with DTT, the reduction sensitive probes (1c-c and 1n-c) were cleaved to yield two distinct fragments with masses corresponding to the expected reduced thiol fragments. Addition of DTT to Probe 1c-c gave two fragments: fragment 1 (at ~7.9 mins) *m/z* calculated: 936.39 observed: 936.40 $[M+H]^+$ and fragment 2 (at ~8.7 mins) *m/z* calculated: 618.18, observed: 618.20 $[M+H]^+$. Addition of DTT to Probe 1n-c also gave two fragments: fragment 1 (at ~7.9 mins) *m/z* calculated: 964.42 observed: 964.40 $[M+H]^+$ and fragment 2 (at ~9.5 mins) *m/z* calculated: 618.18 observed: 618.20 $[M+H]^+$. Probes 2c-n and 2n-n show no cleavage after DTT treatment.

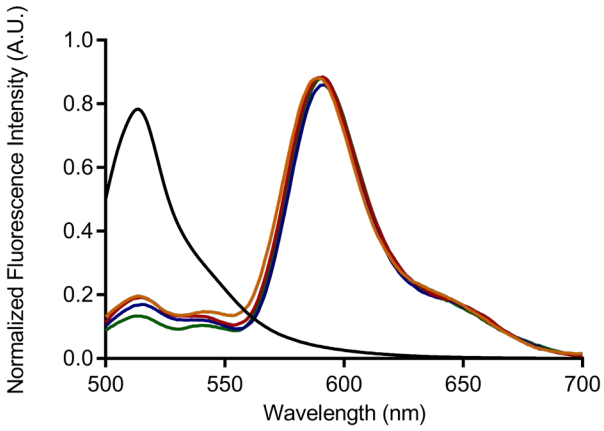

Figure 2.3. Fluorescence emission curves. BODIPY (black), Probe1c-c (green), Probe 1n-c (blue), Probe 2c-n (red), and Probe 2n-n (orange). Fluorescence emission curves were generated at an excitation wavelength of 480 nm for BODIPY NHS (compound **(7)**) and Probe 1c-c, Probe 1n-c, Probe 2c-n, and Probe 2n-n at a concentration of 2.5 μM in PBS pH 7.4.

When conjugated to the green fluorophore BODIPY (Ex/Em: 505/515 nm) and the red fluorophore rhodamine (Ex/Em: 566/586 nm), the oligoTEA-based probes undergo Förster resonance energy transfer (FRET). As such, fluorescence energy transfer can be used as an indicator of bond dissociation by monitoring the loss of FRET due to treatment with $NaIO_4$ and/or DTT. To demonstrate FRET between BODIPY and rhodamine, fluorescence emissions curves were generated for all the FRET oligoTEAs in comparison to the donor fluorophore, BODIPY (Figure 2.3s). These emission curves indicate that when both fluorophores are conjugated to the same probe, BODIPY undergoes intramolecular energy transfer with rhodamine.

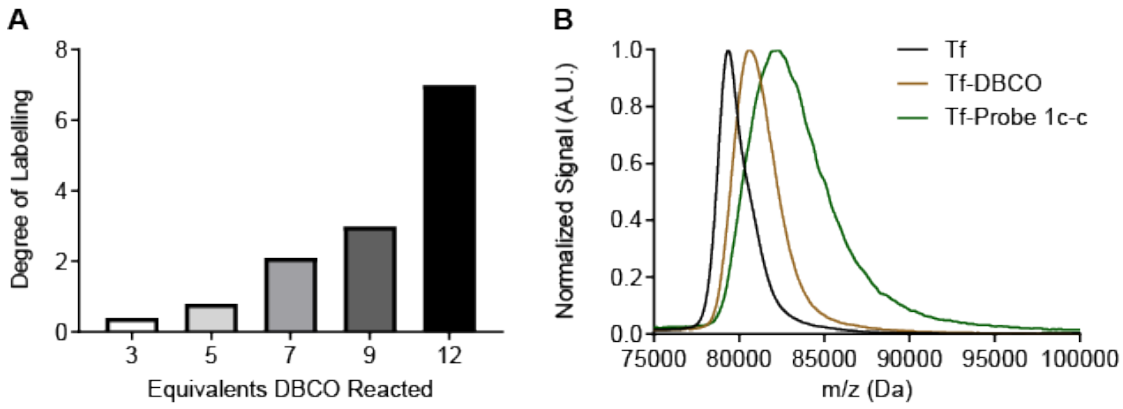

Figure 2.4. Characterization of transferrin conjugates. A) Optimization of labelling of transferrin with dibenzocyclooctyne (DBCO) groups. B) MALDI characterization for transferrin, transferrin-DBCO, and transferrin-Probe 1c-c.

All four fluorescent probes were then conjugated to a model protein - human transferrin, which was modified with a strained dibenzocyclooctyne (DBCO), by coupling to exposed lysine residues on the protein surface. The azide functionality in each probe could then be reacted with DBCO modifications on the protein. Various excesses of DBCO-PEG_4-NHS ester were reacted with transferrin, and the degree of labelling was determined via matrix-assisted laser desorption/ionization (MALDI) (Figure 2.4A). The condition in which 7 equivalents of the NHS ester were reacted with transferrin gave a degree of labelling of approximately 2.1 DBCO groups per protein. This degree of labelling was chosen to prevent fluorescence quenching, retain biological activity of the protein (i.e. binding and internalization), and avoid destabilization/precipitation of the protein. The linker was reacted at 0.5, 1, and 1.5 equivalents of linker relative to the DBCO. The 0.5 equivalents condition gave approximately 1 linker per transferrin, the 1 equivalent condition gave 1.4 linkers per transferrin, and the 1.5 equivalent condition gave 1.1 linkers per transferrin. The 1 equivalent condition was chosen to avoid having much unlabeled protein and to not waste excess linker for the reaction. All transferrin probes were purified by dialysis, and

Probe 1c-c was characterized by matrix-assisted laser desorption/ionization (MALDI) to confirm the degree of labeling for both the DBCO-modified and probe-modified transferrin conjugates (Figure 2.4Bs). MALDI analysis indicated a degree of labeling of approximately one probe per transferrin.

Following confirmation of the probe-modified transferrin conjugates, selective bond cleavage could then be demonstrated via a fluorescent gel shift assay. The readouts of the fluorescent gel shift assay were the appearance and/or disappearance of fluorescence upon BODIPY excitation/emission, rhodamine excitation/emission, and BODIPY excitation/rhodamine emission (FRET) (Figure 2.5).

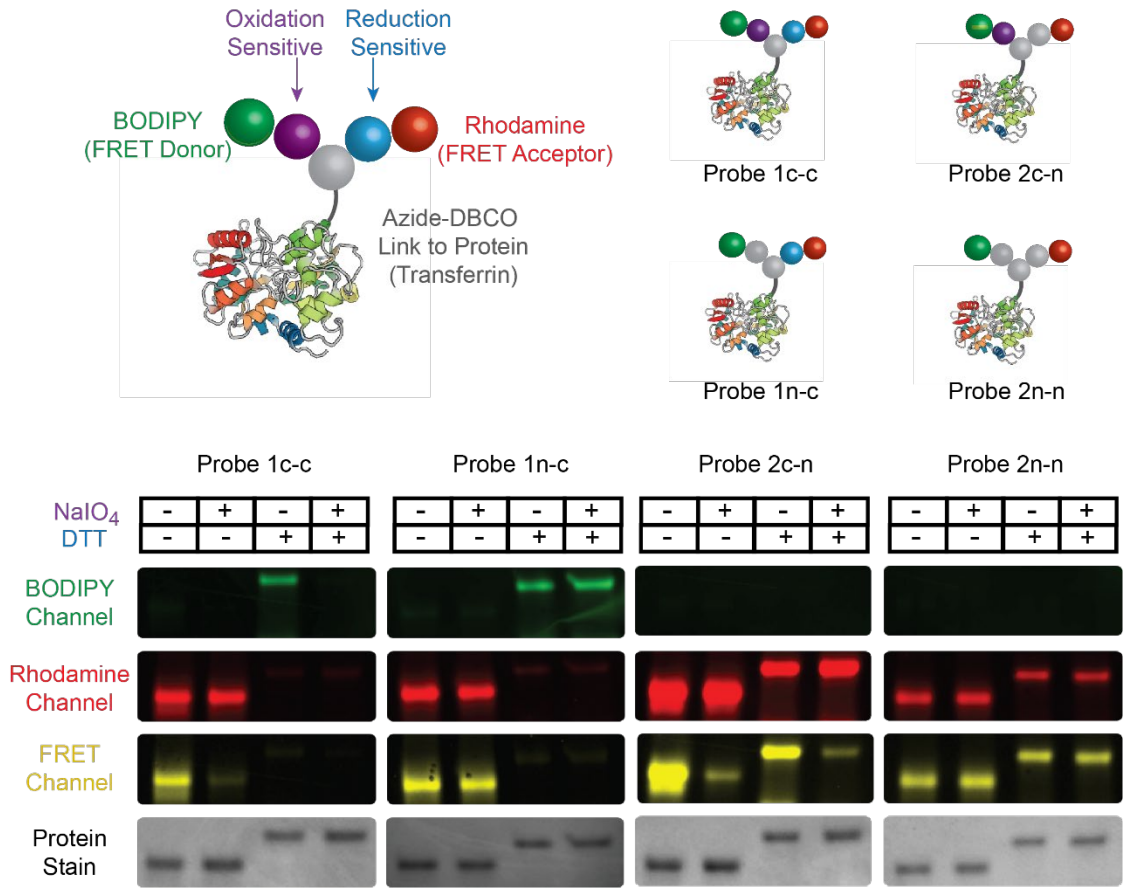

Figure 2.5. Fluorescence gel images of transferrin probes upon treatment with $NaIO_4$ and/or DTT. BODIPY excitation: 488 nm, emission: 500-540 nm; Rhodamine excitation: 561 nm, emission: 573-681 nm. FRET excitation: 488 nm, emission: 578-685 nm; Coomassie blue protein stain. 4-20% SDS-PAGE gel, denatured non-reduced.

With no chemical input, all transferrin probes displayed fluorescence bands for rhodamine emission (red) and FRET emission (yellow), while BODIPY emission (green) was quenched (Figure 2.5). When treated with $NaIO_4$ and/or DTT, the fully non-cleavable Probe 2n-n showed no differences in fluorescence band intensity. The only observed effect was a band shift towards a higher apparent molecular weight when treated with DTT. This was observed for each transferrin probe and is likely due to conformational changes in the protein structure resulting from reduction of native disulfide bonds. When the fully cleavable Probe 1c-c was treated with $NaIO_4$, BODIPY was cleaved from the protein. As such, FRET emission was greatly diminished, and the rhodamine emission stayed constant. Upon DTT induced reduction of the disulfide bond in Probe 1c-c, rhodamine was cleaved from the protein. Thus, a band for BODIPY emission appeared and the rhodamine emission disappeared. Furthermore, the FRET emission disappeared. When treated with both $NaIO_4$ and DTT, both fluorophores were cleaved off the protein leading to a loss of BODIPY, rhodamine, and FRET emission. Probe 1n-c and Probe 2c-n, which should respond to only DTT and $NaIO_4$ treatment respectively, exhibited the expected fluorescence trends. That is, upon treatment with DTT, Probe 1n-c displayed an increase in BODIPY emission, disappearance of rhodamine emission, and a reduction in FRET emission. Upon treatment with $NaIO_4$, Probe 2c-n showed no BODIPY emission, constant rhodamine emission, and diminished FRET emission. Coomassie blue protein stain was used to confirm equal loading between lanes for each probe.

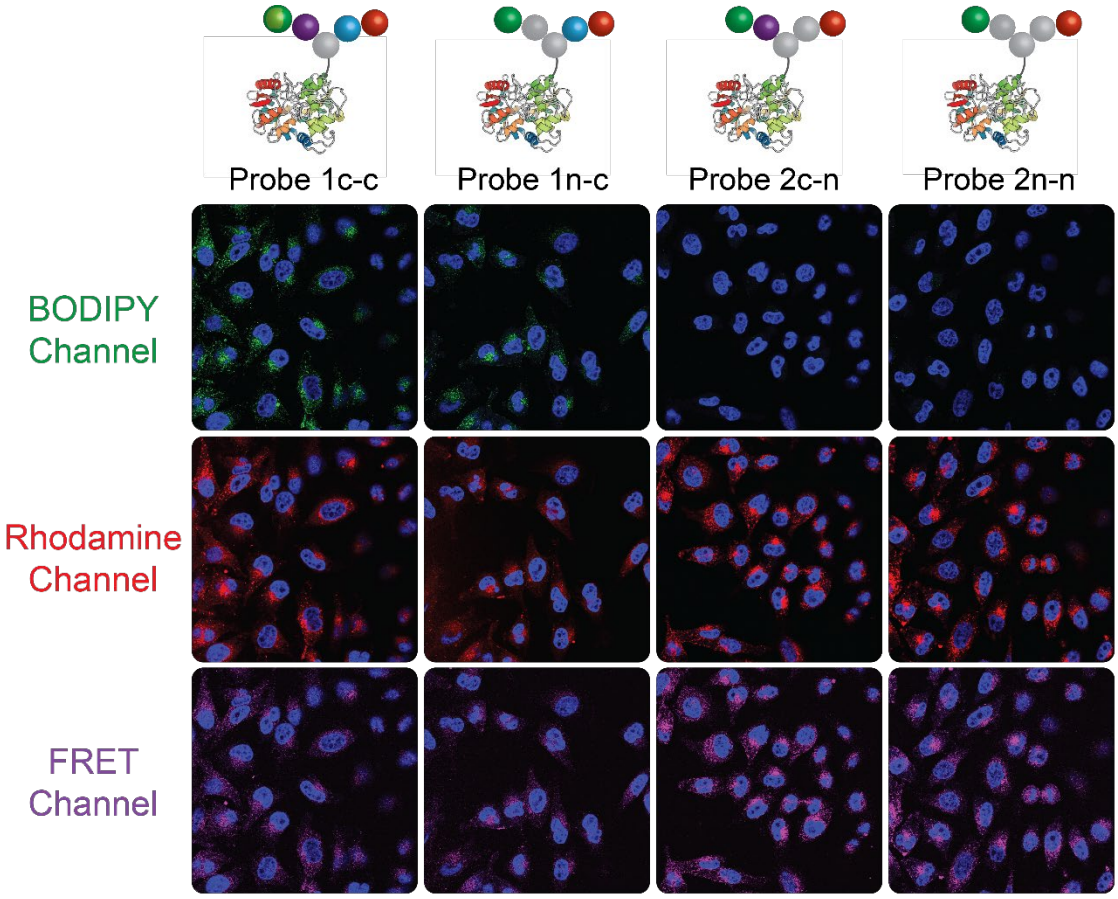

Figure 2.6. Confocal laser-scanning microscopy images of HeLa cells incubated with transferrin probes. Conjugate added at 150 nM. BODIPY excitation: 488 nm, emission: 500-540 nm (green); Rhodamine excitation: 561 nm, emission: 573-681 nm (red); FRET excitation: 488 nm, emission: 578-685 nm (magenta); Hoechst nuclear stain (blue).

To verify the potential of the transferrin probes to function in biological applications, HeLa cells were incubated with the fluorescent transferrin probes and visualized by confocal microscopy. The data confirms that the transferrin probes retain their ability to bind and internalize into HeLa cells.

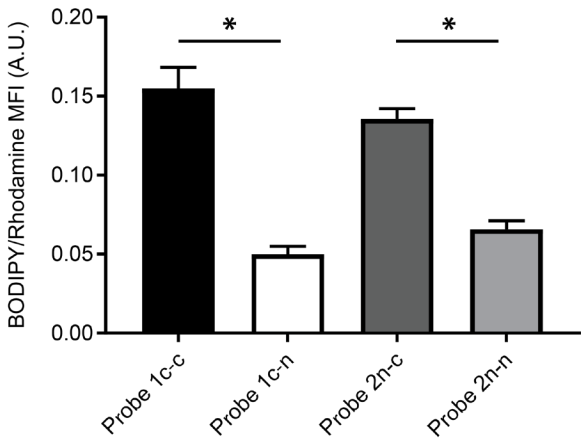

Figure 2.7. Whole cell mean fluorescence intensity quantification of confocal microscopy images. Shown with standard error of the mean (n = 10, * = $p < 0.0001$).

Furthermore, the probes showed differential BODIPY emission intensities with transferrin-Probe 2n-n and transferrin-Probe 2c-n showing the weakest BODIPY emission intensity as expected. Transferrin-Probes 1c-c and 1n-c exhibited quantitatively higher BODIPY fluorescence than transferrin-Probe 2c-n and 2n-n (Figure 2.6, Figure 2.7). This finding indicates that the disulfide bond undergoes cleavage within the endocytic transferrin pathway, in which bound transferrin is internalized via clathrin-coated pits and trafficked through mildly acidic early endosomes and recycling endosomes.5,6 Further studies are currently underway to quantify the kinetics of the cleavage events described above.

2.3. CONCLUSION

In conclusion, we have demonstrated the versatility of the sequence-defined oligothioetheramide (oligoTEA) platform towards the synthesis of four heterotrifunctional crosslinkers comprised of up to two orthogonal internal cleavage sites. These crosslinkers were conjugated to a pair of FRET fluorophores, BODIPY and rhodamine. We demonstrated the chemical cleavage of the resulting probes via LC-MS SIM. Further, we conjugated each of the probes to a model protein – human transferrin.

Cleavage of the transferrin-probes was demonstrated chemically via fluorescent gel electrophoresis and intracellularly via confocal laser-scanning microscopy. Although we synthesized crosslinkers with three reactive groups and two orthogonal cleavage sites, the oligoTEA synthesis shown can be applied iteratively to incorporate additional functional groups and cleavable bonds. These studies demonstrate the utility of oligoTEAs towards the rapid production of structurally diverse heteromultifunctional linkers that can be used in a wide range of biological applications.

2.4. SYNTHETIC CHALLENGES

Rhodamine was incorporated into Probe 1c-c and Probe 1n-c through a thiol-disulfide exchange reaction of the pyridyl disulfide capping group on the oligoTEA and thiol-functionalized rhodamine (sulfo rhodamine amidoethyl mercaptan). The rhodamine thiol was found to be poorly soluble and provided from the commercial supplier as a mixture of the free thiol and the disulfide form. The rhodamine thiol was found to have the most optimal solubility at 0.3 mg/ml in dimethylformamide (DMF). To ensure solubility of the reaction mixture, once dissolved at 0.3 mg/ml in DMF, the stock solution was centrifuged to pellet any insoluble materials. The supernatant was used for reaction and insoluble material was assumed to be dimerized form and left behind.

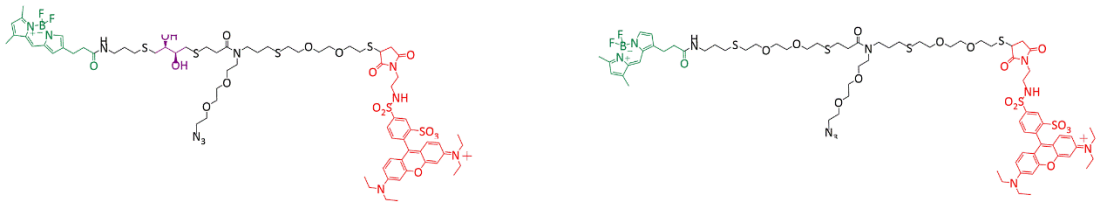

Figure 2.8. FRET cross-linker structures with rhodamine maleimide. Rhodamine is incorporated through a noncleavable thioether linkage via a thiol-maleimide reaction with rhodamine maleimide.

Rhodamine was incorporated into Probe 1c-n and Probe 1n-n through carbodiimide coupling of the carboxylic acid capping group on the oligoTEA and amine-functionalized rhodamine (Compound **(4)**). It was originally attempted to incorporate the rhodamine through a noncleavable thioether linkage via a thiol-maleimide reaction (Figure 2.8). The free thiol at the end of an oligoTEA was reacted with maleimide-functionalized rhodamine. Rhodamine maleimide was obtained commercially and found to have poor solubility. The solubility of rhodamine maleimide was found to be 2 mg/ml in dimethyl sulfoxide (DMSO) and 0.69 mg/ml in other solvents such as DMF, acetonitrile, tetrahydrofuran, and methanol. The oligoTEA was reacted at 420 μM with 5 equivalents of rhodamine maleimide in 28% 1X phosphate-buffered saline (PBS), 72% DMSO for 2 hours. The recovery for the reaction was found to be 3%. The reaction mixture was found to contain rhodamine maleimide, hydrolyzed rhodamine maleimide, rhodamine-modified product, and hydrolyzed rhodamine-modified product. Hydrolysis of rhodamine maleimide occurred readily, wasting fluorophore and hydrolyzing the desired product. The reaction was also carried out in methanol as the solvent with an added 2 equiv of reducing agent (dimethylphenylphosphine, triphenylphosphine, and tris(2-carboxyethyl)phosphine) to reduce dimerization of the thiol-terminated oligoTEA. It was found that the rhodamine maleimide readily formed a phosphine adduct and the thiol-maleimide reaction did not occur.

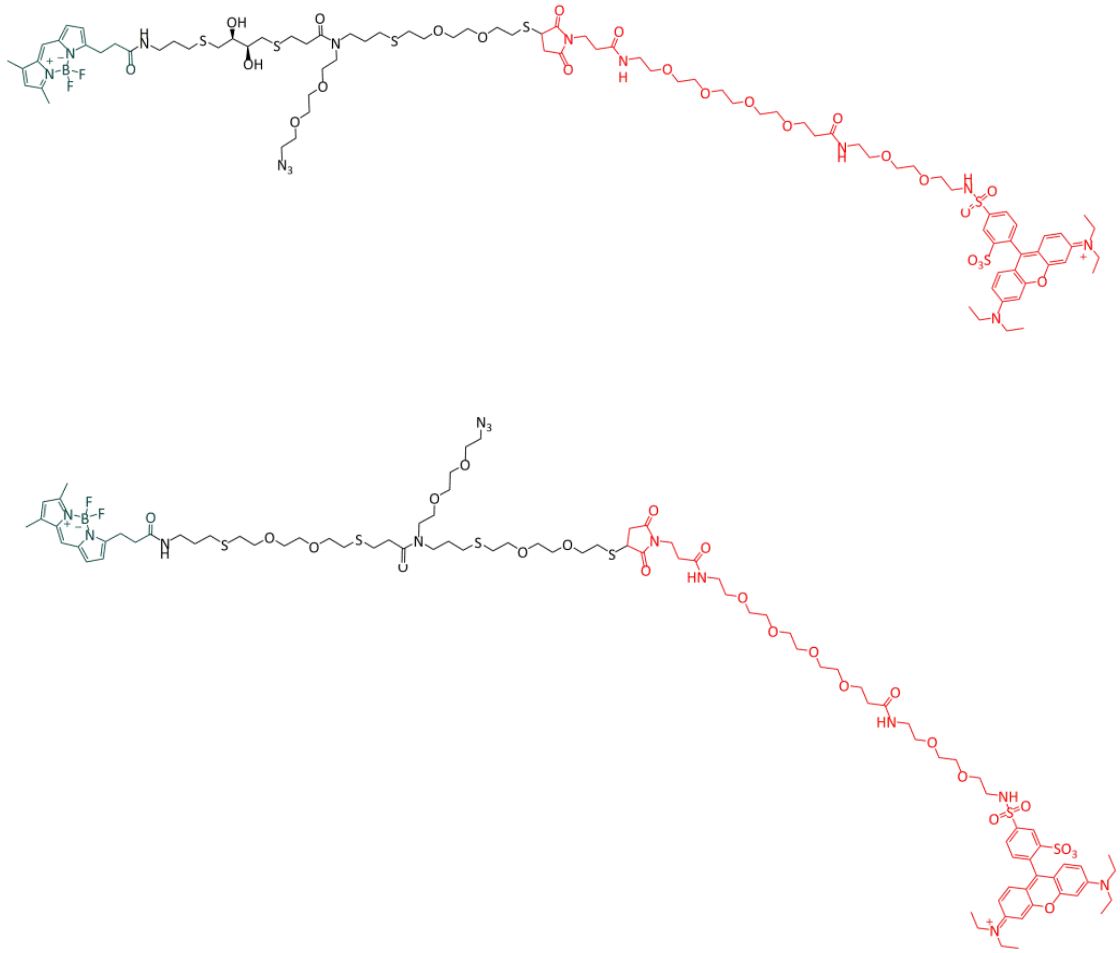

Figure 2.9. FRET cross-linker structures with rhodamine-PEG_6-maleimide. Rhodamine is incorporated through a noncleavable thioether linkage via a thiol-maleimide reaction with rhodamine-PEG_6-maleimide.

To attempt to improve the maleimide reaction, maleimide-functionalized rhodamine was synthesized with a PEG_6 spacer to improve solubility. This fluorophore was found to have 16 times higher solubility in DMSO relative to its non-pegylated counterpart. The reaction was originally carried out with 30% recovery (Figure 2.9). However, this result was found to not be reproducible and the reaction did not occur in subsequent reaction attempts. As such, the EDC coupling reaction was used instead and found to be more consistent.

Chapter 2 – APPENDIX

General Materials

Chemical reagents for synthesis: All chemicals were purchased from Sigma-Aldrich unless stated otherwise. The precursor for *N*-allylacrylamide azide monomer synthesis was purchased from PurePEG LLC. Sulfo rhodamine amidoethyl mercaptan was purchased from Toronto Research Chemicals. The precursor for BODIPY-NHS synthesis, (methyl-3-(2-pyrrolyl)propionate), was purchased from AstaTech, Inc. Materials for cell culture and biological assays were purchased from ThermoFisher Scientific. Fluorous BOC-ON (C_8F_{17} BOC-ON) and fluorous silica were purchased from Boron Specialties.

Reagents for cell culture, gel electrophoresis, and confocal microscopy: Dulbecco's Modified Eagle Medium (DMEM) was purchased from ThermoFisher Scientific containing L-glutamine, pyridoxine hydrochloride and without sodium pyruvate and sodium bicarbonate. Trypsin-EDTA (0.25%), Pen/Strep and fetal bovine serum (FBS) were purchased from ThermoFisher Scientific. HeLa cells were cultured in DMEM supplemented with 10% FBS and 1% Pen/Strep. 4-20% mini-PROTEAN® TGX™ precast protein gels and Coomassie Brilliant Blue R250 Staining Solution were purchased Bio-Rad Laboratories. Hoechst 33342 Solution was purchased from ThermoFisher Scientific.

General Methods

Nuclear Magnetic Resonance (NMR) spectroscopy: ^{1}H NMR spectra were recorded on an INOVA 400 MHz spectrometer. NMR data was analyzed by MestReNova software. ^{1}H NMR chemical shifts are reported in units of ppm relative to tetramethylsilane.

Liquid Chromatography Mass Spectroscopy (LC-MS): LC-MS experiments were carried out on an Agilent 1100 Series LC with a Poroshell 120 EC-C18 column (100 × 3 mm, 2.7 µm, Agilent Technologies) monitoring absorbance at 505 nm and 566 nm and an Agilent G1956B Series Single Quadripole MS in positive ion mode for mass detection. The mobile phase for LC-MS (solvent A) was water with 0.1% v/v acetic acid, and the stationary phase (solvent B) was acetonitrile with 0.1% v/v acetic acid. Compounds were eluted at a flow rate of 0.6 ml min^{-1} using a gradient of 5-100% solvent B (0-10 minutes) followed by 100% solvent B (10-12 minutes) and equilibrated back to 5% solvent B (12-15 minutes).

High Performance Liquid Chromatography (HPLC) Purification: HPLC purification was performed on an Agilent 1100 Series HPLC system equipped with a UV diode array detector and an 1100 Infinity fraction collector using a reversed-phase C18 column (9.4 x 250 mm, 5 µm). The mobile phase for HPLC was water with 0.1% v/v trifluoroacetic acid (solvent A) and acetonitrile with 0.1% v/v trifluoroacetic acid (solvent B). Compounds were eluted at a flow rate of 4 ml min^{-1} with a linear gradient of 5% to 100% solvent B (0-30 minutes), then 100% solvent B (30-40 min), and equilibrated back to 5% solvent B (40-45 minutes). OligoTEAs were collected based on their absorption at 230 nm. Fluorophore-conjugated oligomers were collected based on their absorption at 505 nm and 566 nm. The fractionated oligoTEAs and probes were transferred to microcentrifuge tubes, dried, and stored until further analysis.

High Performance Liquid Chromatography (HPLC) Analysis of FRET Conjugates: Conjugate purify and relative hydrophobicity were analyzed on an Agilent 1100 Series HPLC system equipped with a UV diode array detector and an 1100 Infinity fraction collector using a reversed-phase C18 column (4.6 x 150 mm, 5 µm). The mobile phase for HPLC was water with 0.1% v/v trifluoroacetic acid (solvent A) and acetonitrile with 0.1% v/v trifluoroacetic acid (solvent B). Compounds were eluted at a flow rate of 1 ml min^{-1} with a linear gradient of 5% to 100% solvent B (0-30 minutes), then 100% solvent B (30-35 min), and equilibrated back to 5% solvent B (35-40 minutes). Fluorophore-conjugated oligomers were monitored based on their absorption at 505 nm and 566 nm.

Flash Chromatography: Flash chromatography was performed on a Teledyne ISCO CombiFlash Rf-200i chromatography system equipped with UV-Vis and evaporative light scattering detectors (ELSD).

Fluorescent Gel Electrophoresis of Transferrin-oligoTEA FRET Probes: 2 µg of each of the transferrin probes (2.5 µM final concentration) were reacted either with 1 mM $NaIO_4$ for 30 minutes, 10 mM DTT for 30 minutes, or 1 mM $NaIO_4$ for 30 minutes followed by 10 mM DTT for 30 minutes. The samples were then denatured in the absence of reducing agent by boiling at 100 °C for 5 minutes. A 4-20% mini-PROTEAN® TGX™ precast protein gel was run for 60 minutes at 100V to separate the protein samples. Fluorescence imaging was performed using a GE Healthcare Typhoon 9400 image system set to a photomultiplier tube voltage of 400 with the following fluorescence settings: BODIPY excitation: 488 nm, emission: 500-540 nm; Rhodamine excitation: 561 nm, emission: 573-681 nm. FRET excitation: 488 nm, emission: 578-685 nm. Protein content was visualized using Coomassie Brilliant Blue

R250 Staining Solution according to the manufacturer's instructions and imaged using a Bio-Rad Molecular Imager® ChemiDoc™ XRS+ Imaging System.

Confocal Microscopy of Transferrin-oligoTEA FRET Probes: One day prior to the experiment, cells were plated into an 8-well chambered coverglass slide at 20,000 cells/well in DMEM with 10% FBS and 1% Pen/Strep. The next day, the media was removed, the cells were washed with PBS, and then incubated with 150 nM of the transferrin probes in DMEM with 10% FBS and 1% Pen/Strep for 4.5 hours. After incubation, the cells were washed with PBS. The washed cells were fixed with 4% w/v paraformaldehyde in PBS for 15 minutes at room temprature. The cells were then washed twice with PBS. The fixed cells were incubated with 2 uM Hoechst stain at room temperature for 15 minutes. The fixed and stained cells were washed with PBS, and then incubated in PBS for imaging. Confocal laser scanning microscopy was carried out on a Zeiss LSM710 confocal microscope with a 40x water objective. The green channel was set to excite at 488 nm and emit in the range 491-549 nm with a gain of 570 and 10% laser power. The red channel was set to excite at 561 nm and emit in the range 573-681 nm with a gain of 770 and 10% laser power. The magenta channel was set to excite at 488 nm and emit in the range 578-685 nm with a gain of 620 and 10% laser power. The blue channel was set to excite at 405 nm and emit in the range 415-482 nm with a gain of 800 and a laser power of 1.5%. The brightfield was set to a gain of 300. Gains were set such that a well with cells only did not show any fluorescence in the green, red, magenta, and blue channels. Mean fluorescence intensity for each channel was quantifed for 10 representative cells. Relative bond cleavage of each probe was assessed by dividing the mean fluorescence intensity of the green channel by that of the red channel for each cell. Post-image processing was

performed using Fiji software. Statistical significance was evaluated using One-Way ANOVA (and Nonparametric) analysis in GraphPad Prism 7.0.

Oligothioetheramide Synthesis

Synthesis of fluorous carbamate protected allylamine: 2-[2-(1H,1H,2H,2H-Perfluoro-9-methyldecyl)isopropoxycarbonyloxyimino]-2phenylacetonitrile (fluorous BOC-ON) was dissolved in tetrahydrofuran (THF). To this solution, 1.8 equiv of allylamine and 1.7 equiv of triethylamine (Et_3N) were added. The reaction mixture was stirred at room temperature for 3 hours. The solvent was removed under reduced pressure and the reaction was purified by fluorous solid phase extraction (FSPE), using a fluorophobic wash of 20% water in methanol followed by a fluorophilic wash of 100% methanol. Methanol was evaporated under reduced pressure to yield the fluorous carbamate protected allylamine as a white solid product. The product was characterized by ^1H NMR. ^1H NMR (400 MHz, $CDCl_3$) δ 5.89-5.77 (m, 1H), 5.19-5.08 (m, 2H), 4.66-4.58 (m, 1H), 3.74 (s, 2H), 2.20-2.05 (m, 2H), 2.05-1.95 (m, 2H), 1.48 (s, 6H).

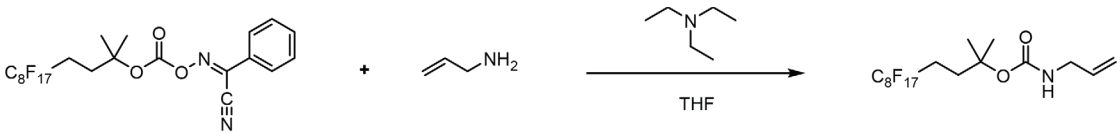

Figure A2.1. Synthesis of fluorous carbamate protected allylamine.

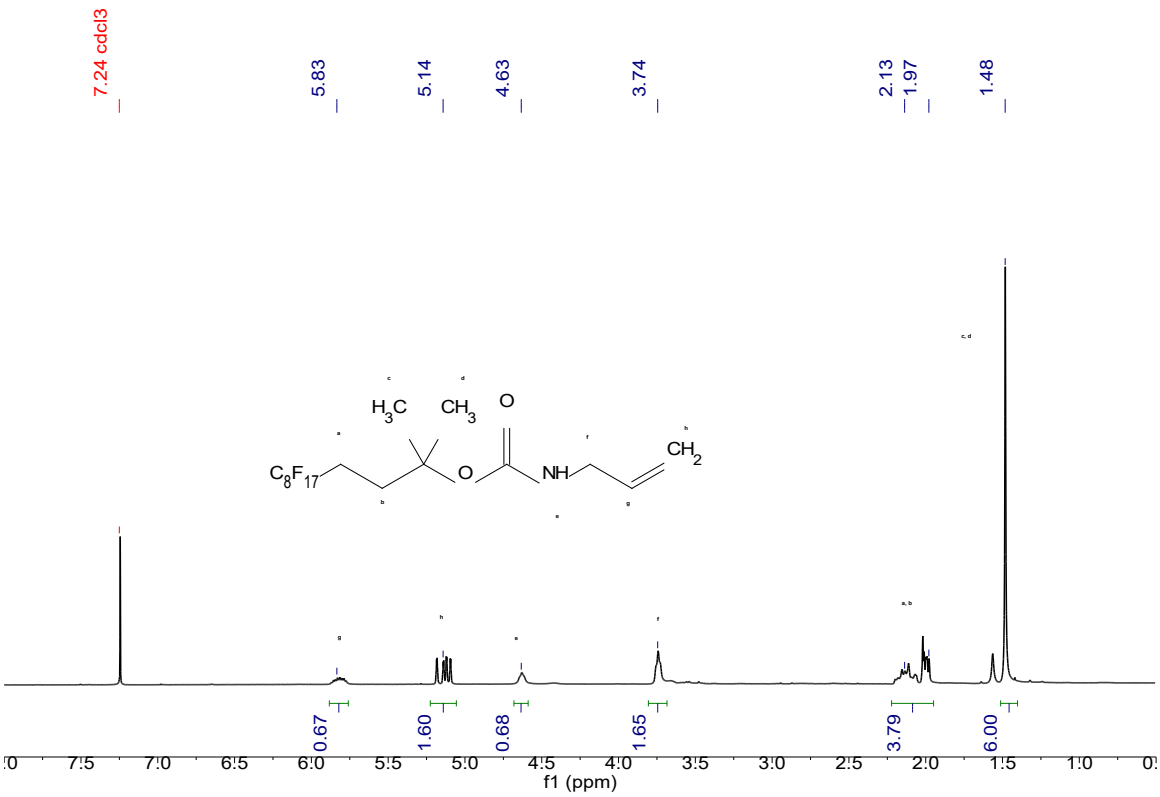

Figure A2.2 ^{1}H NMR (400 MHz, $CDCl_3$) of fluorous carbamate protected allylamine.

Thiol-ene reaction (general conditions): 1 equiv of fluorous-allyl was mixed with 5 equiv of dithiol and 0.25 equiv 2,2-dimethoxy-2-phenylacetophenone (DMPA) at a final concentration of 325 mM in methanol. The mixture was subjected to UV irradiation at 20 mW/cm^2 for 270 s. The product was purified by FSPE, and the methanol was evaporated under reduced pressure to yield the fluorous-thiol product.

Thiol-Michael addition (general conditions): 1 equiv of fluorous-thiol was mixed with 2 equiv of N-allylacrylamide monomer and 0.1 equiv dimethylphenylphosphine (DMPP) at a final concentration of 325 mM in methanol. The mixture was allowed to react until all thiol was consumed, as monitored by the dithiodipyridine (DTDP) assay. The product was purified by FSPE, and the methanol was evaporated under reduced pressure to yield the fluorous-allyl product.

OligoTEA capping with 2,2'-dipyridyl disulfide: 1 equiv of fluorous-thiol was mixed with 5 equiv of 2,2-dipyridyl disulfide and 2 equiv of Et_3N at a final concentration of 225 mM for 2 hours. The product was purified by FSPE, and the methanol was evaporated under reduced pressure to yield the fluorous-pyridyl disulfide product.

Fluorous tag deprotection: Fluorous oligoTEA was mixed at 5 mM in 50% TFA in DCM for 3 hours. The TFA and DCM were then removed under vacuum, and the product was purified by RP-HPLC.

Synthesis of N-[2-[2-(2-azidoethoxy)ethoxy]ethyl]-2-propenamide: 1 equiv of 2-[2-(2-azidoethoxy)ethoxy]-ethanamine (1 g, 5.74 mmol) was dissolved at 150 mM in dichloromethane (DCM). To the solution was added 1.1 equiv of Et_3N (639 mg, 6.31 mmol),and the mixture was allowed to equilibrate for 10 minutes on ice. Next, 1.2 equiv acryloyl chloride (623 mg, 6.89 mmol) dissolved at 1.66 M in DCM was added dropwise for 1 hour. The final concentration of 2-[2-(2-azidoethoxy)ethoxy]-ethanamine was 132 mM. The mixture was left on ice for 1 hour and then removed from the ice and reacted at room temperature for 1 hour. The reaction was quenched with 6 mL of water and extracted with DCM (80 mL, 3x). The DCM layer was collected and concentrated under vacuum. The crude product was used without further purification.

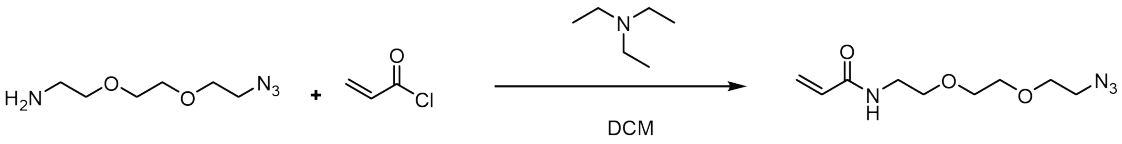

Figure A2.3. Synthesis of *N*-[2-[2-(2-azidoethoxy)ethoxy]ethyl]-2-propenamide.

*Synthesis of **(3)***: 1 equiv of *N*-[2-[2-(2-azidoethoxy)ethoxy]ethyl]-2-propenamide (1.31 g, 5.74 mmol) was dissolved at 378 mM in anhydrous DMF and added to a 246 mM solution of 1.3 equiv NaH (179 mg, 7.46 mmol) in anhydrous DMF. The mixture was allowed to equilibrate for 10 minutes at room temperature. Then, 2.5 equiv of allyl bromide (1.74 g, 14.3 mmol) was added slowly to the reaction mixture over 5 minutes. The mixture was then allowed to react for 1 hour at room temperature. The reaction was quenched with 8 ml of water and extracted with diethyl ether (3x, 70 mL). The organic layer was collected and concentrated under vacuum. The product was purified by flash chromatography (12 g silica, 0-5% MeOH in DCM) in 20% yield. The product was characterized by ^{1}H NMR. ^{1}H NMR (400 MHz, $CDCl_3$) δ 6.72-6.28 (m, 2H), 5.85-5.72 (m, 1H), 5.70-5.60 (m, 1H), 5.22-5.08 (m, 2H), 4.10-4.04 (m, 2H), 3.70-3.45 (m, 10H), 3.40-3.31, (t, J = 5.1 Hz, 2H).

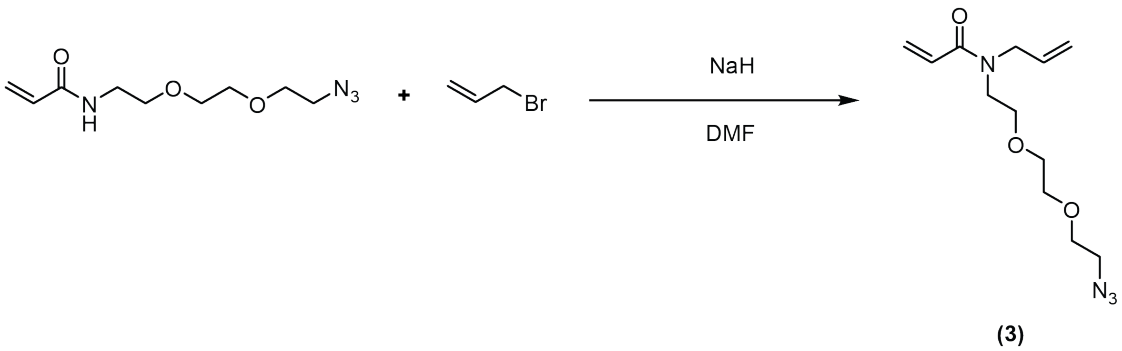

(3)

Figure A2.4. Synthesis of compound **(3)**.

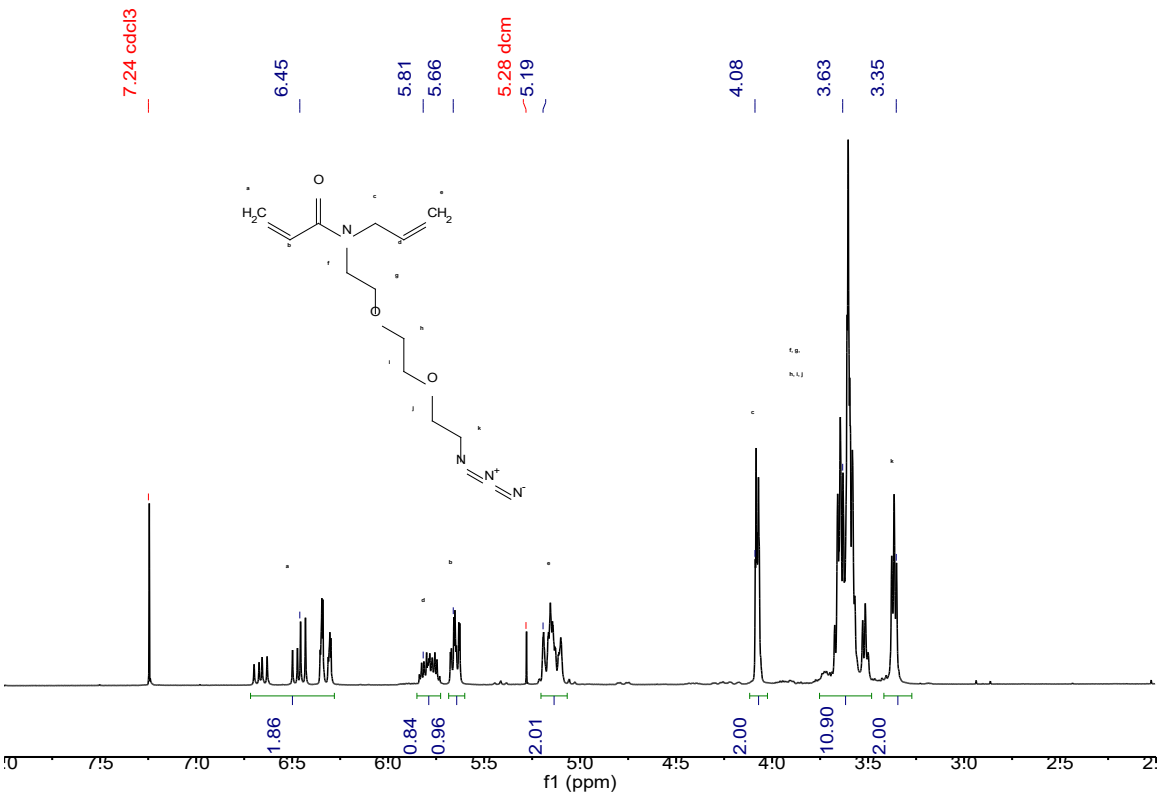

Figure A2.5 ^{1}H NMR (400 MHz, $CDCl_3$) of compound **(3)**.

Fluorophore Synthesis

*Synthesis of **(4)***: 1 equiv of 2,2'-(ethylenedioxy)bis(ethylamine) (257 mg, 1.73 mmol) was dissolved at 550 mM in DCM. To this solution was added 0.2 equiv of Et_3N (35 mg, 0.347 mmol) and 0.015 equiv of 4-dimethylaminopyridine (3.2 mg, 0.026 mmol). The mixture was allowed to equilibrate for 10 minutes at 0 °C in an ice bath. 0.1 equiv of sulforhodamine sulfonyl chloride (100 mg, 0.173 mmol) was then added over 2 hours to the solution. The mixture was removed from the ice bath and allowed to stir at room temperature overnight. The mixture was concentrated under vacuum and purified via semi-preparative RP-HPLC. The product was characterized by LC-MS (*m/z* calculated: 689.27 observed: 689.10 $[M+H]^+$).

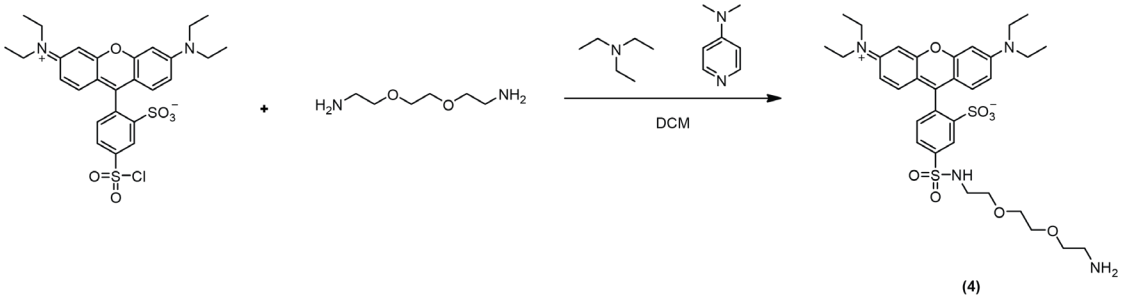

Figure A2.6. Synthesis of compound **(4)**

*Synthesis of **(5)***: 1 equiv of methyl-3-(2-pyrrolyl)propionate (2.71 mmol, 415 mg) and 1.1 equiv 3,5-dimethyl-1H-pyrrole-2-carbaldehyde (2.98 mmol, 367 mg) were dissolved in dry DCM (25 mL) under argon. The mixture was cooled to 0 °C in an ice bath, and 1.1 equiv of phosphorus oxychloride (2.98 mmol, 279 µL) diluted in DCM (2.06 mL) were added dropwise. The reaction was stirred for 30 minutes at 0 °C and then for 6 hours at room temperature. The black solution was cooled to 0 °C and then diisopropylethylamine (16.8 mmol 2.93 mL) and boron trifluoride diethyl etherate (16.26 mmol, 2.04 mL) were added dropwise. The mixture was stirred for 14 hours at room temperature. The reaction was then quenched with water (40mL). The mixture was filtered through Celite and washed with DCM (200mL). The aqueous layer was extracted with DCM (3 x 75 mL). All organic layers were collected, concentrated, and purified by flash chromatography (40 g silica, isocratic gradient, 100% DCM) to yield the red crystalline solid **(5)** in 53% yield.

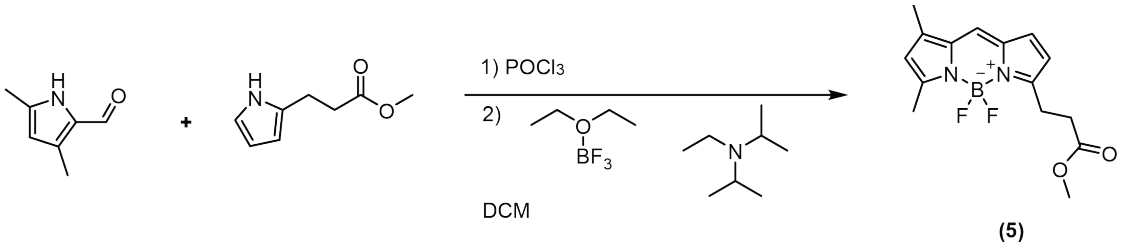

Figure A2.7. Synthesis of compound **(5)**.

Synthesis of (6): The synthesis of **(6)** was completed as previously described with minor modifications. 1 equiv of compound **(5)** (1.43 mmol, 439 mg) was dissolved in THF (65.9 mL) and water (43.9 mL). Concentrated 12N HCl was then added (26.3 mL) to hydrolyze the methyl ester to the carboxylic acid. The reaction was stirred for 36 hours at room temperature. The reaction was diluted with DCM (160 mL) and washed with brine (70 mL). The organic layers were concentrated and quickly purified by flash chromatography (80 g silica, 0-10% MeOH in DCM) to yield **(6)** in 35% yield.

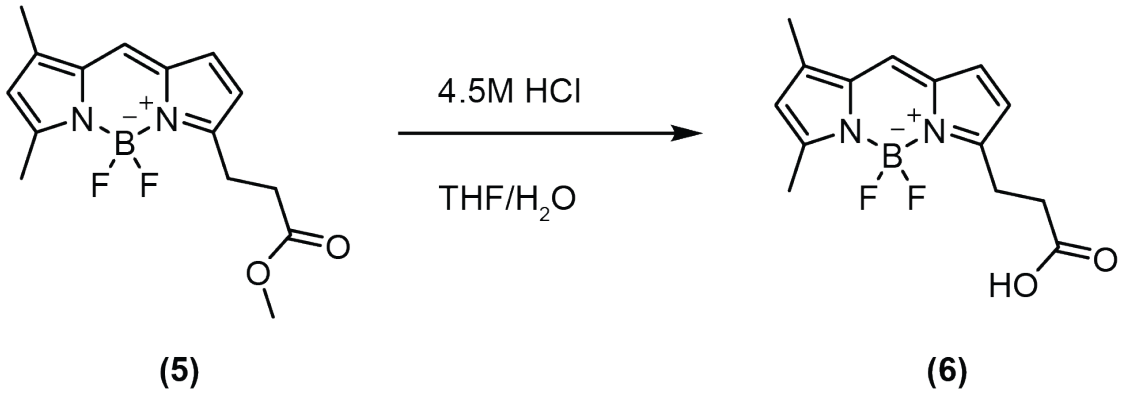

(5) **(6)**

Figure A2.8. Synthesis of compound **(6)**.

*Synthesis of **(7)***: 1 equiv of compound **(6)** (0.311 mmol, 90mg) was dissolved into toluene (10 mL) and 2 equiv of N-hydroxysuccinimide (0.621 mmol 71.5 mg), 2 equiv of dicyclohexylcarbodimide (0.621 mmol, 128.1 mg), and 2 equiv of Et_3N (0.621 mmol, 86.6 uL) were added. The solution was stirred overnight, and centrifuged to remove the isourea byproduct of the dicyclohexylcarbodimide activation of the carboxylic acid. The solids were washed with DCM (3 x 3mL) and the resulting organic solution was concentrated. TLC showed compound **(7)** at an R_f of 0.8 in 5% MeOH in DCM, and two-dimensional TLC demonstrated the degradation of the NHS ester to the acid. Thus, the mixture was purified quickly by flash chromatography (40 g silica, 50-100% ethyl acetate in hexanes in 3.5 minutes and 0-5% MeOH in DCM in 6 minutes) to provide compound **(7)** (0.0653 mmol, 25 mg) in 21% yield. The product was characterized by ^{1}H NMR and LC-MS (*m/z* calculated: 390.15 observed: 390.20 $[M+H]^+$). ^{1}H NMR (400 MHz, $CDCl_3$) δ 7.08 (s, 1H), 6.87 (d, J = 3.9 Hz, 1H), 6.31 (d, J = 3.9 Hz, 1H), 6.11 (s, 1H), 3.36 (t, J = 7.4 Hz, 2H), 3.06 (t, J = 7.4 Hz, 2H), 2.82 (br, 4H), 2.55 (s, 1H), 2.23 (s, 1H).

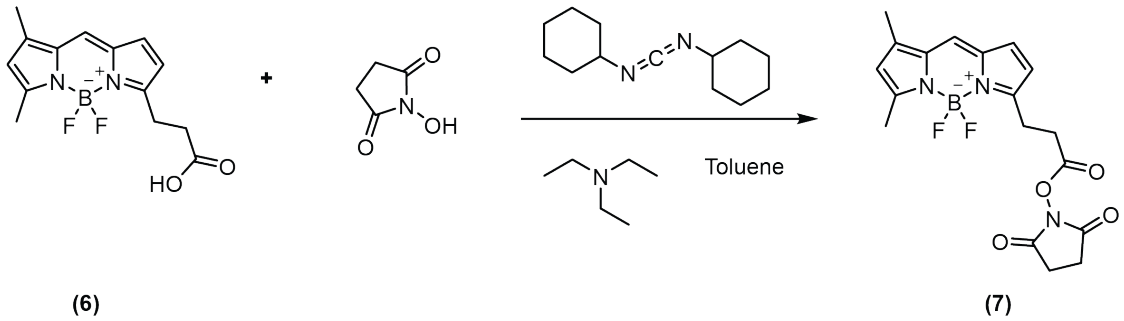

(6) **(7)**

Figure A2.9. Synthesis of compound **(7)**.

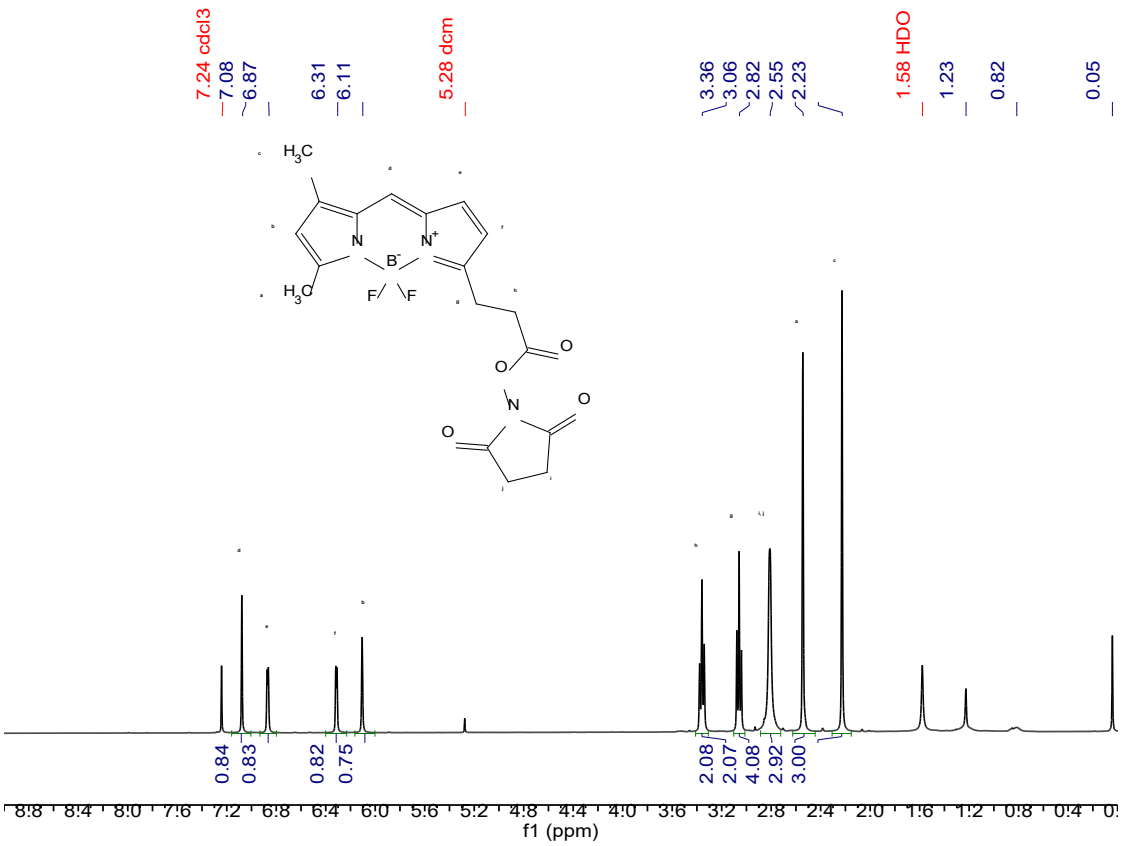

Figure A2.10 ^{1}H NMR (400 MHz, $CDCl_3$) of compound **(7)**.

Fluorophore Conjugation

Synthesis of Probe 1c-c and Probe 1n-c:

Step 1 (Rhodamine Conjugation): 2 equiv of **(1)** were dissolved at 10 mg/mL in dry DMF. To this solution, 1 equiv of sulfo rhodamine amidoethyl mercaptan (0.3 mg/mL in dry DMF) and 15 equiv of Et_3N were added. The final concentration of linker **(1)** was 121 μM. The reaction mixture was stirred overnight, and then purified via semi-preparative RP-HPLC.

Step 2 (BODIPY Conjugation): 1 equiv of **(8)** was dissolved at 10 mg/mL in DMSO. To this solution, 2.25 equiv of compound **(7)** (6 mg/mL in DMSO) and 20 equiv of Et_3N were added. The final concentration of **(5)** was 4.9 mM. The mixture was reacted overnight at room temperature and then purified via semi-preparative RP-HPLC. The product was characterized by LC-MS (Probe 1c-c *m/z* calculated: 1551.54, observed: 1551.50 $[M+H]^+$; Probe 1n-c *m/z* calculated: 1579.57, observed: 1579.49 $[M+H]^+$).

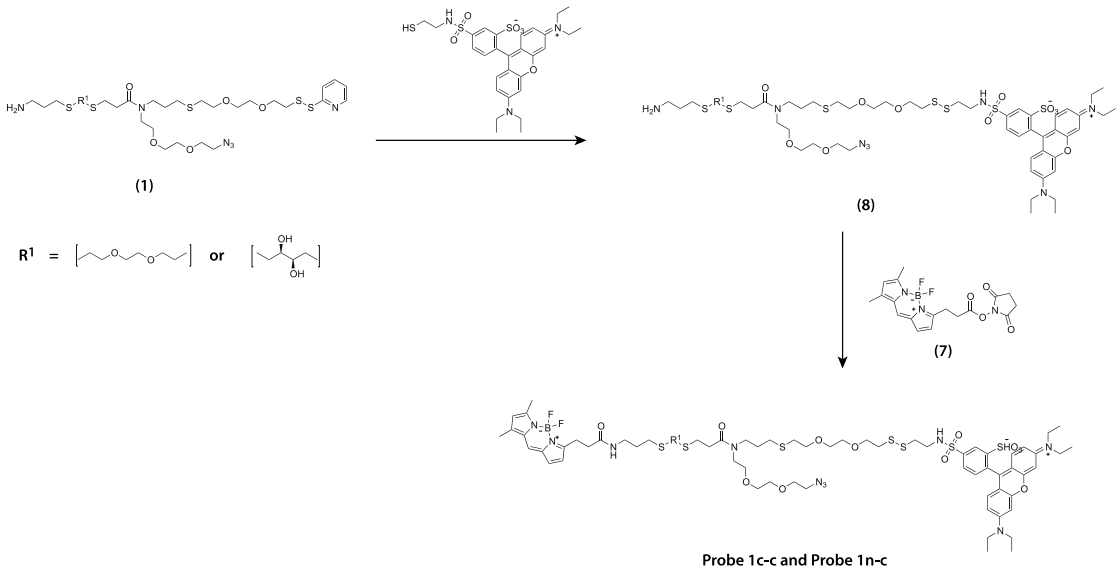

Figure A2.11 Synthesis of Probe 1c-c and Probe 1n-c.

Synthesis of Probe 2c-n and Probe 2n-n:

Step 1 (BODIPY Conjugation): 1 equiv of **(2)** was dissolved at 10 mg/mL in DMSO. To this solution, 2.25 equiv of compound **(7)** (6 mg/mL in DMSO) and 20 equiv of Et_3N were added. The final concentration of the oligoTEA was 4.9 mM. The mixture was reacted overnight at room temperature and then purified via semi-preparative RP-HPLC.

Step 2 (Rhodamine Conjugation): 1 equiv of **(9)** was dissolved at 16 mg/mL in dry DMSO. To the solution was added 5 equiv of 1-ethyl-3-(3-dimethylaminopropyl)carbodiimide (50 mg/mL in dry DMSO), 10 equiv of N-hydroxysuccinimide (100 mg/mL in DMSO), 3 equiv of compound **(4)** (10 mg/mL in DMSO) and 20 equiv of Et_3N. The final concentration of the **(9)** was 3.4 mM. The mixture was reacted overnight at room temperature, and then purified via semi-preparative RP-HPLC. The probes were then characterized by LC-MS (Probe 2c-n *m/z* calculated: 1516.58, observed: 1516.49 $[M+H]^+$; Probe 2n-n *m/z* calculated: 1544.62, observed: 1544.50 $[M+H]^+$).

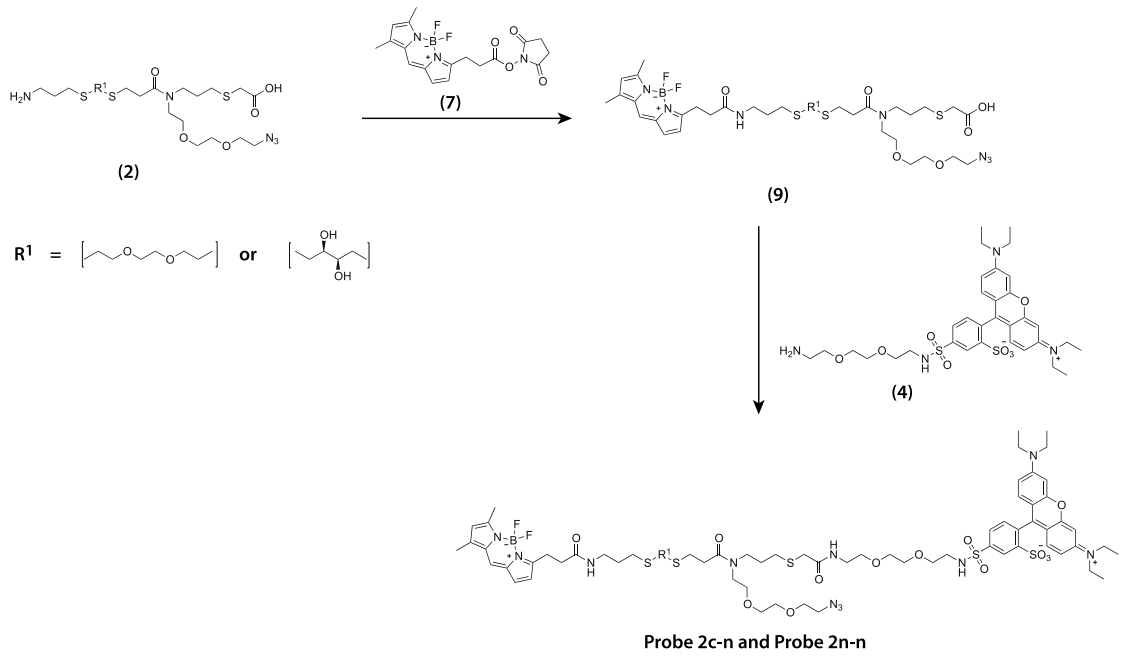

Figure A2.12 Synthesis of Probe 2c-n and Probe 2n-n.

Characterization of Probe Fragments

LC-MS Assay (SIM) to Detect Linker Cleavage: 100 μM of linker was reacted with 1 mM $NaIO_4$ or 2.5 μM linker was reacted with 10 mM DTT in PBS at pH 7.4 for 1 hour. The mixture was then processed with a 10 μL ZipTip® C18 following the manufacturer's protocol to remove excess $NaIO_4$/DTT. The mixture was then injected into the LC-MS to search for ions corresponding to the masses of the expected fragments (Figure 1C and 1D). Figure 2A.13 below shows the reaction scheme and fragments observed for Probe 1c-c after reaction with $NaIO_4$. One peak was observed in the LC-MS SIM corresponding to the singly oxidized BODIPY hydrate. Two peaks were observed in the LC-MS SIM corresponding to the doubly oxidized rhodamine aldehyde (two of the three possible structures shown in Figure 2A.13). The equivalent oxidation products were observed for the reaction of Probe 2c-n with $NaIO_4$ as expected.

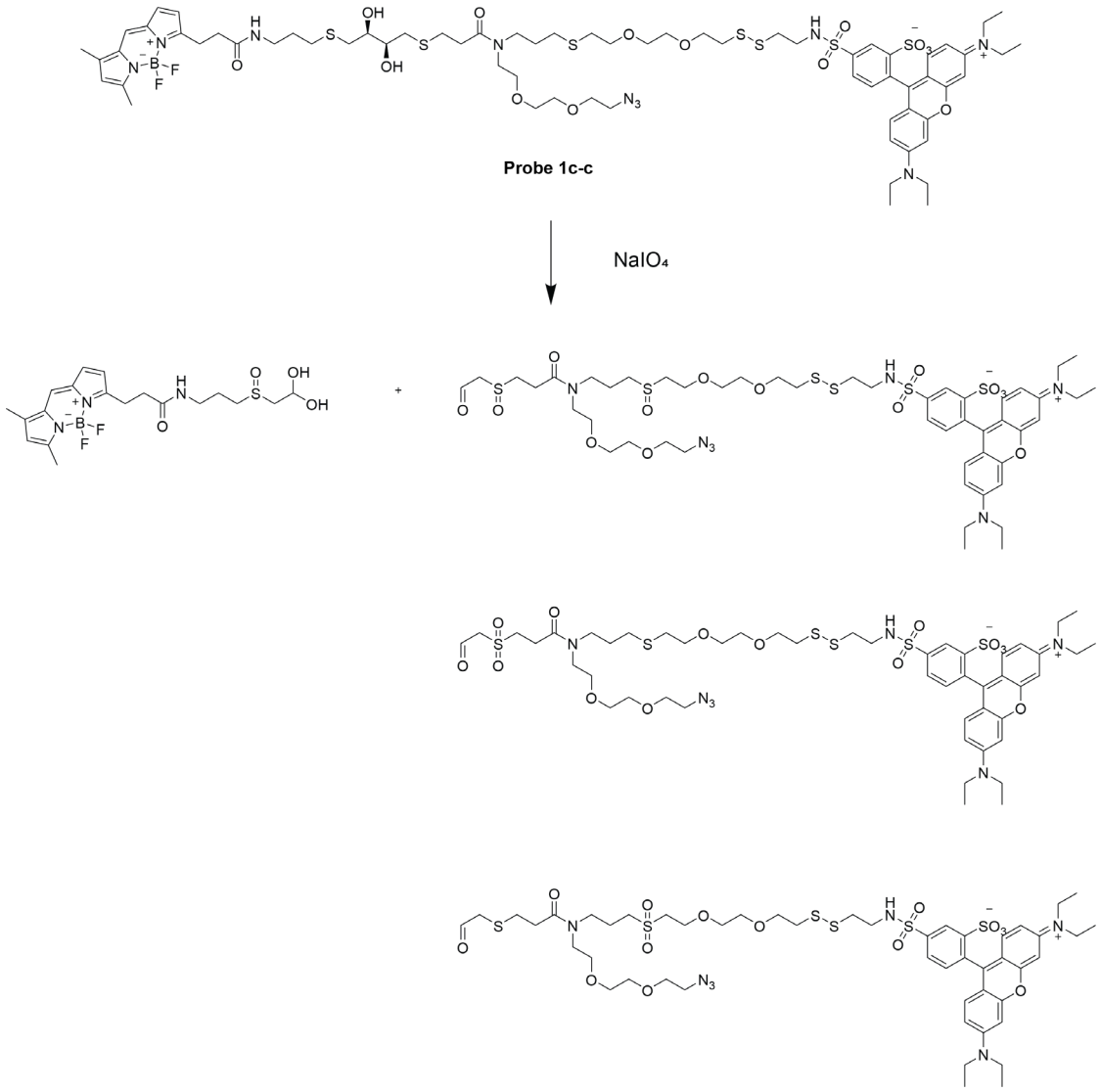

Figure A2.13. Reaction scheme for treatment of Probe 1c-c with $NaIO_4$.

Protein Conjugation

Synthesis of transferrin-DBCO: 1 equiv of human holo-transferrin was reacted with 7 equiv of DBCO-PEG_4-NHS (50 mg/mL in DMSO) in borate-buffered saline (100 mM borate, 150 mM NaCl) pH 8.2 for 5.5 hours. The final concentration of transferrin was 250 μM. The mixture was then dialyzed overnight against ultrapure water in a Slide-A-Lyzer™ MINI Dialysis Device, 3.5K MWCO.

Conjugation of transferrin-DBCO to probes: 1 equiv of transferrin-DBCO (160 μM in ultrapure water) was reacted with 2 equiv of probe (1 mg/mL in DMSO) in PBS pH 7.4 for 24 hours. The mixture was then dialyzed for 5 hours against ultrapure water in a Slide-A-Lyzer™ MINI Dialysis Device, 3.5K MWCO.

MALDI analysis of transferrin conjugates was performed by the MIT Biopolymers Laboratory using a sinapinic acid matrix. MALDI traces confirm modification of transferrin with DBCO groups followed by conjugation to Probe 1c-c. The *m/z* maximum for transferrin was observed to be 79,390 Da. The m/z maximum for the DBCO-modified transferrin (Tf-DBCO) was found to be 80,626 Da. The mass of DBCO-PEG_4-NHS after removal of the N-hydroxysuccinimide ester is 534.59 Da, thus indicating that the transferrin was modified with approximately 2 DBCO groups. The observed mass of the probe-modified conjugate (Tf-Probe 1c-c) was observed to be 82,344 Da. The mass of Probe 1c-c is 1550.53 Da, indicating that the protein was modified on average with approximately 1 probe.

Chapter 2 – REFERENCES

1.Porel, M. & Alabi, C. A. Sequence-defined polymers via orthogonal allyl acrylamide building blocks. *Journal of the American Chemical Society* **136,** 13162–13165 (2014).

2.Alabi, C., Porel, M. & Brown, J. Sequence-Defined Oligothioetheramides. *Synlett* **26,** 565 (2015).

3.Porel, M., Thornlow, D. N., Phan, N. N. & Alabi, C. A. Sequence-defined bioactive macrocycles via an acid-catalysed cascade reaction. *Nature Chemistry* **8,** 590–596 (2016).

4.Porel, M., Thornlow, D. N., Artim, C. M. & Alabi, C. A. Sequence-Defined Backbone Modifications Regulate Antibacterial Activity of OligoTEAs. *ACS Chem Biol* **12,** 715–723 (2017).

5.Qian, Z. M., Li, H., Sun, H. & Ho, K. Targeted drug delivery via the transferrin receptor-mediated endocytosis pathway. *Pharmacol Rev* **54,** 561–587 (2002).

6.Daniels, T. R., Delgado, T., Helguera, G. & Penichet, M. L. The transferrin receptor part II: targeted delivery of therapeutic agents into cancer cells. *Clin Immunol* **121,** 159–176 (2006).

Chapter 3 – REPSONSIVE ANTIBODY CONJUGATES ENABLE QUANTITATIVE DETERMINATION OF INTRACELLULAR BOND DEGRADATION RATE

3.1. INTRODUCTION

To ensure stability in the extracellular milieu and release at the desired intracellular site, a variety of nanoparticle[1] and conjugate-based[2] drug delivery systems have been designed to respond to intracellular stimuli such as pH gradients, reducing environments, and enzymatic activity. Drug payloads have been conjugated to nanoparticles through acid-labile ester[3] and hydrazone[4] linkages as well as reduction-sensitive disulfide bonds.[5] Cleavage of these bonds triggers release of the active drug. For example, CRLX101, a polymeric nanoparticle currently in clinical trials, is comprised of a linear co-polymer backbone incorporating repeating units of cyclodextrin and polyethylene glycol (PEG) blocks.[3] The active drug, camptotechin, is conjugated to the nanoparticle through ester linkages. Hydrolysis of these ester bonds via endosomal pH gradients or intracellular enzymatic activity leads to disassembly of the nanoparticle and subsequent release of camptotechin. Another example is a recently developed nanoparticle conjugate in which the antimitotic agent monomethyl auristatin E (MMAE) is conjugated through disulfide bonds that can be reduced by the high intracellular concentration of glutathione (GSH) found within tumor cells.[6]

In antibody-drug conjugates (ADCs), cytotoxic payloads are attached to monoclonal antibodies through a chemical cross-linker. Cleavable bonds have been incorporated into these chemical cross-linkers to spatiotemporally control the release of drug payload inside the target cell. A variety of cleavable chemistries have been explored for use in ADCs including hydrazone, disulfide, and dipeptide bonds.[2] This cleavage event is critical for ADCs that contain drugs that must be delivered in an unmodified form to be biologically active.[7,8] One of the four ADCs currently on the market, brentuximab vedotin (trade name Adcetris), is composed of an enzymatically

labile, dipeptide linker.[9] A reduction-sensitive disulfide linker has been employed in the ADC IGMN 779 which is currently in clinical trials.[10]

With several promising stimuli-responsive drug delivery systems en route to clinical trials, there is a need to develop methods to quantitatively study their intracellular processing and assess the amount of active payload in the cell. Recently, Maass et al. developed a model to describe the non-specific degradation of ADCs.[11] This model describes intracellular release as mediated by non-specific proteolytic degradation within the lysosomal compartment. While there are ADCs that rely on non-specific degradation,[12,13] a growing number of ADCs utilize specific cleavage chemistries for drug release.[10,14]

The kinetics of bond cleavage is dependent not only on the nature of the cleavable bond, but also on the transient composition of the intracellular environment. At any given time, the type and concentrations of hydrogen ions, enzymes, proteases, and small-molecule reducing agents will vary thus making it difficult to mimic the endocytic compartment in a cell-free well plate assay. Therefore, we sought to develop a method to quantify the intracellular degradation rate of stimuli responsive bonds in a pathway- and cell type-dependent fashion. To this end, we designed a novel, fluorescence-based antibody conjugate probe and developed a model based on mass-action kinetics to describe its intracellular processing. This model was developed in conjunction with live-cell experiments to extract the rate of intracellular bond degradation. In this work, disulfide bond degradation was quantified in SK-BR-3 cells using the HER2 receptor endocytic pathway. The analysis described herein can be performed as a function of bond type, endocytosis pathway, and cell type. In this way, intracellular bond degradation will emerge as a new fundamental parameter to

understand the intracellular processing of stimuli-responsive drug carriers and enable the rational design of new drug delivery systems.

3.2. RESULTS AND DISCUSSION

Design, Synthesis, and Purification of FRET-based Antibody Probes

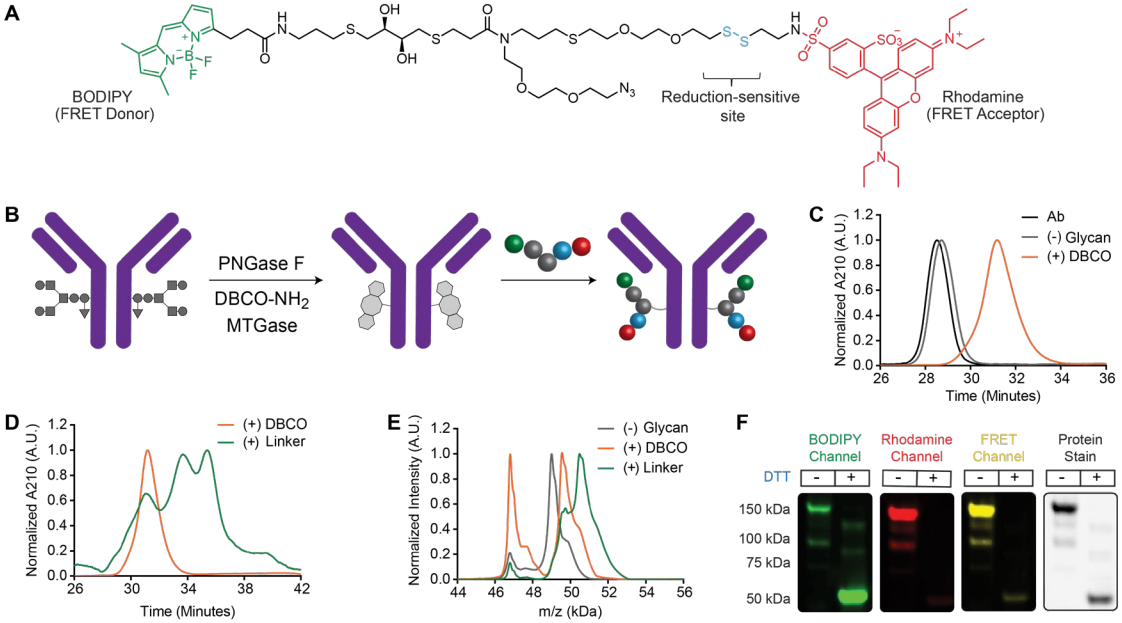

Figure 3.1. Characterization of cleavable probe. A) Chemical structure of Cleavable Cross-linker. B) Schematic of site-specific modification of trastuzumab via microbial transglutaminase. A) HIC characterization indicating modification of trastuzumab with 2 DBCO groups B) HIC characterization of Cleavable Probe. C) MALDI data indicating incorporation of DBCO groups and Cleavable Cross-linker on trastuzumab heavy chain. D) Fluorescent gel electrophoresis showing reduction of the Cleavable Probe by the reducing agent DTT.

To quantify intracellular bond cleavage, we adopted a recently developed reduction sensitive FRET-based cross-linker that can be readily conjugated, via “click” chemistry, to a variety of targeting ligands (Figure 3.1A).[15] This cross-linker was designed and synthesized as described in Chapter 2. In the FRET-labeled cross-linker, the fluorescence emission of BODIPY (FRET donor, Ex/Em: 505/516 nm) is efficiently quenched by rhodamine (FRET acceptor, Ex/Em: 566/586 nm). When the disulfide bond within the cross-linker is cleaved, BODIPY regains its fluorescence emission.

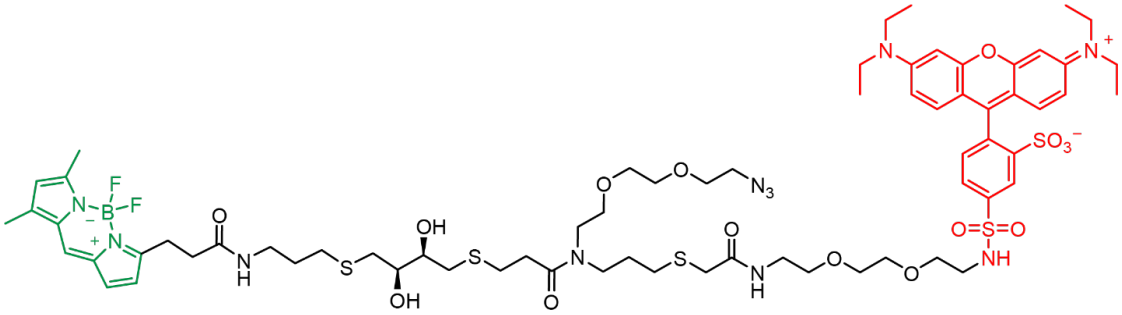

Figure 3.2. Chemical structure of control cross-linker containing stable sulfonamide bond.

The resulting FRET cross-linker will henceforth be referred to as the Cleavable Cross-linker (Figure 3.1A). A Control Cross-linker in which the disulfide bond was replaced with an amide bond was synthesized as a noncleavable control (Figure 3.2).

HER2 (human epidermal growth factor receptor 2) was chosen as the target receptor for this study due to its therapeutic relevance.[16,17] HER2 is a membrane tyrosine kinase which has been found to be overexpressed on 20-30% of breast cancer cells.[18-20] Trastuzumab is a humanized monoclonal antibody against the HER2 receptor.[21] Trastuzumab has been used alone as a therapeutic (known by the trade name Herceptin) as well as in an FDA approved antibody-drug conjugate, Kadcyla.

In the area of ADCs, there has been an increasing push towards site-specific modification of antibodies to increase homogeneity and stability.[2] As such, site-specific labeling strategies were adapted for this work. Trastuzumab probes were synthesized using the transglutaminase-based chemo-enzymatic method for site-specific antibody modification.[22,23] In this method, first, the *N*-linked glycans on the antibody are enzymatically removed by Peptide-N-Glycosidase F (PNGase F). Next, the exposed glutamine residues (Q295 within the IgG heavy chain) are reacted with an amine-bearing substrate using microbial transglutaminase (MTGase) to catalyze the formation

of a Gln-Lys isopeptide bond (Figure 3.1B). This set of reactions yields an antibody modified site-specifically with two of these substrates on the heavy chain. In this work, the transglutaminase-based method was used to modify trastuzumab site-specifically with two strained dibenzocylooctyne (DBCO) functionalities. The DBCO-modified antibody was purified via a protein A/G column. The DBCO groups were then reacted with the azide functionality on each cross-linker through copper-free “click” chemistry (Figure 3.1B). The final trastuzumab probe was purified using dialysis to remove excess FRET cross-linker.

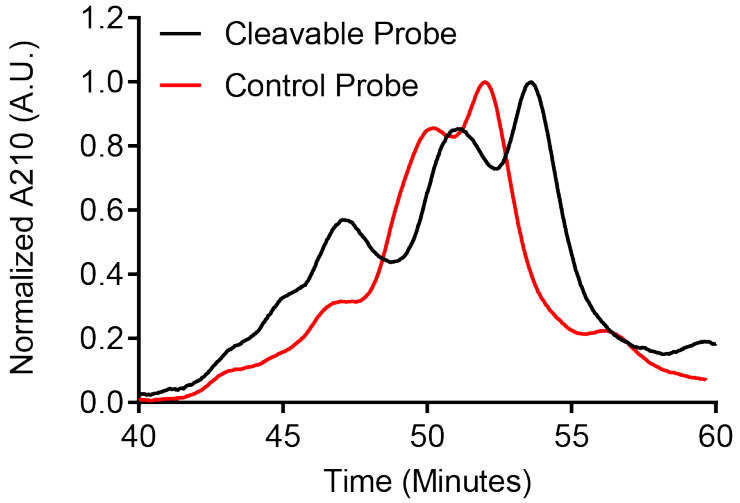

Figure 3.3. HIC characterization comparison of cleavable probe and control probe. By area under the curve estimates, the degree of labelling for both probes is approximately 1.3 FRET cross-linkers per antibody.

Synthesis of the probe was monitored via hydrophobic interaction chromatography (HIC). A slight hydrophobic shift is observed when the glycans are removed from the antibody (Figure 3.1C). Next, a large hydrophobic shift from the antibody without the glycan is observed following modification with an amino-DBCO substrate, indicating complete incorporation of DBCO groups. Following conjugation of this DBCO-trastuzumab conjugate with the Cleavable Probe, the HIC trace shows a

mixture composed of 0, 1, and 2 cross-linkers per antibody (Figure 3.1D). The area under the curve was measured for each peak and weighted by its corresponding cross-linker labeling to give an approximate degree of labeling of 1.3 probes per antibody. The Control Probe was also characterized by HIC and found to have a similar degree of labeling (Figure 3.3).

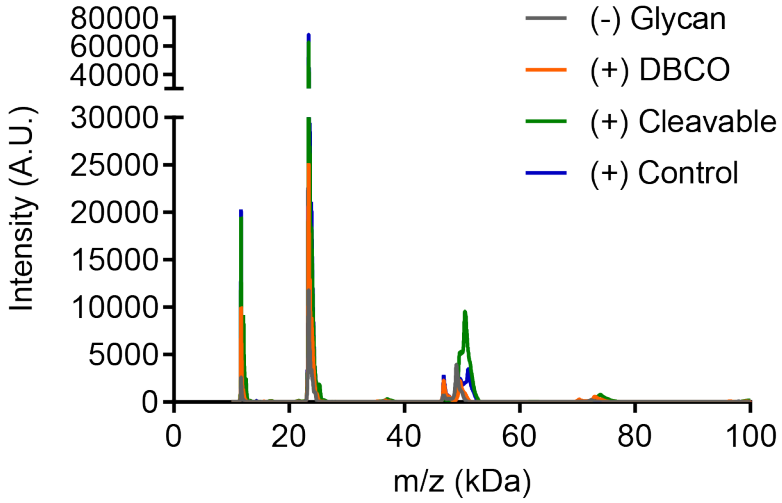

	Observed m/z (Da)	Expected m/z (Da)
(-) Glycan	49021.19	
(+) DBCO	49610.72	49544.46
(+) Cleavable	50544.54	50479.84
(+) Control	51083.18	51060.04

Figure 3.4. MALDI analysis of conjugates. Full MALDI spectra of trastuzumab conjugates (Top) and expected and observed masses (Bottom).

Additionally, MALDI-MS was used to confirm the expected increase in the molecular weight of the IgG heavy chain (Figure 3.1E and Figure 3.4). The peak that appears at 46.8 kDa in the MALDI spectrum corresponds to the double mass of the light chain and remains constant for each conjugate (full spectra in Figure 3.4).

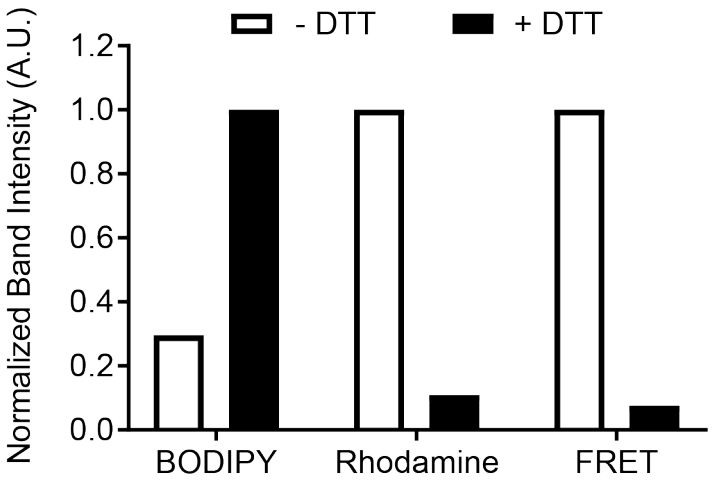

Figure 3.5. Quantification of fluorescence band intensity in gel of cleavable probe.

A fluorescent gel shift assay was used to demonstrate selective cleavage of the disulfide bond within the probe (Figure 3.1F). Trastuzumab probes were treated with the reducing agent dithiothreitol (DTT) at room temperature for 1 hour. Fluorescence was measured for BODIPY excitation/emission, rhodamine excitation/emission, and BODIPY excitation/rhodamine emission (i.e. the FRET). When the FRET probes were intact, fluorescence bands were visualized for BODIPY emission (green), rhodamine emission (red) and FRET emission (yellow). The BODIPY emission was relatively low due to quenching by the rhodamine dye. Coomassie blue protein stain confirmed equal loading between lanes for each probe and indicated that the fluorescence observed was associated with a full antibody structure with a molecular weight of 150 kDa.

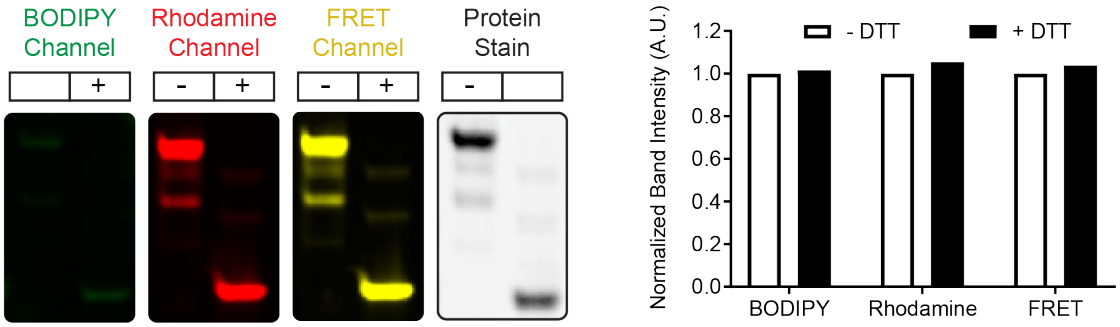

Figure 3.6. Fluorescent gel characterization of control probe. Probe. Fluorescent gel electrophoresis showing effect of DTT on Control Probe (Left). No differences in fluorescence intensity were seen after DTT treatment as confirmed by fluorescence band quantification (Right). All bands shifted to lower molecular weight due to cleavage of interchain disulfide bonds in the IgG structure.

When treated with DTT, all bands shifted to lower molecular weight due to cleavage of interchain disulfide bonds in the IgG structure. Fluorescence is visualized on the band corresponding to the molecular weight of a heavy chain (50 kDa). When the Cleavable Probe was treated with DTT, rhodamine was cleaved from the antibody, leading to an increase in BODIPY fluorescence emission (dequenching). Rhodamine emission and FRET emission almost vanished due to the loss of the rhodamine fluorophore. The relative changes in fluorescence with and without DTT treatment were quantified for the Cleavable Probe (Figure 3.5). The Control Probe showed no differences in fluorescence intensity (Figure 3.6).

Visualization of Intracellular Bond Cleavage

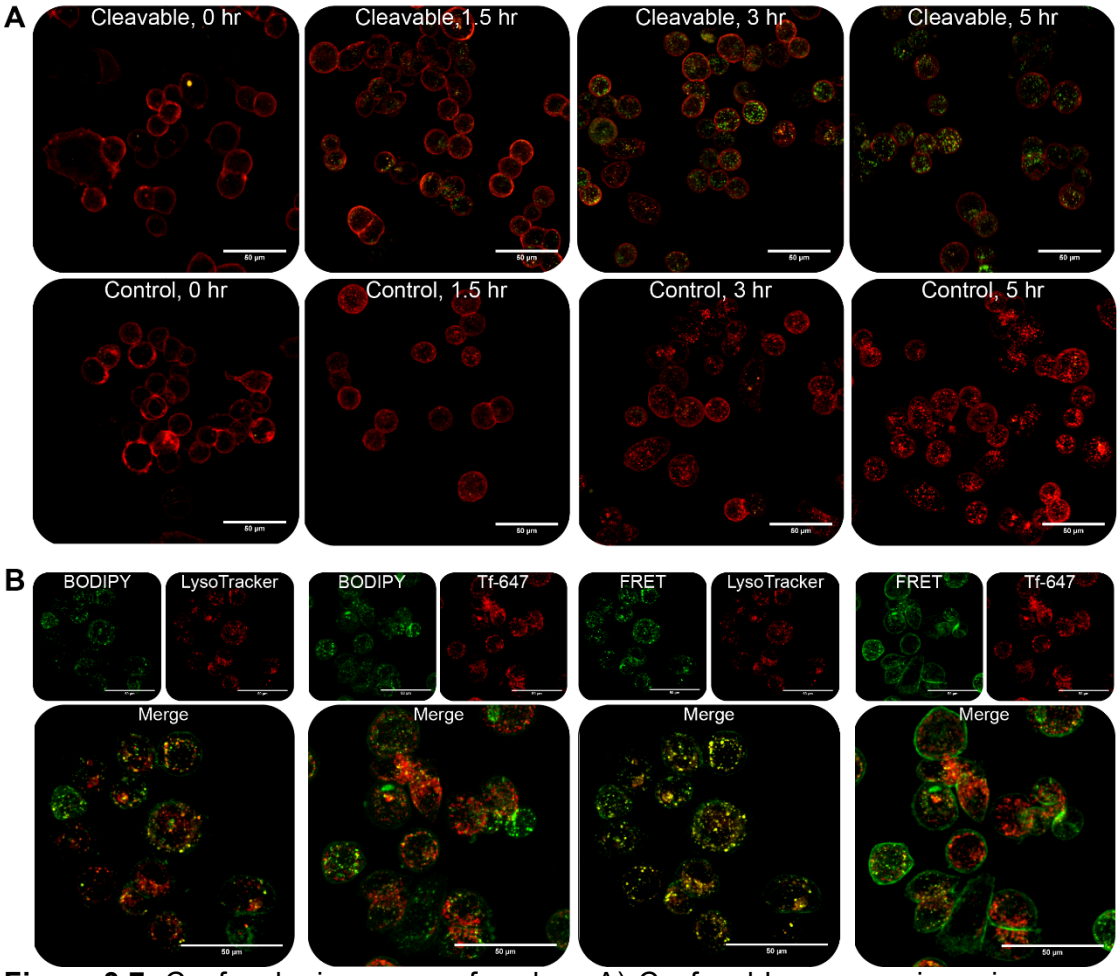

Figure 3.7. Confocal microscopy of probes. A) Confocal laser scanning microscopy images of Cleavable Probe and Control Probe incubated with SK-BR-3 cells. BODIPY excitation and emission is shown in green. BODIPY excitation with rhodamine emission (FRET) is shown in red. Scale bar is 50 μm. B) Colocalization of BODIPY excitation/emission of Cleavable Probe with LysoTracker Deep Red and Tf-AF647 after 3 hours of incubation (Left). Colocalization of BODIPY excitation/Rhodamine emission of Cleavable Probe with LysoTracker Deep Red and Tf-AF647 after 3 hours of incubation (Left). Scale bar is 50 μm.

SK-BR-3 cells are a human breast cancer cell line that has been shown to possess a high level of the HER2 receptor (approximately 1.5 million receptors per cell).[24] We incubated SK-BR-3 cells at 4 °C with 10 nM of the trastuzumab probes to prevent internalization and to saturate surface receptors. Probe solution was then removed, fresh media was added, and the cells were incubated at 37 °C to allow for

internalization and intracellular processing. The 37 °C incubation was carried out for varying amounts of time (0, 1.5, 3, and 5 hours) and cellular fluorescence was visualized via live-cell confocal microscopy (Figure 3.7). FRET emission is shown in red and BODIPY emission is shown in green. Initially, FRET emission is visualized on the cell surface and there is no BODIPY emission.

In the panel with the Cleavable Probe, FRET emission intensity decreases over time and BODIPY emission intensity increases. However, in the panel with the Control Probe, overall FRET emission intensity remains the same and there is no BODIPY emission over the time course of the experiment. These results indicate that disulfide bond reduction occurs in the HER2 pathway in SK-BR-3 cells. Researchers have previously shown that trastuzumab is endocytosed and undergoes rapid and efficient recycling.[20,25] Over time for both probes, fluorescence emission appears intracellularly as punctate spots, indicating localization within endosomes. To confirm endocytic localization, the Cleavable Probe was incubated with transferrin, an established marker for recycling endosomes,[26] and LysoTracker Deep Red, a standard lysosomal marker.[27] We found that after 3 hours of uptake, cleaved probe co-localizes more with lysosomes than recycling endosomes (Figure 3.7B). Additionally, the intact trastuzumab Cleavable Probe shows colocalization with lysosomes and recycling endosomes.

Theoretical Model

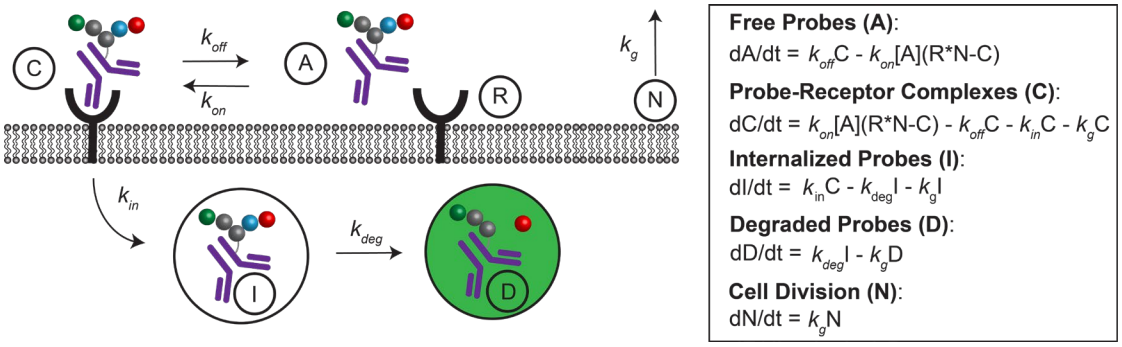

Figure 3.8. Kinetic model to describe the intracellular processing of the cleavable probe. The total number of receptors, *R*, and rate constants k_{on}, k_{off}, and k_g were obtained from literature[11] as 3.9×10^{-5} nM/cell, 0.014 hr^{-1}, 0.37 hr^{-1}, and 0.011 hr^{-1}, respectively.

In order to quantify the intracellular bond degradation rate, we expanded the kinetic model developed by Maass et al.[11] to describe the processing of our Cleavable Probe. In our model (Figure 3.8), the trastuzumab Cleavable Probe binds to its respective receptor yielding species C, the probe-receptor complex. This association with a free surface receptor is defined by the rate constant k_{on}. The probe can dissociate from its receptor to give species A (unbound probe) and R (free surface receptor) given by the rate constant k_{off}. The probe-receptor complex, species C, is internalized with an internalization rate constant k_{in} to yield species I (internalized, intact probe). The cleavable bond in the internalized, intact probe (I) is then degraded to yield species D (degraded probe). This degradation event is characterized by the rate constant k_{deg}. Cell growth dilutes intracellular contents and is accounted for by the rate constant k_g.

This model assumes bond degradation over a time period less than the timescale of proteolytic degradation of the antibody within the lysosomal compartment. It has been shown that the half-life for non-specific degradation of trastuzumab in SK-BR-3 cells is 16.1 hours.[11,25] As shown by confocal microscopy, the degradation of the disulfide bond occurs within a 5-hour timeframe. By assuming that lysosomal

degradation of the antibody is negligible, we can also assume that there is no exocytosis of the donor fluorophore within the time scale of our experiment. Complete degradation of the antibody would have to occur for the FRET probe to detach from the antibody and allow BODIPY to exit from the cell. The number of each of species over time can be described by a set of differential equations based on mass-action kinetics (Figure 3.8). The differential equation corresponding to degraded ADCs over time corresponds to the increase in fluorescence observed when the Cleavable Probe is cleaved and BODIPY is no longer quenched by rhodamine. This is the cleavage event we observed via confocal microscopy (Figure 3.7). To determine kinetic parameters, this cleavage event must be quantified as a function of time.

Quantification of Intracellular and In-Solution Measurements

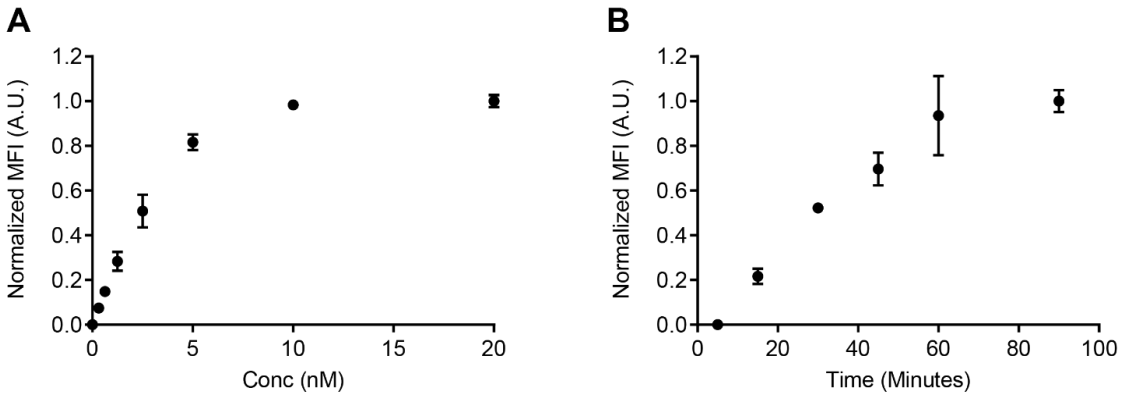

Figure 3.9. Flow cytometry determination of "pulse" concentration and time. A) SK-BR-3 cells were incubated with various concentrations of BODIPY-labelled trastuzumab. B) SK-BR-3 cells were incubated with 10 nM of BODIPY-labelled trastuzumab for various amounts of time.

To solve the set of differential equations in Figure 3.8, initial conditions were set based on experimental design. Intracellular disulfide bond degradation was quantitatively measured with live-cell flow cytometry via a “pulse-chase” experiment (Figure 3.9).

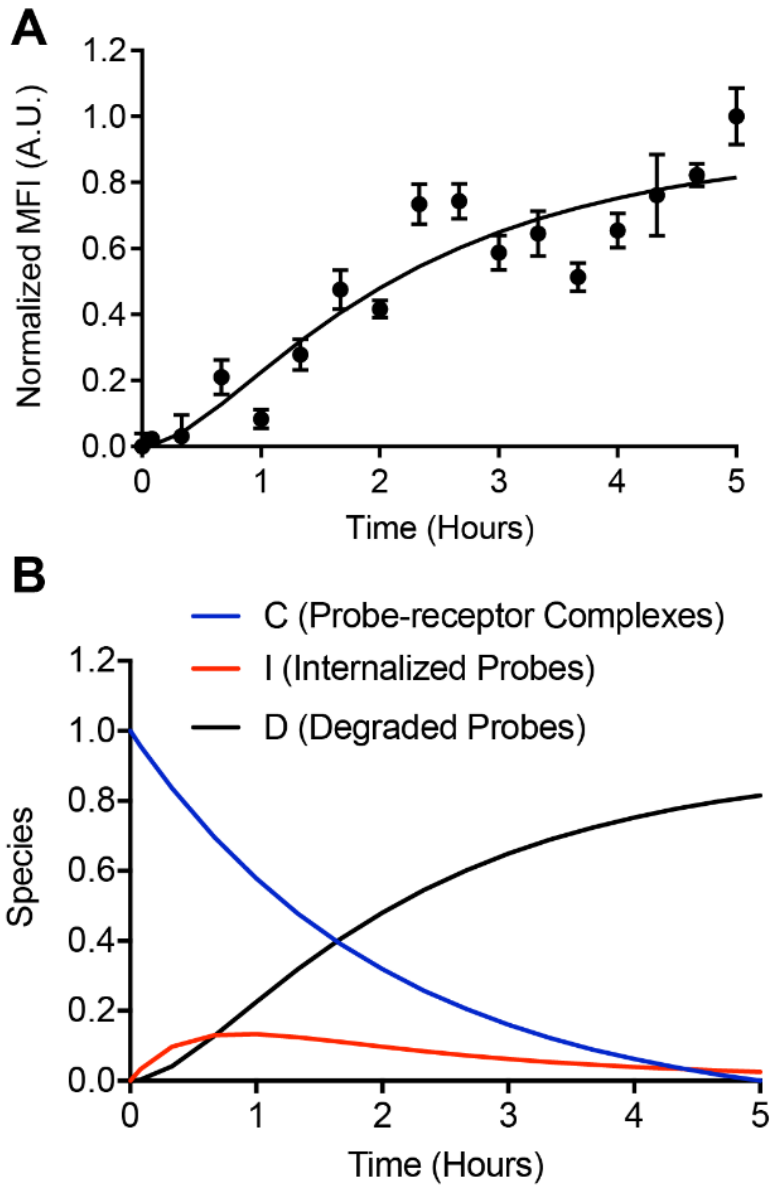

Figure 3.10. Intracellular data and model fit. A) Intracellular disulfide bond degradation in SK-BR-3 cells measured via flow cytometry. Data is reported as fluorescence of Cleavable Probe minus fluorescence of Control Probe and normalized on a 0 to 1 scale. n = 3 biological replicates with 2 technical replicates per biological replicate. Error bars shown indicate SEM. B) Kinetic plots of probe-receptor complexes, internalized probes, and degraded probes as a function of time.

Similar to confocal studies, SK-BR-3 cells were pulsed at 4 °C with a saturating concentration (Figure 3.9, 10 nM) of the trastuzumab probes and all unbound probes were washed off. This ensured that at time t = 0 of the chase experiment, all surface

HER2 receptors were bound to trastuzumab probes (Figure 3.10, state C). After various amounts of “chase” time intervals, the cells were trypsinized and total fluorescence was measured via flow cytometry.

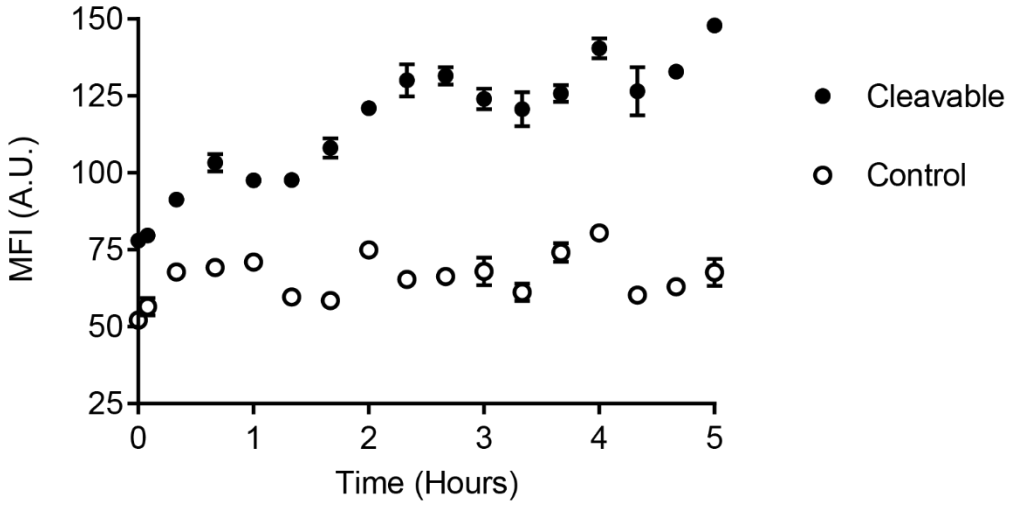

Figure 3.11. Raw fluorescence values as measured via flow cytometry for cleavable probe and control probe in SK-BR-3 cells.

Fluorescence values attained for the Control Probe were subtracted from the fluorescence values measured for the Cleavable Probe (raw data shown in Figure 3.11). The constants R, k_{on}, k_{off}, and k_g were obtained from literature.[11] The remaining rate constants k_{in} and k_{deg} were determined by fitting the kinetic data for bond cleavage to the model. The rate constant for internalization was determined to be 2.2 hr^{-1} and the rate constant for disulfide bond cleavage in the HER2 pathway in SK-BR-3 cells was calculated to be 0.45 hr^{-1}, corresponding to a half-life of 92 minutes. The internalization rate constants of ligands to the HER2 receptor that have been previously measured[25,28-30] vary depending on the cell type, the nature of the ligand, and the measurement method.

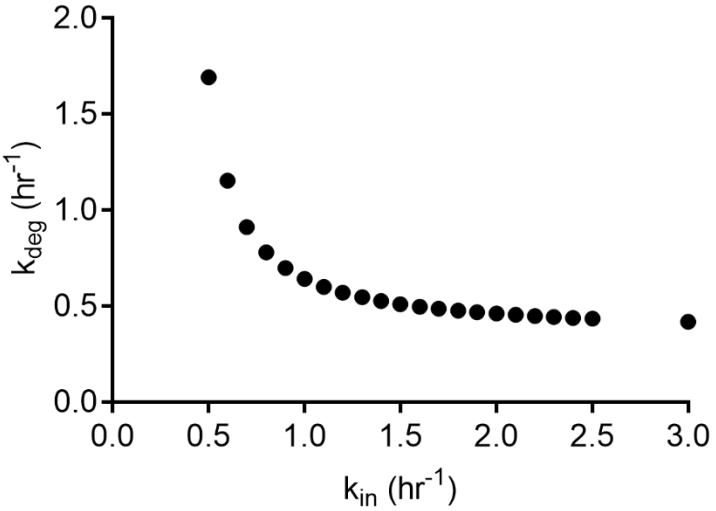

Figure 3.12. Dependence of k_{deg} on k_{in} for the cleavable probe. All other rates are held constant.

Using our kinetic model, we found that the degradation rate constant is sensitive to the value of k_{in} (Figure 3.12) for slow internalization processes, i.e. where $k_{in} < 1$ hr^{-1}. This framework for quantifying intracellular bond degradation would be best used to determine the intracellular bond degradation rate in other pathways (given the same assumptions) wherein the internalization rate is well characterized and quantified. Alternatively, the approach as outlined here could be applied to quantify the internalization rate constant and degradation rate constant simultaneously. Finally, the kinetic model enables tracking of the relative amount of each species (probe-receptor complexes, degraded probes, and internalized probes) as a function of time (Figure 3.10). Here, we see that after 30 minutes of incubation, there are more degraded probes in the cell than internalized probes. Furthermore, the model also indicates that there are more degraded internalized probes than surface bound probe-receptor complexes after the two-hour time point. These results are in qualitative agreement with confocal data in Figure 2A and highlight the utility of the kinetic model.

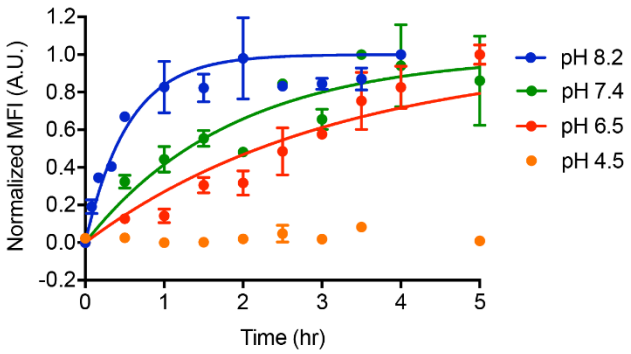

Figure 3.13. In-solution cleavage of trastuzumab cleavable probe by glutathione. Cleavage at pH 8.2, pH 7.4, pH 6.5, and pH 4.5. n = 2 technical replicates. Error bars shown indicate SEM.

For comparison to our intracellular measurement, disulfide bond degradation of the antibody probe was measured in buffered solution with the tripeptide glutathione (GSH) which is found to be in the range of 1-10 mM in the cytosol of cells.[31] The cleavable trastuzumab probe was incubated at 5 μM in buffer (pH 8.2, pH 7.4, pH 6.5, and pH 4.5) with 1.5 mM reduced glutathione at 37 °C. Fluorescence was measured as a function of time with a microplate reader (Figure 3.13). By fitting this data using pseudo first-order association kinetics, the rate constant for disulfide bond degradation at pH 8.2 was found to be 1.84 hr^{-1}. The rate constant for disulfide bond degradation at pH 7.4 (cytosolic pH) was found to be 0.54 hr^{-1} and at pH 6.5 (the pH associated with early endosomes[32]), the rate constant was found to be 0.32 hr^{-1}. At pH 4.5 (the pH associated with lysosomes[32]), there was no observable cleavage up to 5 hours of incubation with reduced glutathione. The corresponding half-lives under these conditions is listed in Table 3.1. This acute dependence of cleavage rate on pH, and presumably other components, highlights the difficulty of using cell-free assays to predict intracellular rates.

Table 3.1. Degradation rate constant and half-lives from fits of intracellular and in-solution data. [a]Intracellular data was fit to the kinetic model of intracellular processing of the Cleavable Probe. [b]In-solution data was fit using pseudo first-order association kinetics. [b]In-solution kinetic data was too slow to fit to a kinetic model (nd – not determined).

Environment	k_{deg} (hr^{-1})	$t_{1/2}$ (min)
[a]Intracellular	0.45	92
[b]Solution (pH 8.2)	1.84	23
[b]Solution (pH 7.4)	0.54	77
[b]Solution (pH 6.5)	0.32	132
[c]Solution (pH 4.5)	nd	nd

There is some uncertainty with respect to what agent is responsible for cleaving disulfide bonds in the endocytic pathway as well as its concentration. The endocytic compartment is an oxidizing environment making it unfavorable for GSH to exist in its reduced form. Furthermore, GSH mediated cleavage is non-existent at lysosomal pH 4.5 (Figure 3.13), which is in direct contrast with intracellular experiments (Figure 3.7 and 3.11). Thus, we believe that the agent responsible for disulfide reduction in the endocytic pathway is not a glutathione but rather an enzyme. There is indeed evidence of an enzyme, GILT (gamma interferon-inducible lysosomal thiol reductase), that catalyzes disulfide bond reduction and is optimally active at low pH.[33-35] There are other known redox enzymes present in the intracellular milieu such as thioredoxin,

glutaredoxin, and protein disulfide isomerase.[36] However, these enzymes are optimally active at neutral pH. There also maybe be other enzymes involved in disulfide bond reduction in the endocytic pathway that have yet to be identified. Although the exact identity of the enzyme(s) responsible for endosomal cleavage of the trastuzumab probes is unknown at this time, it is clear that endo/lysosomal disulfide bond cleavage occurs in the HER2 pathway at a fairly rapid rate.

3.3. CONCLUSIONS

In conclusion, we have developed a modular platform to quantify the intracellular degradation rate of stimuli-responsive bonds in a pathway- and cell type-dependent manner. We synthesized a FRET-based cross-linker containing a reduction-sensitive disulfide bond. This cross-linker was conjugated to a therapeutically relevant antibody against the HER2 receptor, trastuzumab. Cleavage of the trastuzumab probe was demonstrated chemically using a fluorescent gel shift assay. Intracellular bond cleavage was visualized via live-cell confocal microscopy and then measured kinetically with flow cytometry. By fitting this kinetic data to our model of intracellular processing of the trastuzumab probe, we have quantified the fundamental rate constant of intracellular disulfide bond degradation in the HER2 pathway in SK-BR-3 cells. Given the modular nature of our bioconjugate-based approach, it would be interesting to explore this bond degradation as a function of cell type, endocytic pathway, and carrier protein. Additionally, the method described here can be used to quantify the degradation rate constant of other therapeutically relevant bond types, such as hydrazone,[3] dipeptide,[37] and glucuronide[38] chemistries. Further, this system could be used in conjunction with genome editing techniques to quantitate the effect of various

intracellular agents on bond cleavage. This would further inform the design of stimuli-responsive drug delivery systems.

Chapter 3 – APPENDIX

General Materials

All chemicals were purchased from MilliporeSigma unless stated otherwise. Materials for cell culture and biological assays were purchased from ThermoFisher Scientific unless stated otherwise. DBCO-PEG_4-NH_2 was purchased from BroadPharm. Transglutaminase was purchased from Amazon as Transglutaminase (Meat Glue) – RM Formula by Moo Gloo. Recombinant PNGase F was purchased from New England BioLabs. SK-BR-3 cells were purchased from ATCC. SK-BR-3 cells were cultured in McCoy's 5A (Modified) Medium supplemented with 10% fetal bovine serum (FBS) and 1% Penicillin Streptomycin (Pen/Strep) at 37 °C with with 5% CO_2. 4-20% mini-PROTEAN TGX precast protein gels and Bio-Safe Coomassie Stain were purchased from Bio-Rad Laboratories. Glass bottom dishes for confocal imaging and flow cytometry were purchased from Cellvis. Trastuzumab was produced as described previously.[39]

General Methods

Analytical Hydrophobic Interaction Chromatography (HIC) of Trastuzumab Probes: HIC characterization of trastuzumab conjugates was performed on an Agilent 1100 Series HPLC system equipped with a UV diode array detector and an 1100 Infinity fraction collector using a Tosoh Biosciences TSK Gel Phenyl-5PW HPLC column (7.55 mm ID x 7.5 cm, 10 µm). The mobile phase for HPLC was 1.5 M ammonium sulfate, 25 mM potassium phosphate pH 7 (solvent A) and 18.75 mM potassium phosphate, 25% IPA pH 7 (solvent B). Compounds were eluted at a flow rate of 1 mL/min with a linear gradient of 0% to 100% solvent B (0-60 minutes), then 100% solvent B (60-65 min) and equilibrated back to 5% solvent B (65-70 minutes). Absorbance at 210 nm was analyzed.

Matrix Assisted Laser Desorption Ionization (MALDI) of Trastuzumab Probes: MALDI was performed by MIT Biopolymer Laboratory. Each sample was reduced with tris(2-carboxyethyl)phosphine (TCEP) for 1 hour at a final concentration of TCEP in solution of 50 mM. Each reduced sample was desalted by a C4 zip-tip, eluted in 5 µl of 70% acetonitrile, 0.1% trifluoroacetic acid, and 29.9% water. Then, 1 µl of each reduced and desalted sample was mixed with 1 µl of sinapinic acid matrix solution. The mixture was spotted and analyzed within the range 10-100 kDa on a microflex MALDI-TOF MS (Bruker Daltonics) with the following settings: PIE delay of 600 ns, laser repetition rate of 60 Hz, linear detector voltage of 3.158 kV, reflector detector voltage of 1.909 kV, ion source voltage 1 of 20 kV, ion source voltage 2 of 18.1 kV, ion source lens voltage of 9 kV, and 256 shots.

Fluorescent Gel Electrophoresis of Trastuzumab Probes: 2 µg of each of the trastuzumab probes (15 µM in 1X phosophate buffered saline (PBS) pH 7.4) were reacted with 10 mM DTT for 30 minutes. The final concentration of trastuzumab was 2.5 µM in PBS. The samples were then denatured in the absence of reducing agent by boiling at 100 °C for 5 minutes. A 4-20% mini-PROTEAN® TGX™ precast protein gel was run for 60 minutes at 100V to separate the protein samples. Fluorescence imaging was performed using a GE Healthcare Typhoon 9400 image system set to a photomultiplier tube voltage of 400 with the following fluorescence settings: BODIPY excitation: 488 nm, emission: 500-540 nm; Rhodamine excitation: 561 nm, emission: 573-681 nm. FRET excitation: 488 nm, emission: 578-685 nm. Protein content was visualized using Bio-Safe Coomassie Stain according to the manufacturer's instructions and imaged using a Bio-Rad Chemidoc MP Imaging System. Fluorescence intensity was analyzed using Fiji software.

Confocal Microscopy Time Course of Trastuzumab Probes: One day prior to the experiment, SK-BR-3 cells were plated into a 4-chamber 35 mm glass bottom dish with 20 mm microwell, #1.5 cover glass at 75,000 cells/chamber in McCoy's 5A (Modified) Medium with 10% FBS and 1% Pen/Strep. The next day, the media was removed, the cells were washed with 1X PBS pH 7.4, and then incubated at 4 °C with 10 nM of the probes in McCoy's 5A (Modified) Medium with 10% FBS and 1% Pen/Strep for 1 hour. After incubation, the cells were washed twice with PBS and fresh media was added. Cells were incubated at 37 °C and 5% CO_2 for varying amounts of time (0, 1.5, 3, and 5 hours). After the desired length of time, confocal laser scanning microscopy was carried out on a Zeiss LSM 800 Confocal Laser Scanning Microscope with a 20x objective. The BODIPY channel was set to excite at 488 nm and emit in the range 400-

545 nm with 1% laser power and a detector gain of 650 V. The rhodamine channel was set to excite at 561 nm and emit in the range 565-700 nm with 1% laser power and a detector gain of 675 V. The FRET channel was set to excite at 488 nm and emit in the range 565-700 nm with 1% laser power and a detector gain of 675 V. Phase images were collected in the range 400-700nm with a detector gain of 300 V. Post-image processing was performed using Fiji software.

Confocal Microscopy Colocalization of Cleavable Probe: One day prior to the experiment, SK-BR-3 cells were plated into a 4-chamber 35 mm glass bottom dish with 20 mm microwell, #1.5 cover glass at 75,000 cells/chamber in McCoy's 5A (Modified) Medium with 10% FBS and 1% Pen/Strep. For colocalization with transferrin, the next day the media was removed, the cells were washed with 1X PBS pH 7.4, and then incubated at 4 °C with 10 nM of the Cleavable Probe and 150 nM of Tf-AF647 in McCoy's 5A (Modified) Medium with 10% FBS and 1% Pen/Strep for 1 hour. After incubation, the cells were washed twice with PBS and 150 nM of Tf-AF647 was added in fresh media. Cells were incubated at 37 °C and 5% CO_2 for 3 hours. After the desired length of time, confocal laser scanning microscopy was carried out on a Zeiss LSM 800 Confocal Laser Scanning Microscope with a 20x objective. For colocalization with LysoTracker Deep Red, the next day the media was removed, the cells were washed with 1X PBS pH 7.4, and then incubated at 4 °C with 10 nM of the Cleavable Probe in McCoy's 5A (Modified) Medium with 10% FBS and 1% Pen/Strep for 1 hour. After incubation, the cells were washed twice with PBS and 150 nM of Tf-AF647 was added in fresh media. Cells were incubated at 37 °C and 5% CO_2 for 3 hours, with 150 nM of LysoTracker Deep Red added in the last hour of incubation. After the desired length of time, confocal laser scanning microscopy was carried out on a Zeiss LSM 800 Confocal

Laser Scanning Microscope with a 20x objective. The BODIPY channel was set to excite at 488 nm and emit in the range 400-545 nm with 1% laser power and a detector gain of 650 V. The rhodamine channel was set to excite at 561 nm and emit in the range 565-700 nm with 1% laser power and a detector gain of 675 V. The FRET channel was set to excite at 488 nm and emit in the range 565-700 nm with 1% laser power and a detector gain of 675 V. Phase images were collected in the range 400-700nm with a detector gain of 300 V. Post-image processing was performed using Fiji software.

Flow Cytometry of Trastuzumab Probes: One day prior to the experiment, cells were plated into a 4-chamber 35 mm glass bottom dish with 20 mm microwell, #1.5 cover glass at 75,000 cells/well in McCoy's 5A (Modified) Medium with 10% FBS and 1% Pen/Strep. The next day, the media was removed, the cells were washed with PBS, and then incubated at 4 °C with 10 nM of the probes in McCoy's 5A (Modified) Medium with 10% FBS and 1% Pen/Strep for 1 hour. After incubation, the cells were washed twice with PBS and fresh media was added. Cells were incubated at 37 °C and 5% CO_2 for varying amounts of time (20 minute intervals from 0 to 5 hours). Cells were then washed with PBS, trypsinized, pelleted, and resuspended in PBS for flow cytometry analysis. Green fluorescence was measured on a BD FACS Calibur with the following instrument settings: FSC detector: E-1 Voltage, 3 Amp Gain, SSC detector: 400 Voltage, 1 Amp Gain, FL1 detector: 600 Voltage, 1 Amp Gain. Data was collected for 3 biological replicates with 2 technical replicates per biological replicate. Data processing was performed using FlowJo software.

Fluorescence Spectroscopy of Trastuzumab Probes: Trastuzumab probes were incubated at 5 μM in buffer (100 mM Tris with 150 mM NaCl pH 8.2, 1X PBS pH 7.4, 1X PBS pH 6.5, or 20 mM citrate with 50 mM NaCl pH 4.5) with 1.5 mM of L- glutathione (reduced). At various time points, 0.5 μL of the solution was removed, diluted to 100 nM, and transferred to a low volume 384-well black flat bottom plate. The fluorescence was then measured at an excitation wavelength of 490 nm and an emission wavelength of 515 nm on a Tecan M1000 Pro microplate reader. Data was analyzed in GraphPad Prism and fit to one-phase association nonlinear regression.

Site-Specific Antibody Modification

Synthesis of DBCO-modified trastuzumab: 600 units/mg of PNGase F (500,000 U/mL) were added to 1 equiv of trastuzumab (40 mg/mL in 1X PBS pH 7.4). To this mixture was added 160 equivalents of N-(14-amino-3,6,9,12-tetraoxatetradec-1-yl)-11,12-didehydro-γ-oxodibenz[b,f]azocine-5(6H)-butanamide (100 mM in "10X Buffer" (100 mM phosphate, 27 mM KCl, and 137 mM NaCl)) and 66.7% v/v of Transglutaminase (Meat Glue) (500 mg/mL in 10X Buffer). The final trastuzumab concentration was 8 mg/mL in 10X Buffer. The antibody was reacted at 37 °C for 24 hours. The mixture was then purified using NAb Protein A/G 0.2 mL spin columns according to the manufacturer's instructions.

Synthesis of Cleavable and Control Probes: 1 equiv of DBCO-modified trastuzumab (10 uM in 100 mM Tris pH 7) was reacted with 5 equivalents of FRET cross-linker (10 mg/mL in DMSO). The final concentration of DBCO-modified trastuzumab was 10 μM in 1X PBS pH 7.4 with 10% DMSO. The mixture was reacted for 24 hours at room temperature and then purified and concentrated using an Amicon Ultra-0.5 mL centrifugal filter with a 30 kDa molecular weight cut off.

Supplementary Software

MATLAB Code. The code is comprised of a script that calls a custom function. Within the function are the differential equations that describe the processing of the probe as well as the associated known rate constants.

Script:

```
close all

global M1 M2 M3 M4 M5

filename = 'Deg_data5.txt';
fileopen=fopen(filename,'r');
filein = fscanf(fileopen,'%f',[2 Inf]);
data = zeros(length(filein),2);
data = filein';
fclose('all');

t = data(:,1);
y = data(:,2);

%initial values of k
k0=[0.5;0.05]; %the first is kdeg and the second is ke-internalization

%Plot curve with initial values
figure(1), clf
plot(t,SKBR3_2(k0,t),'r')
plot(t,y,'o',t,SKBR3_2(k0,t),'r')

%bounds for parameter
lb = [0.1;0.01]; %lower boundary for parameters
ub = [10;10]; %upper boundary for parameters

%options for running algorithms
options = optimoptions('lsqcurvefit','Algorithm','trust-region-reflective');
options.OptimalityTolerance = 1.0000e-09;
options.FiniteDifferenceStepSize = 1; % default is eps
options.FiniteDifferenceType = 'central';
options.Diagnostics = 'on';
options.Display = 'iter';
options.FunctionTolerance = 1.0000e-016;
options.FunValCheck = 'on';
```

```
options.MaxIterations = 1000;
options.StepTolerance = 1.0000e-016;

%fit the data
[k,resnorm,output,exitflag] = lsqcurvefit(@SKBR3_2,k0,t,y);

%see results
figure(2), clf
plot(t,y,'o',t,SKBR3_2(k,t),'r');
```

Function:

```
function R = SKBR3_2(k,t)

global M1 M2 M3 M4 M5

kon=0.37;     % association rate constant (h-1 nM-1)
koff=0.014;   % dissociation rate constant (h-1)
u=0.011;      % cell growth rate (h-1)
HER2=2.36*10^-5;     % HER2 concentration in well volume per cell (nM/cell)

y0 = [(HER2*7.5*10^4);0;0;0;7.5*10^4]; %initial conditions

ode_options = odeset('RelTol', 1e-8, 'AbsTol', 1e-08, 'Stats','on');
[~,Fit]=ode15s(@DiffEq,t,y0,ode_options);
R = Fit(:,3); % pulling just y3

M1 = Fit(:,1);
M2 = Fit(:,2);
M3 = Fit(:,3);
M4 = Fit(:,4);
M5 = Fit(:,5);

function dy = DiffEq(t,y)

%answer matrix
dydt=zeros(5,1);

%Model equations
dydt(1) = kon * y(4) * ((HER2*y(5))-y(1)) - koff * y(1) - k(2) * y(1) - u * y(1); %
dC/dt (# of ADC-receptor complexes on cell surface)
dydt(2) = k(2) * y(1) - k(1) * y(2) - u * y(2); % dI/dt (Intact internalized ADCs per
cell)
dydt(3) = k(1) * y(2) - u * y(3); %dD/dt (degraded ADCs per cell)
dydt(4) = (koff * y(1) - kon * y(4) * ((HER2*y(5))-y(1))); % dA/dt (antibody in
media)
dydt(5) = u * y(5) ; % dN/dt (cell count)
```

```
dy=dydt;

end %SKBR3


end %main
```

Chapter 3 – REFERENCES

1.Davis, M. E., Chen, Z. G. & Shin, D. M. Nanoparticle therapeutics: an emerging treatment modality for cancer. *Nanoscience and Technology* 239 (2009). doi:10.1142/9789814287005_0025

2.Beck, A., Goetsch, L., Dumontet, C. & Corvaïa, N. Strategies and challenges for the next generation of antibody-drug conjugates. *Nature Reviews Drug Discovery* **16,** 315–337 (2017).

3.Davis, M. E. Design and development of IT-101, a cyclodextrin-containing polymer conjugate of camptothecin. *Advanced Drug Delivery Reviews* **61,** 1189–1192 (2009).

4.Liao, J. *et al.* Tumor-targeting and pH-responsive nanoparticles from hyaluronic acid for the enhanced delivery of doxorubicin. *Int J Biol Macromol* **113,** 737–747 (2018).

5.Hong, R. *et al.* Glutathione-mediated delivery and release using monolayer protected nanoparticle carriers. *Journal of the American Chemical Society* **128,** 1078–1079 (2006).

6.Qi, R. *et al.* Nanoparticle conjugates of a highly potent toxin enhance safety and circumvent platinum resistance in ovarian cancer. *Nat Commun* **8,** 2166 (2017).

7.Staben, L. R. *et al.* Targeted drug delivery through the traceless release of tertiary and heteroaryl amines from antibody-drug conjugates. *Nature Chemistry* **8,** 1112–1119 (2016).

8.Koga, Y. *et al.* Antitumor effect of antitissue factor antibody-MMAE conjugate in human pancreatic tumor xenografts. *Int J Cancer* **137,** 1457–1466 (2015).

9.Senter, P. D. & Sievers, E. L. The discovery and development of brentuximab vedotin for use in relapsed Hodgkin lymphoma and systemic anaplastic large cell lymphoma. *Nat Biotechnol* **30,** 631–637 (2012).

10.Kovtun, Y. *et al.* IMGN779, a Novel CD33-Targeting Antibody-Drug Conjugate with

DNA-Alkylating Activity, Exhibits Potent Antitumor Activity in Models of AML. … *Cancer Therapeutics* **17,** 1271–1279 (2018).

11.Maass, K. F., Kulkarni, C., Betts, A. M. & Wittrup, K. D. Determination of Cellular Processing Rates for a Trastuzumab-Maytansinoid Antibody-Drug Conjugate (ADC) Highlights Key Parameters for ADC Design. *The AAPS Journal* **18,** 635–646 (2016).

12.Oflazoglu, E. *et al.* Potent anticarcinoma activity of the humanized anti-CD70 antibody h1F6 conjugated to the tubulin inhibitor auristatin via an uncleavable linker. *Clin Cancer Res* **14,** 6171–6180 (2008).

13.Lambert, J. M. & Chari, R. V. J. Ado-trastuzumab Emtansine (T-DM1): an antibody-drug conjugate (ADC) for HER2-positive breast cancer. *J Med Chem* **57,** 6949–6964 (2014).

14.Katz, J., Janik, J. E. & Younes, A. Brentuximab Vedotin (SGN-35). *Clin Cancer Res* **17,** 6428–6436 (2011).

15.Sorkin, M. R., Walker, J. A., Brown, J. S. & Alabi, C. A. Versatile Platform for the Synthesis of Orthogonally Cleavable Heteromultifunctional Cross-Linkers. *Bioconjugate Chemistry* **28,** 907–912 (2017).

16.Ahmed, S., Sami, A. & Xiang, J. HER2-directed therapy: current treatment options for HER2-positive breast cancer. *Breast Cancer* **22,** 101–116 (2015).

17.Escrivá-de-Romaní, S., Arumí, M., Bellet, M. & Saura, C. HER2-positive breast cancer: Current and new therapeutic strategies. *Breast* **39,** 80–88 (2018).

18.Arteaga, C. L. *et al.* Treatment of HER2-positive breast cancer: current status and future perspectives. *Nat Rev Clin Oncol* **9,** 16–32 (2011).

19.Mitri, Z., Constantine, T. & O'Regan, R. The HER2 Receptor in Breast Cancer: Pathophysiology, Clinical Use, and New Advances in Therapy. *Chemother Res Pract* **2012,** 743193 (2012).

20.Bertelsen, V. & Stang, E. The Mysterious Ways of ErbB2/HER2 Trafficking. *Membranes (Basel)* **4,** 424–446 (2014).

21.Gemmete, J. J. & Mukherji, S. K. Trastuzumab (herceptin). *AJNR Am J Neuroradiol* **32,** 1373–1374 (2011).

22.Dennler, P., Schibli, R. & Fischer, E. Enzymatic antibody modification by bacterial transglutaminase. *Methods Mol Biol* **1045,** 205–215 (2013).

23.Dennler, P. *et al.* Transglutaminase-based chemo-enzymatic conjugation approach yields homogeneous antibody-drug conjugates. *Bioconjugate Chemistry* **25,** 569–578 (2014).

24.Li, J. Y. *et al.* A Biparatopic HER2-Targeting Antibody-Drug Conjugate Induces Tumor Regression in Primary Models Refractory to or Ineligible for HER2-Targeted Therapy. *Cancer Cell* **29,** 117–129 (2016).

25.Austin, C. D. *et al.* Endocytosis and sorting of ErbB2 and the site of action of cancer therapeutics trastuzumab and geldanamycin. *Mol Biol Cell* **15,** 5268–5282 (2004).

26.Kobayashi, H. & Fukuda, M. Arf6, Rab11 and transferrin receptor define distinct populations of recycling endosomes. *Commun Integr Biol* **6,** e25036 (2013).

27.Fan, F. *et al.* Labeling lysosomes and tracking lysosome-dependent apoptosis with a cell-permeable activity-based probe. *Bioconjugate Chemistry* **23,** 1309–1317 (2012).

28.Hendriks, B. S., Opresko, L. K., Wiley, H. S. & Lauffenburger, D. Coregulation of epidermal growth factor receptor/human epidermal growth factor receptor 2 (HER2) levels and locations: quantitative analysis of HER2 overexpression effects. *Cancer research* **63,** 1130–1137 (2003).

29.Hendriks, B. S., Opresko, L. K., Wiley, H. S. & Lauffenburger, D. Quantitative analysis of HER2-mediated effects on HER2 and epidermal growth factor receptor endocytosis: distribution of homo- and heterodimers depends on relative HER2 levels.

J Biol Chem **278,** 23343–23351 (2003).

30.Hendriks, B. S. *et al.* Impact of tumor HER2/ERBB2 expression level on HER2-targeted liposomal doxorubicin-mediated drug delivery: multiple low-affinity interactions lead to a threshold effect. *… Cancer Therapeutics* **12,** 1816–1828 (2013).

31.Forman, H. J., Zhang, H. & Rinna, A. Glutathione: overview of its protective roles, measurement, and biosynthesis. *Mol Aspects Med* **30,** 1–12 (2008).

32.Hu, Y.-B., Dammer, E. B., Ren, R.-J. & Wang, G. The endosomal-lysosomal system: from acidification and cargo sorting to neurodegeneration. *Transl Neurodegener* **4,** 18 (2015).

33.Sinnathamby, G., Maric, M., Cresswell, P. & Eisenlohr, L. C. Differential Requirements for Endosomal Reduction in the Presentation of Two H2-Ed-Restricted Epitopes from Influenza Hemagglutinin. *J Immunol* **172,** 6607 (2004).

34.Arunachalam, B., Phan, U. T., Geuze, H. J. & Cresswell, P. Enzymatic reduction of disulfide bonds in lysosomes: characterization of a gamma-interferon-inducible lysosomal thiol reductase (GILT). *Proc Natl Acad Sci USA* **97,** 745–750 (2000).

35.Hastings, K. T. & Cresswell, P. Disulfide reduction in the endocytic pathway: immunological functions of gamma-interferon-inducible lysosomal thiol reductase. *Antioxidants & Redox Signaling* **15,** 657–668 (2011).

36.Feener, E. P., Shen, W. C. & Ryser, H. J. Cleavage of disulfide bonds in endocytosed macromolecules. A processing not associated with lysosomes or endosomes. *J Biol Chem* **265,** 18780–18785 (1990).

37.Sanderson, R. J. *et al.* In vivo drug-linker stability of an anti-CD30 dipeptide-linked auristatin immunoconjugate. *Clin Cancer Res* **11,** 843–852 (2005).

38.Burke, P. J. *et al.* Optimization of a PEGylated Glucuronide-Monomethylauristatin E Linker for Antibody-Drug Conjugates. *… Cancer Therapeutics* **16,** 116–123 (2016).

39.Thornlow, D. N. *et al.* Dual Site-Specific Antibody Conjugates for Sequential and Orthogonal Cargo Release. *Bioconjugate Chemistry* (2019). doi:10.1021/acs.bioconjchem.9b00244

Chapter 4 – DEVELOPMENT OF ALTERNATIVE QUENCHED PROBES FOR MONITORING INTRACELLULAR BOND DEGRADATION

4.1. INTRODUCTION

Fluorescence spectroscopy has often been used to detect and visualize biological structures and processes. Quenching is a process that results in the decrease of fluorescence intensity. The ground state of a fluorophore refers to its low-energy, stable configuration in which it does not fluoresce. The excited state of a fluorophore refers to a higher-energy state that results when it absorbs light.

Dynamic quenching, also known as collisional quenching, occurs when an excited state fluorophore interacts with a quencher, resulting in deactivation of the fluorophore to the ground state.[1] An example of dynamic quenching is Förster resonance energy transfer (FRET). In FRET, energy is transferred from an excited fluorophore (the donor) to another fluorophore (the acceptor) through long-range intermolecular interactions. The efficiency of FRET is inversely dependent on the distance between the donor and the acceptor. The highest FRET efficiency occurs within what is known as the Förster radius, a distance of 3-6 nm between donor and acceptor. As such, FRET has been used extensively to measure biological processes that occur when proximity is changed.

Static quenching, also known as contact quenching, occurs when a fluorophore and quencher form a ground state complex before excitation occurs. Hydrophobic dye molecules interact in such a way to minimize contact with water. In contrast to FRET in which the absorption spectra of the donor and acceptor molecules do not change, the formation of the complex in static quenching leads to a change in the absorption spectra of the fluorophore and quencher molecules. In this interaction, a non-fluorescent intramolecular dimer is formed, which possesses its own distinct absorption spectrum.

We previously developed a reduction-sensitive FRET-based cross-linker that was used to qualitatively detect intracellular bond degradation within the transferrin pathway in HeLa cells.[2] Towards quantifying this degradation event, we modified our cross-linker structure to contain a fluorescent reporter and a quencher dye instead of a FRET pair of fluorophores. We hypothesized that this type of "turn on" system would offer reduced background signal and thus improved contrast and sensitivity over a FRET-based system. A fluorophore-quencher system would exhibit contact quenching.[3]

4.2. RESULTS AND DISCUSSION

Chemical Structures of Quenched Cross-linkers

Cleavable Cross-Linker (BODIPY-ss-DNP)

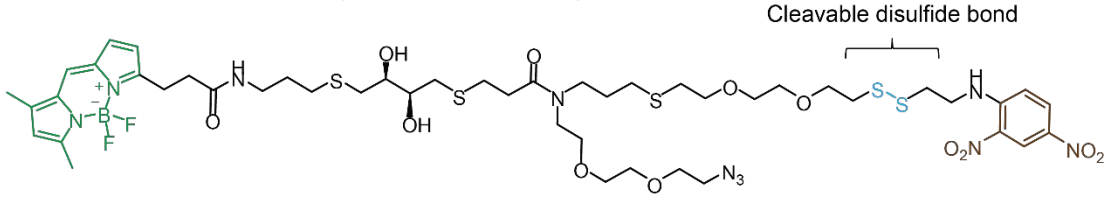

Control Cross-Linker (BODIPY-mal-DNP)

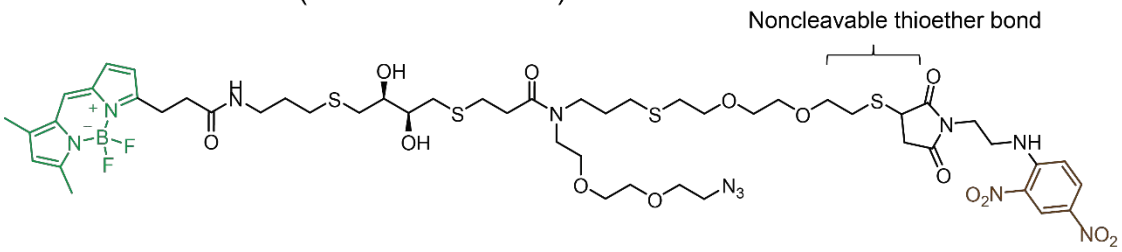

Figure 4.1. Chemical structures of quenched cross-linkers with BODIPY and DNP as fluorophore-quencher pair. The Cleavable Cross-linker contains a reduction-sensitive disulfide bond. The Control Cross-linker contains a noncleavable thiol-maleimide bond.

We first adapted our cross-linker to contain the fluorophore-quencher pair, BODIPY and 2,4-dinitrophenyl (DNP). This pair has been used for intracellular fluorescence imaging.[4,5] The fluorophore BODIPY was previously used in our FRET

cross-linkers as the FRET donor.[2] The FRET acceptor rhodamine was replaced with the quencher DNP, which is more hydrophilic. It is beneficial to improve hydrophilicity to improve conjugation efficiency of the cross-linker to a protein or antibody of interest. The chemical structures of the Cleavable Cross-linker and the Control Cross-linker are shown in Figure 4.1.

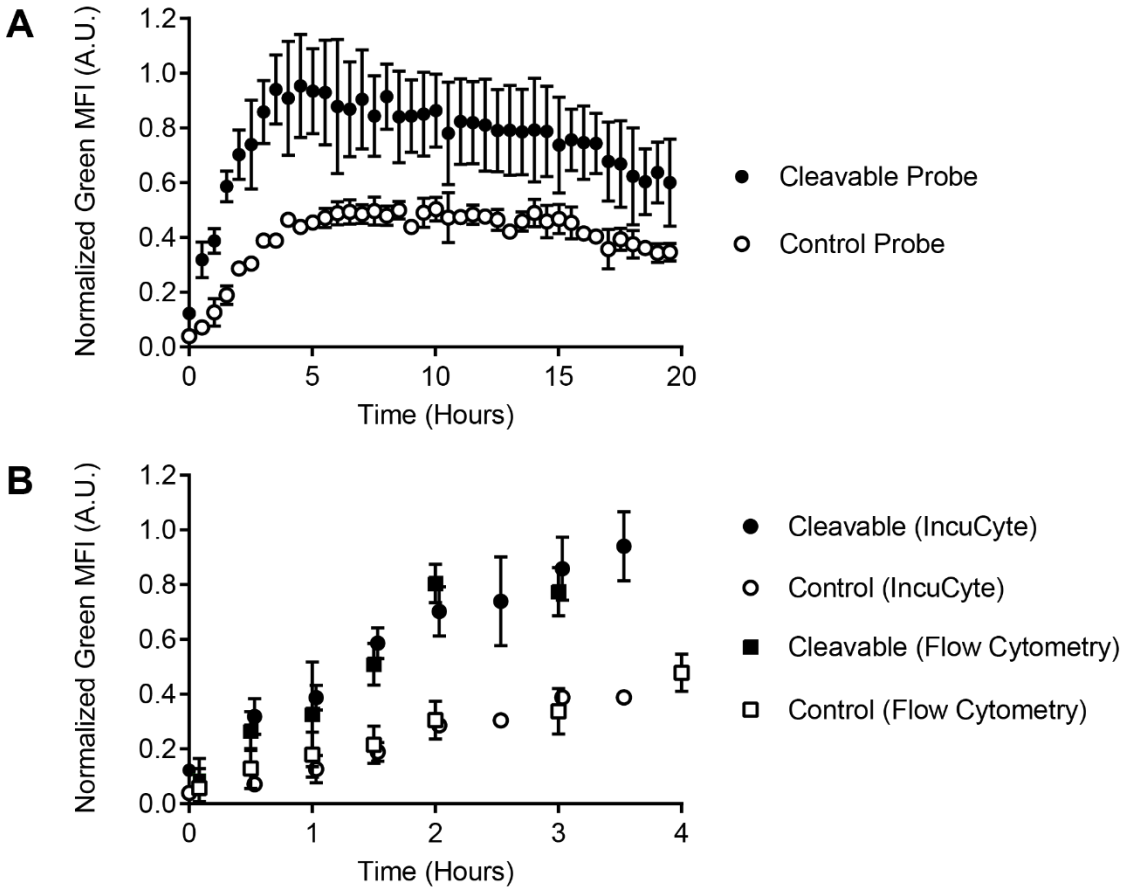

Figure 4.2. IncuCyte analysis of probes. A) IncuCyte analysis of Cleavable Probe and Control Probe. B) Comparison of IncuCyte data to flow cytometry data.

Live-cell Imaging via IncuCyte

In addition to improving the system with a fluorophore-quencher pair, we sought to develop a high throughput technique based on the IncuCyte ZOOM automated live-cell imaging system to measure the kinetics of intracellular bond cleavage. The IncuCyte system is a live-cell imaging and analysis platform that enables real-time visualization of cell behavior by combining image-based analysis with the throughput of well-plate assays. The system is contained within a standard cell incubator and comprised of a tray for up to six microplates of any size and a camera with imaging modes for phase-contrast and red and green fluorescence. Cells remain stationary and undisturbed in the incubator while the optics move. Images are collected at desired time points and analyzed to calculate fluorescence intensity and phase confluency. Additionally, the system is fitted with 4x, 10x, and 20x objectives which can capture hundreds of cells in one image. This platform has been referenced in over 1,000 publications. The IncuCyte has been used to study other “turn on” systems such as in the quantification of macrophage phagocytosis pathogens labeled with a pH-sensitive dye[6]. The Cleavable Probe was analyzed with the IncuCyte system (Figure 4.2A). We benchmarked this data by conducting the experiment and measuring fluorescence via flow cytometry (Figure 4.2B). The data for the first four hours of cleavage qualitatively matches the trend shown via flow cytometry.

Flipped Cross-Linker (DNP-ss-BODIPY)

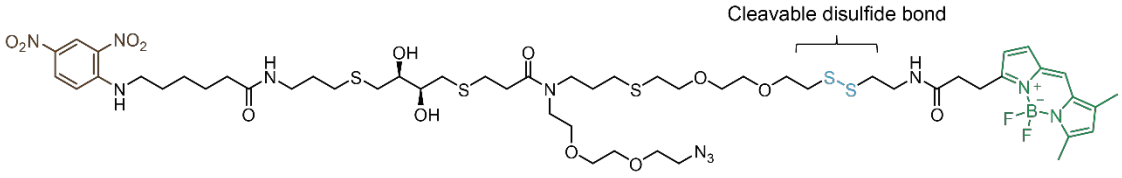

Control Cross-Linker (BODIPY-mal-DNP)

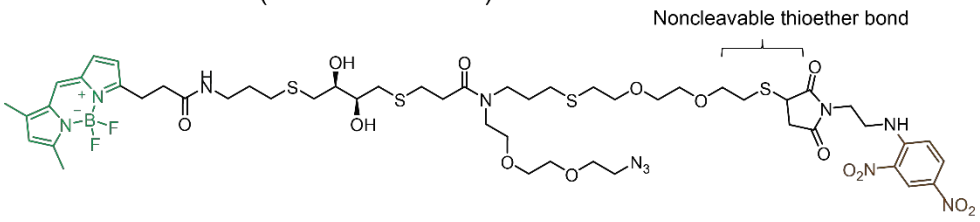

Figure 4.3. Chemical structures of flipped cross-linker and control cross-linker. The Flipped Cross-linker releases the quencher upon cleavage of the disulfide bond.

Recycling Effects on Fluorescence

Given this kinetic data, we wanted to confirm that the increase in fluorescence of the Cleavable Probe over time was due to bond cleavage. When the quencher is cleaved off the probe, it effectively generates an “Always On” control containing only the fluorophore. Given the recycling nature of the transferrin endocytic pathway, it is possible that the “Always On” probe generated would be recycled back to the surface. The probe could then bind iron in the media and be internalized again, leading to an increase in fluorescence that was not due to bond cleavage. To demonstrate that the increase in signal observed by IncuCyte is not due to recycling, a Flipped Cross-Linker was synthesized in which the location of the fluorophore and quencher were switched. This cross-linker was conjugated to transferrin to yield a Flipped Probe. When this probe is cleaved, the fluorophore would be detached from the protein and only the quencher would remain. Recycling of this probe would not yield any green fluorescence signal.

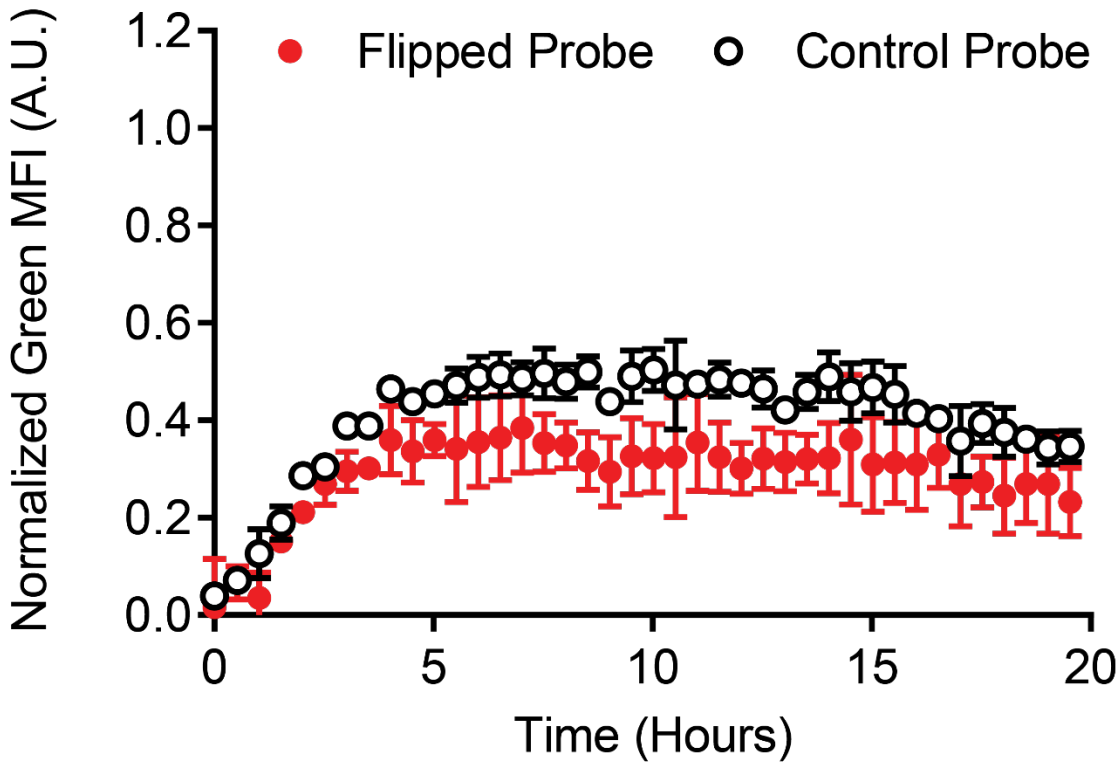

Figure 4.4. IncuCyte analysis of flipped probe and control probe.

The Flipped Probe was analyzed via IncuCyte (Figure 4.4). The fluorescence curve for the Flipped Probe matched that of the Control Probe. This result seemed to indicate that no significant disulfide cleavage seemed to be occurring in the transferrin pathway. However, we found that this overlap in fluorescence signal arose due to exocytosis of BODIPY. It has been shown that BODIPY can exit the cell by passive diffusion through membranes.[7] Thus, when the BODIPY was released from the Flipped Probe due to disulfide bond cleavage, it likely exited the cell and its fluorescence could not be measured.

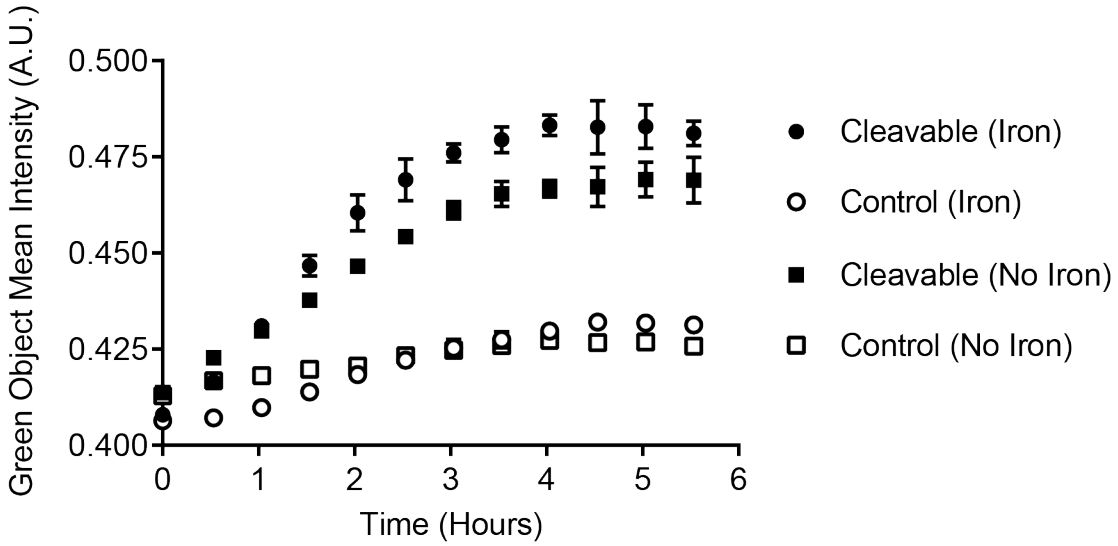

Figure 4.5. Effect of iron on fluorescence signal associated with the cleavable control and control probe.

As it would not be feasible to use a probe in which the fluorophore is released, we decided to test whether the iron concentration in media was high enough to enable reassociation of recycled, cleaved probe with the transferrin receptor. We carried out IncuCyte analysis of the Cleavable Probe and Control Probe in media with and without iron. As shown in Figure 4.5, there was not a significant effect on fluorescence with versus without iron for the Cleavable Probe. As such, we decided to move forward with the original probe design in which the quencher is released upon cleavage.

Control Cross-Linker 3º (BODIPY-DNP, Tertiary)

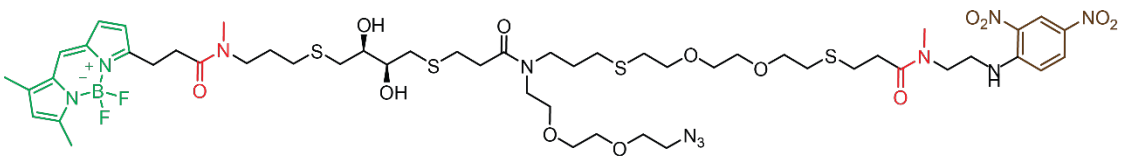

Figure 4.6. Chemical structure of control cross-linker 3° with no secondary amides. The tertiary amides that replaced the secondary amides in the original Control Cross-Linker structure are highlighted in red.

Investigating Fluorescence Increase of Control Probe

As seen in the IncuCyte data in Figure 4.2 and Figure 4.4, however, the fluorescence of the Control Probe trends upwards. It would be expected that this probe would not show any increase in fluorescence signal over time, as it should remain intact and therefore quenched. We believed that this increase in fluorescence might have been due to nonspecific proteolytic cleavage of secondary amides in the probe structure. Additionally, the thiol-maleimide bond within the Control Probe is also susceptible to hydrolysis, which generates another secondary amide in the structure. Another disadvantage of the maleimide chemistry is that it is reversible and nonspecific deconjugation has been shown under biological conditions.[8]

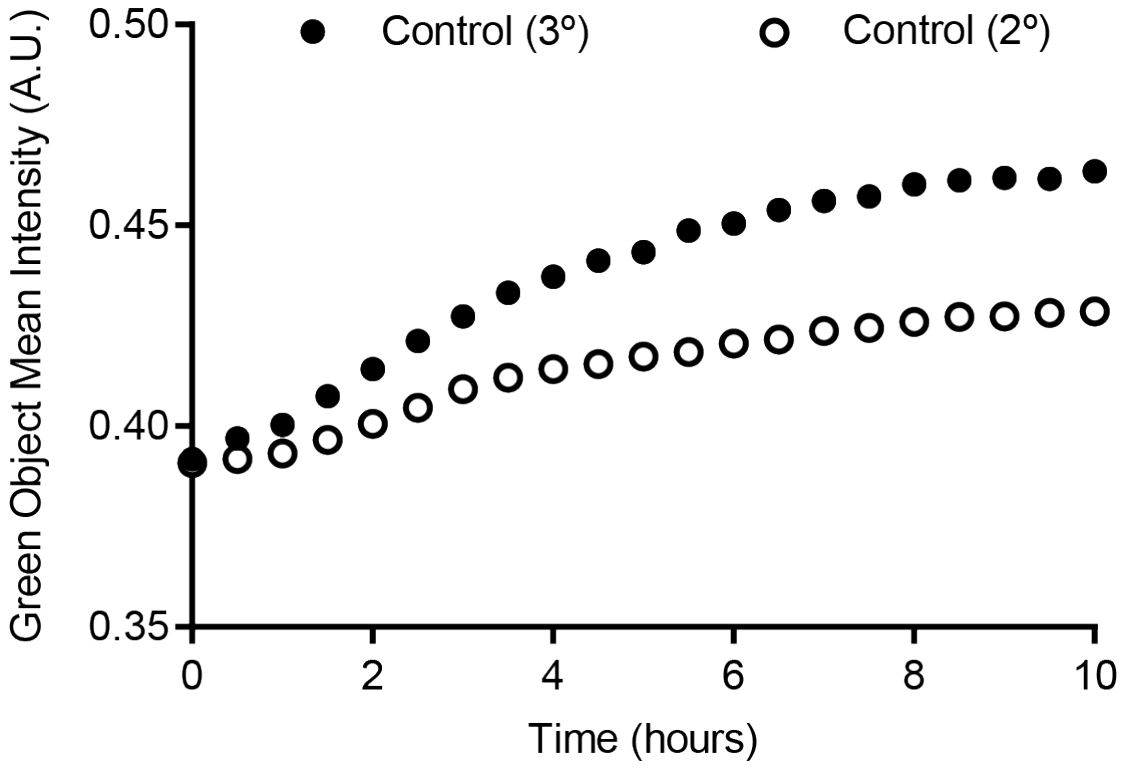

Figure 4.7. Comparison of control probe with tertiary amides to control probe with secondary amides.

We sought to remedy these issues by synthesizing new variants of the probes with tertiary amides that would be stable to nonspecific proteolytic degradation. We designed and synthesized a Control Cross-Linker with no secondary amides in the structure (Figure 4.6). This cross-linker was conjugated to transferrin and the resulting probe was analyzed via IncuCyte (Figure 4.7). The results of the IncuCyte experiment indicated that the fluorescence increase was not due to the presence of secondary amides in the structure.

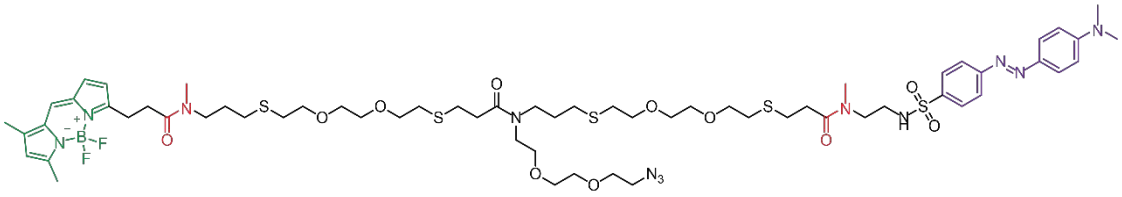

Figure 4.8. Chemical structure of control cross-linker with Dabcyl as the quencher.

One remaining possibility for the increase in signal of the Control Probes is accumulation of fluorescence from incomplete quenching. Another alternative Control Cross-linker was synthesized with Dabcyl as the quencher molecule instead of DNP and no secondary amides in the structure.

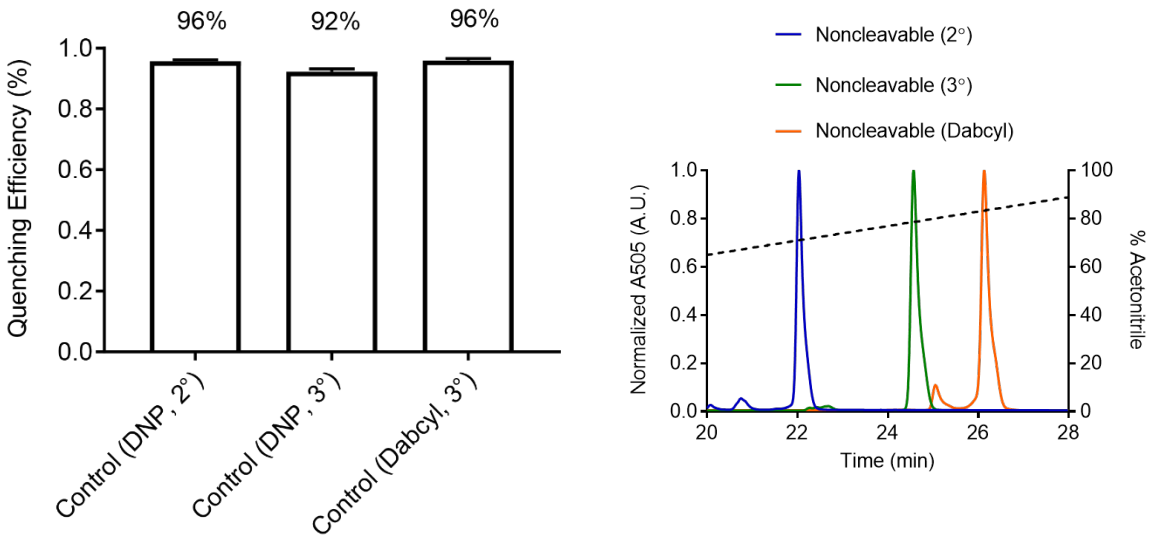

Figure 4.9. Comparison of cross-linker properties. Quenching efficiencies of Control Cross-linker variants (Left) and relative hydrophobicity comparison via RP-HPLC (Right).

The quenching efficiency of the cross-linker was quantified in solution relative to the other two Control Cross-linker variants and it was found to have comparable quenching efficiency (Figure 4.9). We decided not to pursue this Dabcyl cross-linker further due to the similarity in quenching as well as its higher hydrophobicity relative to the cross-linkers with DNP. As analyzed by RP-HPLC, the Dabcyl cross-linker eluted at 83% acetonitrile + 0.1% TFA. The DNP cross-linker with tertiary amides eluted at 80% acetonitrile + 0.1% TFA. The DNP cross-linker with secondary amide eluted at 71% acetonitrile + 0.1% TFA. The Dabcyl cross-linker and DNP cross-linker with tertiary amides are more hydrophobic than the DNP cross-linker with secondary amides. Higher hydrophobicity would translate to decreased solubility in aqueous solvent, thus hampering conjugation to transferrin and other proteins or antibodies. These structural variants also did not improve upon the issue of the noncleavable probe showing increasing intracellular fluorescence over time.

Confocal Imaging for Visualization of Subcellular Localization

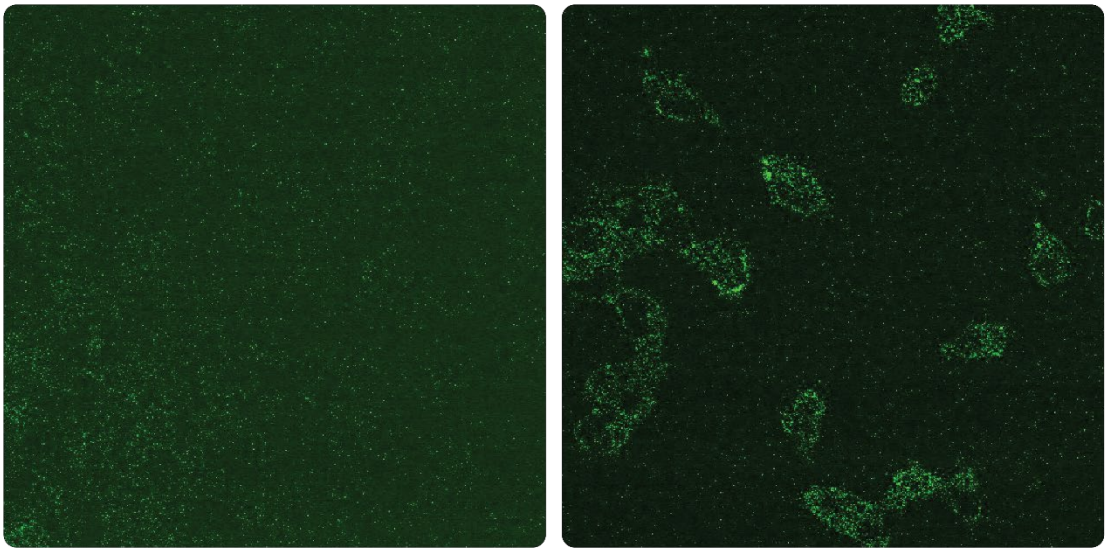

Figure 4.10. Visualization of HeLa cells via confocal laser scanning microscopy of "always on" probes with degree of labelling of 0.6 and 2 cross-linkers per transferrin.

We decided to switch from the IncuCyte technique to live-cell imaging via confocal microscopy in order to obtain information regarding subcellular localization of our probes. When imaging an “always on” probe with comparable degree of labelling to our Cleavable Probe (DOL of approximately 0.6 cross-linkers per transferrin), we found that it was difficult to visualize the fluorescence. Using an “always on” probe with a higher degree of labelling of 2 cross-linkers per transferrin would enable optimal visualization of our cells.

Improving Limitation of Probes with BODIPY

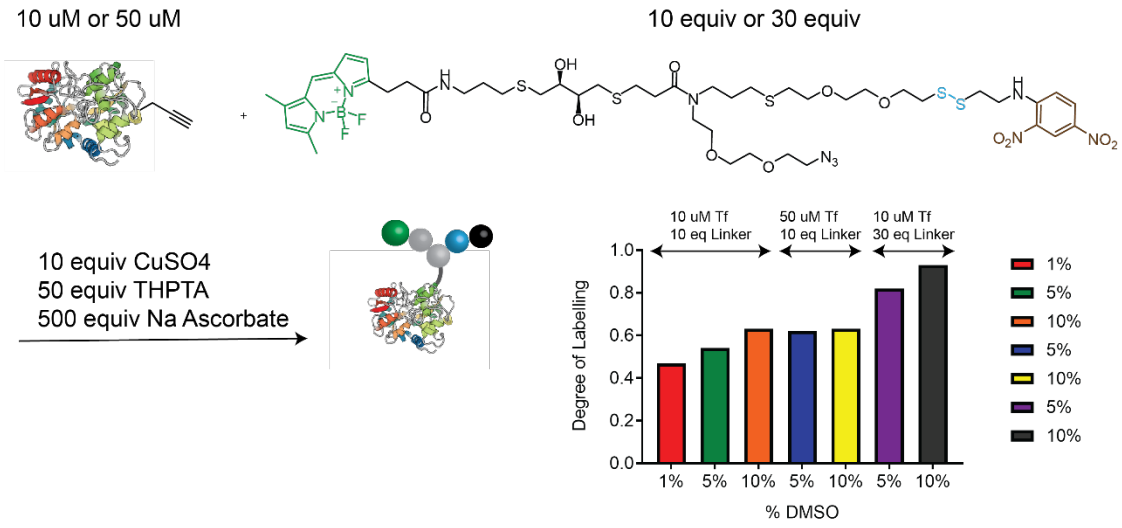

Figure 4.11. Degree of labelling achieved from reacting various excess of the cleavable cross-linker with various concentrations of transferrin.

We attempted to increase the degree of labelling to transferrin by modifying the protein with alkyne groups which are more hydrophilic than DBCO groups. We could then carry out a copper-click reaction with the azide functionality on our probes. The final transferrin probes would be purified by size-exclusion chromatography to remove copper which is toxic to cells. We tried several different conditions to achieve a degree of labelling via this copper-click route, but the highest degree of labelling achieved was 0.9 due to a solubility issue in reacting the relatively hydrophobic Cleavable Cross-linker with the protein (Figure 4.10).

The BODIPY fluorophore had been difficult to work with in general since the boron center is very sensitive to acid. Further, BODIPY NHS is precious as it is time-consuming to synthesize from scratch and too expensive to purchase in the quantities needed for synthesis. As a result, I investigated other options for fluorophores that could be quenched by DNP.

Cleavable Cross-linker (Rhodamine-ss-DNP)

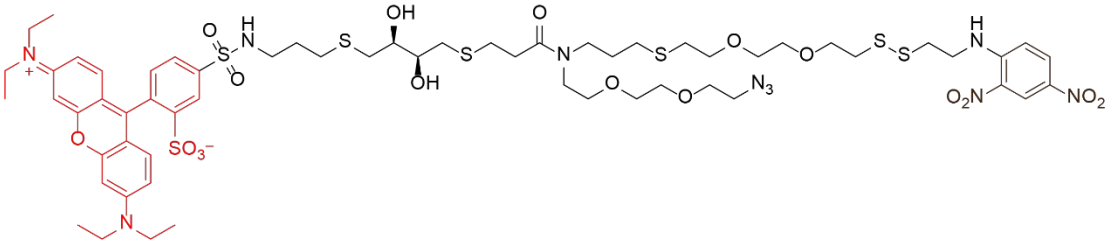

Control Cross-linker (Rhodamine-mal-DNP)

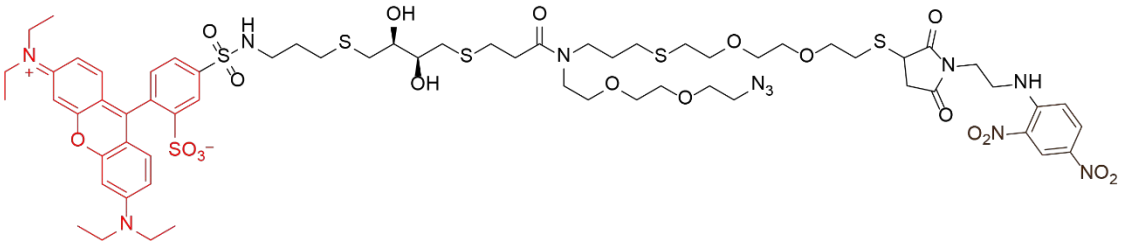

Figure 4.12. Chemical structures of quenched rhodamine-DNP cross-linkers.

It would be ideal to switch to a red fluorophore to improve signal-to-noise relative to cell autofluorescence. We found that the red fluorophore, sulforhodamine B can be quenched by DNP. Rhodamine is also advantageous because it is not as expensive as most fluorophores; the sulfonyl chloride form can be easily modified and costs about $0.30 per mg whereas BODIPY NHS is sold at $110 per mg. This would allow us to scale up synthesis once we have validated the system. Further, from previous conjugation experience, we have found that this fluorophore is fairly stable and insensitive to the concentrations and types of acid and base that it may be exposed to in reactions and purification. Thus, we worked towards synthesizing new variants of our cleavable and control quenched probes in which the BODIPY fluorophore was switched to rhodamine. The structures of these quenched probes are shown in Figure 4.12.

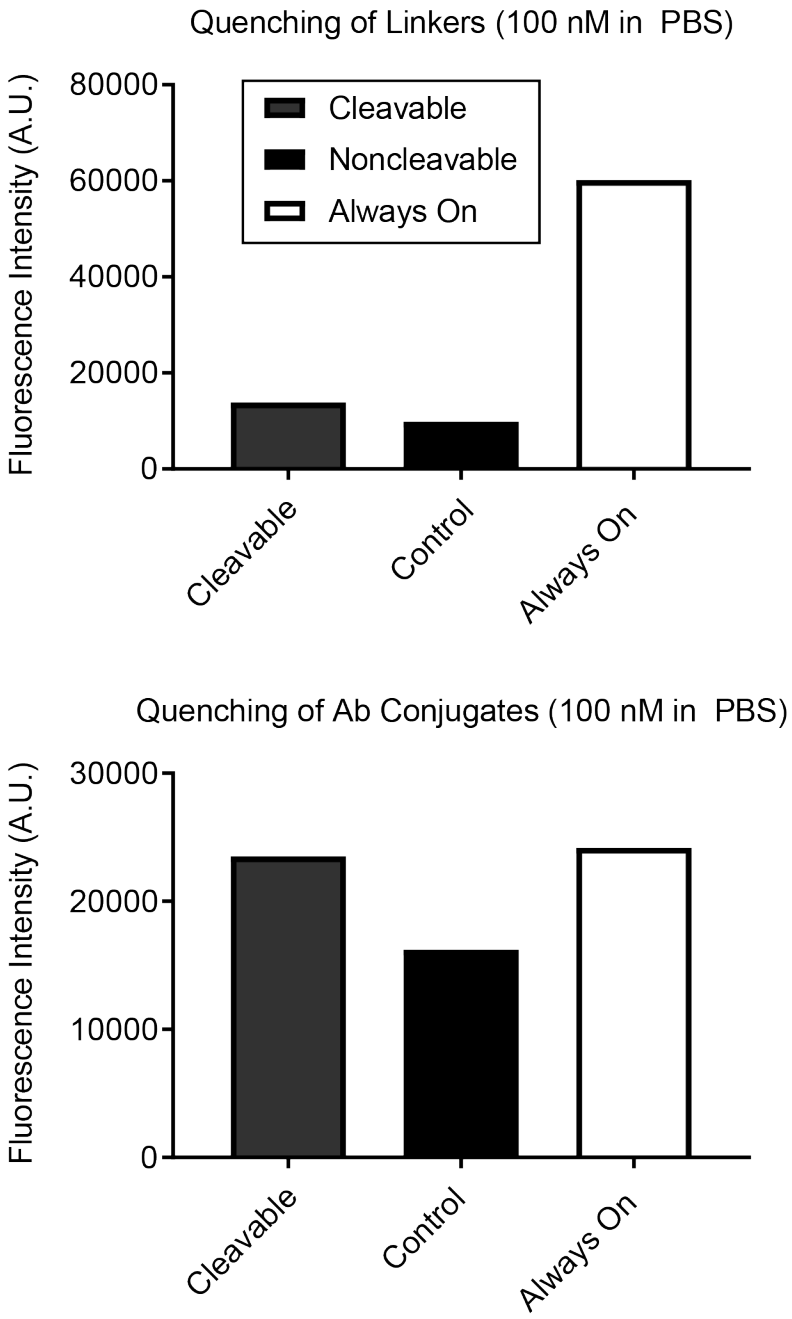

Figure 4.13. Quenching efficiencies of rhodamine-DNP cross-linkers and antibody conjugates.

Another change that was made was the choice of targeting ligand. We wanted to move towards a more therapeutically relevant system, so we decided to conjugate the cross-linkers to trastuzumab, a humanized antibody against the HER2 receptor.

Trastuzumab was modified with 2 DBCO groups using the method for site-specific antibody modification via microbial transglutaminase as shown in Chapter 3. The azide functionalized cross-linkers were then reacted with the DBCO functionality on the antibody to create the final trastuzumab probes. Unfortunately, we found that when conjugated to the antibody the rhodamine-DNP probes were no longer quenched (Figure 4.12). We hypothesize that the orientation of the cross-linkers on the antibody disrupts the contact needed between rhodamine and DNP to achieve quenching.

Cathepsin B Cleavable Probes

In addition to reduction-sensitive disulfide bonds, proteolytically-sensitive dipeptide bonds have been incorporated into antibody-drug conjugates. As such, we synthesized a quenched cross-linker containing the dipeptide valine-citrulline in order to investigate its cleavage. The dipeptide was incorporated with a self-immolating spacer as is used in ADCs to release free drug in its unmodified form. The chemical structures of the cleavable dipeptide probe and the noncleavable control are shown in Figure 4.14.

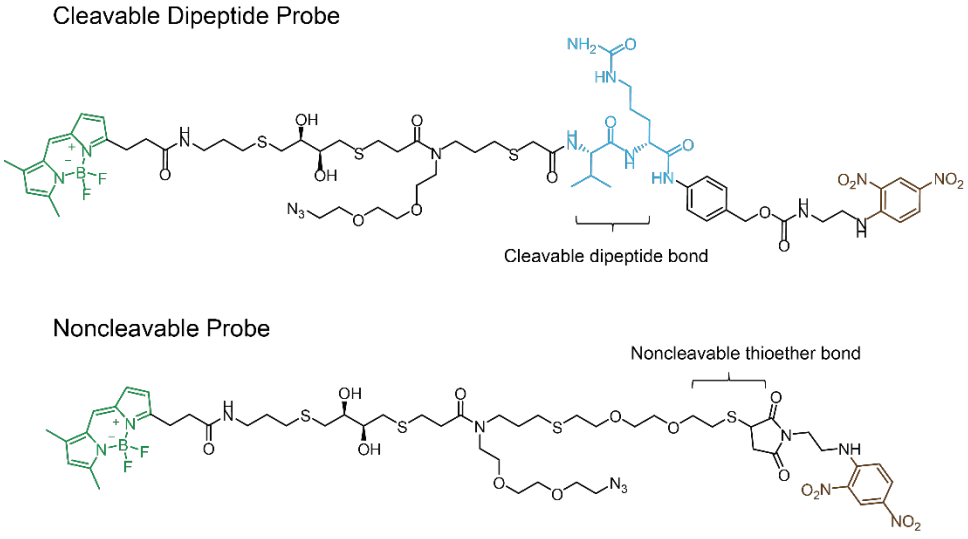

Figure 4.14. Chemical structures of cleavable dipeptide probe and corresponding non-cleavable control.

Enzymatic cleavage of the dipeptide bond was verified by treatment with cathepsin B isolated from human placenta (Sigma) in PBS with EDTA pH 6.0 at 37 °C. The cleavable dipeptide probe showed an increase in fluorescence signal upon treatment with the enzyme, while the noncleavable probe remained quenched (Figure 4.15).

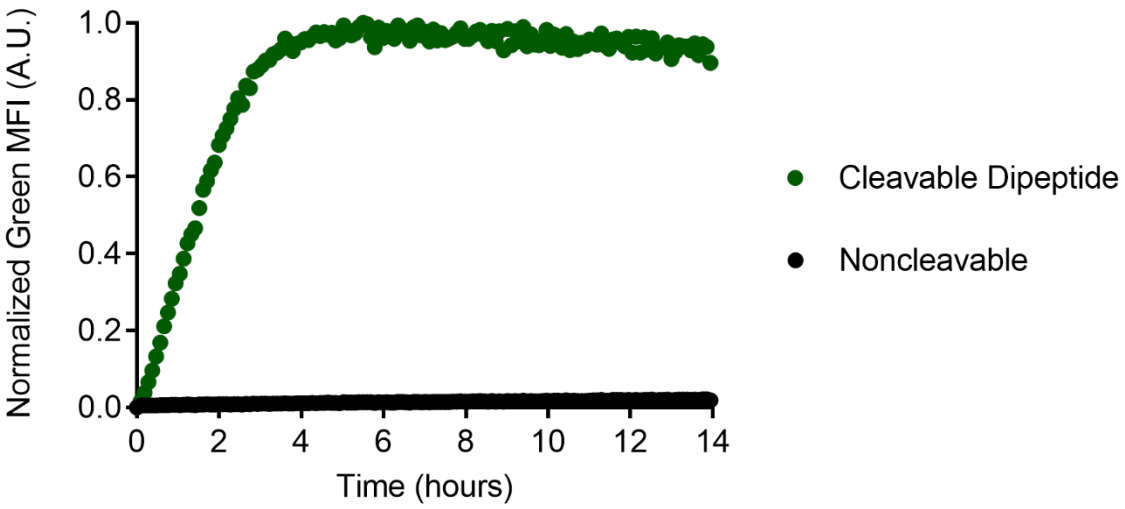

Figure 4.15. Fluorescence dequenching of cleavable dipeptide probe upon treatment with cathepsin B.

The cleavable dipeptide probe was also conjugated to human transferrin through nonspecifically incorporated DBCO groups as previously described and analyzed with the IncuCyte system (Figure 4.16). The results indicated that no significant cleavage was detected within the transferrin-mediated endocytosis pathway.

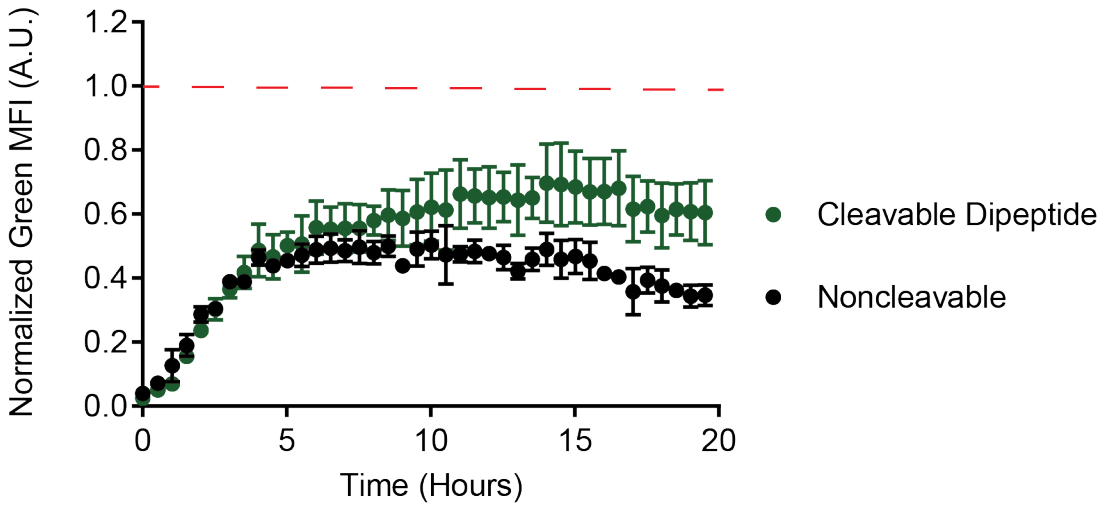

Figure 4.16. IncuCyte analysis of cleavable dipeptide transferrin probe and non-cleavable transferrin probe. The red dashed line represents the "always on" probe.

Confocal microscopy with fixed HeLa cells was then carried out to validate the IncuCyte data and confirm internalization of the cleavable dipeptide probe. Quantification of the confocal images confirmed that there was no significant difference between the cleavable transferrin probe and the noncleavable control (Figure 4.17).

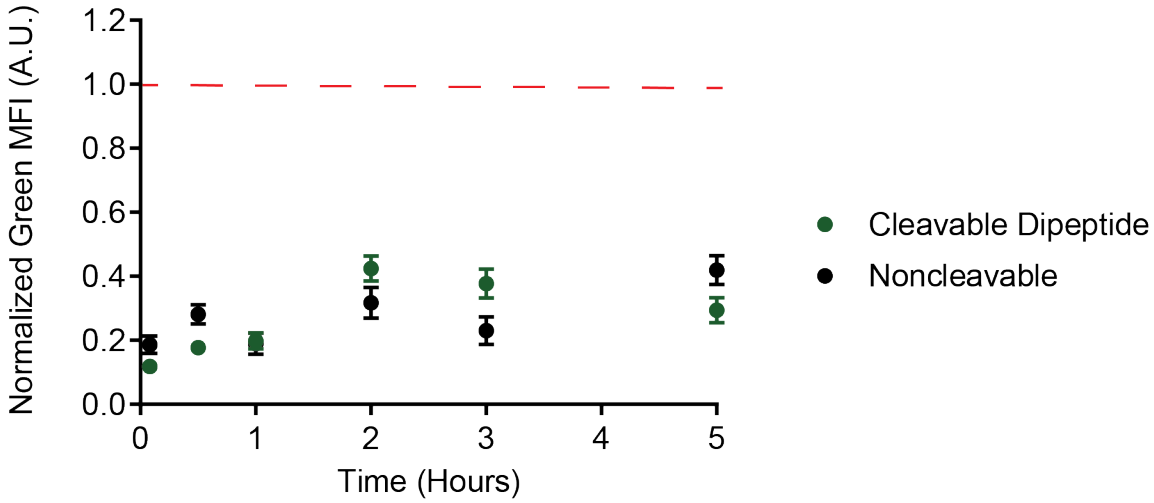

Figure 4.17. Confocal analysis of cleavable disulfide transferrin probe and non-cleavable transferrin probe. The red dashed line represents the "always on" probe.

We had previously tested the cleavage of the dipeptide linker treated with cathepsin B in PBS. However, it is possible that the dipeptide transferrin probe does not cleave due to steric effects from the protein. To verify that the dipeptide probe could be cleaved, it was treated with cathepsin B at 37 °C as described previously. The results shown in Figure 4.18 confirmed that the probe was cleavable.

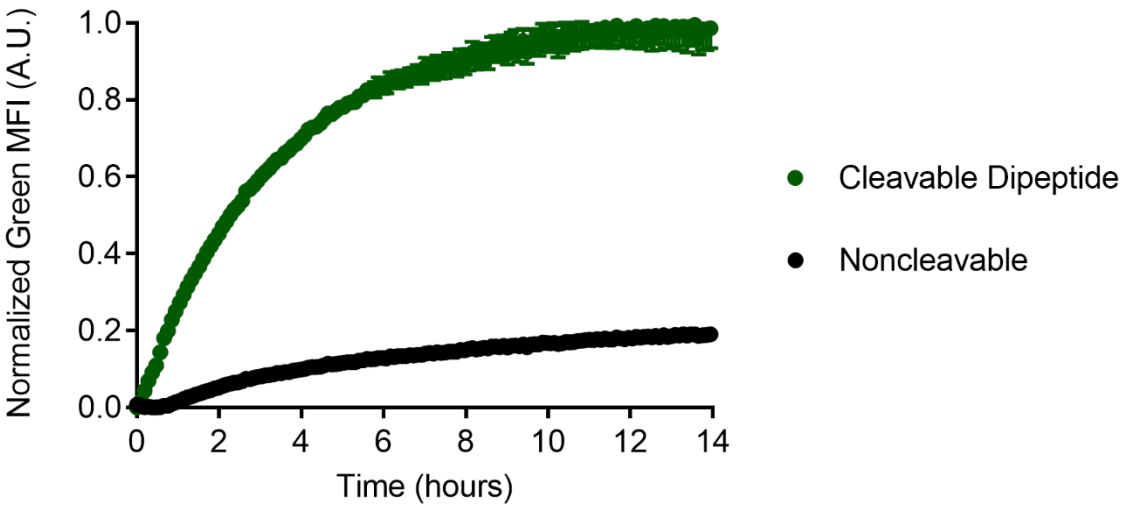

Figure 4.18. Fluorescence dequenching of cleavable dipeptide transferrin probe upon treatment with cathepsin B.

4.3. CONCLUSIONS

In conclusion, we attempted to synthesize “turn on” probes with an improved signal-to-noise ratio for monitoring intracellular bond cleavage. We encountered various issues with these structures. We found that the control cross-linker with BODIPY and DNP as the fluorophore-quencher pair increased in fluorescence over time inside of cells. In an effort to remedy this fluorescence increase, we synthesized a control cross-linker with tertiary amides in its backbone that would not be potentially susceptible to hydrolysis by proteases as are secondary amides. The incorporation of

tertiary amides did not resolve the fluorescence increase. Another control cross-linker was synthesized with Dabcyl as a quencher instead of DNP. This cross-linker did not show improve quenching efficiency and was too hydrophobic for conjugation to proteins and antibodies. Another set of cross-linkers was synthesized with rhodamine and DNP as the fluorophore-quencher pair. However, it was found that once conjugated to an antibody, the structure was no longer quenched. These results seem to indicate that the orientation of the cross-linker on the antibody prevents formation of the ground state complex between the fluorophore and the quencher as needed for contact quenching. A FRET-based system would not experience this loss of quenching upon conjugation. Further, a carefully selected FRET pair in which the donor fluorophore is effectively quenched by the acceptor could essentially be treated as a “turn on” system, as was done in the previous chapter.

Chapter 4 – APPENDIX

General Materials

All chemicals were purchased from MilliporeSigma unless stated otherwise. “Click” chemistry reagents (Alkyne-PEG_4-NHS Ester, Methyltetrazine-PEG_4-NHS Ester, DBCO-PEG_4-NHS Ester, NH_2-PEG_6-Alkyne, and NHS-PEG_6-Alkyne) were purchased from Click Chemistry Tools. Fmoc-N-amido-$dPEG_{12}$-TFP ester was purchased from Quanta BioDesign. Lissamine rhodamine B sulfonyl chloride was purchased from ThermoFisher Scientific.

General Methods

Nuclear Magnetic Resonance (NMR) spectroscopy: ^{1}H NMR spectra were recorded on an INOVA 400 MHz spectrometer. NMR data was analyzed by MestreNova software. ^{1}H NMR chemical shifts are reported in units of ppm relative to chloroform-D ($CDCl_3$, ^{1}H NMR 7.26 ppm).

Liquid Chromatography Mass Spectroscopy (LC-MS): LC-MS experiments were carried out on an Agilent 1100 Series LC with a Poroshell 120 EC-C18 column (100 × 3 mm, 2.7 µm, Agilent Technologies) and an Agilent G1956B Series Single Quadripole MS in positive ion mode for mass detection. The mobile phase for LC-MS (solvent A) was water with 0.1% v/v acetic acid, and the stationary phase (solvent B) was acetonitrile with 0.1% v/v acetic acid. Compounds were eluted at a flow rate of 0.6 mL/min using a gradient of 5-100% solvent B (0-10 minutes) followed by 100% solvent B (10-12 minutes) and equilibrated back to 5% solvent B (12-15 minutes).

High Performance Liquid Chromatography (HPLC) Purification: HPLC purification was performed on an Agilent 1100 Series HPLC system equipped with a UV diode array detector and an 1100 Infinity fraction collector using a reversed-phase C18 column (9.4 x 250 mm, 5 µm). For reagent not solution or acid-sensitive, the mobile phase for HPLC was water with 0.1% v/v trifluoroacetic acid (solvent A) and acetonitrile with 0.1% v/v trifluoroacetic acid (solvent B). For solution and/or acid-sensitive reagents, the mobile phase for HPLC was water (solvent A) and acetonitrile (solvent B). Compounds were eluted at a flow rate of 4 mL/min with a linear gradient of 5% to 95% solvent B (0-30 minutes), 95% to 100% solvent B (30-32.5 minutes), then 100% solvent B (32.5-42.5 min) and equilibrated back to 5% solvent B (42.5-50 minutes) unless stated otherwise. The oligomer was collected based on its absorption at 230 nm. Fluorophore-conjugated oligomer was collected based on its absorption at 566 nm and 647 nm. The fractionated

compounds were transferred to microcentrifuge tubes, dried, and stored until further analysis.

Flash Chromatography: Flash chromatography was performed on a Teledyne ISCO CombiFlash Rf-200i chromatography system equipped with UV-Vis and evaporative light scattering detectors (ELSD).

IncuCyte Live-cell Analysis of Transferrin Probes - One day prior to the experiment, HeLa cells were plated into a 24-well tissue culture treated plate at 50,000 cells/well in DMEM with 10% FBS and 1% Pen/Strep. The media was then removed, the cells were washed with PBS, and then incubated with 150 nM of the transferrin probes in FluoroBrite DMEM with 10% FBS and 1% Pen/Strep. The IncuCyte was equipped with a 10x objective and set to image phase and green fluorescence at 30 minute time intervals. After 24 hours, the images were analyzed using the IncuCyte ZOOM software with phase filters with a minimum area of 100 μm^2 and hole fill cleanup of 100 μm^2. Green fluorescence was analyzed with top-hat background subtraction with a radius of 30 μm and a threshold of 0.3 GCU, edge sensitivity of -59, hole fill cleanup of 10 μm^2, and minimum area filter 30 μm^2.

Nonspecific Protein Conjugation

Nonspecific Alkyne Modification of Trastuzumab - 1 equiv of human holo-transferrin was reacted with 20 equiv of 4,7,10,13,16-pentaoxanonadec-18-ynoic acid N-succinimidyl ester (50 mg/mL in dry DMSO) in borate-buffered saline (100 mM borate, 150 mM NaCl) pH 8.2 for 5.5 hours at room temperature. The final concentration of transferrin was 250 μM. The mixture was then spin filtered with phosphate-buffered saline (137 mM NaCl, 2.7 mM KCl, 10 mM Na_2HPO_4, 1.8 mM KH_2PO_4) pH 7.4 using an Amicon Ultra-0.5 centrifugal filter unit with Ultracel-30 membrane.

Conjugation of Alkyne-modified Transferrin to Azide-functionalized Linkers - 1 equiv of transferrin-alkyne (350 μM in PBS pH 7.4) was reacted with 10 or 30 equiv of quenched linker (10 mg/ml in dry DMSO), 10 equiv of copper sulfate pentahydrate, 50 equiv of tris(3-hydroxypropyltriazolylmethyl)amine, and 500 equiv of sodium ascorbate in 1X PBS pH 7.4 with up to 10% DMSO for 5 hours at room temperature. The final concentration of transferrin-alkyne was either 10 μM or 50 mM. The mixture was then spin filtered with 1X PBS pH 7.4 using an Amicon Ultra-0.5 centrifugal filter unit with Ultracel-30 membrane.

Site-Specific Antibody Modification

Site-Specific Dibenzocyloocytne (DBCO) Modification of Trastuzumab via Microbial Transglutaminase (MTG): 1 equiv of trastuzumab at 24 mg/ml in phosphate-buffered saline (137 mM NaCl, 2.7 mM KCl, 10 mM Na_2HPO_4, 1.8 mM KH_2PO_4) pH 7.4 was reacted with 240 units of PNGase F (500 units/μL in 50% glycerol). The final concentration of antibody was 1 mg/mL in phosphate-buffered saline pH 7.4. The reaction was carried out for 1 day at 37 °C. To this mixture was then added 160 equiv of DBCO-PEG_4-NH_2 (100 mM in ultrapure water) and 0.75 equiv microbial transglutaminase (159 μM in sodium acetate buffer (50 mM NaOAc, 300 mM NaCl) pH 5). The MTG reaction was carried out for 2 days at 37 °C. The mixture was then spin filtered with phosphate-buffered saline pH 7.4 using an Amicon Ultra-0.5 centrifugal filter unit with Ultracel-50 membrane.

Reaction of DBCO-modified Trastuzumab with Azide Functionalized Linkers: 1 equiv of DBCO-modified trastuzumab at 290 μM in phosphate-buffered saline pH 7.4 was reacted with 10 equiv of linker (25 mg/ml in dimethyl sulfoxide (DMSO)). The reaction was carried out for 1 day at 37 °C. The final concentration of antibody was 10 μM in phosphate-buffered saline pH 7.4 with 5% DMSO. The mixture was then spin filtered with phosphate-buffered saline pH 7.4 using an Amicon Ultra-0.5 centrifugal filter unit with Ultracel-50 membrane.

Biological Assays

Cathepsin B Cleavage Assay - Each linker was incubated at 2.5 μM with 1.8 μM cathepsin B in pH 6 buffer (352mM KH_2PO_4; 48mM NaH_2PO_4; 4mM EDTA) at 40°C. Fluorescence measurements were taken at regular intervals on the TECAN M1000 Pro Plate Reader using an excitation of 490 nm and an emission of 515 nm. Signals were normalized to fluorescence of the sample incubated in a buffer control.

Synthesis of 2-(phenyldithio)-ethanamine – 1 equiv of **tert-butyl N-(2-mercaptoethyl)carbamate was mixed with 1 equiv of 2,2'-dithiodipyridine and 2 equiv of Et_3N. The final concentration** of **tert-butyl N-(2-mercaptoethyl)carbamate was 500 mM in DMSO. The mixture was reacted overnight at room temperature and purified via semi-preparative RP-HPLC. The** compound was eluted at a flow rate of 4 mL/min with a linear gradient of 5% to 95% solvent B (0-15 minutes), then 95% solvent B (15-20 min) and equilibrated back to 5% solvent B (20-30 minutes). **The product eluted at 12.4 minutes.** The HPLC-purified product was then mixed at 50 mM in 50% trifluoroacetic acid (TFA) in DCM for 1 hour. The TFA and DCM were then removed under vacuum to yield the desired product, 2-(phenyldithio)-ethanamine.

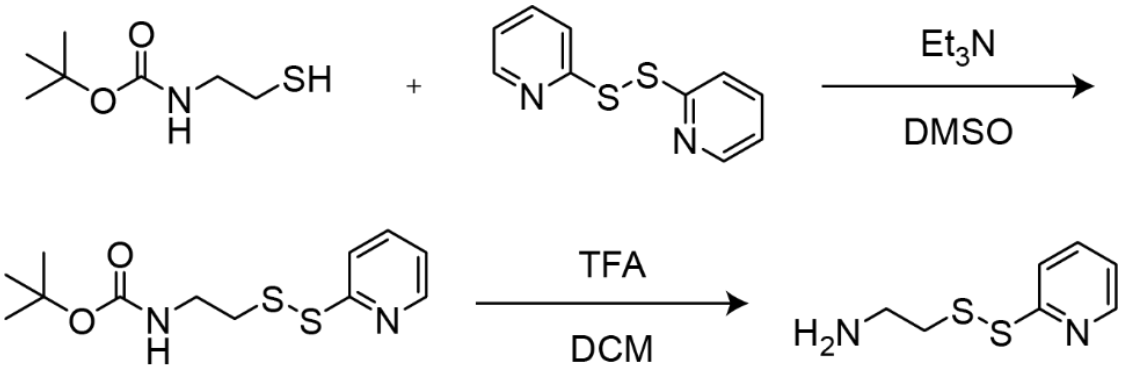

Figure A4.1. Scheme for synthesis of 2-(phenyldithio)-ethanamine.

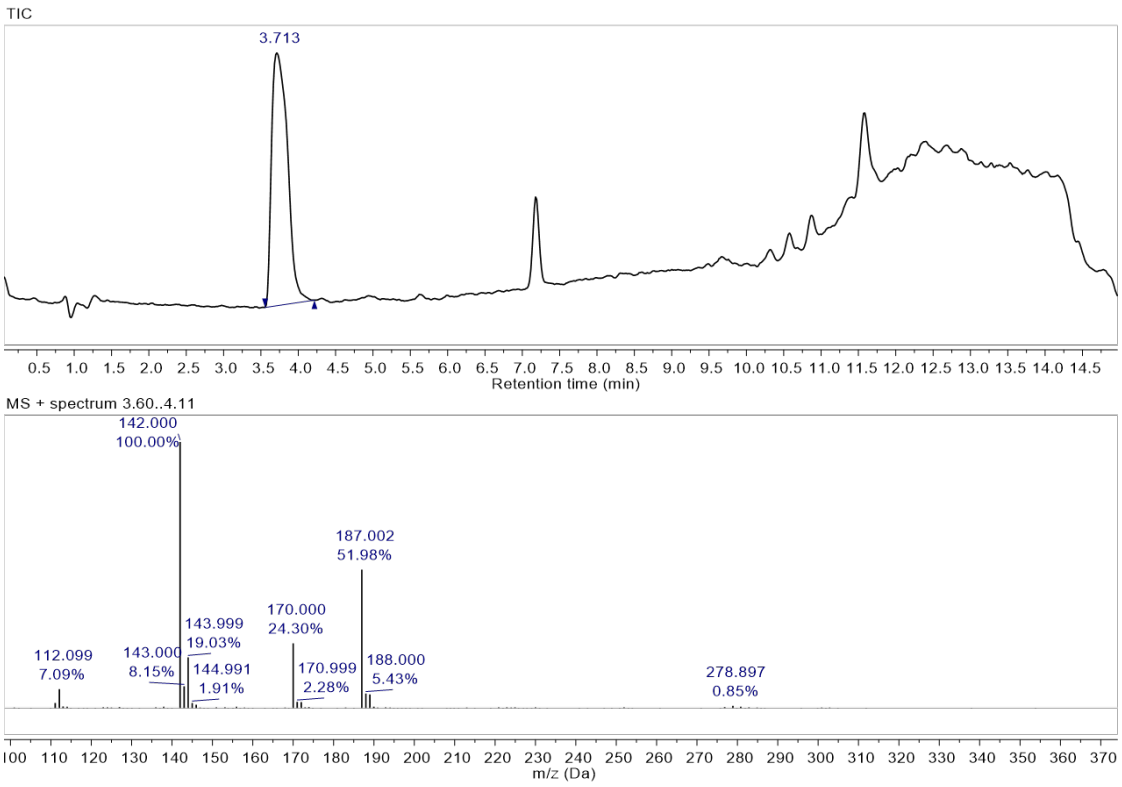

Figure A4.2. LC-MS of 2-(phenyldithio)-ethanamine.

Synthesis of 2,4-dinitro-N-(2-(pyridin-2-yldisulfaneyl)ethyl)aniline: 1 equiv of chloro-2,4-dinitrobenzene was dissolved at 100 mg/ml in DMSO. To this solution was added 1.5 equiv of 2-(phenyldithio)-ethanamine (50 mg/ml in DMSO) and 4 equivalents of Et_3N. The final concentration of chloro-2,4-dinitrobenzene was 105 mM. The mixture was reacted overnight at room temperature and then purified via semi-preparative RP-HPLC. **The** compound was eluted at a flow rate of 4 mL/min with a linear gradient of 5% to 95% solvent B (0-45 minutes), then 95% solvent B (45-55 min) and equilibrated back to 5% solvent B (55-60 minutes). The product eluted at 31.5 minutes in 86% yield. The product was characterized by LC-MS (*m/z* calculated: 353.04 observed: 353.00 $[M+H]^+$).

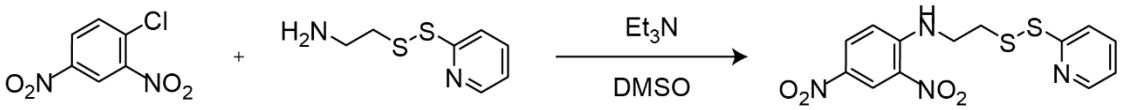

Figure A4.3. Reaction scheme for synthesis of 2,4-dinitro-N-(2-(pyridin-2-yldisulfaneyl)ethyl)aniline.

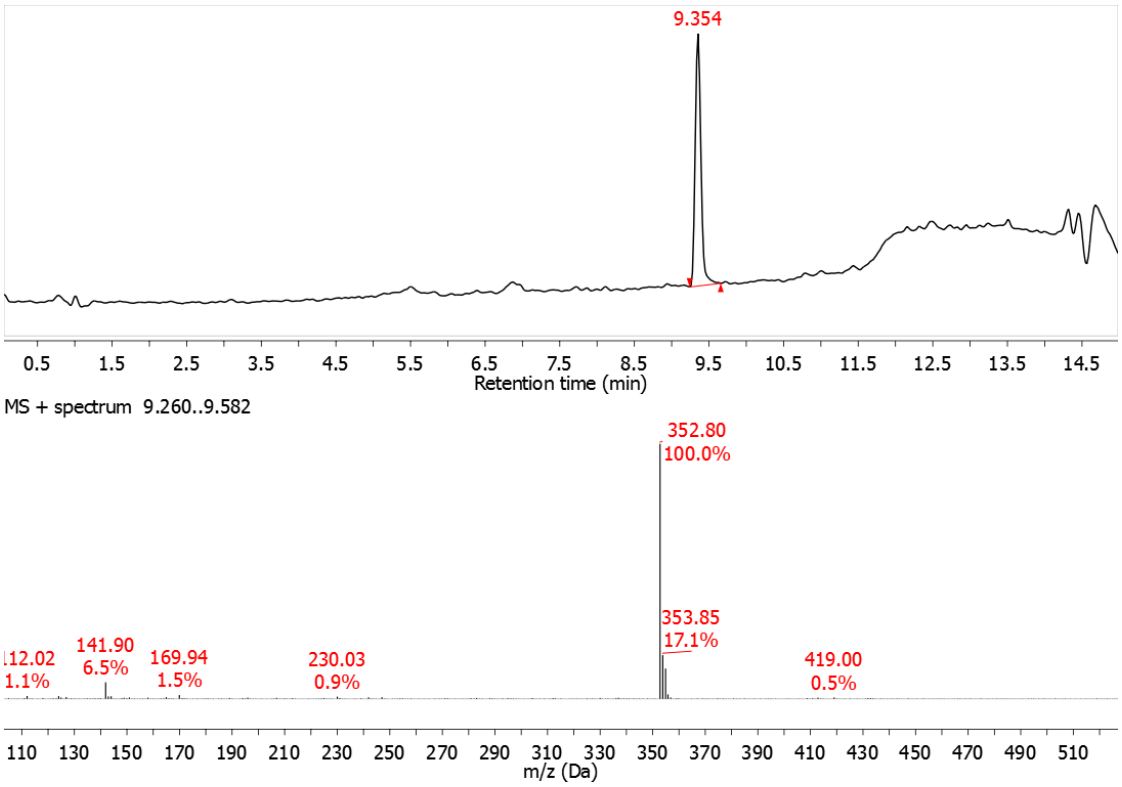

Figure A4.4. LC-MS spectra of 2,4-dinitro-N-(2-(pyridin-2-yldisulfaneyl)ethyl)aniline.

*Synthesis of Compound **(2)*** - 1 equiv of Compound **(1)** was dissolved at 10 mg/ml in DMSO. To this solution was added 5 equiv of 2,4-dinitro-N-(2-(pyridin-2-yldisulfaneyl)ethyl)aniline (39 mg/ml in DMSO) and 10 equiv of Et_3N. The final concentration of Compound **(1)** was 9.7 mM in DMSO. The mixture was reacted overnight at room temperature and purified via semi-preparative RP-HPLC. The product eluted at 19.6 minutes. The product was characterized by LC-MS (*m/z* calculated: 903.29 observed: 903.10 $[M+H]^+$).

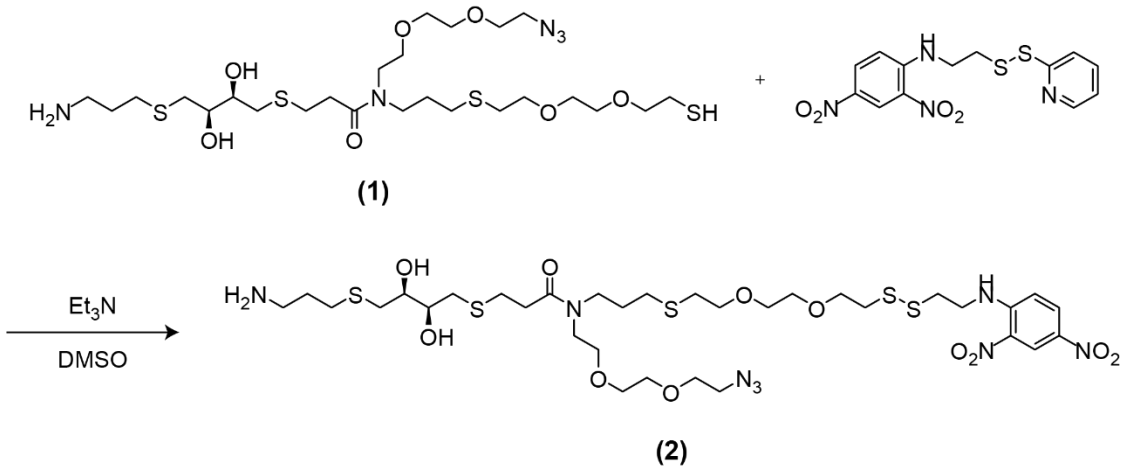

Figure A4.5. Reaction scheme for synthesis of Compound **(2)**.

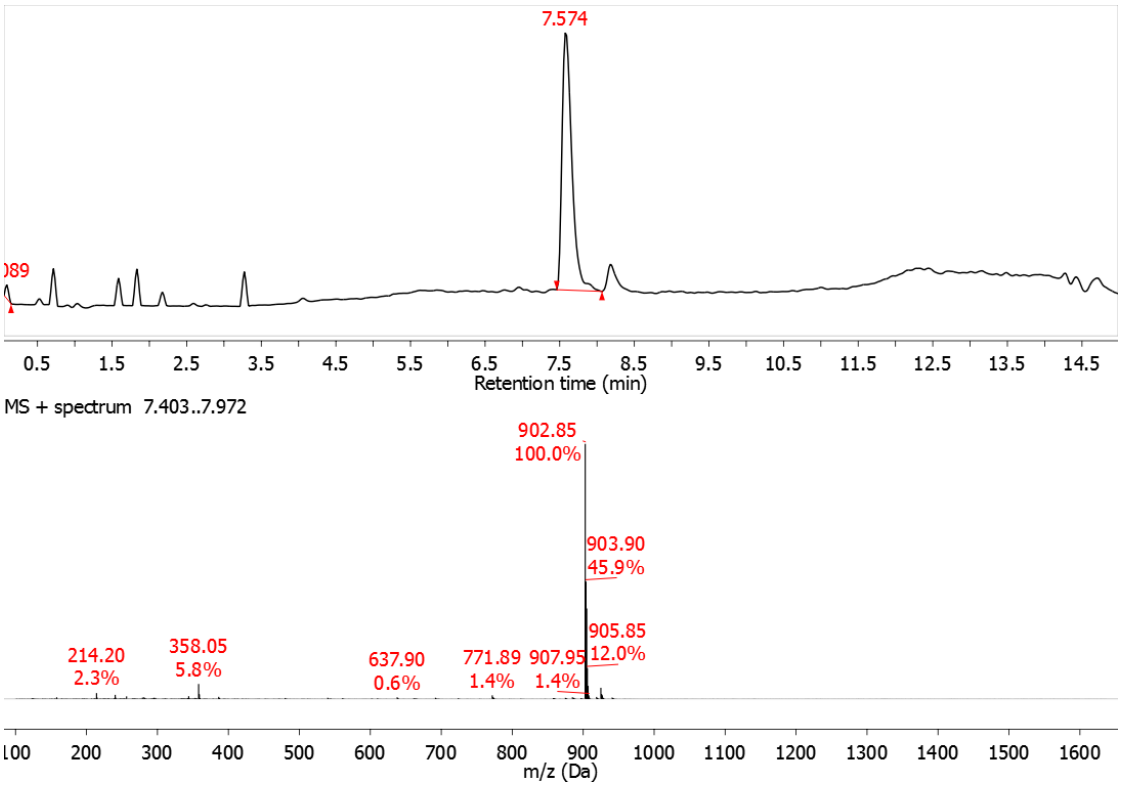

Figure A4.6. LC-MS of Compound **(2)**.

*Synthesis of Compound **(4)*** - 1 equiv of Compound **(2)** was dissolved at 7.1 mg/ml in DMSO. To this solution was added 2.5 equiv of Compound **(3)** (6 mg/ml in DMSO) and 20 equiv of Et_3N. The final concentration of linker was 5.2 mM in DMSO. The mixture was reacted overnight at room temperature and then purified via semi-preparative RP-HPLC. **The** compound was eluted at a flow rate of 4 mL/min with a linear gradient of 5% to 95% solvent B (0-45 minutes), then 95% solvent B (45-55 min) and equilibrated back to 5% solvent B (55-60 minutes). The product eluted at 35.7 minutes. The product was characterized by LC-MS (*m/z* calculated: 1177.40 observed: 1177.20 $[M+H]^+$).

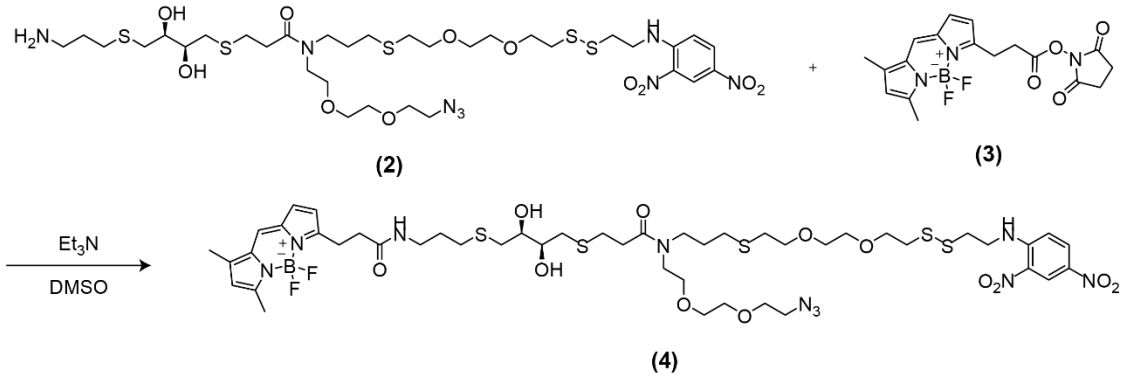

Figure A4.7. Reaction scheme for synthesis of Compound **(4)**.

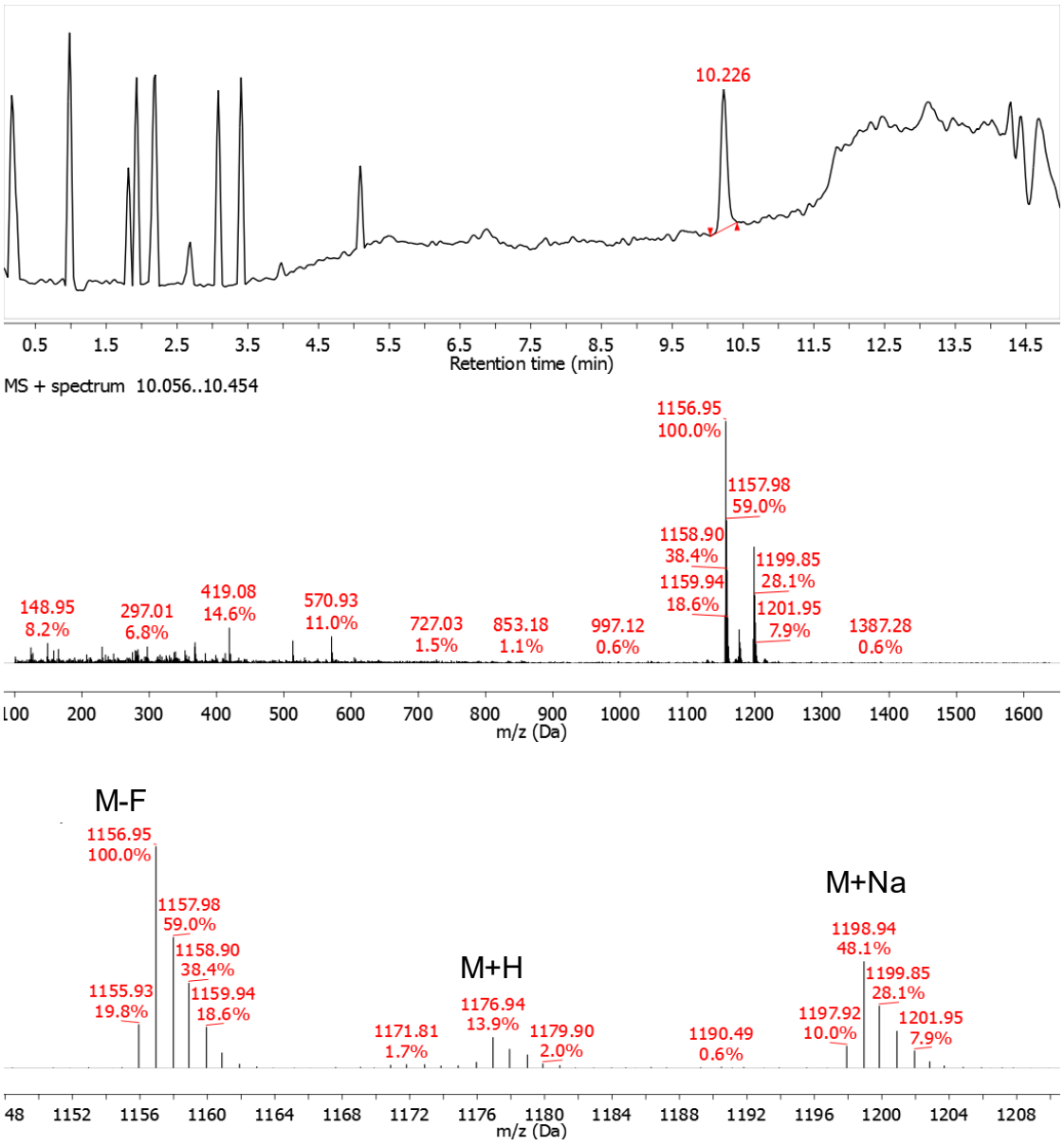

Figure A4.8. LC-MS of Compound **(4)** with zoom in showing fragmentation typically seen with BODIPY-containing compounds.

*Synthesis of Compound **(5)*** – 1 equiv of Compound **(1)** was dissolved at 10 mg/ml in DMSO. To this solution was added 1.5 equiv of 1-2-((2,4-dinitrophenyl)amino)ethyl)-1H-pyrrole-2,5-dione (16.7 mg/ml in DMSO). The final concentration of Compound **(1)** was 3.1 mM in 21% 1X phosphate-buffered saline (PBS) in DMSO. The mixture was reacted overnight at room temperature and purified via semi-preparative RP-HPLC. **The** compound was eluted at a flow rate of 4 mL/min with a linear gradient of 5% to 95% solvent B (0-45 minutes), then 95% solvent B (45-55 min) and equilibrated back to 5% solvent B (55-60 minutes). The product eluted at 24.5 minutes. The product was characterized by LC-MS (*m/z* calculated: 968.34 observed: 968.10 $[M+H]^+$).

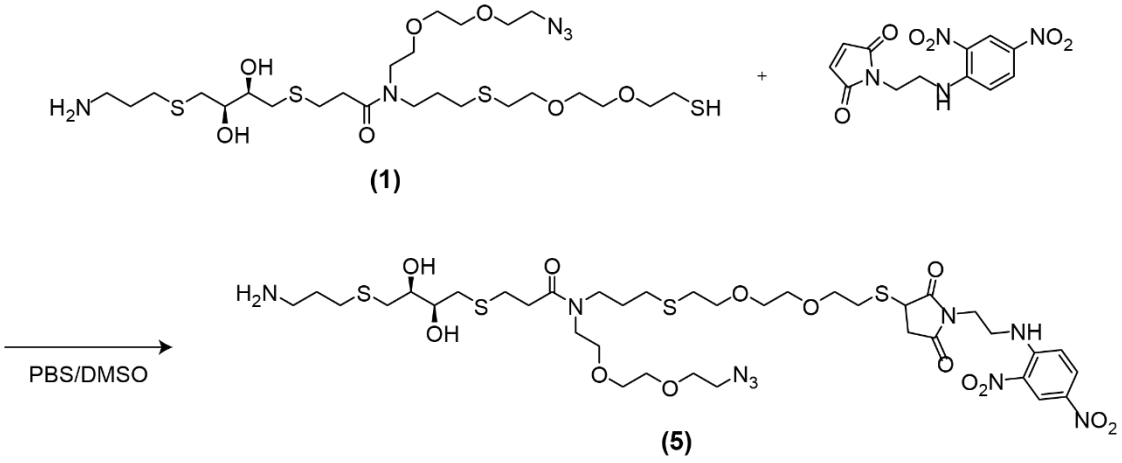

Figure A4.9. Reaction scheme for synthesis of Compound **(5)**.

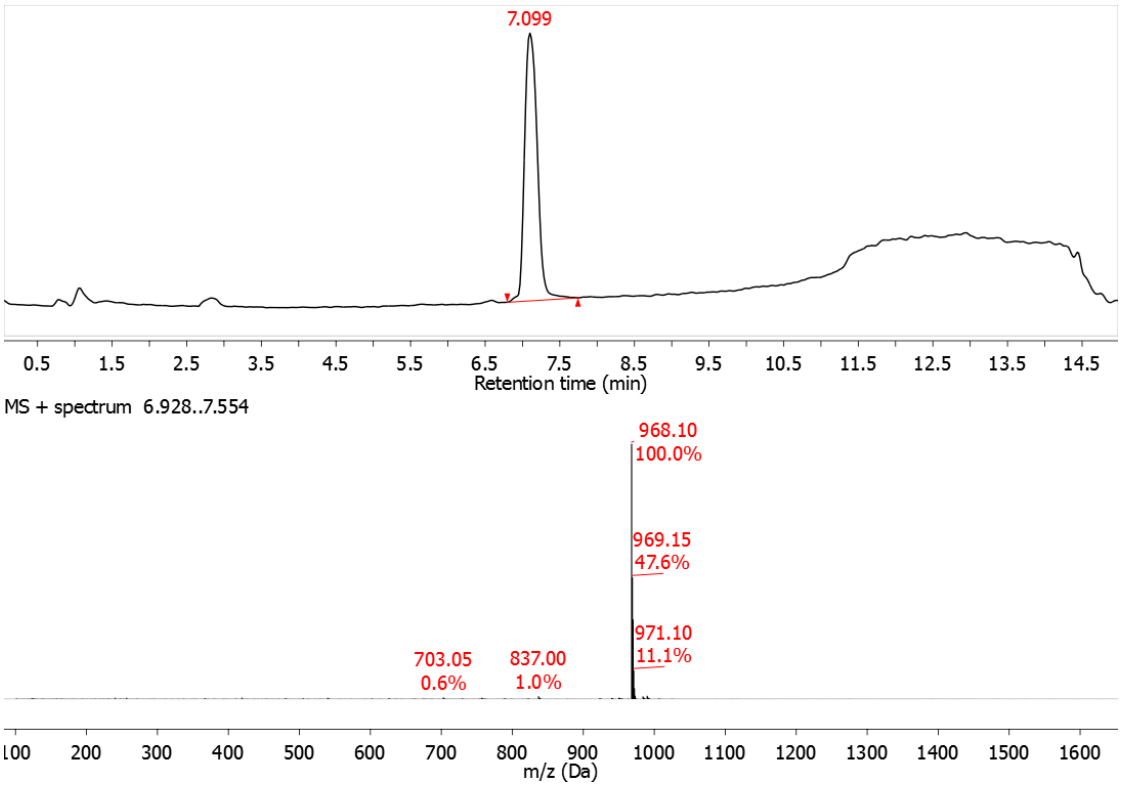

Figure A4.10. LC-MS of Compound **(5)**.

*Synthesis of Compound **(6)*** – 1 equiv of Compound **(5)** was dissolved at 10.5 mg/ml in DMSO and mixed with 2.5 equiv of Compound **(3)** (6 mg/ml in DMSO) and 20 equivalents of Et_3N. The final concentration of linker was 3.76 mM in DMSO. The mixture was reacted overnight at room temperature and purified via semi-preparative RP-HPLC. **The** compound was eluted at a flow rate of 4 mL/min with a linear gradient of 5% to 95% solvent B (0-45 minutes), then 95% solvent B (45-55 min) and equilibrated back to 5% solvent B (55-60 minutes). The product eluted at 41 minutes. The product was characterized by LC-MS (*m/z* calculated: 1242.45 observed: 1242.00 $[M+H]^+$).

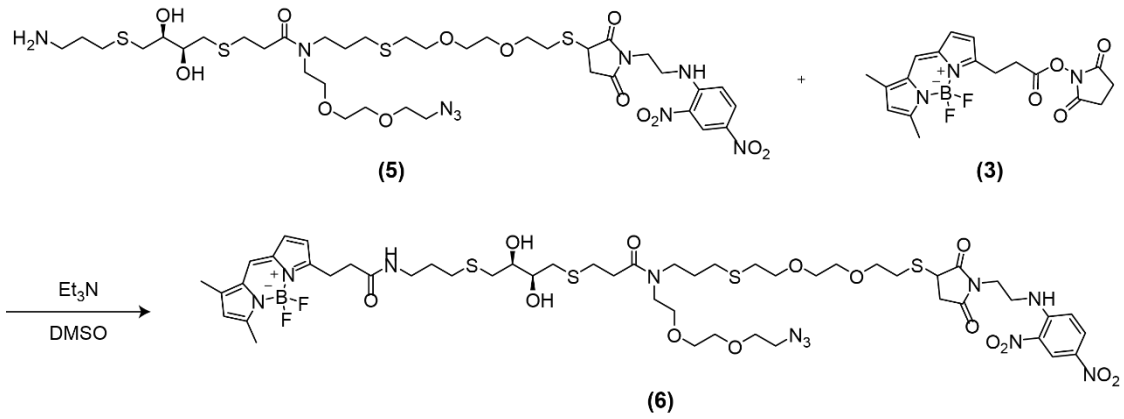

Figure A4.11. Reaction scheme for synthesis of Compound **(6)**.

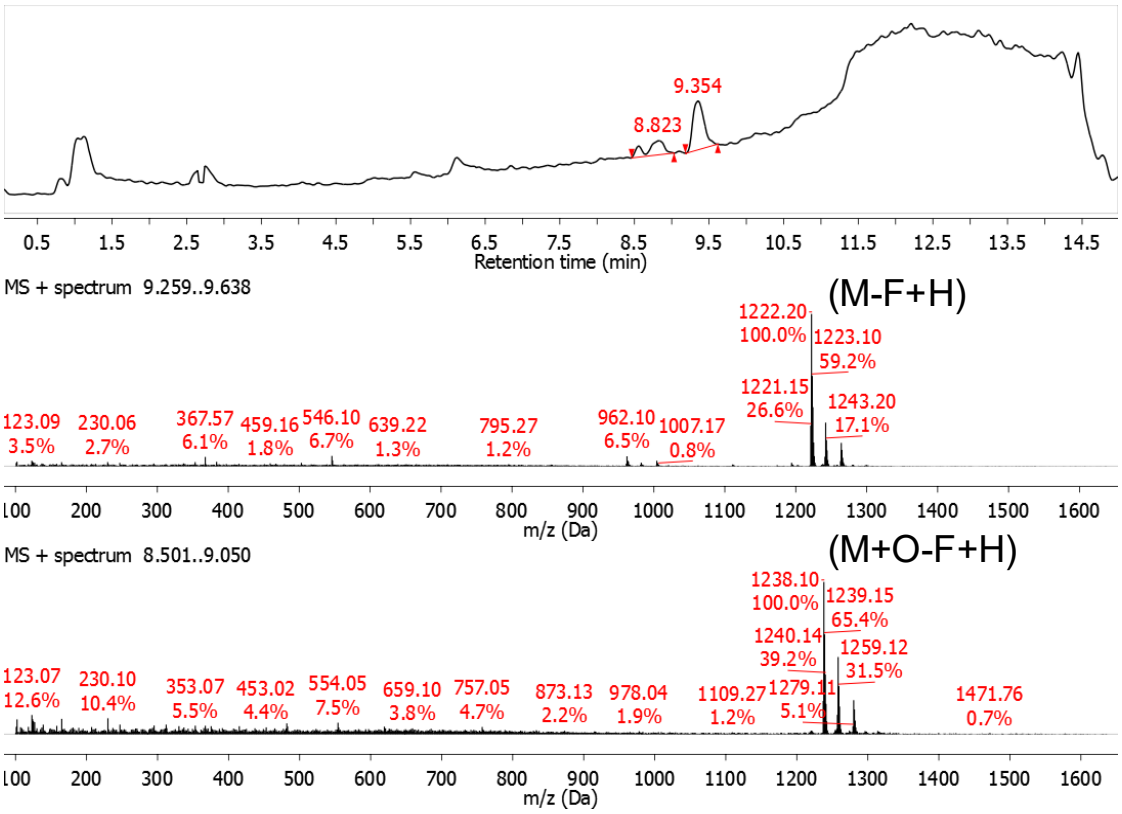

Figure A4.12. LC-MS of Compound **(6)** indicating BODIPY fragmentation and thioether oxidation.

Synthesis of (2) – 1 equiv of **(1)** was dissolved at 6 mg/ml in dry DMSO. To this solution, 3 equiv of 2-(2-pyridyldithio)ethylamine hydrochloride (100 mg/ml in dry DMSO) and 2 equiv of Et_3N were added. The final concentration of **(1)** was 13.7 mM. The mixture was reacted overnight at room temperature and then purified via semi-preparative RP-HPLC. The product was characterized by LC-MS (*m/z* calculated: 461.15 observed: 461.10 $[M+H]^+$).

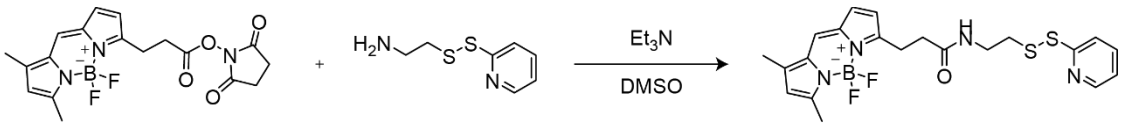

(3) **(7)**

Figure A4.13. Reaction scheme for synthesis of Compound **(7)**.

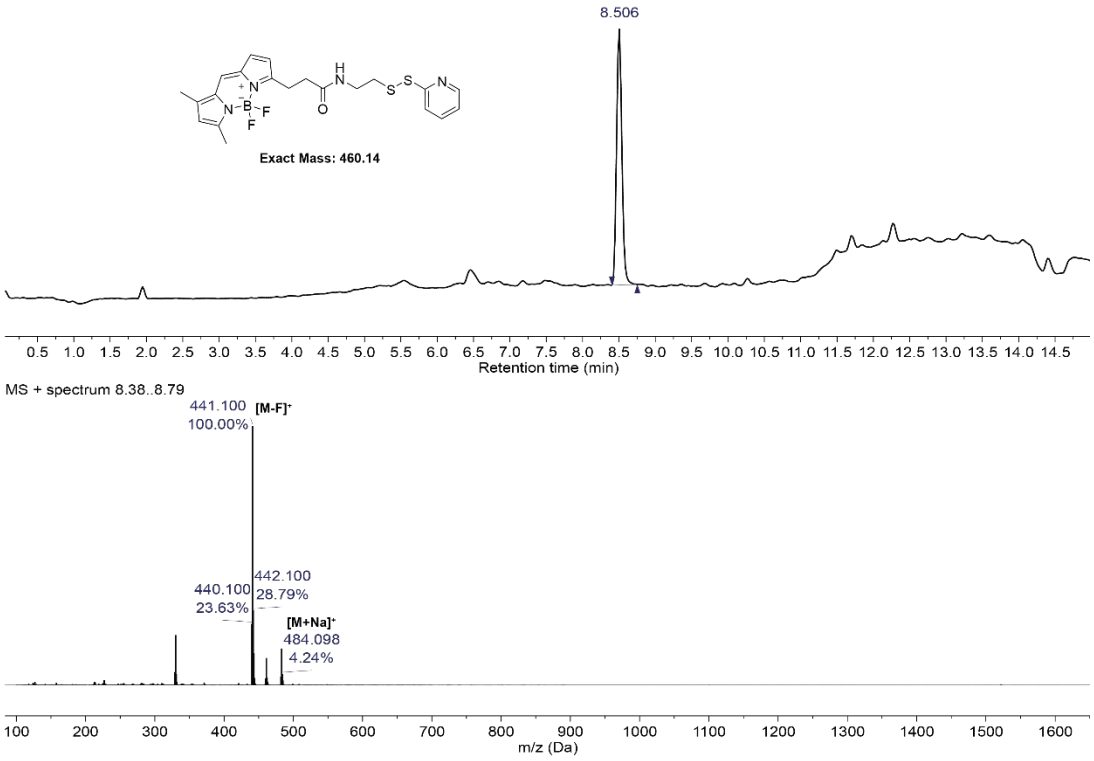

Figure A4.14. LC-MS of Compound **(7)**.

Synthesis of (4) – 1 equiv of **(1)** was dissolved at 10 mg/ml in dry DMSO. To this solution, 1 equiv of **(3)** and 20 equiv of Et_3N were added. The mixture was reacted overnight at room temperature. To the mixture was then added 3 equiv of 6-(2,4-dinitrophenyl)aminohexanoic acid succinimidyl ester (25 mg/ml in dry DMSO). The final concentration of **(1)** was 1.7 mM in DMSO. The resulting mixture was reacted overnight and then purified via semi-preparative RP-HPLC. **The** compound was eluted at a flow rate of 4 mL/min with a linear gradient of 5% to 95% solvent B (0-45 minutes), then 95% solvent B (45-55 min) and equilibrated back to 5% solvent B (55-60 minutes). The product eluted at 35 minutes. The product was characterized by LC-MS (*m/z* calculated: 1290.49 observed: 1290.20 $[M+H]^+$).

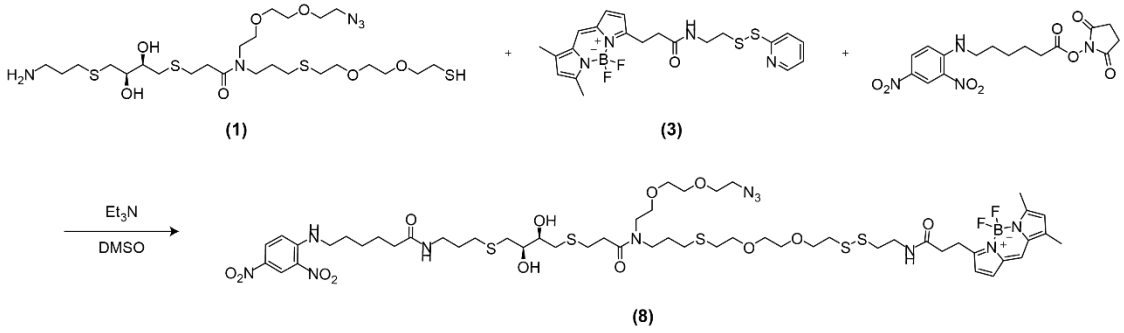

Figure A4.15. Synthesis of compound **(8)**.

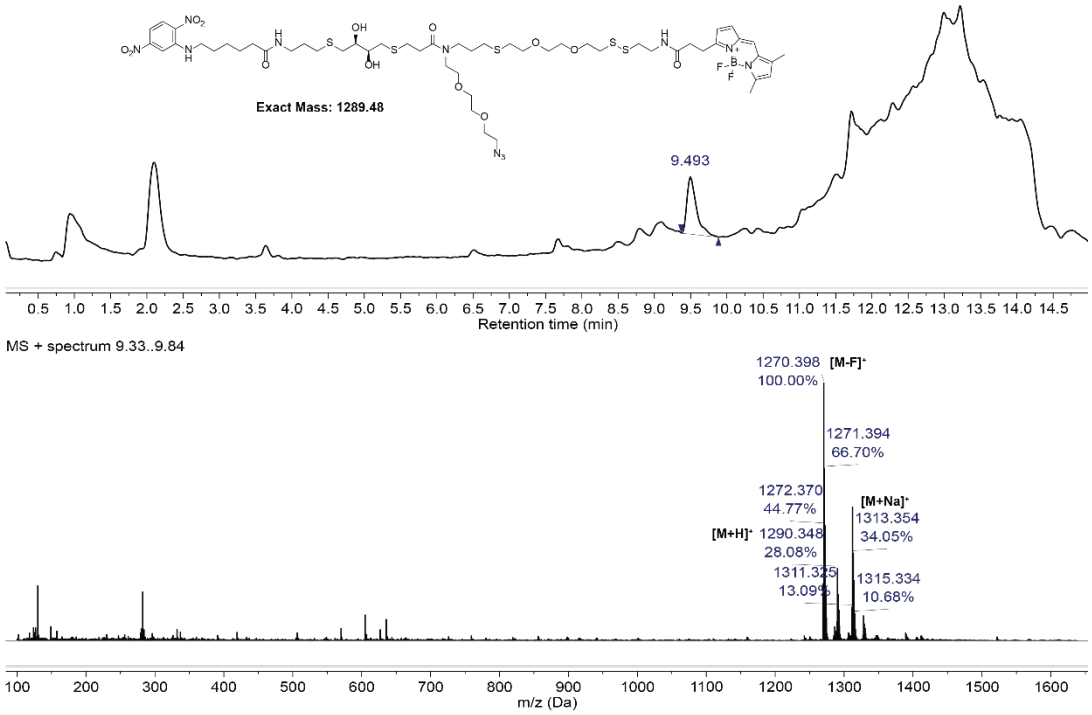

Figure A4.16. LC-MS of Compound **(8)**.

Synthesis of tert-butyl N-methyl-N-(prop-2-en-1-yl)carbamate – N-allylmethylamine (427 mg, 6 mmol) was dissolved at 151 mM in dichloromethane (DCM). To this solution was added 1.2 equiv of $E_{t3}N$ (729 mg, 7.2 mmol) and the mixture was allowed to equilibrate for 10 minutes on ice. Next, 1.2 equiv of di-tert-butyl dicarbonate (1090.9 mg, 5 mmol) dissolved at 1.6 M in DCM was added over 5 minutes. The final concentration of N-allylmethylamine was 132 mM. The mixture was left on ice for 1 hour and then removed from the ice and reacted at room temperature overnight. The reaction was quenched with 100 mL of water and extracted with DCM (100 mL, 3x). The DCM layer was collected and concentrated under vacuum in 82% yield. The crude product was used without further purification. The product was characterized by ^{1}H NMR and LC-MS (*m/z* calculated: 116.07 observed: 116.00 $[M\text{-t-Butyl+H}]^+$). ^{1}H NMR (400 MHz, $CDCl_3$) δ 5.82-5.70 (m, 1H), 5.18-5.07 (m, 2H), 3.87-3.74 (m, 2H), 2.86-2.76 (s, 3H), 1.52-1.37 (s, 9H).

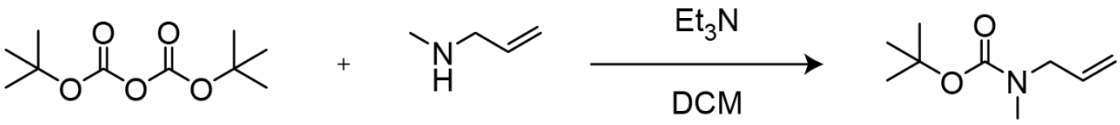

Figure A4.17. Scheme for synthesis of tert-butyl N-methyl-N-(prop-2-en-1-yl) carbamate.

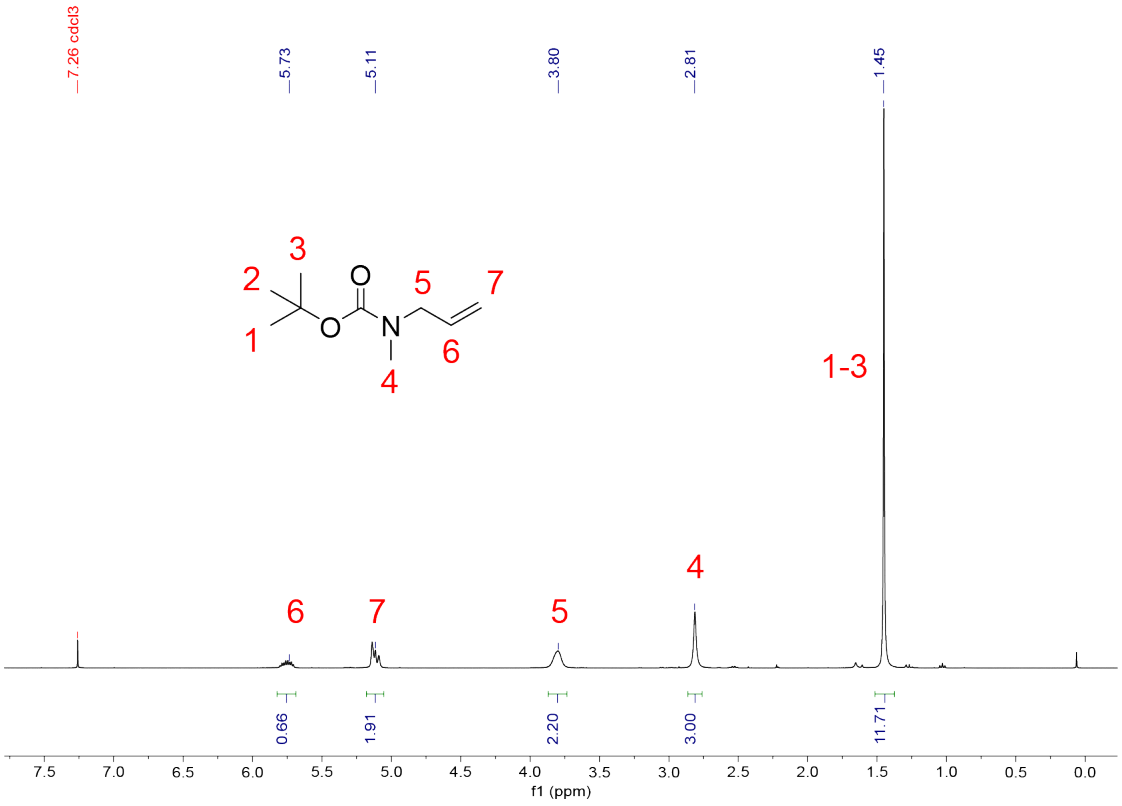

Figure A4.18. ^{1}H NMR (400 MHz, $CDCl_3$) of tert-butyl N-methyl-N-(prop-2-en-1-yl) carbamate.

Synthesis of S-[2-[2-(2-mercaptoethoxy)ethoxy]ethyl] ester ethanethioic acid – 2,2'-(ethylenedioxy)diethanethiol (500 mg, 2.7 mmol) was dissolved at 150 mM in THF. To this solution was added 3 equiv of Et_3N (832 mg, 8.2 mmol) and the mixture was allowed to equilibrate on ice for 10 minutes. Next, 1.05 equiv of acetyl chloride (216 mg, 2.9 mmol) dissolved at 1.6 M in THF was added over 2 hours. The mixture was then removed from the ice and reacted at room temperature overnight. The reaction was quenched with 100 mL of water and extracted with EtOAc (100 mL, 3x). The EtOAc layer was collected and concentrated under vacuum, and the product was purified by flash chromatography (12 g silica, 0-40% ethyl acetate in hexanes) in 42% yield. The product was characterized by ^{1}H NMR. ^{1}H NMR (400 MHz, $CDCl_3$) δ 3.64-3.54 (m, 8H), 3.11-3.05 (t, 2H), 2.72-2.64 (q, 2H), 2.35-2.29 (s, 3H), 1.61-1.54 (t, 1H).

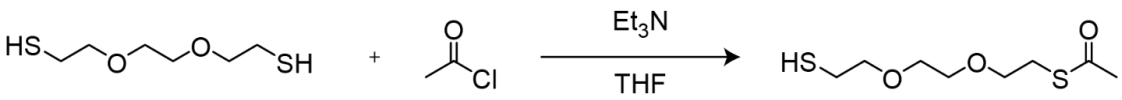

Figure A4.19. Scheme for synthesis of *S*-[2-[2-(2-mercaptoethoxy)ethoxy]ethyl] ester ethanethioic acid.

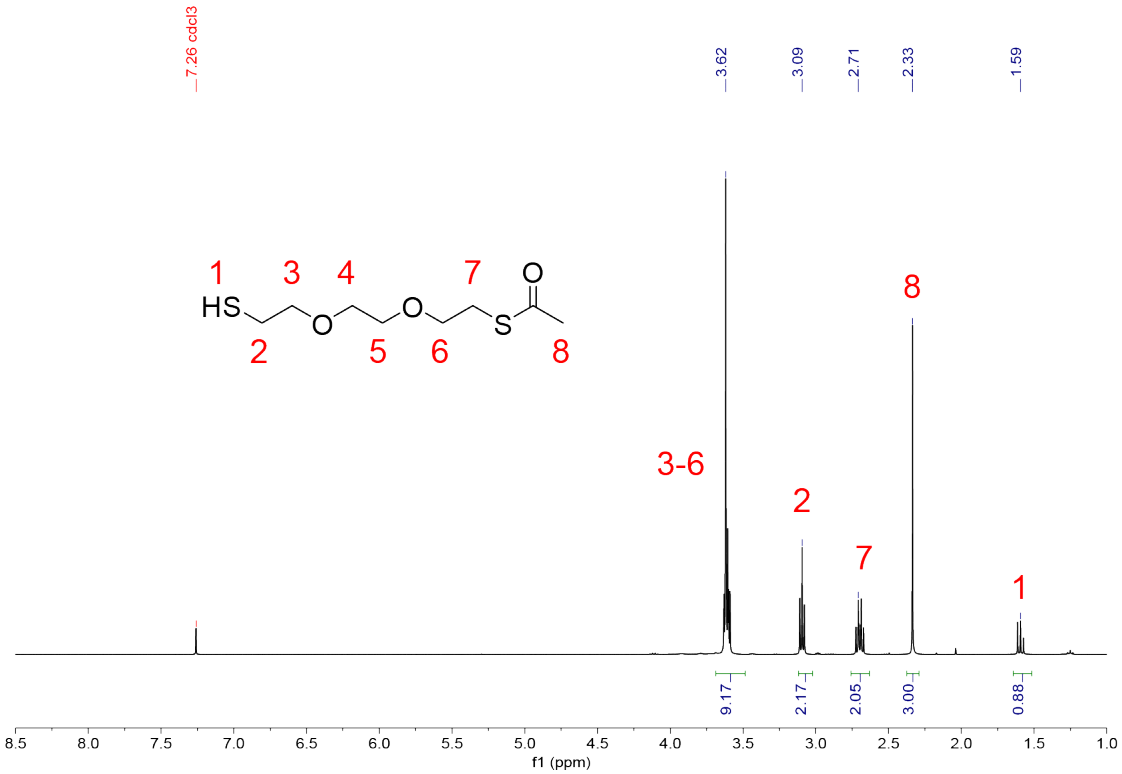

Figure A4.20. ^{1}H NMR (400 MHz, $CDCl_3$) of *S*-[2-[2-(2-mercaptoethoxy)ethoxy]ethyl] ester ethanethioic acid.

Synthesis of 2,[2-(2-azidoethoxy)ethoxy]ethyl-4-methylbenzenesulfonate – P-toluenesulfonyl chloride (3.5 g, 18.4 mmol) was dissolved at 175 mM in dichloromethane (DCM). Separately, 4 equiv of triethylene glycol (11 g, 73 mmol) was dissolved at 110 mM in DCM. To this solution was added 1.05 equiv of Et_3N (1.95 g, 19 mmol) and 0.02 equiv of 4-dimethylaminopyridine (DMAP, 46 mg, 0.3 mmol), and the mixture was allowed to equilibrate for 10 minutes on ice. The solution of p-toluenesulfonyl chloride in DCM was then added dropwise to the mixture over 2 hours. The mixture was subsequently removed from the ice and reacted at room temperature overnight. The reaction was quenched with 100 mL of water and extracted with DCM (100 mL, 3x). The DCM layer was collected and concentrated under vacuum in 98% yield. The crude product was used without further purification. The product was characterized by ^1H NMR and LC-MS (*m/z* calculated: 305.20 observed: 305.09 $[M+H]^+$). ^1H NMR (400 MHz, $CDCl_3$) δ 7.82-7.75 (d, 2H), 7.37-7.30 (d, 2H), 4.19-4.08 (m, 2H), 3.78-3.52 (br, 10H), 2.47-2.40 (s, 3H).

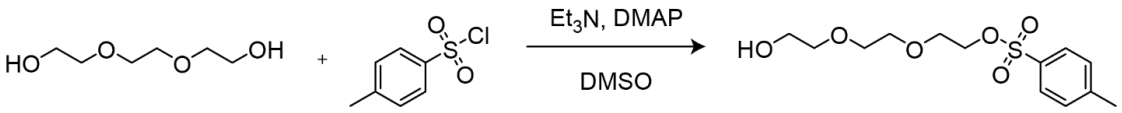

Figure A4.21. Scheme for synthesis of 2,[2-(2-azidoethoxy)ethoxy]ethyl-4-methylbenzenesulfonate.

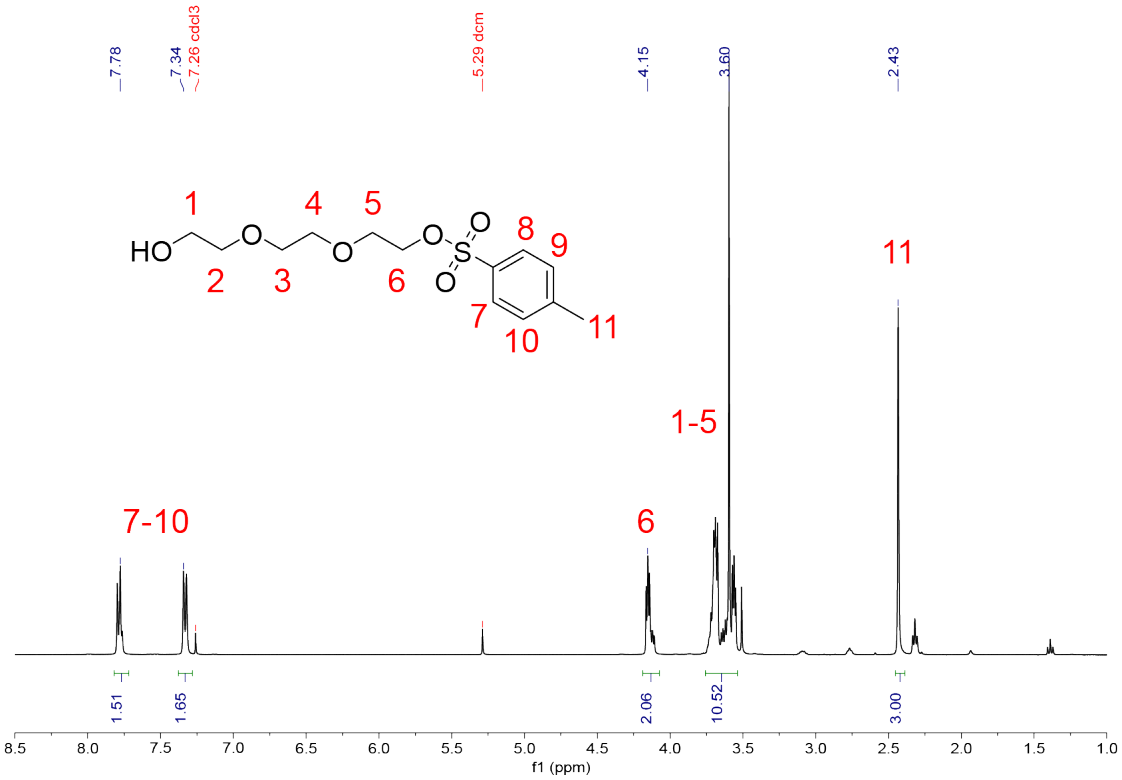

Figure A4.22. ^{1}H NMR (400 MHz, $CDCl_3$) of 2,[2-(2-azidoethoxy)ethoxy]ethyl-4-methylbenzenesulfonate.

Synthesis of 2-(2-(2-azidoethoxy)ethoxy) ethanol – 2,[2-(2-azidoethoxy)ethoxy]ethyl-4-methylbenzenesulfonate was dissolved at 739 mM in dry dimethylformamide (DMF). To this solution was added 2 equiv of sodium azide (2 g, 32 mmol) and the mixture was reacted overnight at 80 °C. The mixture was then concentrated under vacuum and the residue was resuspended in diethyl ether and filtered through celite. The ether was collected and concentrated under vacuum in 96% yield. The crude product was used without further purification. The product was characterized by ^{1}H NMR. ^{1}H NMR (400 MHz, $CDCl_3$) δ 3.74-3.70 (t, 2H), 3.69-3.64 (br, 6H), 3.62-3.58 (m, 6H), 3.41-3.35 (t, 2H).

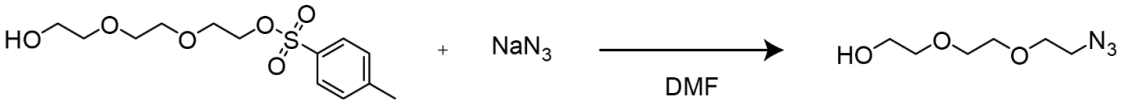

Figure A4.23. Scheme for synthesis of 2-(2-(2-azidoethoxy)ethoxy) ethanol.

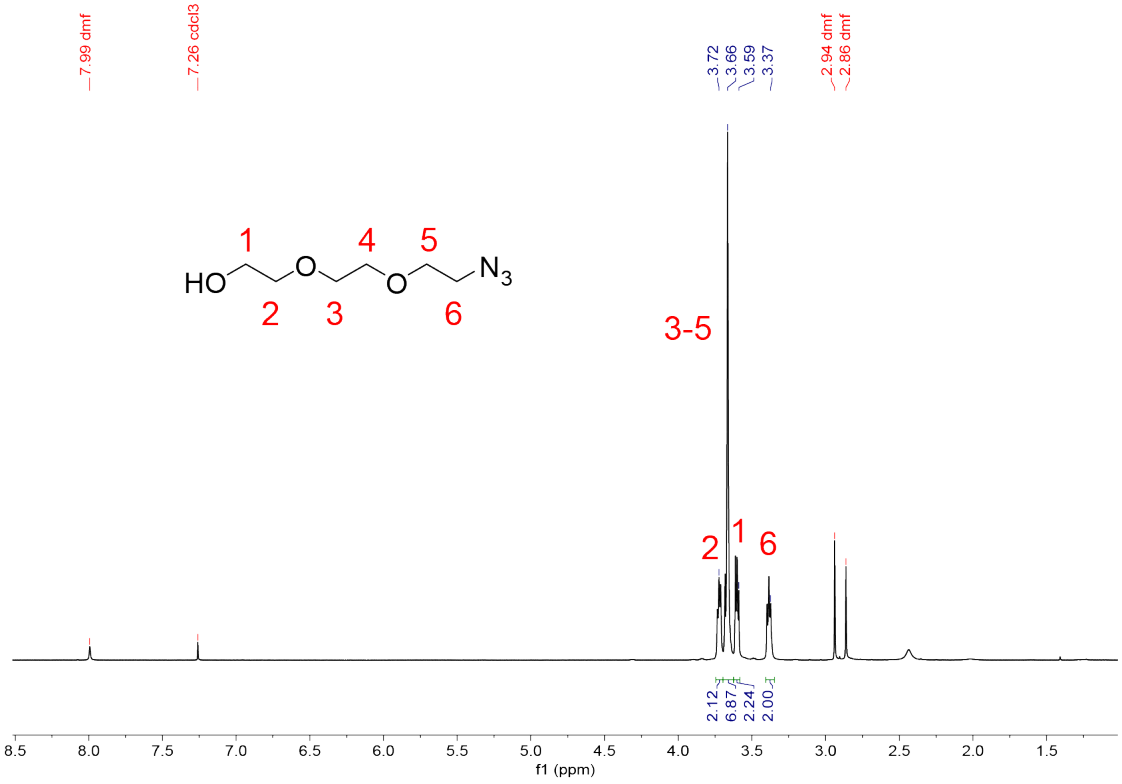

Figure A4.24. ^{1}H NMR (400 MHz, $CDCl_3$) of 2-(2-(2-azidoethoxy)ethoxy) ethanol.

Synthesis of 1-[2-(2-azidoethoxy)ethoxy]-2-bromoethane – 2-(2-(2-azidoethoxy)ethoxy) ethanol (1 g, 5.8 mmol) was dissolved at 342 mM in anhydrous chloroform ($CHCl_3$). To this solution was added 2 equiv of phosphorus tribromide (3.1 g, 12 mmol) over 5 minutes. The mixture was then refluxed overnight at 50 °C. The reaction was quenched on ice over 30 minutes with 75 mL of saturated sodium bicarbonate solution and extracted with $CHCl_3$ (100 mL, 3x). The $CHCl_3$ layer was collected and concentrated under vacuum in 30% yield. The crude product was used without further purification. The product was characterized by ^{13}C NMR. ^{13}C NMR (400 MHz, $CDCl_3$) δ 71.41 70.83 70.73 70.68 70.29 50.85 30.52.

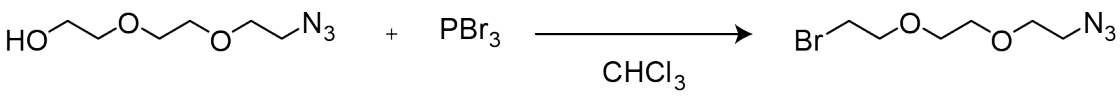

Figure A4.25. Scheme for synthesis of 1-[2-(2-azidoethoxy)ethoxy]-2-bromoethane.

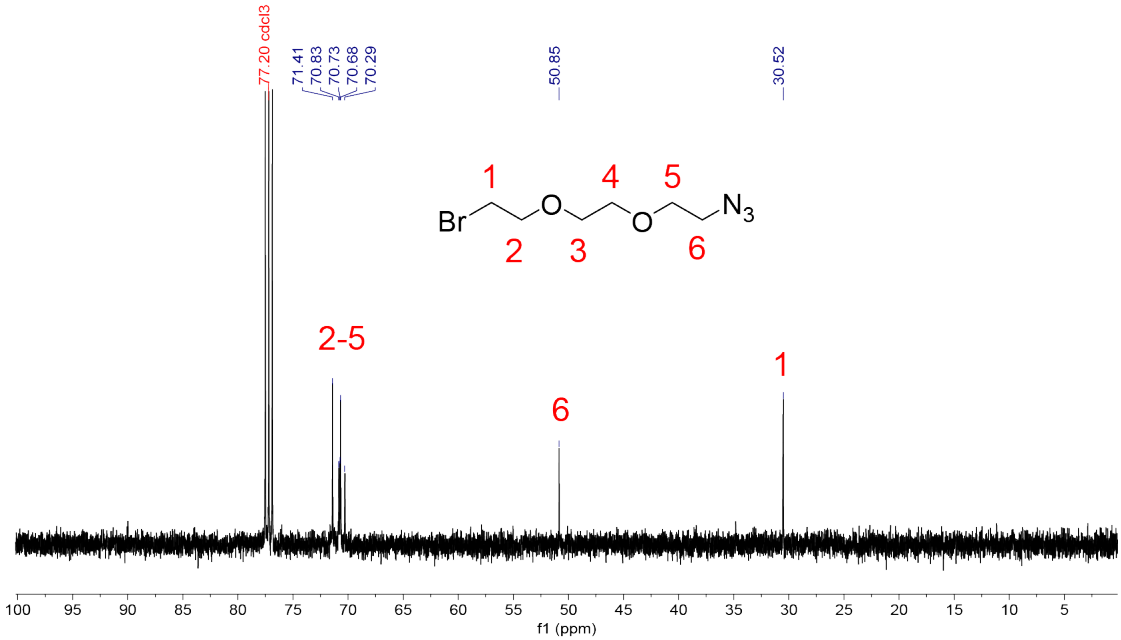

Figure A4.26. ^{13}C NMR (400 MHz, $CDCl_3$) of 1-[2-(2-azidoethoxy)ethoxy]-2-bromoethane.

Synthesis of N-[2-[2-(2-azidoethoxy)ethoxy]ethyl]-2-propen-1-amine - 1 equiv of 1-[2-(2-azidoethoxy)ethoxy]-2-bromoethane (888 mg, 3.73 mmol) was added to 1.2 equiv of potassium carbonate (619 mg, 4.48 mmol) and 10 equiv allylamine (2.1 g, 37.3 mmol). The mixture was allowed to react overnight at room temperature. The reaction was then filtered through celite and concentrated under vacuum in 85% recovery. The crude product was used without further purification. The product was characterized by ^{1}H NMR. ^{1}H NMR (400 MHz, $CDCl_3$) δ 5.99-5.86 (m,1H), 5.24-5.07 (dd, 1H), 3.75-3.58 (br, 8H), 3.46-3.38 (t, 2H), 3.31-3.25 (d, 2H), 2.83-2.79 (t, 2H).

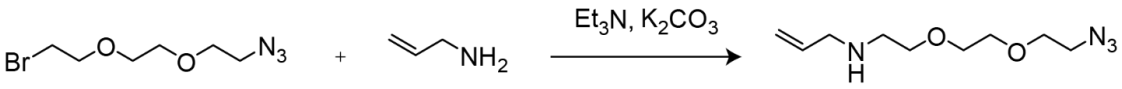

Figure A4.27. Scheme for synthesis of *N*-[2-[2-(2-azidoethoxy)ethoxy]ethyl]-2-propen-1-amine.

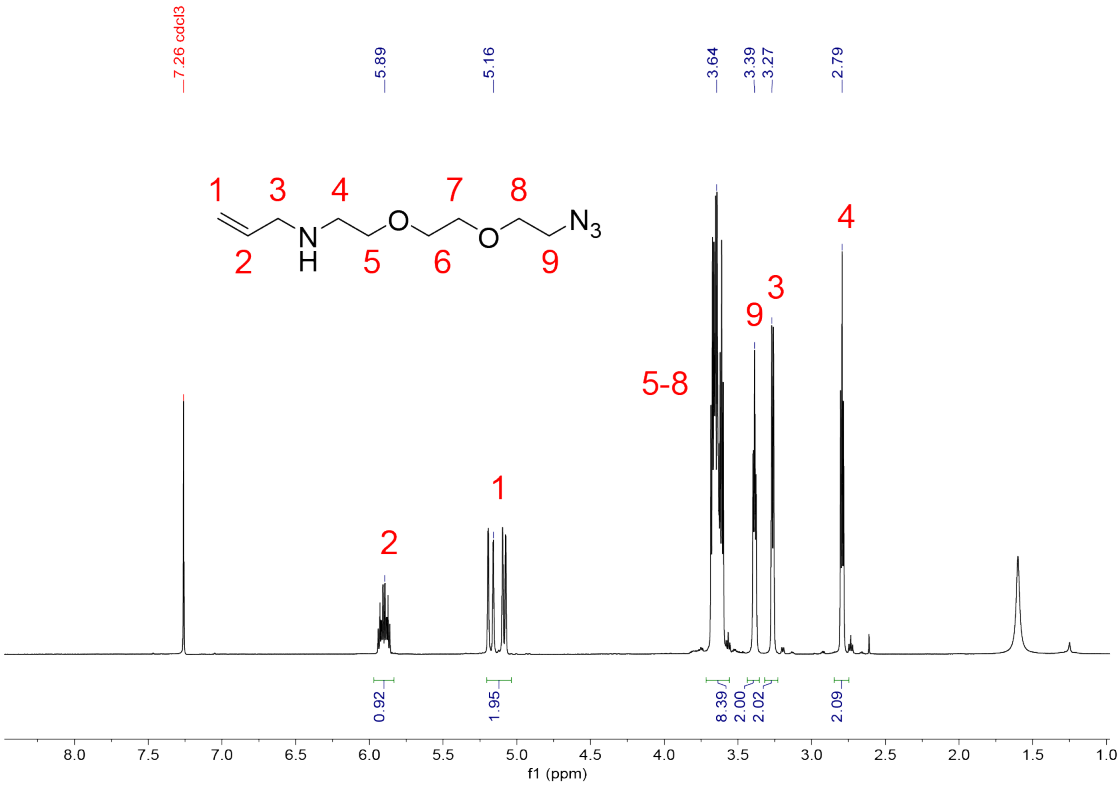

Figure A4.28. ^{1}H NMR (400 MHz, $CDCl_3$) of *N*-[2-[2-(2-azidoethoxy)ethoxy]ethyl]-2-propen-1-amine.

*Synthesis of Compound **(9)*** – 1 equiv of *N*-[2-[2-(2-azidoethoxy)ethoxy]ethyl]-2-propen-1-amine (668 mg, 3.1 mmol) was dissolved at 151 mM in dichloromethane (DCM). To the solution was added 1.1 equiv of Et_3N (347 mg, 3.4 mmol), and the mixture was allowed to equilibrate for 10 minutes on ice. Next, 1.3 equiv acryloyl chloride (367 mg, 4.1 mmol) dissolved at 1.66 M in DCM was added dropwise for 1 hour. The final concentration of *N*-[2-[2-(2-azidoethoxy)ethoxy]ethyl]-2-propen-1-amine was 132 mM. The mixture was then removed from the ice and reacted at room temperature for 1 hour. The reaction was quenched with 6 mL of water and extracted with DCM (80 mL, 3x). The DCM layer was collected and concentrated under vacuum. The product was purified by flash chromatography (12 g silica, 0-5% MeOH in DCM) in 30% yield. The product was characterized by ^{1}H NMR and LC-MS (*m/z* calculated: 269.16 observed: 269.20 $[M+H]^+$). ^{1}H NMR (400 MHz, $CDCl_3$) δ 6.72-6.28 (m, 2H), 5.85-5.72 (m, 1H), 5.70-5.60 (m, 1H), 5.22-5.08 (m, 2H), 4.10-4.04 (m, 2H), 3.70-3.45 (m, 10H), 3.40-3.31, (t, J = 5.1 Hz, 2H).

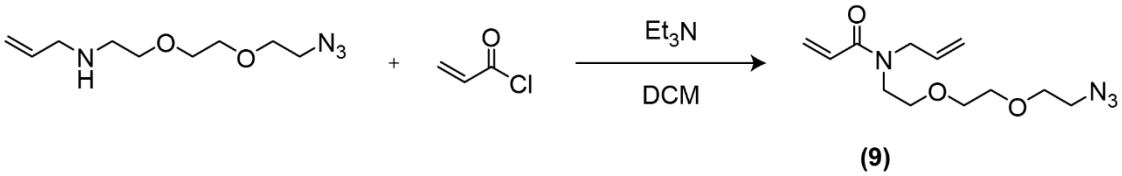

(9)

Figure A4.29. Scheme for synthesis of Compound **(9)**.

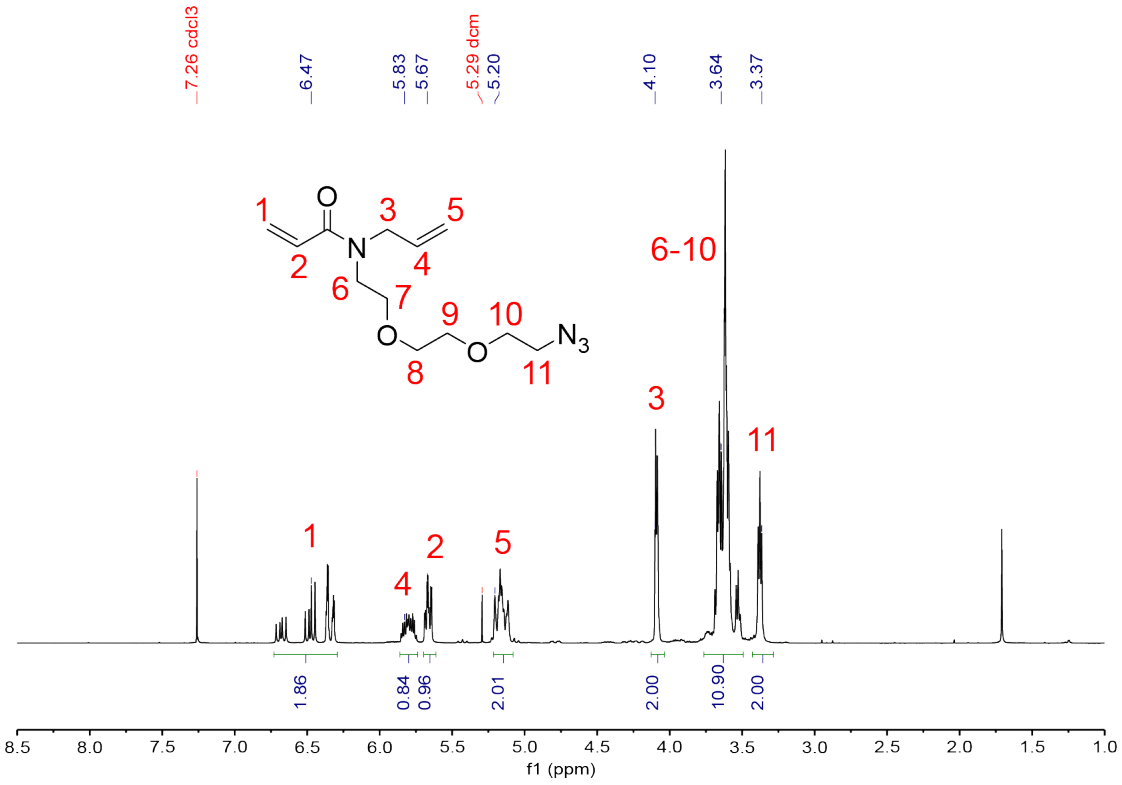

Figure A4.30. ^{1}H NMR (400 MHz, $CDCl_3$) of Compound **(9)**.

*Synthesis of Compound **(10)*** – Tert-butyl N-methyl-N-(prop-2-en-1-yl)carbamate was dissolved at 500 mg/ml in methanol (MeOH). To this solution was added 0.1 equiv of 2,2-dimethoxy-2-phenylacetophenone (DMPA) and 5 equiv of 2,2'-(ethylenedioxy)diethanethiol. The final concentration of tert-butyl N-methyl-N-(prop-2-en-1-yl)carbamate was 306 mM in MeOH. The mixture was subjected to UV irradiation at 5 mW/cm^2 for 270 s. The methanol was then evaporated under reduced pressure, and the product was purified by flash chromatography (40 g silica, 0-20% ethyl acetate in hexanes). The product was characterized by ^{1}H NMR. ^{1}H NMR (400 MHz, $CDCl_3$) δ 3.67-3.54 (m, 8H), 3.31-3.22 (t, 2H), 2.85-2.79 (s, 3H), 2.74-2.65 (m, 4H), 2.56-2.48 (t, 2H), 1.83-1.71 (q, 2H), 1.62-1.54 (t, 1H), 1.47-1.37 (s, 9H).

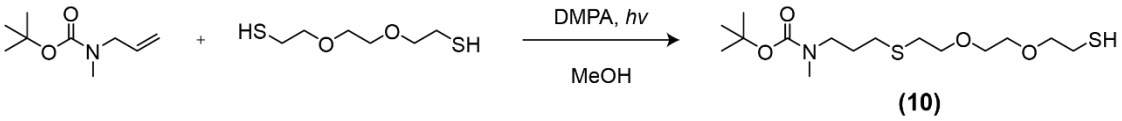

Figure A4.31. Synthesis of Compound **(10)**.

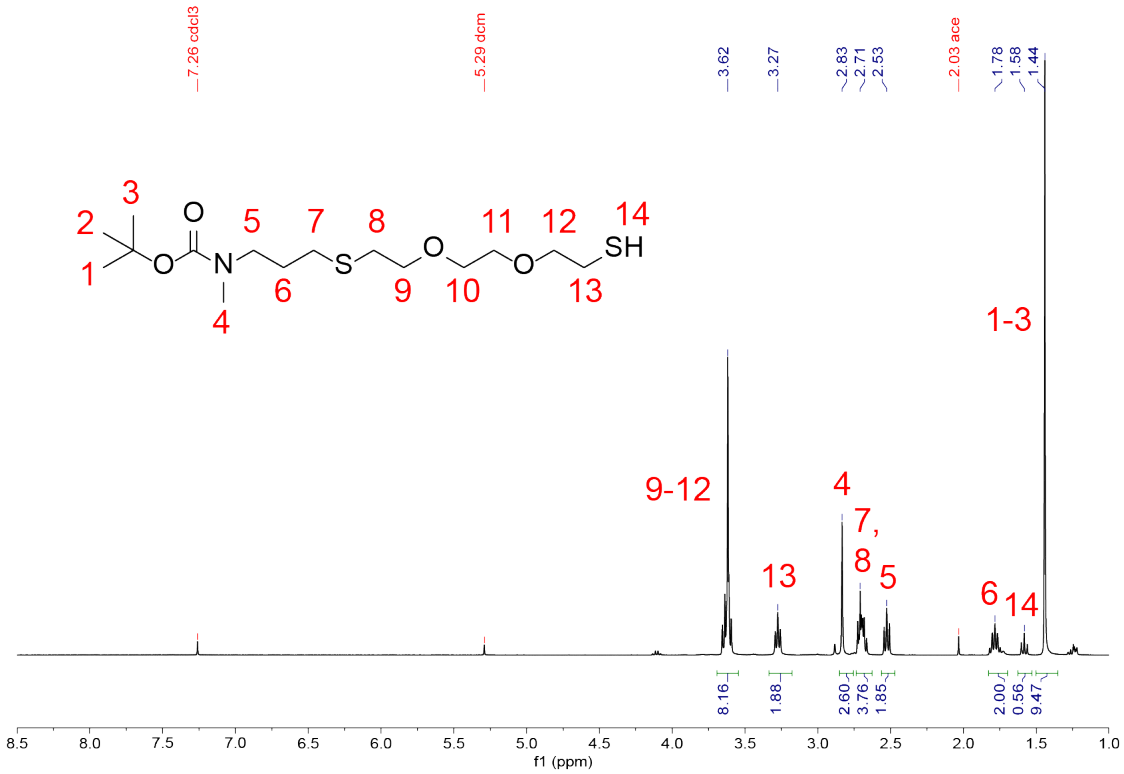

Figure A4.32. ^{1}H NMR (400 MHz, $CDCl_3$) of Compound **(10)**.

*Synthesis of Compound **(11)*** – 1 equiv of Compound **(10)** was mixed with 1 equiv of Compound **(9)** and 0.05 equiv 1,8-diazabicyclo[5.4.0]undec-7-ene (DBU) at a final concentration of 600 mM in acetonitrile (ACN). The mixture was reacted overnight at room temperature. The product was characterized by LC-MS (*m/z* calculated: 644.31 observed: 644.20 $[M+Na]^+$) and used without further purification.

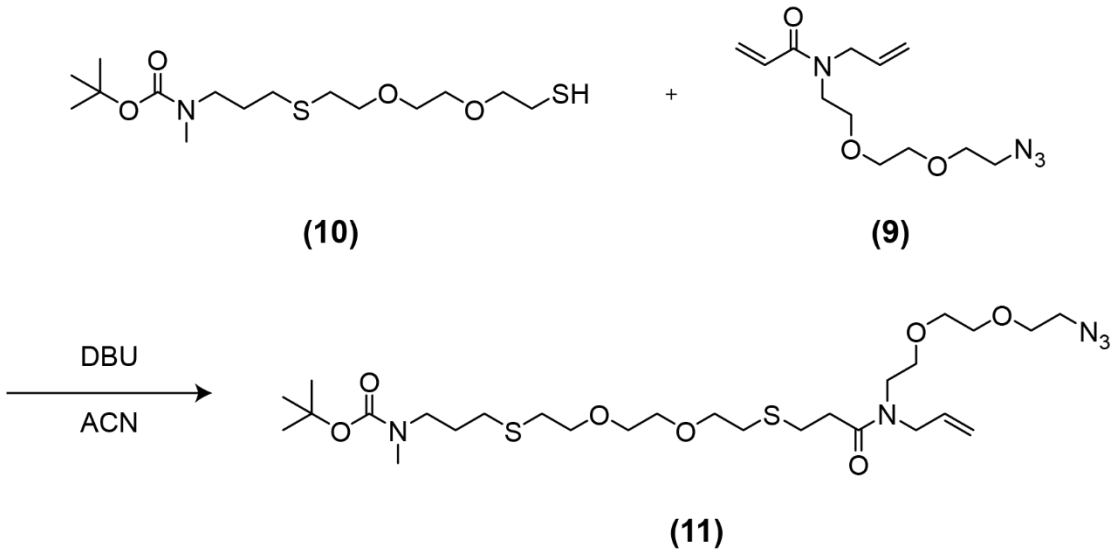

Figure A4.33. Scheme for synthesis of Compound **(11)**.

*Synthesis of Compound **(12)*** – 1 equiv of Compound **(11)** was mixed with 2.2 equiv of *S*-[2-[2-(2-mercaptoethoxy)ethoxy]ethyl] ester ethanethioic acid and 0.2 equiv of DMPA at a final concentration of 600 mM in MeOH. The mixture was subjected to UV irradiation at 5 mW/cm^2 for 270 s. **The mixture was purified via semi-preparative RP-HPLC (mobile phase without TFA).** The product eluted at 37.9 minutes and was characterized by ^{1}H NMR and LC-MS (*m/z* calculated: 868.37 observed: 868.20 $[M+Na]^+$). ^{1}H NMR (400 MHz, $CDCl_3$) δ 3.67-3.54 (br, 24H), 3.53-3.40 (m, 4H), 3.39-3.35 (t, 2H), 3.28-3.23 (m, 2H), 3.09-3.05 (t, 2H), 2.86-2.47 (m, 16H), 2.33-2.39 (s, 2H), 1.87-1.73 (m, 4H), 1.45-1.40 (s, 9H).

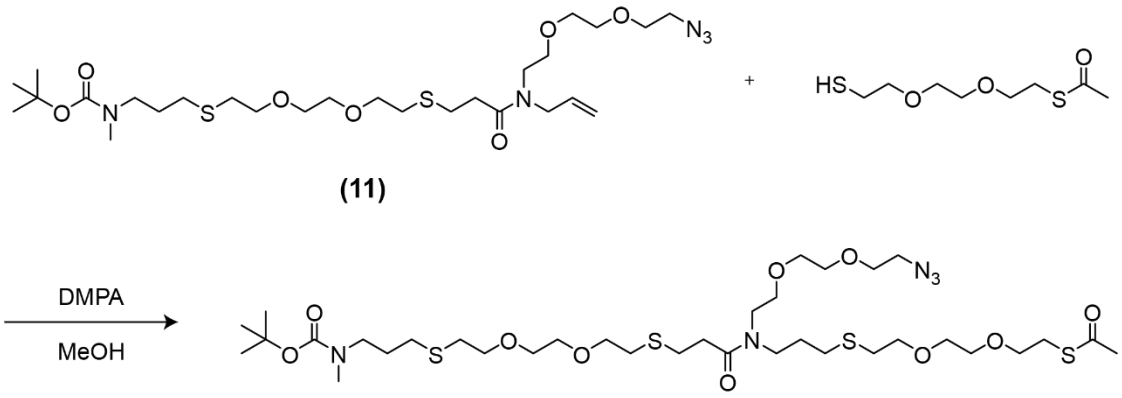

Figure A4.34. Scheme for synthesis of Compound **(12)**.

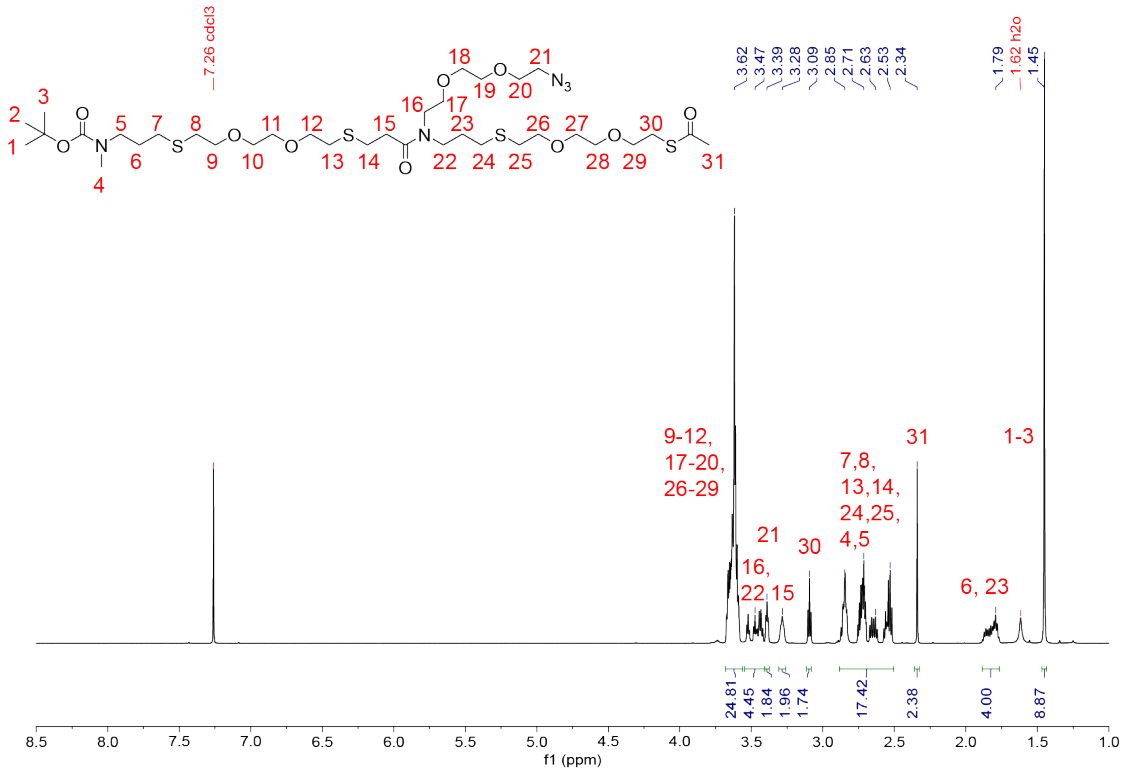

Figure A4.35. ^{1}H NMR (400 MHz, $CDCl_3$) of Compound **(12)**.

*Tert-butoxy carbamate (Boc) Deprotection of Compound **(12)*** – Compound **(12)** was mixed at 5 mM in 50% trifluoroacetic acid (TFA) in DCM for 3 hours. The TFA and DCM were then removed under vacuum. The product was characterized by LC-MS (*m/z* calculated: 746.33 observed: 746.20 $[M+H]^+$).

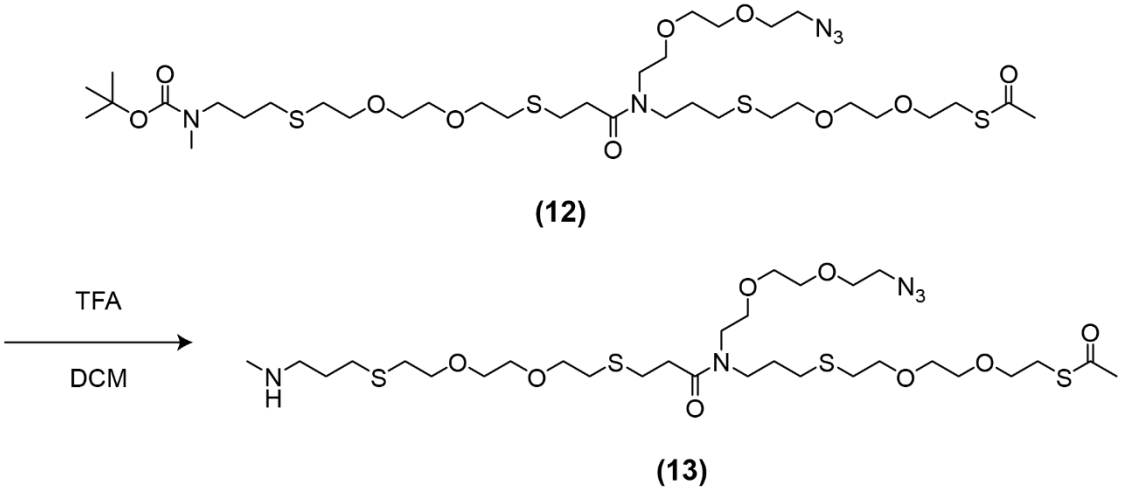

(12)

(13)

Figure A4.36. Scheme for synthesis of Compound **(13)**.

*Synthesis of Compound **(14)*** – 2,4-dinitrochlorobenzene (584 mg, 2.9 mmol) was dissolved at 100 mM in THF. To this solution was added 2 equiv of N1-boc-N1-methyl-1,2-ethylenediamine (1 g, 5.8 mmol) and 3 equiv of Et_3N (875 mg, 8.6 mmol). The mixture was reacted overnight at room temperature. The reaction was quenched with 100 mL of water and extracted with ethyl acetate (EtOAc) (100 mL, 3x). The EtOAc layer was collected and concentrated under vacuum, and the product was purified by flash chromatography (12 g silica, 0-60% ethyl acetate in hexanes). The product was characterized by ^1H NMR. ^1H NMR (400 MHz, $CDCl_3$) δ 9.18-8.15 (m, 3H), 7.05-6.90 (m, 1H), 3.66-3.47 (m, 4H), 2.99-2.80 (s, 3H), 1.53-1.37 (s, 9H).

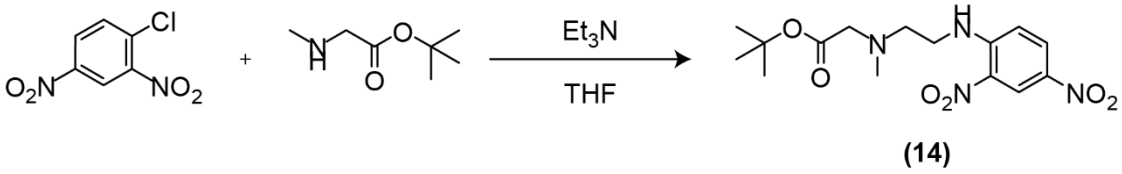

(14)

Figure A4.37. Scheme for synthesis of Compound **(14)**.

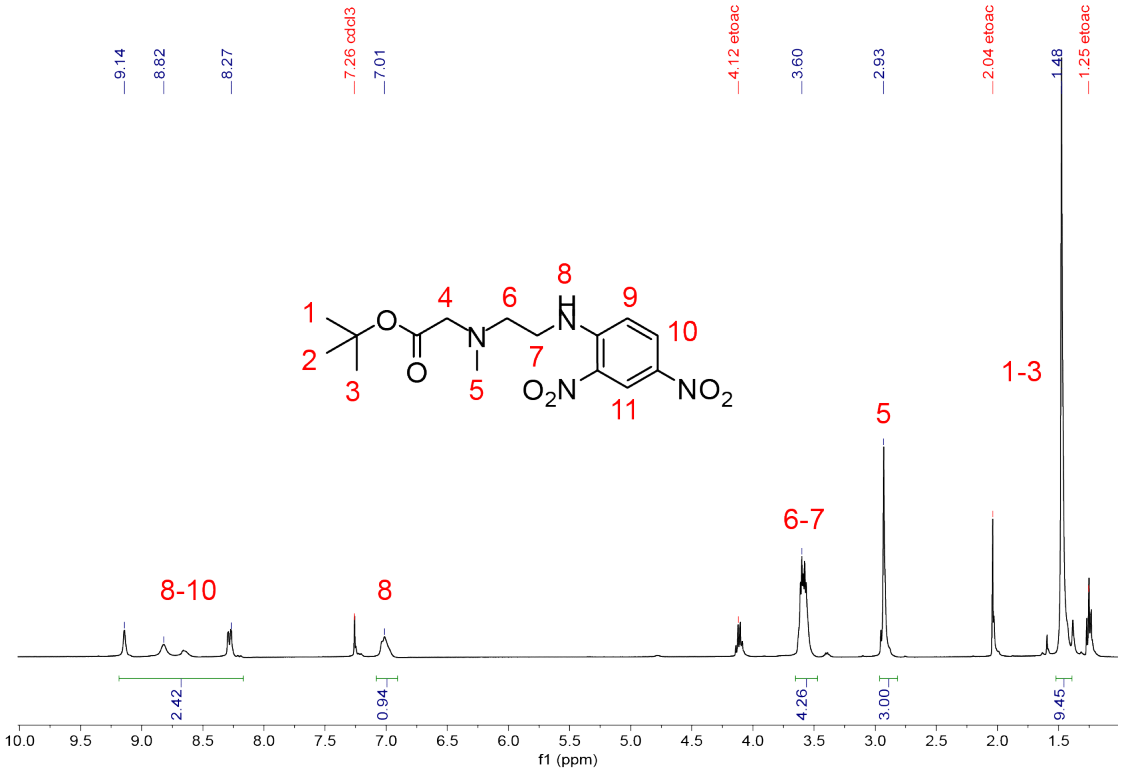

Figure A4.38. ^{1}H NMR (400 MHz, $CDCl_3$) of Compound **(14)**.

*Tert-butoxy carbamate (Boc) Deprotection of Compound **(14)*** – Compound **(14)** was mixed at 50 mM in 50% trifluoroacetic acid (TFA) in DCM for 1 hour. The TFA and DCM were then removed under vacuum. The product was characterized by LC-MS (*m/z* calculated: 241.10 observed: 240.90 $[M+H]^+$).

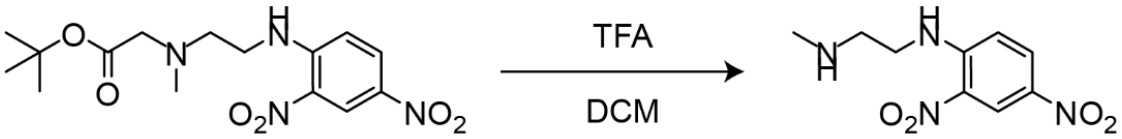

(14) **(15)**

Figure A4.39. Scheme for synthesis of Compound **(15)**.

*Synthesis of Compound **(16)*** – Compound **(15)** (403 mg, 1.68 mmol) was dissolved at 150 mM in DCM. To this solution was added 1.1 equiv of Et_3N (343 mg, 3.4 mmol) and the mixture was allowed to equilibrate on ice for 10 minutes. Next, 1.3 equiv of acryloyl chloride (197 mg, 2.2 mmol) dissolved at 1.6 M in DCM was added over 1 hour. The mixture was then removed from the ice and reacted at room temperature overnight. The reaction was quenched with 10 mL of water and extracted with DCM (100 mL, 3x). The DCM layer was collected and concentrated under vacuum, and the product was purified by flash chromatography (12 g silica, 0-20% ethyl acetate in hexanes). The product was characterized by ^1H NMR. The product was characterized by ^1H NMR and LC-MS (*m/z* calculated: 295.11 observed: 295.10). ^1H NMR (400 MHz, $CDCl_3$) δ 9.17-8.26 (m, 3H), 7.22-7.14 (d, 1H), 6.65-6.35 (m, 2H), 5.85-5.70 (d, 1H), 3.82-3.61 (m, 4H), 3.22-3.10 (s, 3H).

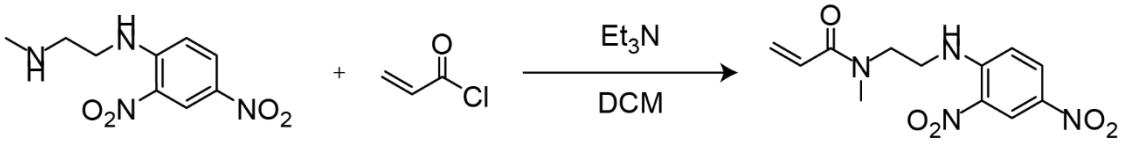

(15) **(16)**

Figure A4.40. Synthesis of compound **(16).**

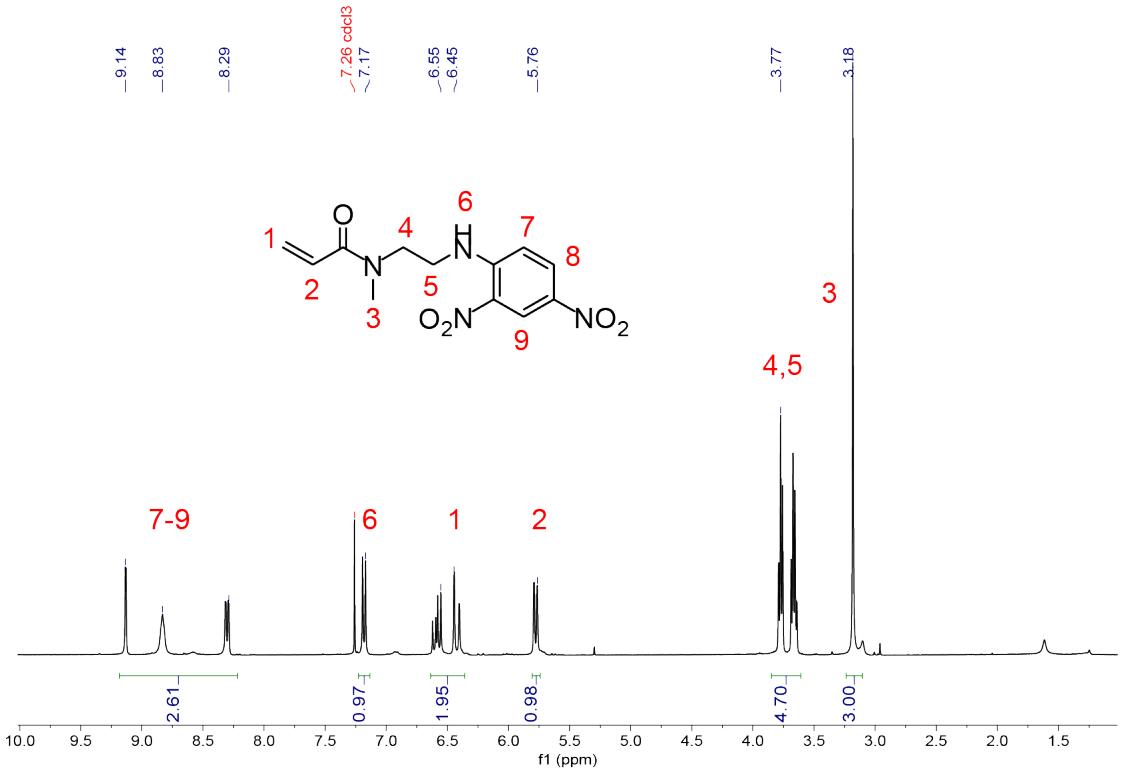

Figure A4.41. ^{1}H NMR (400 MHz, $CDCl_3$) of Compound **(16)**.

Synthesis of (7) – Compound **(6)** (5 mg, 0.0059 mmol) was dissolved at 59 mM in 7 N ammonia in MeOH and reacted for 1 hour at room temperature. The reaction was then diluted to 5.8 mM in ACN and the ammonia, MeOH, and 90% of the ACN were evaporated under reduced pressure. To this solution was added 3 equiv of compound **(4)** and 0.15 equiv of 1,8-diazabicyclo(5.4.0)undec-7-ene (DBU) at a final concentration of 54 mM in ACN. The mixture was reacted at room temperature overnight. The product was then purified via RP-HPLC and characterized by LC-MS (*m/z* calculated: 1098.47 observed: 1098.40). The product eluted at 27 minutes.

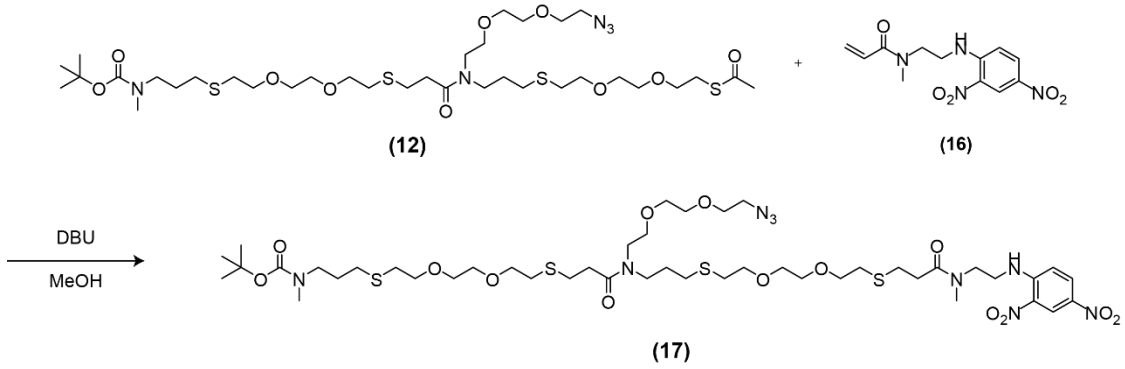

Figure A4.42. Synthesis of compound **(17).**

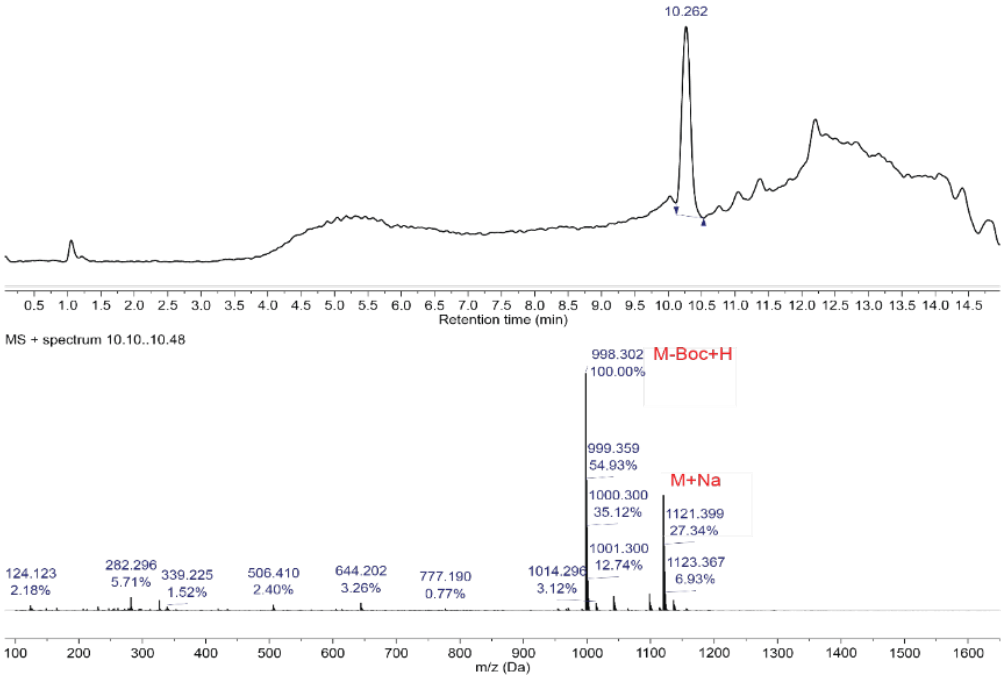

Figure A4.43. LC-MS of Compound **(17)**.

*Tert-butoxy carbamate (Boc) Deprotection of Compound **(17)*** – Compound **(17)** was mixed at 5 mM in 50% trifluoroacetic acid (TFA) in DCM for 3 hours. The TFA and DCM were then removed under vacuum.

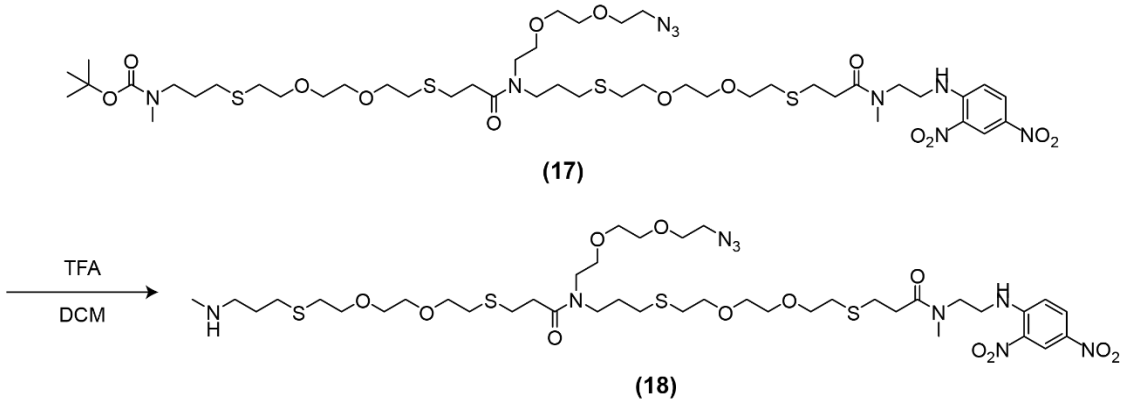

(17)

(18)

Figure A4.44. Scheme for synthesis of Compound **(18)**.

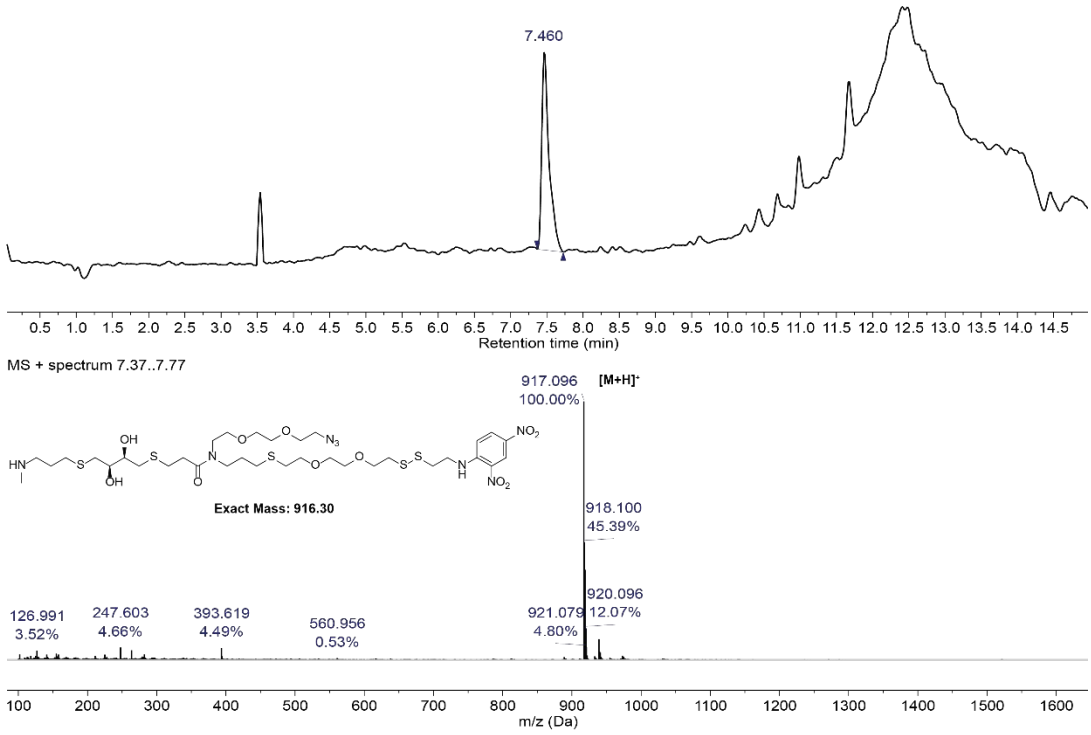

Figure A4.44. LC-MS of Compound **(18)**.

*Synthesis of Compound **(19)*** – Compound **(18)** (3.27 mg 0.003 mmol) was dissolved at 50 mg/ml in dry DMSO. To this solution was added 10 equiv of Et_3N (3.3 mg, 0.033 mmol) and 1.5 equiv of Compound **(3)**. The final concentration of Compound **(18)** was 8.4 mM in DMSO. The mixture was reacted at room temperature overnight. The product was then purified via RP-HPLC and characterized by LC-MS (*m/z* calculated: 1272.53 observed: 1272.50). The product eluted at 27 minutes.

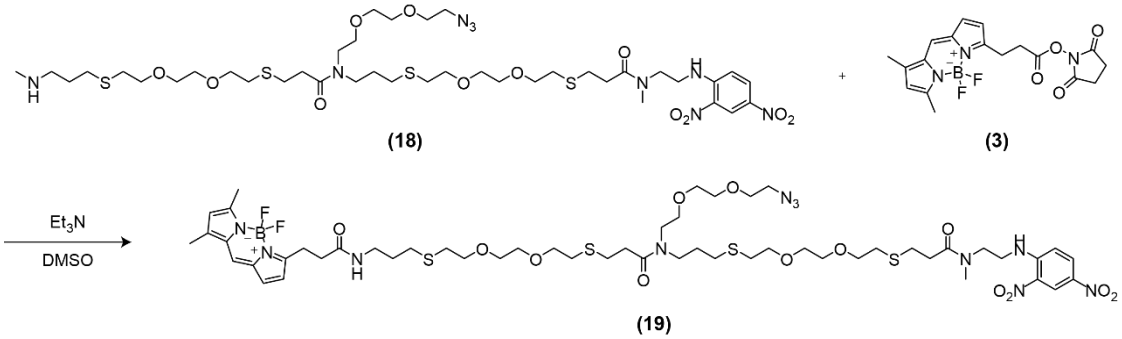

Figure A4.45. Scheme for synthesis of Compound **(19)**.

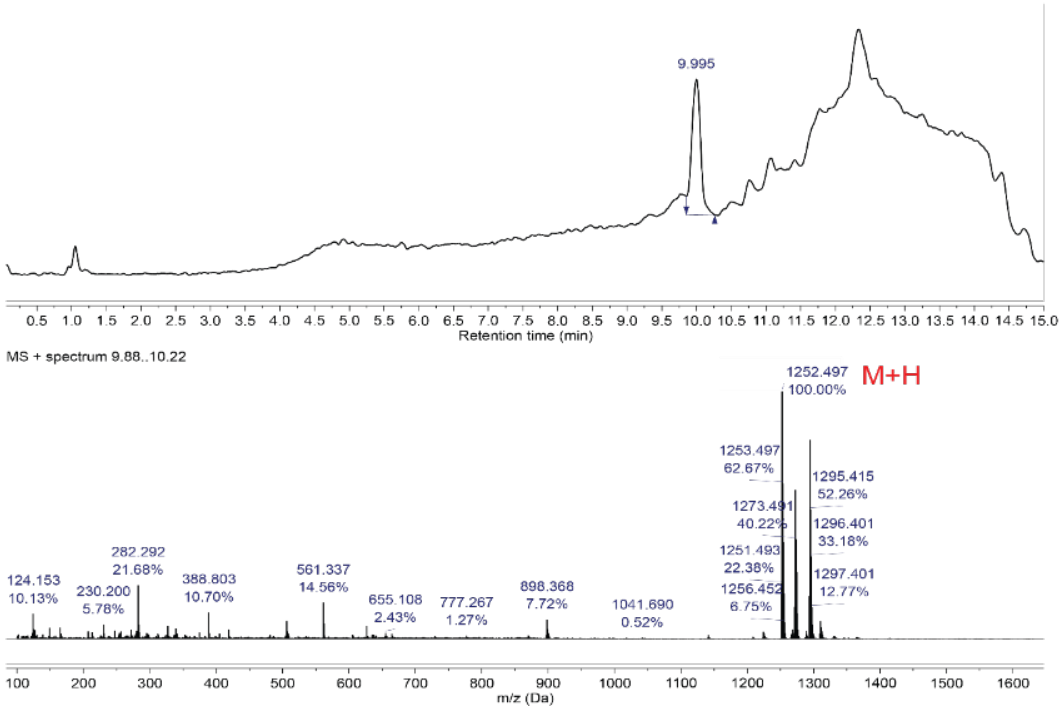

Figure A4.46. LC-MS of Compound **(19)**.

*Synthesis of Compound **(20)*** - 1 equiv of Compound **(2)** (55 mg/ml in anhydrous dimethylformamide (DMF)) was reacted with 2.5 equiv of lissamine rhodamine B sulfonyl chloride (mixed isomers, 100 mg/ml in DMF) and 15 equiv of Et_3N. The final concentration of Compound **(2)** was 30 mM. The mixture was reacted overnight at room temperature. The reaction was purified via semi-preparative RP-HPLC. The product eluted at 24 minutes. The product was characterized by LC-MS (*m/z* calculated: 1443.43 observed: 1443.80 $[M+H]^+$).

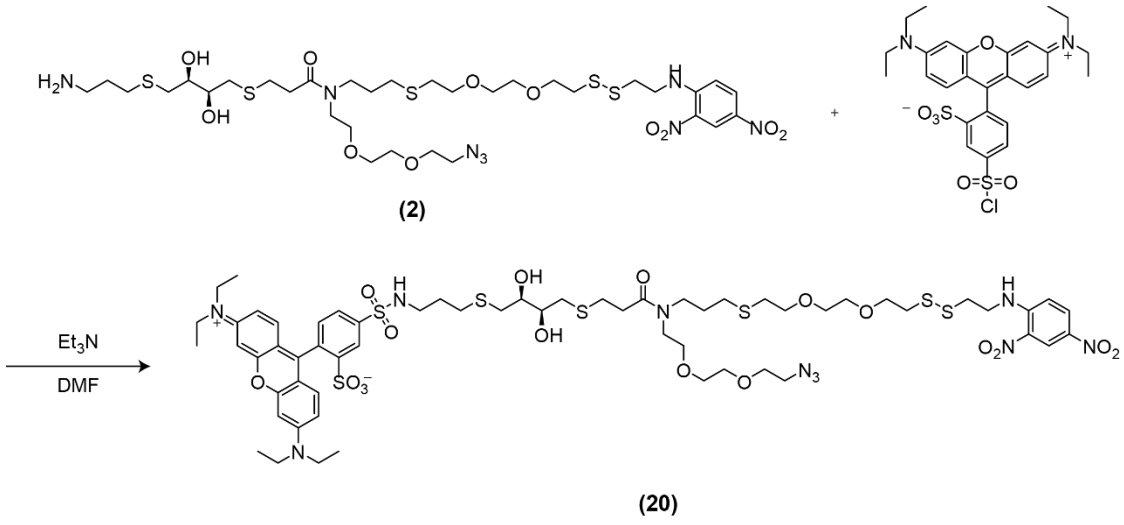

(2) **(20)**

Figure A4.47. Scheme for synthesis of Compound **(20)**.

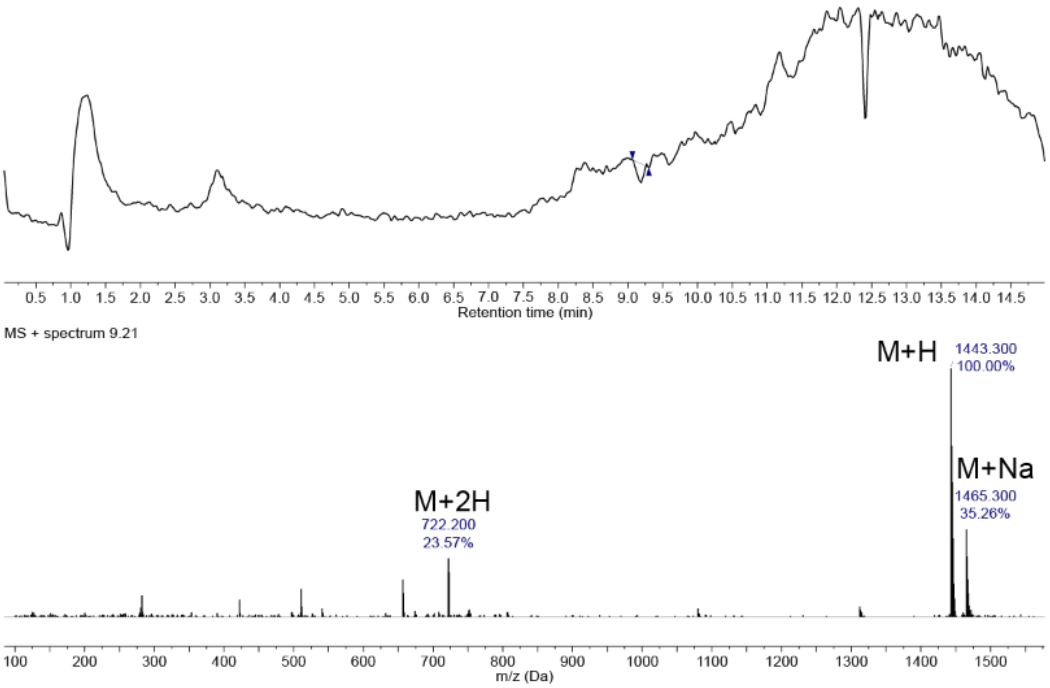

Figure A4.48. LC-MS of Compound **(20)**.

*Synthesis of Compound **(21)*** - 1 equiv of Compound **(5)** (55 mg/ml in anhydrous dimethylformamide (DMF)) was reacted with 2.5 equiv of lissamine rhodamine B sulfonyl chloride (mixed isomers, 100 mg/ml in DMF) and 15 equiv of Et_3N. The final concentration of Compound **(5)** was 30 mM. The mixture was reacted overnight at room temperature. The reaction was purified via semi-preparative RP-HPLC. The product eluted at 30 minutes. The product was characterized by LC-MS (*m/z* calculated: 1508.48 observed: 1508.40 $[M+H]^+$).

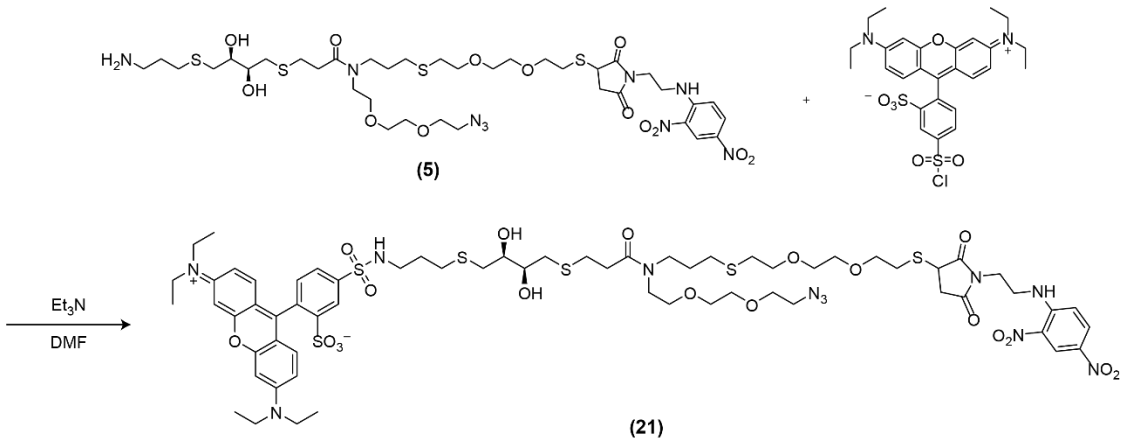

Figure A4.49. Scheme for synthesis of Compound **(21)**.

Chemical Synthesis:

Synthesis of (3) – 1 equiv of **(1)** was dissolved at 10 mg/ml in dry DMSO. To this solution, 1.5 equiv of **(2)** (6 mg/ml in dry DMSO) and 15 equiv of Et_3N were added. The final concentration of **(1)** was 6.4 mM. The mixture was reacted overnight at room temperature and then purified via semi-preparative RP-HPLC. The product was characterized by LC-MS (m/z calculated: 826.33 observed: 826.30 $[M-F]^+$).

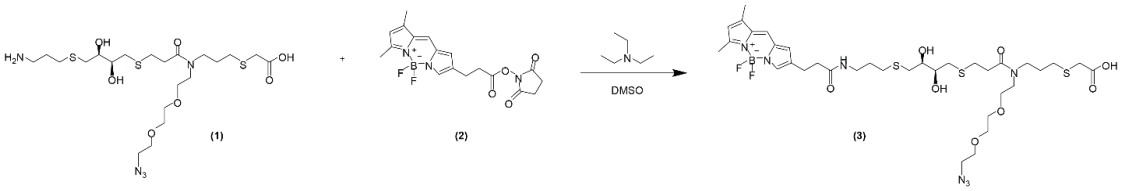

Figure A4.50. Synthesis of compound **(3)**.

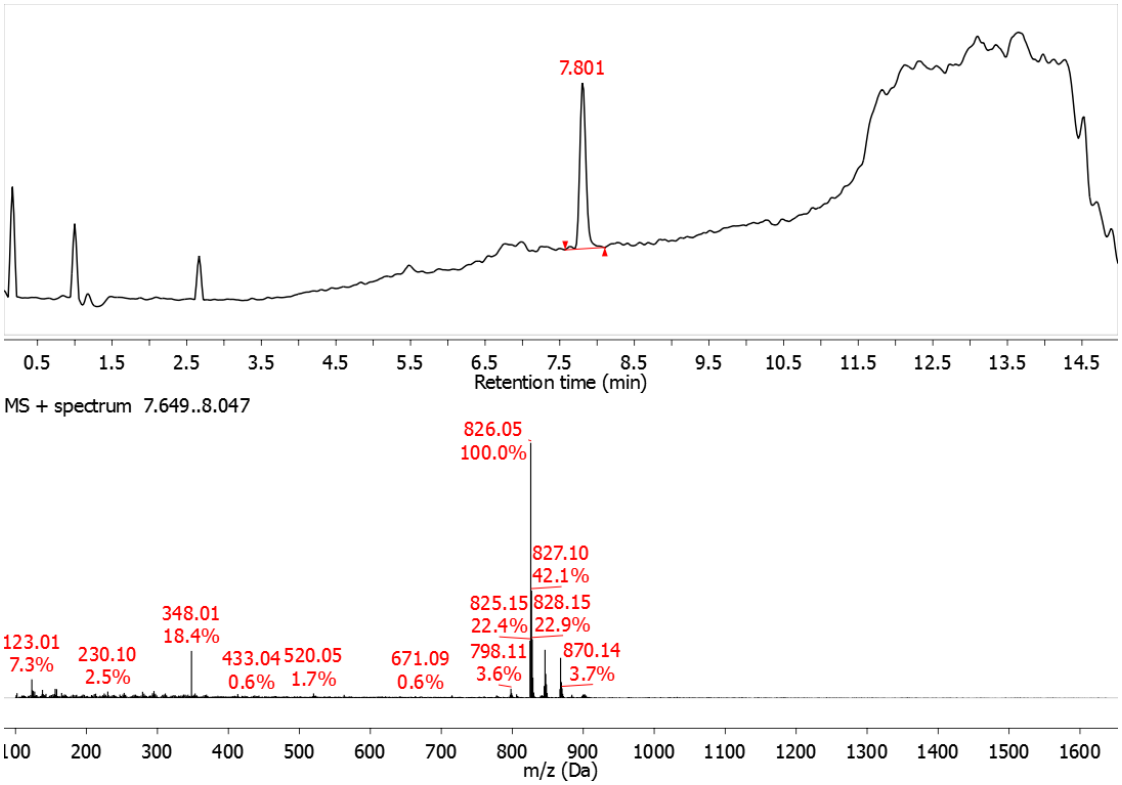

Figure A4.51. LC-MS of Compound **(3)**.

Synthesis of (5) – 1 equiv of **(4)** was dissolved at 10 mg/ml in dry DMSO. To this solution, 2.2 equiv of N1-(2,4-dinitro-phenyl)-ethane-1,2-diamine (10 mg/ml in dry DMSO) and 10 equiv of Et_3N were added. The final concentration of **(1)** was 7.8 mM. The mixture was reacted for 6 hours at room temperature after which 10% v/v piperidine was added and the resulting mixture was reacted overnight at room temperature. The reaction was purified via semi-preparative RP-HPLC, and the product was characterized by LC-MS (*m/z* calculated: 632.28 observed: 632.29 $[M+H]^+$).

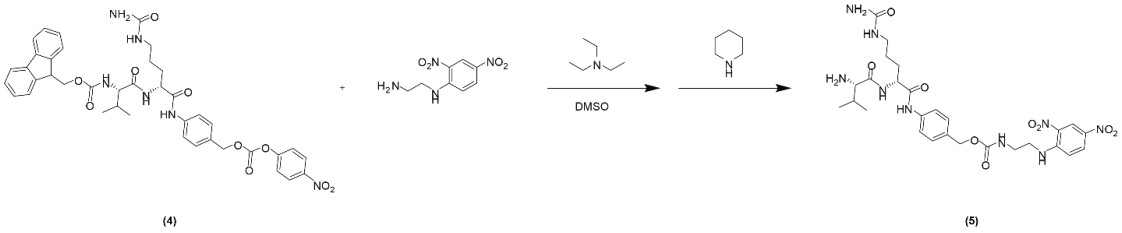

Figure A4.52. Synthesis of compound **(5)**.

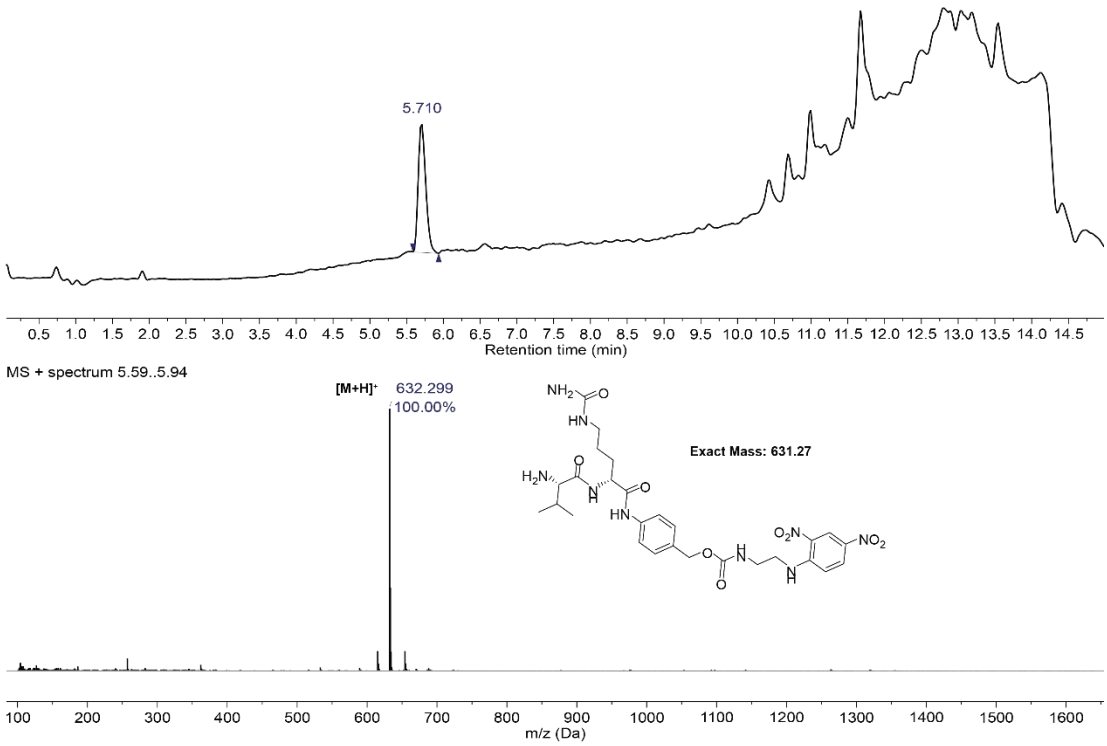

Figure A4.53. LC-MS of Compound **(5)**.

Synthesis of (6) – 1 equiv of **(3)** was dissolved at 23 mg/ml in dry DMSO. To this solution, 2.5 equiv of **(5)**, 4 equiv of 1-ethyl-3-(3-dimethylaminopropyl)carbodiimide, 4 equiv of N-hydroxysuccinimide, and 30 equiv of Et_3N were added. The final concentration of **(6)** was 5.1 mM. The mixture was reacted overnight at room temperature and then purified via semi-preparative RP-HPLC. The product was characterized by LC-MS (*m/z* calculated: 1459.60 observed: 1459.40 $[M+H]^+$).

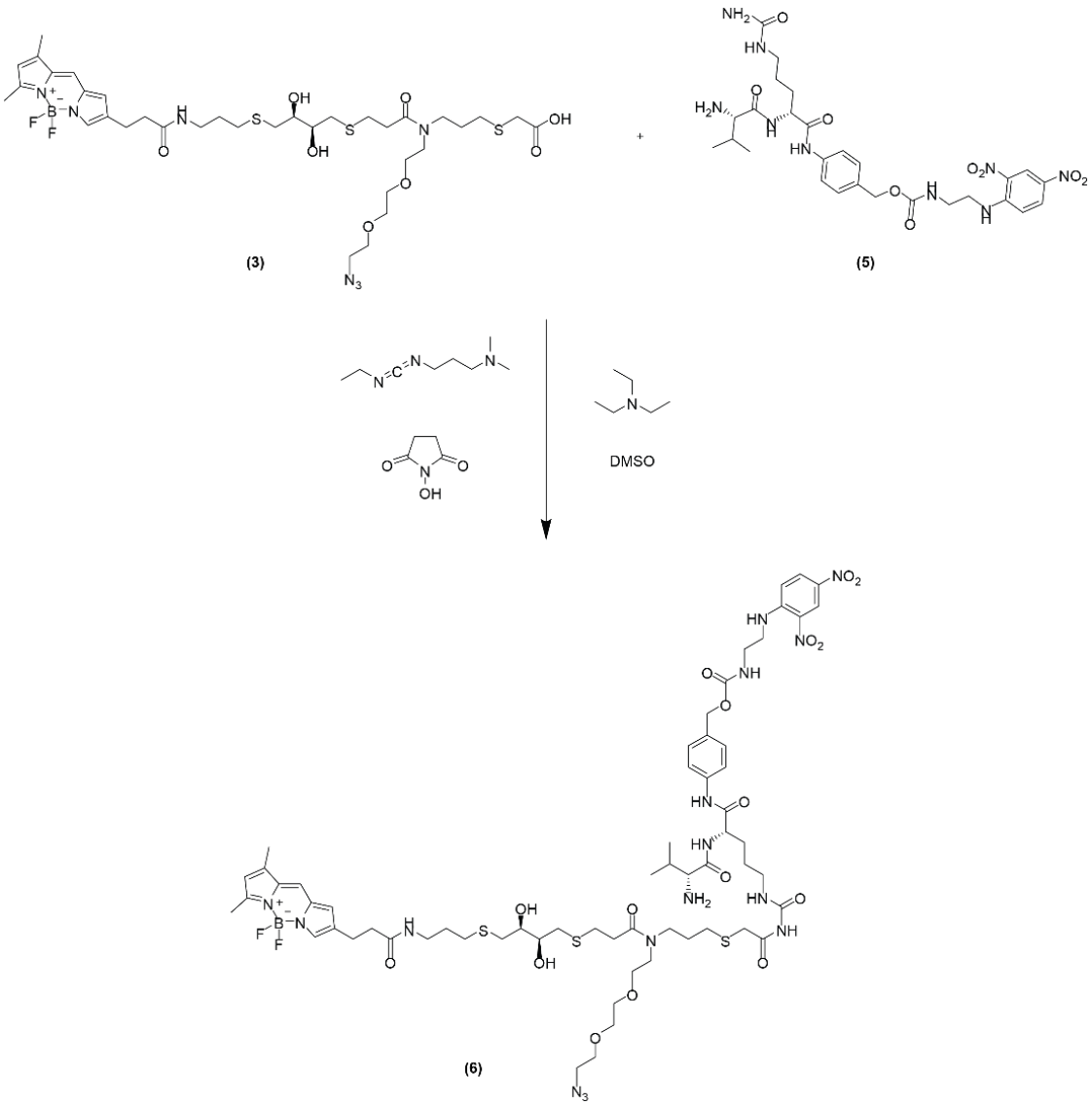

Figure A4.54. Synthesis of compound **(6)**.

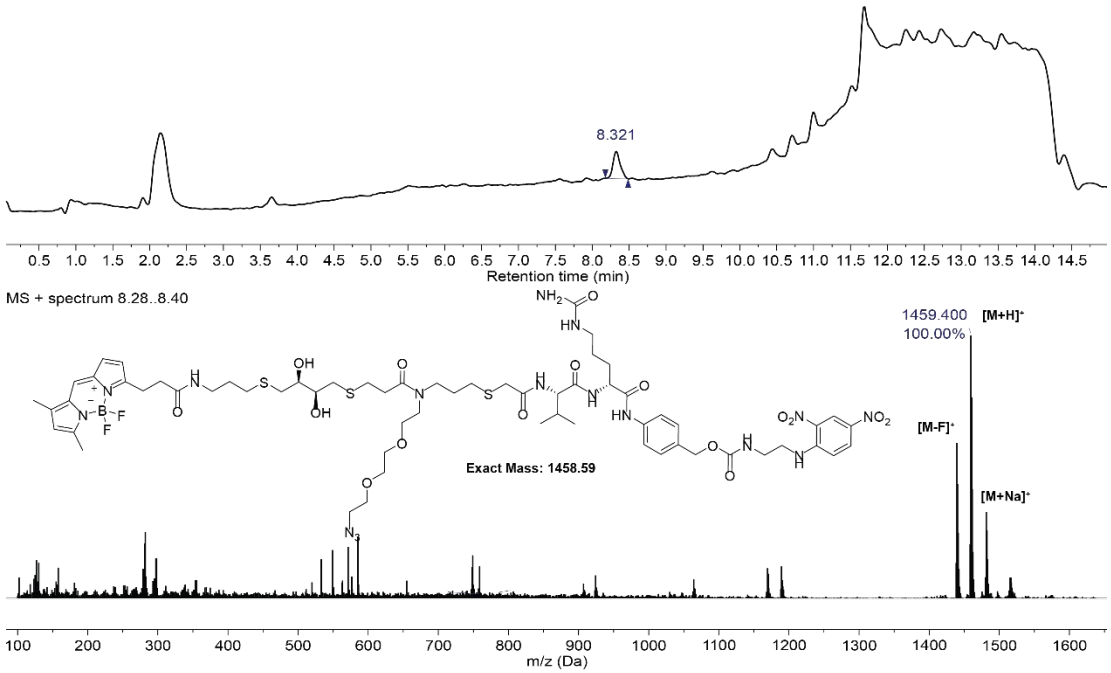

Figure A4.55. LC-MS of Compound **(6)**.

Chapter 4 – REFERENCES

1.Clavé, G. *et al.* A novel heterotrifunctional peptide-based cross-linking reagent for facile access to bioconjugates. Applications to peptide fluorescent labelling and immobilisation. *Organic & Biomolecular Chemistry* **6,** 3065–3078 (2008).

2.Sorkin, M. R., Walker, J. A., Brown, J. S. & Alabi, C. A. Versatile Platform for the Synthesis of Orthogonally Cleavable Heteromultifunctional Cross-Linkers. *Bioconjugate Chemistry* **28,** 907–912 (2017).

3.Marras, S. A. E., Kramer, F. R. & Tyagi, S. Efficiencies of fluorescence resonance energy transfer and contact-mediated quenching in oligonucleotide probes. *Nucleic Acids Res* **30,** e122 (2002).

4.Cho, W. Seeing is believing: real-time cellular activity assay for phospholipase A2. *ACS Chem Biol* **1,** 65–66 (2006).

5.Hendrickson, H. S., Hendrickson, E. K., Johnson, I. D. & Farber, S. A. Intramolecularly quenched BODIPY-labeled phospholipid analogs in phospholipase A(2) and platelet-activating factor acetylhydrolase assays and in vivo fluorescence imaging. *Anal Biochem* **276,** 27–35 (1999).

6.Kapellos, T. S. *et al.* A novel real time imaging platform to quantify macrophage phagocytosis. *Biochem Pharmacol* **116,** 107–119 (2016).

7.Cilliers, C., Liao, J., Atangcho, L. & Thurber, G. M. Residualization Rates of Near-Infrared Dyes for the Rational Design of Molecular Imaging Agents. *Mol Imaging Biol* **17,** 757–762 (2015).

8.Marras, S. A. E., Kramer, F. R. & Tyagi, S. Efficiencies of fluorescence resonance energy transfer and contact-mediated quenching in oligonucleotide probes. *Nucleic Acids Res* **30,** e122 (2002).

Chapter 5 – SUPER-RESOLUTION IMAGING OF THE GLYCOCALYX VIA MODULAR "CLICK" PROBES

5.1. INTRODUCTION

Expansion microscopy (ExM) is a powerful technique that enables super-resolution imaging via a conventional light microscope.[1-6] In traditional optical microscopy, refraction is used to magnify images.[7] Expansion microscopy is a means to circumvent the diffraction limit of light by physically magnifying samples through isotropic chemical expansion.[3] As such, details smaller than the diffraction limit of light (~250 nm) are resolvable on a standard confocal microscope. The traditional workflow for ExM includes the following steps: fixing and labelling, anchoring and gelation, digestion, and expansion.[2] First, the sample is fixed and labelled with a fluorescently labelled antibody or fluorescent protein (Figure 5.1). Second, the sample is modified with methacrylamide groups that are used as handles to crosslink the sample into a polyelectrolyte gel. Next, the underlying biological structure (i.e. proteins, lipids, cell membrane) is digested away using a mixture of proteases and denaturing reagents. This step effectively transfers biological information into the gel network. Finally, the entire sample is swelled via dialysis in low-salt buffer or water to increase the physical size of the gel and improve resolution over 4 times.

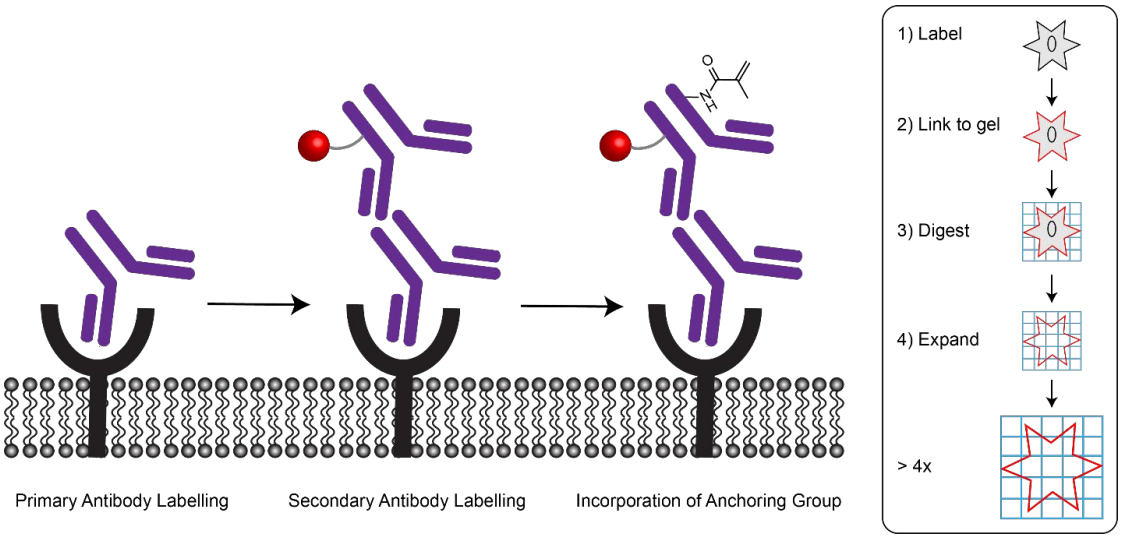

Figure 5.1. Traditional workflow for expansion microscopy.

Glycans are fundamental to a diversity of biological processes such as anticoagulation,[8] cell development,[9] and immune recognition.[10] Determining how glycans encode spatial information would enable the programing of cellular behavior on demand. Expansion microscopy could be a powerful tool for studying glycans. Methacrylamide labelling in the second step of the ExM workflow is achieved by reacting lysine residues on the fluorescent antibody or protein with the N-hydroxysuccinimide ester (NHS ester) of 6-((acryloyl)amino)hexanoic acid (AcX).[6] Glycolipids and glycoproteins have few primary amines and as such are poorly incorporated into the gel during traditional expansion microscopy. Further, current probes for ExM such as proteins and antibodies are large (~150 kDa) and bulky, which may impair binding to cell surface glycans. As such, we developed a modular chemical cross-linker that enables ExM imaging of the glycocalyx in metabolically-labeled cells and tissues.

An additional, significant benefit of our chemical cross-linker is proteolytic stability. The originally described method of expansion microscopy uses a label comprised of an oligonucleotide with a fluorophore and a methacryloyl group.[3] The

oligonucleotide was hybridized to a complementary sequence attached to an affinity tag such as a secondary antibody. This method does not allow for the retention of proteins in the gel. As such, the method has since been modified to protein retention ExM (proExM)[6]. In proExM, fluorescent proteins or fluorescently labelled antibodies are used to stain samples. The proteins or antibodies are then modified with methacrylamide groups that enable anchoring into the gel. To remove the underlying biological structure before expansion, it is necessary to carry out a strong protease digestion. By chance, in the proExM technique, proteins or antibodies are sufficiently retained for visualization. To enhance fluorescence signal and improve visualization, it would be ideal to develop a reagent that is stable to the strong proteolysis that is required for reliable expansion. The modular chemical cross-linker we developed was synthesized using the oligoTEA methodology described in Chapter 1. As mentioned previously, oligoTEAs do not contain secondary amides in their structure as peptides do and as such as stable to proteolytic degradation.

5.2. RESULTS AND DISCUSSION

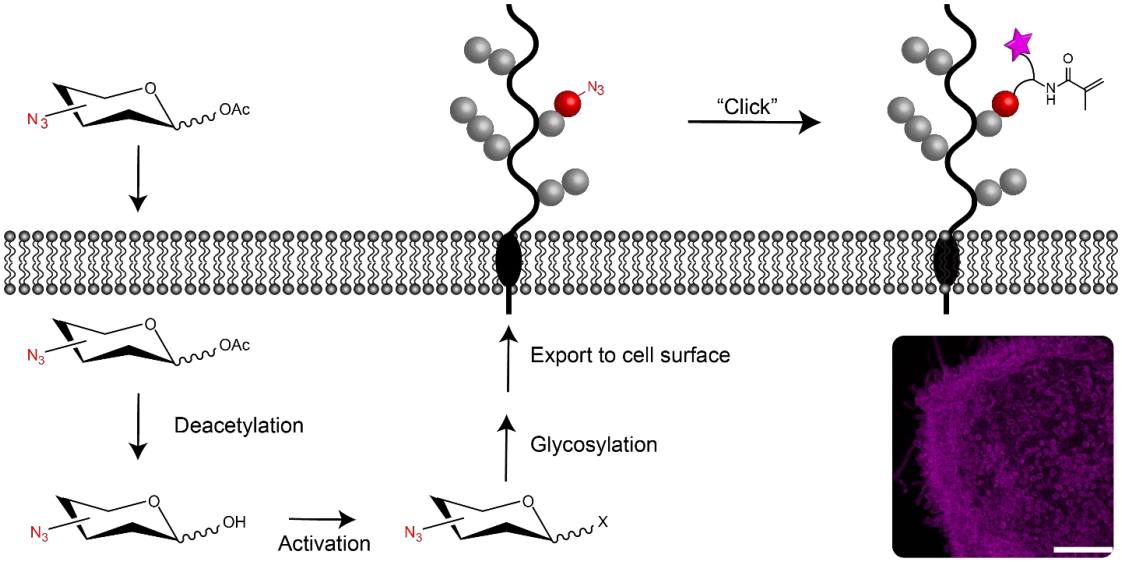

Figure 5.2. Scheme for visualization of the cell surface glycocalyx with "click" ExM probe.

To visualize the cell surface glycocalyx, our collaborators in the Paszek lab at Cornell University, Marshall J. Colville and Joe C.H. Kuo, developed a strategy involving metabolic labeling of cell surface glycans (Figure 5.2). Cells are fed azide-modified sugars based on the method developed by the Bertozzi group.[11] The sugars are processed inside of cells and incorporated into cell surface glycoproteins. We envisioned using these azide functional groups as a chemical handle to attach a molecular probe for expansion microscopy.

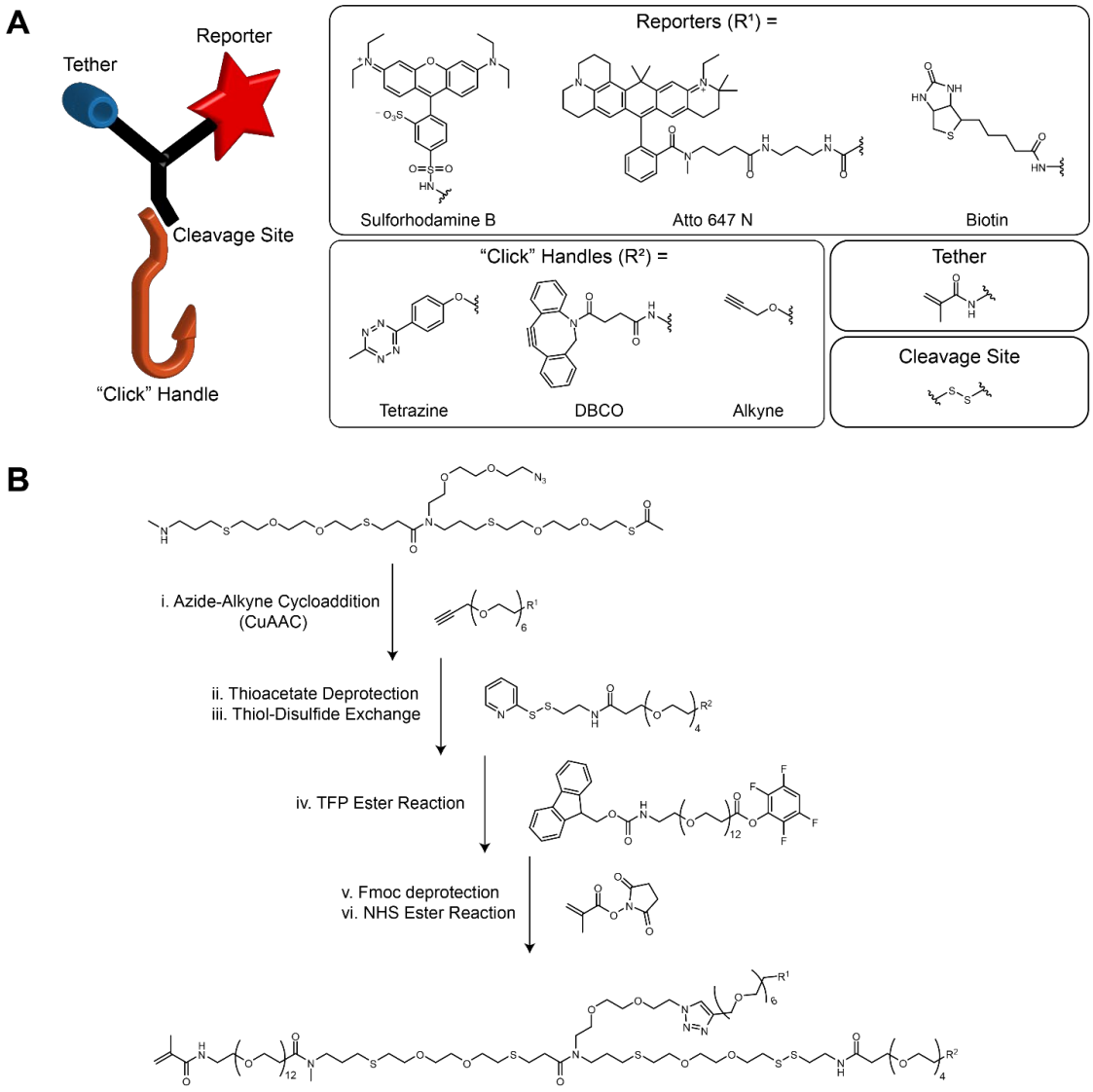

Figure 5.3. Structures and synthesis of "click" ExM probes. A) Cartoon of "click" ExM probe. Reporters, "click handles", tether, and cleavage site used in this work. B) Scheme for synthesizing "click" ExM probes from modular oligoTEA-based heterotrifunctional cross-linker.

The oligoTEA-based chemical cross-linker that we designed is composed of three distinct functional groups: a secondary amine for conjugation with an activated ester, an azide group that can undergo copper-catalyzed alkyne-azide cycloaddition (CuAAC), and a thioacetate for thiol-disulfide exchange (Figure 5.2B). This cross-linker can be modified with a variety of reporters and "click" handles and a methacrylamide anchoring group to generate "click" ExM probes (Figure 5.3A).

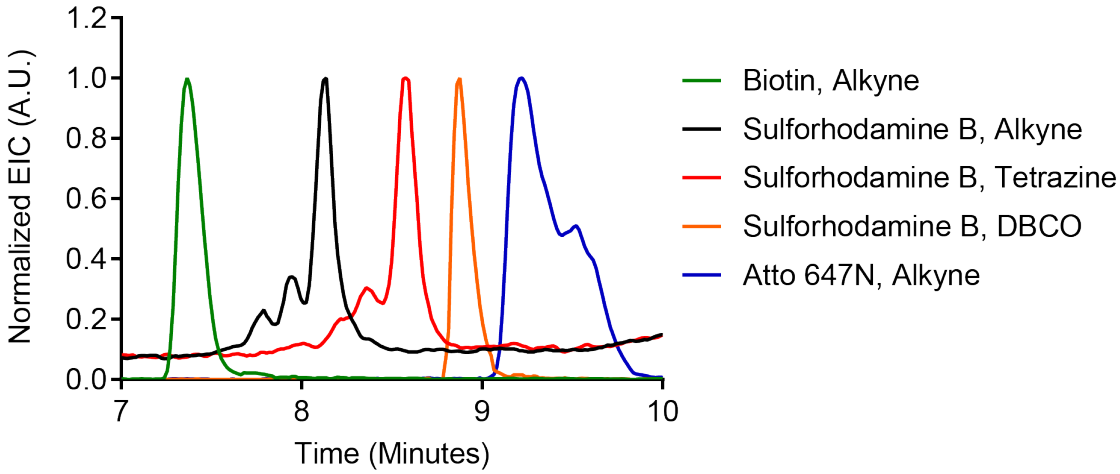

Figure 5.4. Extracted ion count (EIC) of "click" ExM probes via LC-MS indicating relative hydrophobicity.

To synthesize these probes, first, the azide functionality on the cross-linker was reacted with an alkyne-modified reporter with a PEG_6 space (Figure 5.3). We found that adding a PEG_6 spacer to the reporter improved solubility and reaction yield. Next, the thioacetate was deprotected and reacted with a pyridyl disulfide-modified “click” handle with a PEG_4 spacer. The “click” functional group enables glycan-directed labeling via derivatized sugars (Figure 5.2). A reduction-sensitive disulfide bond was incorporated to remove dye that was not incorporated into the gel and thus decrease background. The secondary amine was then reacted with Fmoc-amido-PEG_{12}-TFP ester. The Fmoc was deprotected and the resultant primary amine was reacted with methacrylic acid NHS. The methacrylamide group was attached via a PEG_{12} spacer to improve the accessibility of the methacrylamide group and increase gel incorporation efficiency. Purification was carried out after each step via reversed phase high-performance liquid chromatography (RP-HPLC). Products were characterized with liquid chromatography-mass spectrometry (LC-MS). Through this approach, we synthesized “click” ExM probes containing sulforhodamine B, Atto 647N, and biotin as reporters. The “click” handles that have been incorporated are methyltetrazine,

dibenzocyclooctyne (DBCO), and linear alkyne. The relative hydrophobicity of these probes is shown in Figure 4.4.

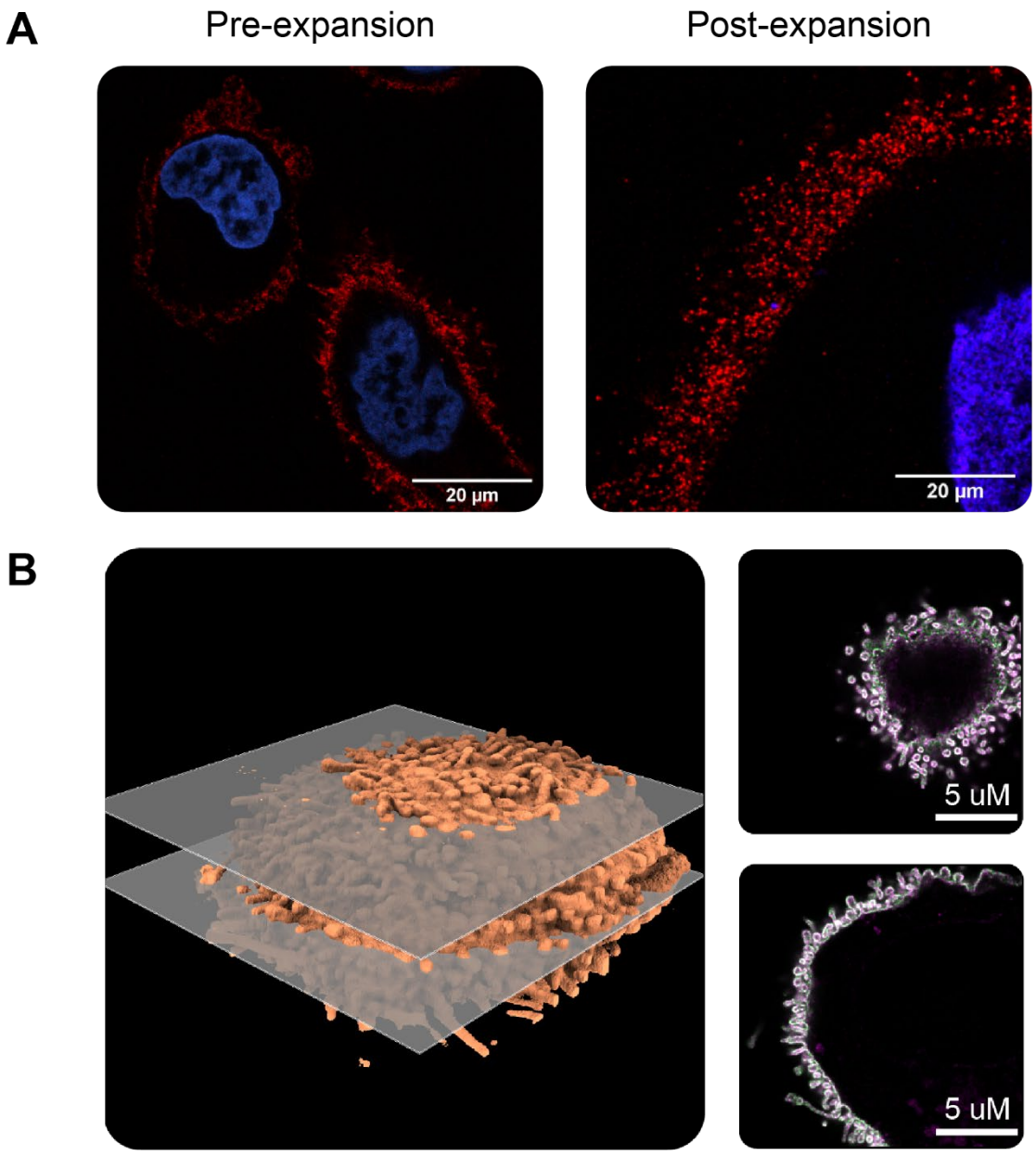

Figure 5.5. ExM imaging of the glycocalyx. A) General demonstration of the expansion process with the probe in MCF 10A cells. Shown in red is the glycan labelled with the probe. B) 3D rendering of cell surface glycosylation (Left). Z slices through the rendering showing colocalization of the probe (green) and Muc1 (magenta) (Right).

Our collaborators have used the strategy outlined in Figure 5.2 with a “click” ExM probe comprised of sulforhodamine B as a reporter and a linear alkyne “click” handle to visualize the cell surface glycocalyx. After expansion, you can see more defined localized spots and increased resolution than in the pre-expansion image (Figure 5.5A). Figure 5.5B shows a 3D rendering of cell surface glycosylation, with Z slices taken through the 3D rendering. In this experiment MCF 10A cells were labelled with the probe shown in green. Shown in magenta is a nanobody targeted against a specific cell-surface glyocoprotein, Muc1. These images demonstrate colocalization of the probe and Muc1 on the cell surface.

5.3. CONCLUSION

We are currently using the other probes that have been synthesized to demonstrate the versatility of this “click” ExM approach. Probes containing a methyltetrazine “click” handle will be used for site-specific protein labeling to small peptide tags. DBCO and linear alkyne probes will be used with metabolic labeling of live worms and cells. Thus, our novel “click” ExM probes have enabled visualization of cellular structures that could not be visualized via previous expansion microscopy techniques. Further, our collaborators have shown that our “click” ExM probes show enhanced signal relative to the traditional reagent used for proExM. In the proExM technique, a portion of the fluorescent proteins or antibodies that are used are digested away. As a result, fluorophore is lost because it is no longer anchored into the gel. Our oligoTEA-based cross-linker is stable to proteolytic digestion and the fluorophore is always retained.

Chapter 5 – APPENDIX

General Materials

All chemicals were purchased from MilliporeSigma unless stated otherwise. “Click” chemistry reagents (Alkyne-PEG_4-NHS Ester, Methyltetrazine-PEG_4-NHS Ester, DBCO-PEG_4-NHS Ester, NH_2-PEG_6-Alkyne, and NHS-PEG_6-Alkyne) were purchased from Click Chemistry Tools. Fmoc-N-amido-$dPEG_{12}$-TFP ester was purchased from Quanta BioDesign. Lissamine rhodamine B sulfonyl chloride was purchased from ThermoFisher Scientific.

General Methods

Nuclear Magnetic Resonance (NMR) spectroscopy: ^{1}H NMR spectra were recorded on an INOVA 400 MHz spectrometer. NMR data was analyzed by MestreNova software. ^{1}H NMR chemical shifts are reported in units of ppm relative to chloroform-D ($CDCl_3$, ^{1}H NMR 7.26 ppm).

Liquid Chromatography Mass Spectroscopy (LC-MS): LC-MS experiments were carried out on an Agilent 1100 Series LC with a Poroshell 120 EC-C18 column (100 × 3 mm, 2.7 µm, Agilent Technologies) and an Agilent G1956B Series Single Quadripole MS in positive ion mode for mass detection. The mobile phase for LC-MS (solvent A) was water with 0.1% v/v acetic acid, and the stationary phase (solvent B) was acetonitrile with 0.1% v/v acetic acid. Compounds were eluted at a flow rate of 0.6 mL/min using a gradient of 5-100% solvent B (0-10 minutes) followed by 100% solvent B (10-12 minutes) and equilibrated back to 5% solvent B (12-15 minutes).

High Performance Liquid Chromatography (HPLC) Purification: HPLC purification was performed on an Agilent 1100 Series HPLC system equipped with a UV diode array detector and an 1100 Infinity fraction collector using a reversed-phase C18 column (9.4 x 250 mm, 5 µm). For reagent not solution or acid-sensitive, the mobile phase for HPLC was water with 0.1% v/v trifluoroacetic acid (solvent A) and acetonitrile with 0.1% v/v trifluoroacetic acid (solvent B). For solution and/or acid-sensitive reagents, the mobile phase for HPLC was water (solvent A) and acetonitrile (solvent B). Compounds were eluted at a flow rate of 4 mL/min with a linear gradient of 5% to 95% solvent B (0-30 minutes), 95% to 100% solvent B (30-32.5 minutes), then 100% solvent B (32.5-42.5 min) and equilibrated back to 5% solvent B (42.5-50 minutes) unless stated otherwise. The oligomer was collected based on its absorption at 230 nm. Fluorophore-conjugated oligomer was collected based on its absorption at 566 nm and 647 nm. The fractionated

compounds were transferred to microcentrifuge tubes, dried, and stored until further analysis.

Flash Chromatography: Flash chromatography was performed on a Teledyne ISCO CombiFlash Rf-200i chromatography system equipped with UV-Vis and evaporative light scattering detectors (ELSD).

Oligomer Synthesis

Synthesis of tert-butyl N-methyl-N-(prop-2-en-1-yl)carbamate – N-allylmethylamine (427 mg, 6 mmol) was dissolved at 151 mM in dichloromethane (DCM). To this solution was added 1.2 equiv of $E_{t3}N$ (729 mg, 7.2 mmol) and the mixture was allowed to equilibrate for 10 minutes on ice. Next, 1.2 equiv of di-tert-butyl dicarbonate (1090.9 mg, 5 mmol) dissolved at 1.6 M in DCM was added over 5 minutes. The final concentration of N-allylmethylamine was 132 mM. The mixture was left on ice for 1 hour and then removed from the ice and reacted at room temperature overnight. The reaction was quenched with 100 mL of water and extracted with DCM (100 mL, 3x). The DCM layer was collected and concentrated under vacuum in 82% yield. The crude product was used without further purification. The product was characterized by ^{1}H NMR and LC-MS (*m/z* calculated: 116.07 observed: 116.00 $[M\text{-t-Butyl+H}]^+$). ^{1}H NMR (400 MHz, $CDCl_3$) δ 5.82-5.70 (m, 1H), 5.18-5.07 (m, 2H), 3.87-3.74 (m, 2H), 2.86-2.76 (s, 3H), 1.52-1.37 (s, 9H).

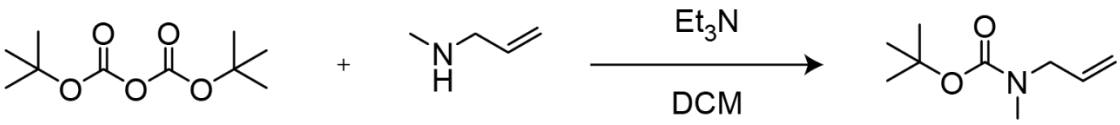

Figure A5.1. Scheme for synthesis of tert-butyl N-methyl-N-(prop-2-en-1-yl) carbamate.

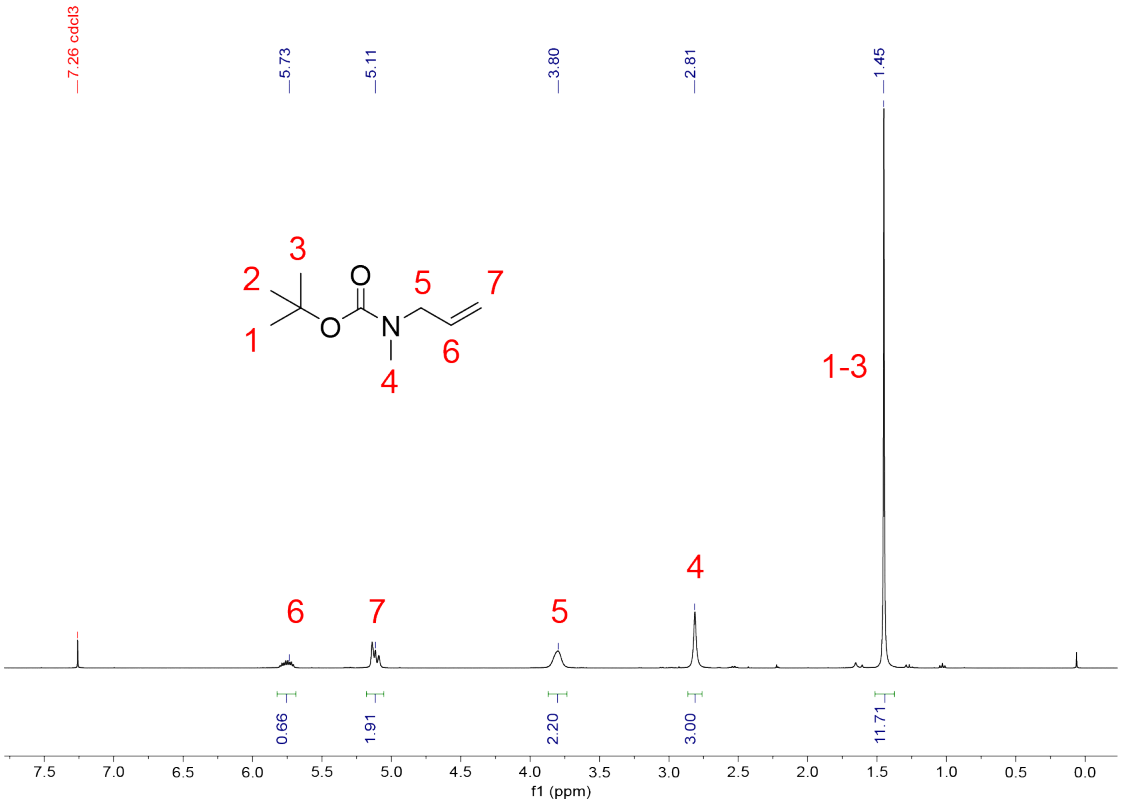

Figure A5.2. ^{1}H NMR (400 MHz, $CDCl_3$) of tert-butyl N-methyl-N-(prop-2-en-1-yl) carbamate.

Synthesis of S-[2-[2-(2-mercaptoethoxy)ethoxy]ethyl] ester ethanethioic acid – 2,2'-(ethylenedioxy)diethanethiol (500 mg, 2.7 mmol) was dissolved at 150 mM in THF. To this solution was added 3 equiv of Et_3N (832 mg, 8.2 mmol) and the mixture was allowed to equilibrate on ice for 10 minutes. Next, 1.05 equiv of acetyl chloride (216 mg, 2.9 mmol) dissolved at 1.6 M in THF was added over 2 hours. The mixture was then removed from the ice and reacted at room temperature overnight. The reaction was quenched with 100 mL of water and extracted with EtOAc (100 mL, 3x). The EtOAc layer was collected and concentrated under vacuum, and the product was purified by flash chromatography (12 g silica, 0-40% ethyl acetate in hexanes) in 42% yield. The product was characterized by ^{1}H NMR. ^{1}H NMR (400 MHz, $CDCl_3$) δ 3.64-3.54 (m, 8H), 3.11-3.05 (t, 2H), 2.72-2.64 (q, 2H), 2.35-2.29 (s, 3H), 1.61-1.54 (t, 1H).

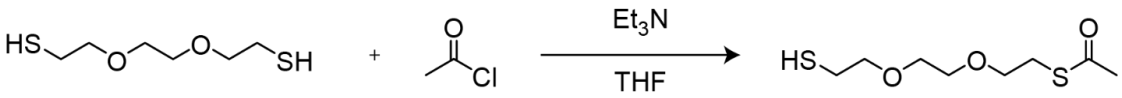

Figure A5.3. Scheme for synthesis of *S*-[2-[2-(2-mercaptoethoxy)ethoxy]ethyl] ester ethanethioic acid.

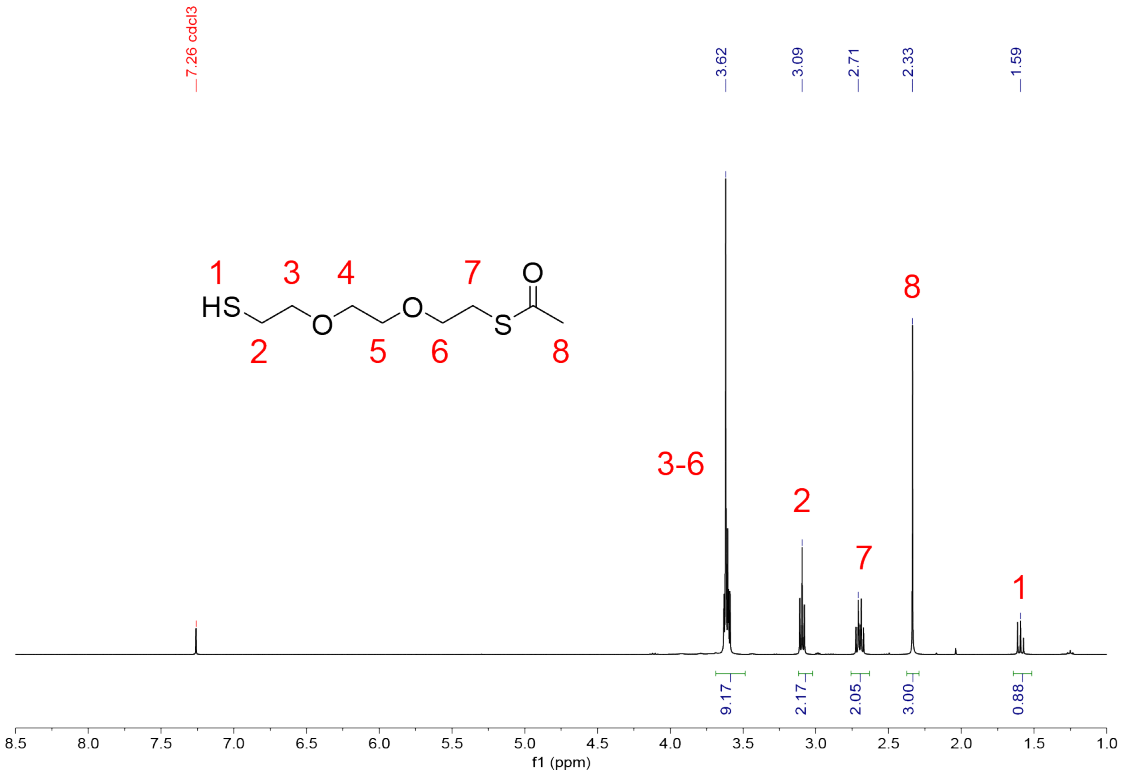

Figure A5.4. ^{1}H NMR (400 MHz, $CDCl_3$) of *S*-[2-[2-(2-mercaptoethoxy)ethoxy]ethyl] ester ethanethioic acid.

Synthesis of 2,[2-(2-azidoethoxy)ethoxy]ethyl-4-methylbenzenesulfonate – P-toluenesulfonyl chloride (3.5 g, 18.4 mmol) was dissolved at 175 mM in dichloromethane (DCM). Separately, 4 equiv of triethylene glycol (11 g, 73 mmol) was dissolved at 110 mM in DCM. To this solution was added 1.05 equiv of Et_3N (1.95 g, 19 mmol) and 0.02 equiv of 4-dimethylaminopyridine (DMAP, 46 mg, 0.3 mmol), and the mixture was allowed to equilibrate for 10 minutes on ice. The solution of p-toluenesulfonyl chloride in DCM was then added dropwise to the mixture over 2 hours. The mixture was subsequently removed from the ice and reacted at room temperature overnight. The reaction was quenched with 100 mL of water and extracted with DCM (100 mL, 3x). The DCM layer was collected and concentrated under vacuum in 98% yield. The crude product was used without further purification. The product was characterized by ^1H NMR and LC-MS (*m/z* calculated: 305.20 observed: 305.09 $[M+H]^+$). ^1H NMR (400 MHz, $CDCl_3$) δ 7.82-7.75 (d, 2H), 7.37-7.30 (d, 2H), 4.19-4.08 (m, 2H), 3.78-3.52 (br, 10H), 2.47-2.40 (s, 3H).

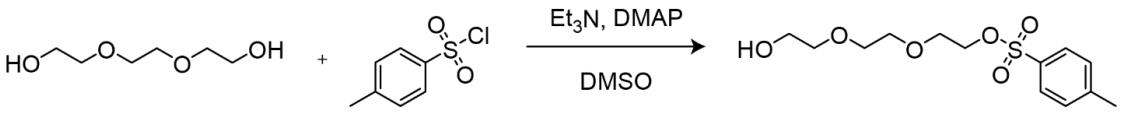

Figure A5.5. Scheme for synthesis of 2,[2-(2-azidoethoxy)ethoxy]ethyl-4-methylbenzenesulfonate.

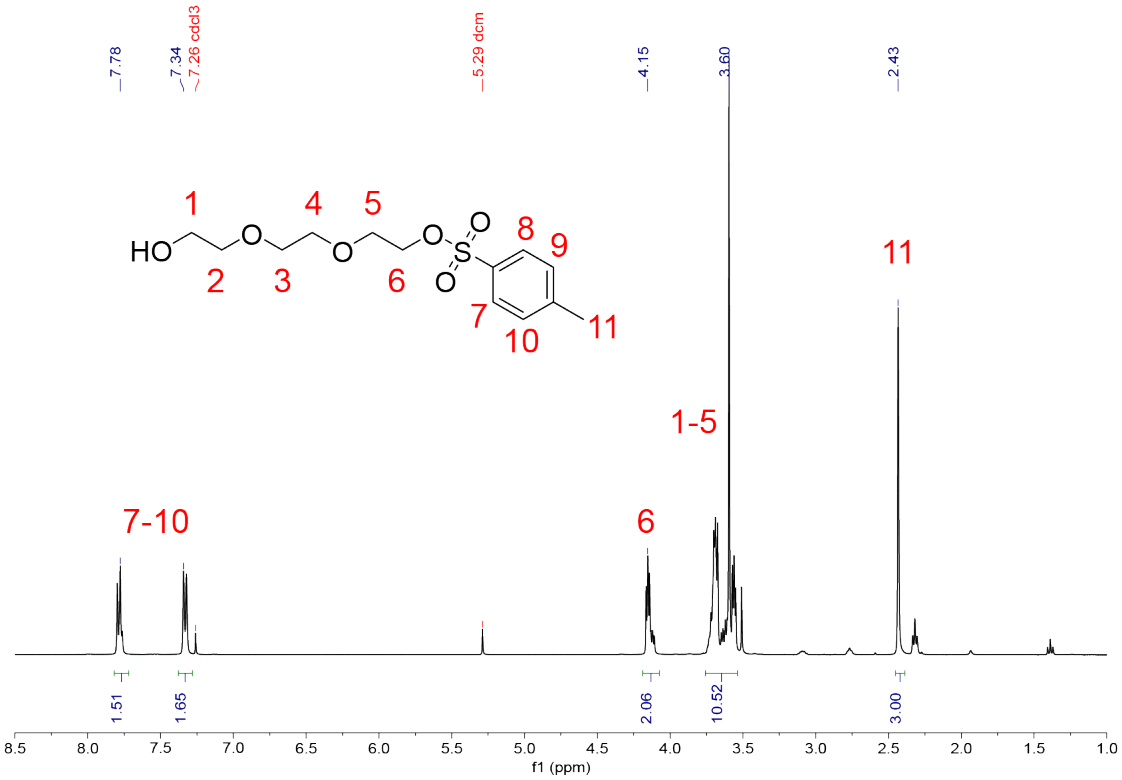

Figure A5.6. ^{1}H NMR (400 MHz, $CDCl_3$) of 2,[2-(2-azidoethoxy)ethoxy]ethyl-4-methylbenzenesulfonate.

Synthesis of 2-(2-(2-azidoethoxy)ethoxy) ethanol – 2,[2-(2-azidoethoxy)ethoxy]ethyl-4-methylbenzenesulfonate was dissolved at 739 mM in dry dimethylformamide (DMF). To this solution was added 2 equiv of sodium azide (2 g, 32 mmol) and the mixture was reacted overnight at 80 °C. The mixture was then concentrated under vacuum and the residue was resuspended in diethyl ether and filtered through celite. The ether was collected and concentrated under vacuum in 96% yield. The crude product was used without further purification. The product was characterized by ^{1}H NMR. ^{1}H NMR (400 MHz, $CDCl_3$) δ 3.74-3.70 (t, 2H), 3.69-3.64 (br, 6H), 3.62-3.58 (m, 6H), 3.41-3.35 (t, 2H).

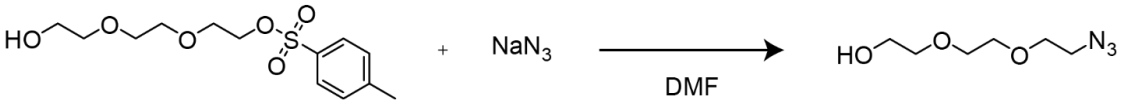

Figure A5.7. Scheme for synthesis of 2-(2-(2-azidoethoxy)ethoxy) ethanol.

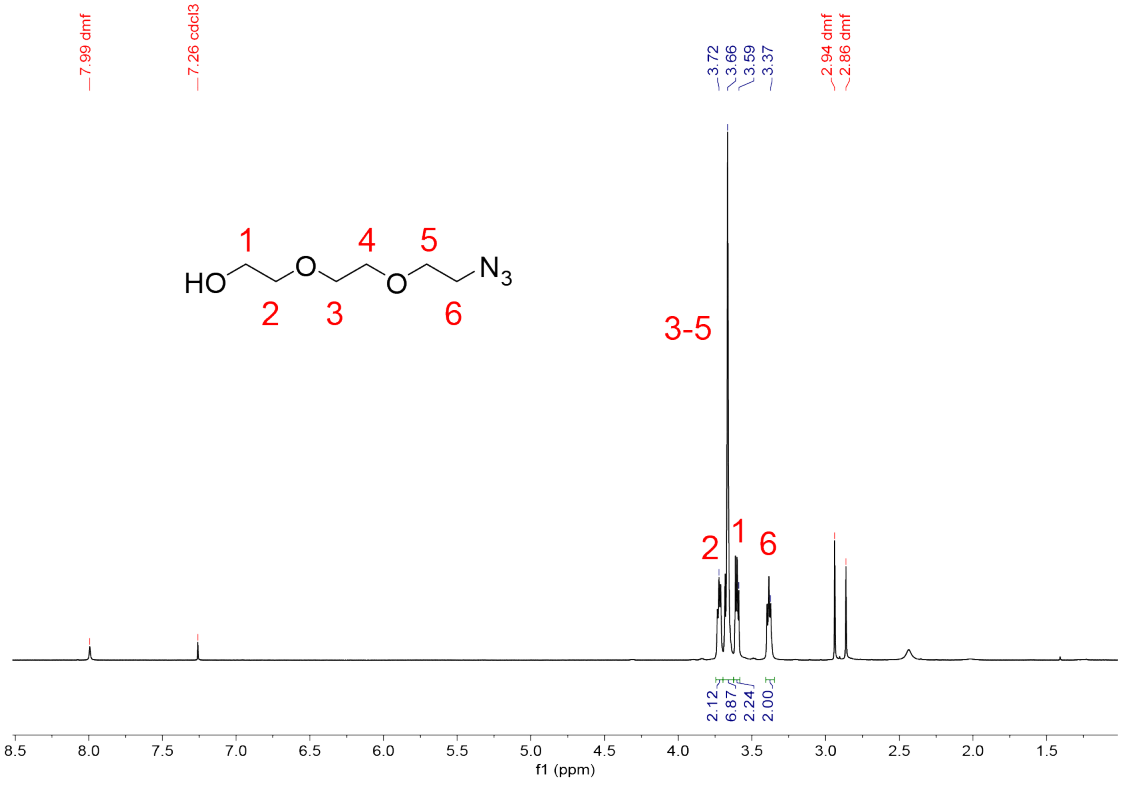

Figure A5.8. ^{1}H NMR (400 MHz, $CDCl_3$) of 2-(2-(2-azidoethoxy)ethoxy) ethanol.

Synthesis of 1-[2-(2-azidoethoxy)ethoxy]-2-bromoethane – 2-(2-(2-azidoethoxy)ethoxy) ethanol (1 g, 5.8 mmol) was dissolved at 342 mM in anhydrous chloroform ($CHCl_3$). To this solution was added 2 equiv of phosphorus tribromide (3.1 g, 12 mmol) over 5 minutes. The mixture was then refluxed overnight at 50 °C. The reaction was quenched on ice over 30 minutes with 75 mL of saturated sodium bicarbonate solution and extracted with $CHCl_3$ (100 mL, 3x). The $CHCl_3$ layer was collected and concentrated under vacuum in 30% yield. The crude product was used without further purification. The product was characterized by ^{13}C NMR. ^{13}C NMR (400 MHz, $CDCl_3$) δ 71.41 70.83 70.73 70.68 70.29 50.85 30.52.

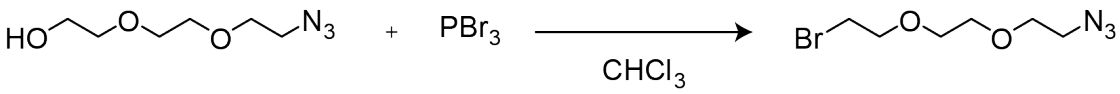

Figure A5.9. Scheme for synthesis of 1-[2-(2-azidoethoxy)ethoxy]-2-bromoethane.

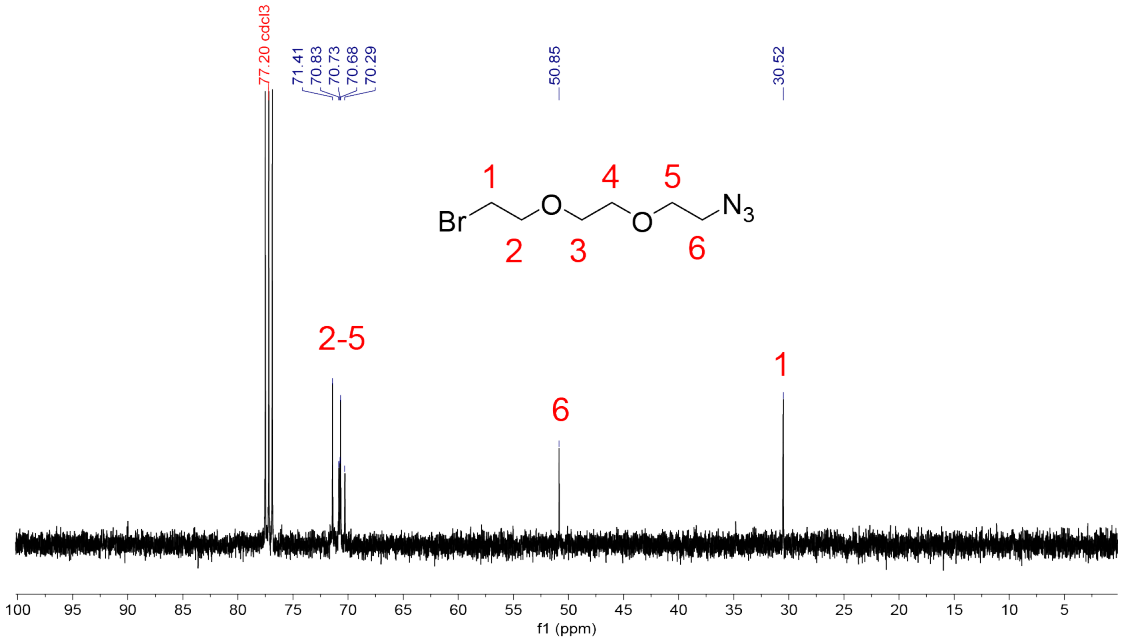

Figure A5.10. ^{13}C NMR (400 MHz, $CDCl_3$) of 1-[2-(2-azidoethoxy)ethoxy]-2-bromoethane.

Synthesis of N-[2-[2-(2-azidoethoxy)ethoxy]ethyl]-2-propen-1-amine - 1 equiv of 1-[2-(2-azidoethoxy)ethoxy]-2-bromoethane (888 mg, 3.73 mmol) was added to 1.2 equiv of potassium carbonate (619 mg, 4.48 mmol) and 10 equiv allylamine (2.1 g, 37.3 mmol). The mixture was allowed to react overnight at room temperature. The reaction was then filtered through celite and concentrated under vacuum in 85% recovery. The crude product was used without further purification. The product was characterized by ^{1}H NMR. ^{1}H NMR (400 MHz, $CDCl_3$) δ 5.99-5.86 (m,1H), 5.24-5.07 (dd, 1H), 3.75-3.58 (br, 8H), 3.46-3.38 (t, 2H), 3.31-3.25 (d, 2H), 2.83-2.79 (t, 2H).

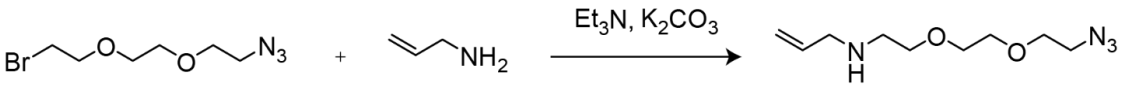

Figure A5.11. Scheme for synthesis of *N*-[2-[2-(2-azidoethoxy)ethoxy]ethyl]-2-propen-1-amine.

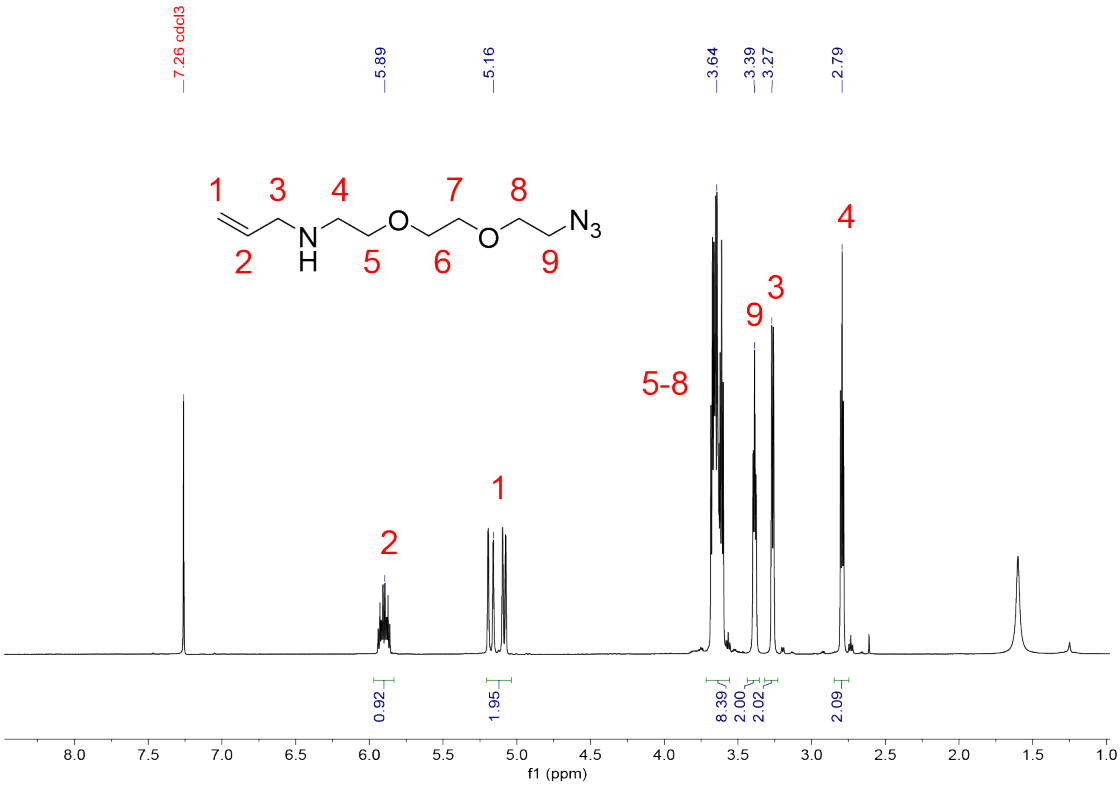

Figure A5.12. ^{1}H NMR (400 MHz, $CDCl_3$) of *N*-[2-[2-(2-azidoethoxy)ethoxy]ethyl]-2-propen-1-amine.

*Synthesis of Compound **(1)*** – 1 equiv of *N*-[2-[2-(2-azidoethoxy)ethoxy]ethyl]-2-propen-1-amine (668 mg, 3.1 mmol) was dissolved at 151 mM in dichloromethane (DCM). To the solution was added 1.1 equiv of Et_3N (347 mg, 3.4 mmol), and the mixture was allowed to equilibrate for 10 minutes on ice. Next, 1.3 equiv acryloyl chloride (367 mg, 4.1 mmol) dissolved at 1.66 M in DCM was added dropwise for 1 hour. The final concentration of *N*-[2-[2-(2-azidoethoxy)ethoxy]ethyl]-2-propen-1-amine was 132 mM. The mixture was then removed from the ice and reacted at room temperature for 1 hour. The reaction was quenched with 6 mL of water and extracted with DCM (80 mL, 3x). The DCM layer was collected and concentrated under vacuum. The product was purified by flash chromatography (12 g silica, 0-5% MeOH in DCM) in 30% yield. The product was characterized by ^{1}H NMR and LC-MS (*m/z* calculated: 269.16 observed: 269.20 $[M+H]^+$). ^{1}H NMR (400 MHz, $CDCl_3$) δ 6.72-6.28 (m, 2H), 5.85-5.72 (m, 1H), 5.70-5.60 (m, 1H), 5.22-5.08 (m, 2H), 4.10-4.04 (m, 2H), 3.70-3.45 (m, 10H), 3.40-3.31, (t, J = 5.1 Hz, 2H).

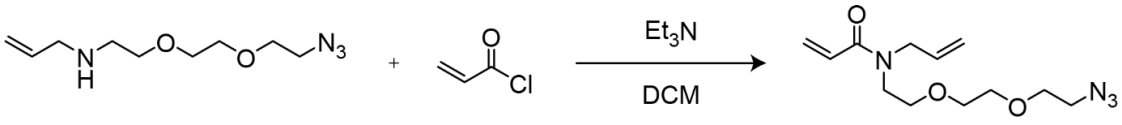

(1)

Figure A5.13. Scheme for synthesis of Compound **(1)**.

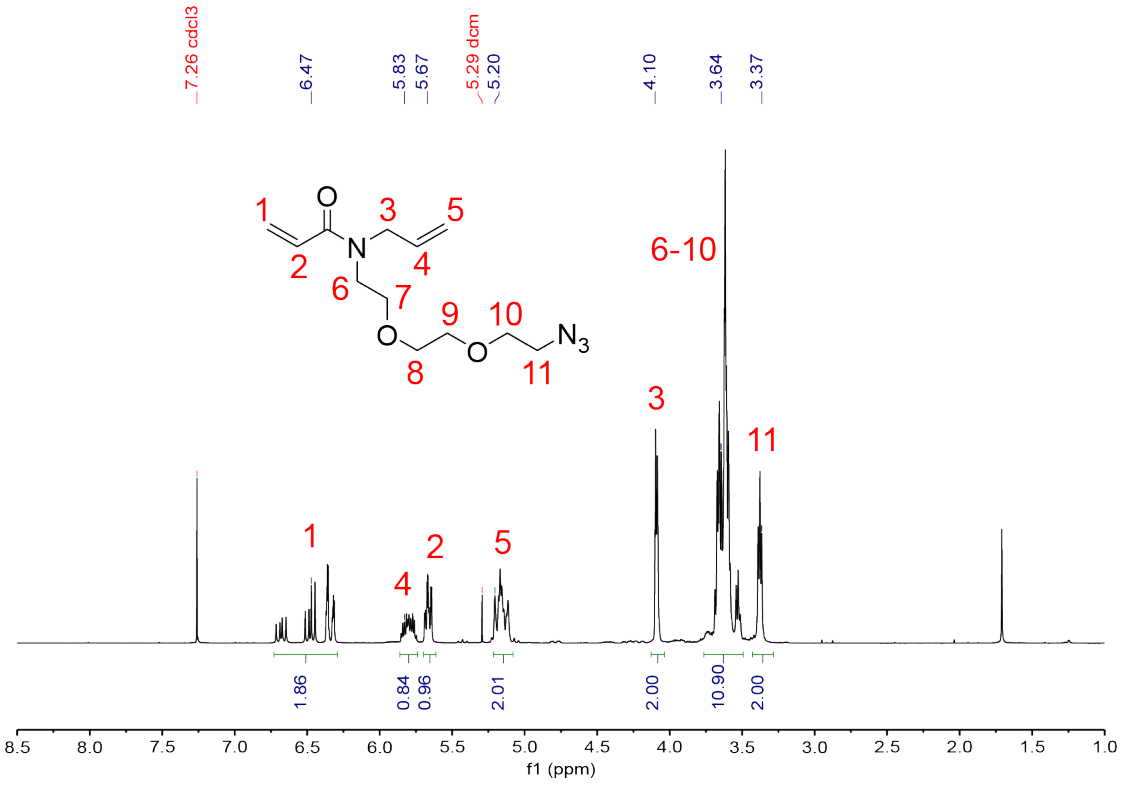

Figure A5.14. ^{1}H NMR (400 MHz, $CDCl_3$) of Compound **(1)**.

Synthesis of Compound ***(2)*** – Tert-butyl N-methyl-N-(prop-2-en-1-yl)carbamate was dissolved at 500 mg/ml in methanol (MeOH). To this solution was added 0.1 equiv of 2,2-dimethoxy-2-phenylacetophenone (DMPA) and 5 equiv of 2,2'-(ethylenedioxy)diethanethiol. The final concentration of tert-butyl N-methyl-N-(prop-2-en-1-yl)carbamate was 306 mM in MeOH. The mixture was subjected to UV irradiation at 5 mW/cm^2 for 270 s. The methanol was then evaporated under reduced pressure, and the product was purified by flash chromatography (40 g silica, 0-20% ethyl acetate in hexanes). The product was characterized by ^{1}H NMR. ^{1}H NMR (400 MHz, $CDCl_3$) δ 3.67-3.54 (m, 8H), 3.31-3.22 (t, 2H), 2.85-2.79 (s, 3H), 2.74-2.65 (m, 4H), 2.56-2.48 (t, 2H), 1.83-1.71 (q, 2H), 1.62-1.54 (t, 1H), 1.47-1.37 (s, 9H).

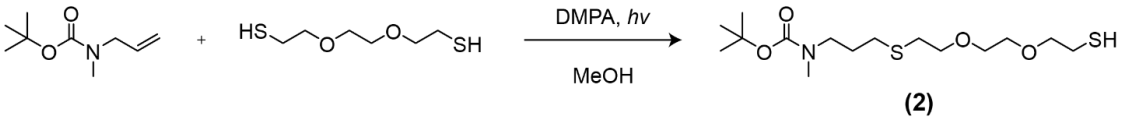

Figure A5.15. Synthesis of Compound **(2)**.

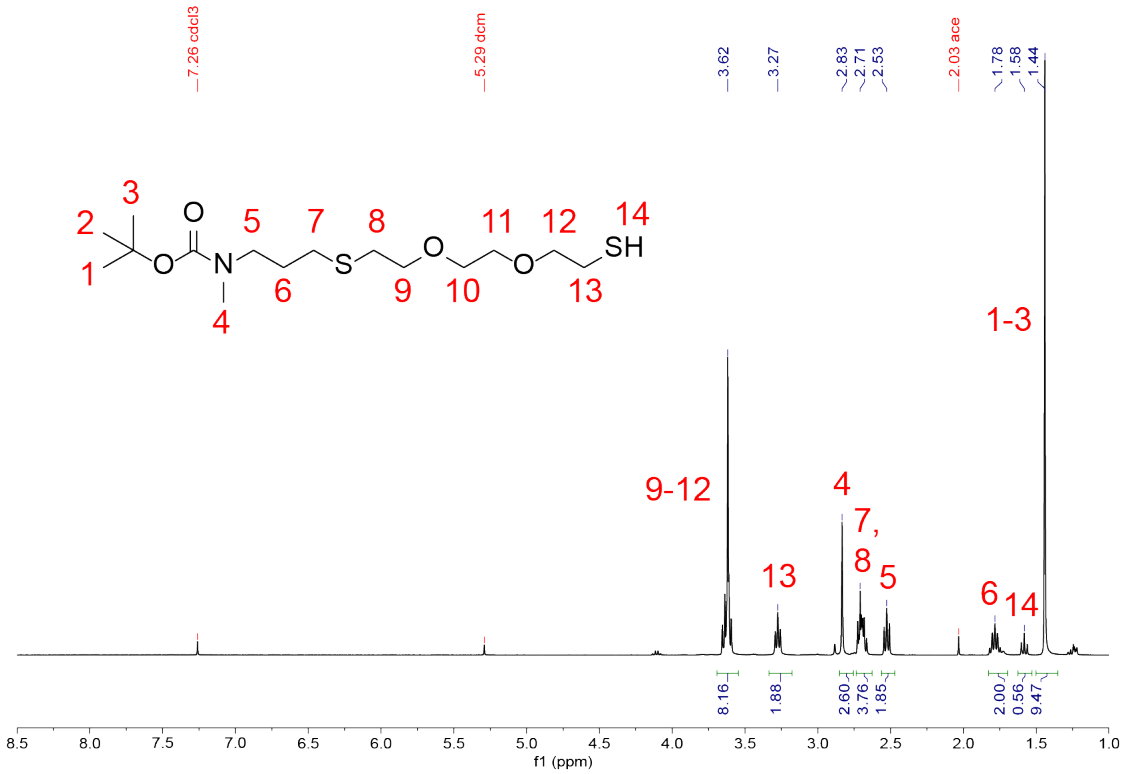

Figure A5.16. ^{1}H NMR (400 MHz, $CDCl_3$) of Compound **(2)**.

*Synthesis of Compound **(3)*** – 1 equiv of Compound **(2)** was mixed with 1 equiv of Compound **(1)** and 0.05 equiv 1,8-diazabicyclo[5.4.0]undec-7-ene (DBU) at a final concentration of 600 mM in acetonitrile (ACN). The mixture was reacted overnight at room temperature. The product was characterized by LC-MS (*m/z* calculated: 644.31 observed: 644.20 $[M+Na]^+$) and used without further purification.

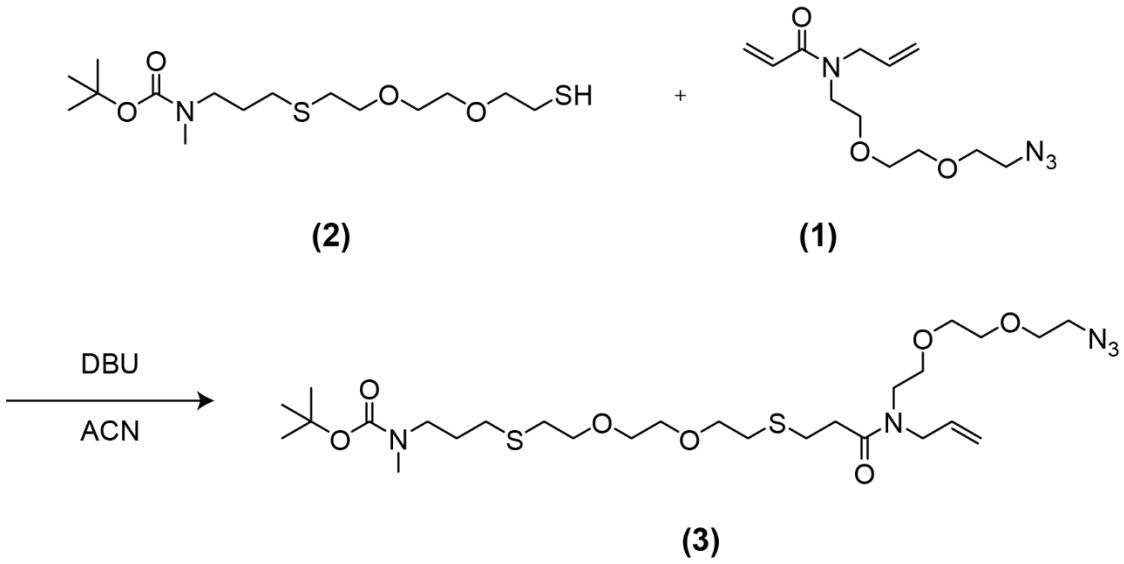

(2) **(1)** **(3)**

Figure A5.17. Scheme for synthesis of Compound **(3)**.

*Synthesis of Compound **(4)*** – 1 equiv of Compound **(3)** was mixed with 2.2 equiv of *S*-[2-[2-(2-mercaptoethoxy)ethoxy]ethyl] ester ethanethioic acid and 0.2 equiv of DMPA at a final concentration of 600 mM in MeOH. The mixture was subjected to UV irradiation at 5 mW/cm^2 for 270 s. **The mixture was purified via semi-preparative RP-HPLC (mobile phase without TFA).** The product eluted at 37.9 minutes and was characterized by ^{1}H NMR and LC-MS (*m/z* calculated: 868.37 observed: 868.20 $[M+Na]^+$). ^{1}H NMR (400 MHz, $CDCl_3$) δ 3.67-3.54 (br, 24H), 3.53-3.40 (m, 4H), 3.39-3.35 (t, 2H), 3.28-3.23 (m, 2H), 3.09-3.05 (t, 2H), 2.86-2.47 (m, 16H), 2.33-2.39 (s, 2H), 1.87-1.73 (m, 4H), 1.45-1.40 (s, 9H).

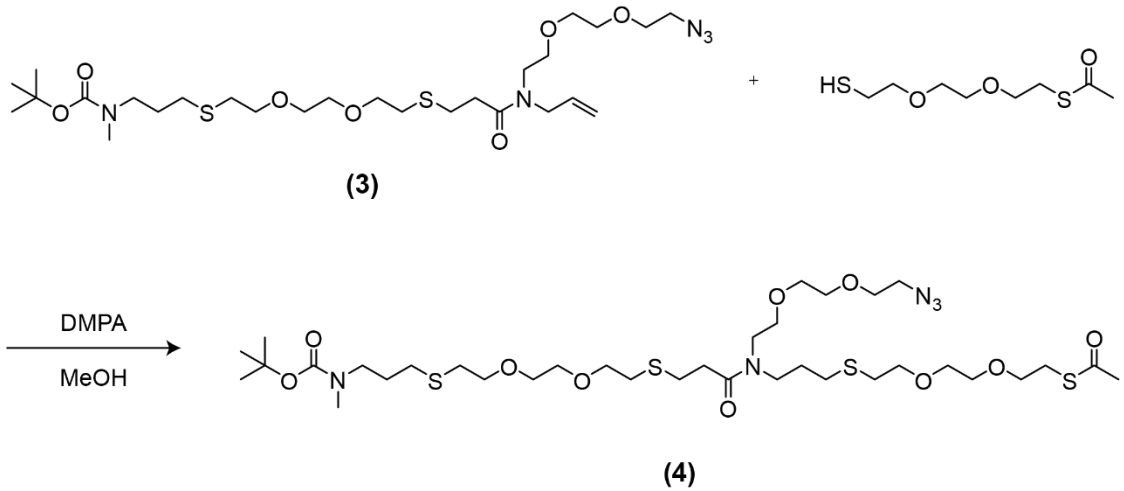

Figure A5.18. Scheme for synthesis of Compound **(4)**.

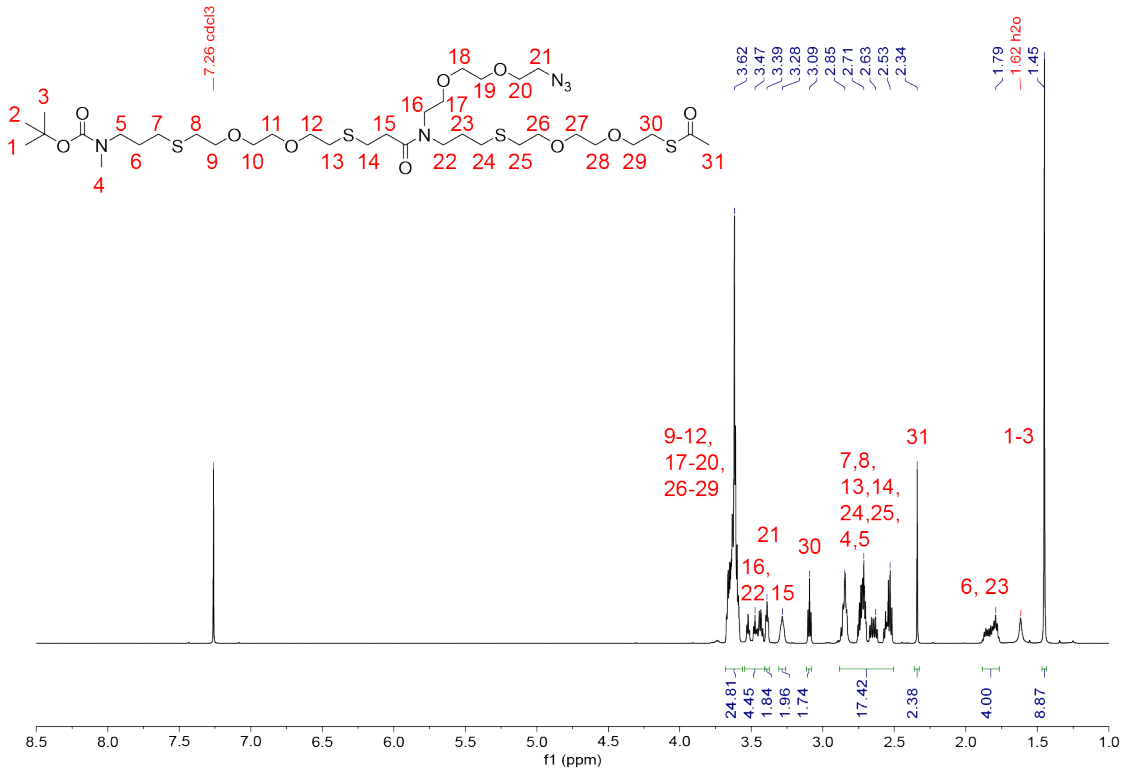

Figure A5.19. ^{1}H NMR (400 MHz, $CDCl_3$) of Compound **(4)**.

*Tert-butoxy carbamate (Boc) Deprotection of Compound **(4)*** – Compound **(4)** was mixed at 5 mM in 50% trifluoroacetic acid (TFA) in DCM for 1 hour. The TFA and DCM were then removed under vacuum. The product was characterized by LC-MS (*m/z* calculated: 746.33 observed: 746.20 $[M+H]^+$).

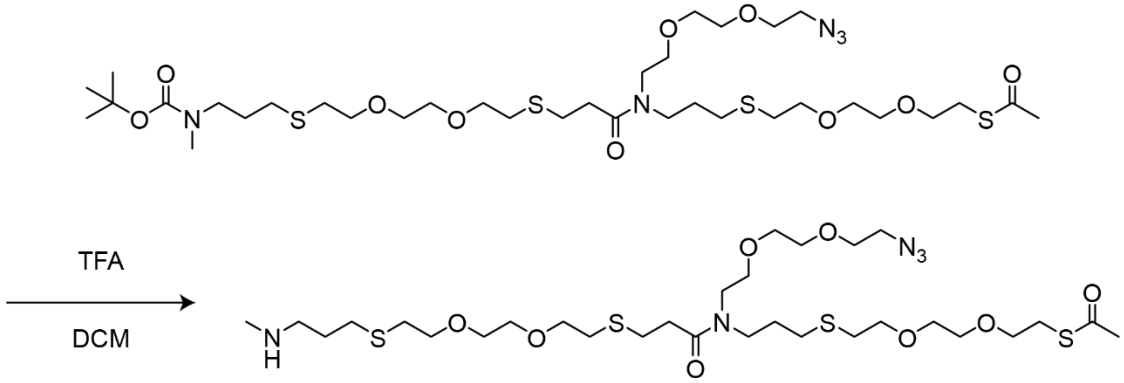

(5)

Figure A5.20. Synthesis of Compound **(5)**.

Oligomer Conjugation to Reporter, "Click" Handle, and Anchoring Group

Synthesis of 2-(phenyldithio)-ethanamine – 1 equiv of **tert-butyl N-(2-mercaptoethyl)carbamate was mixed with 1 equiv of 2,2'-dithiodipyridine and 2 equiv of Et_3N. The final concentration** of **tert-butyl N-(2-mercaptoethyl)carbamate was 500 mM in DMSO. The mixture was reacted overnight at room temperature and purified via semi-preparative RP-HPLC (mobile phase with TFA). The** compound was eluted at a flow rate of 4 mL/min with a linear gradient of 5% to 95% solvent B (0-15 minutes), then 95% solvent B (15-20 min) and equilibrated back to 5% solvent B (20-30 minutes). **The product eluted at 12.4 minutes.** The HPLC-purified product was then mixed at 50 mM in 50% trifluoroacetic acid (TFA) in DCM for 1 hour. The TFA and DCM were then removed under vacuum to yield the desired product, 2-(phenyldithio)-ethanamine.

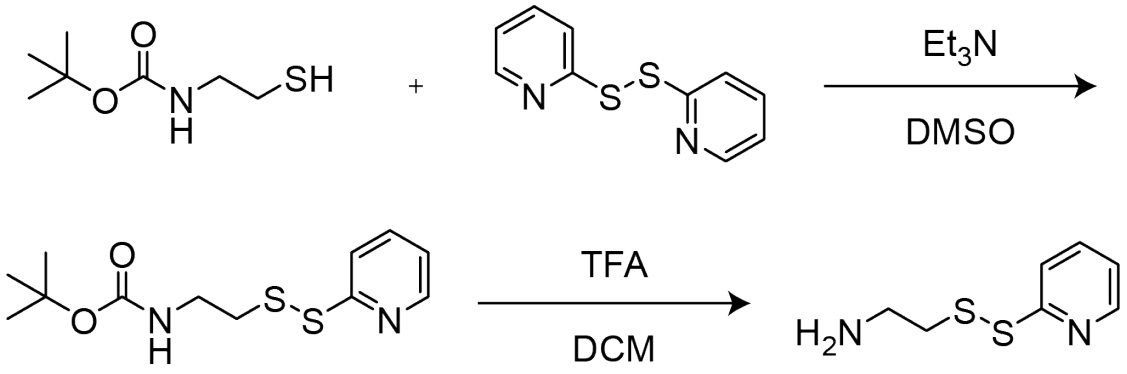

Figure A5.21. Scheme for synthesis of 2-(phenyldithio)-ethanamine.

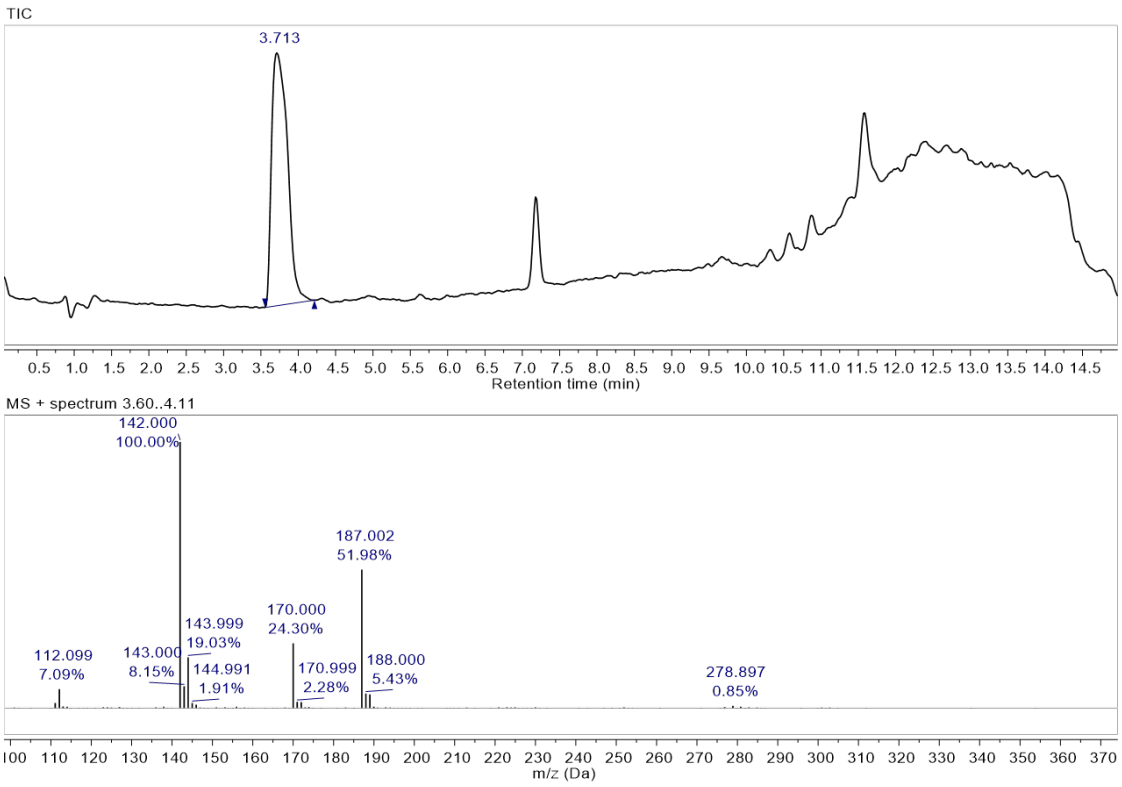

Figure A5.22. LC-MS of 2-(phenyldithio)-ethanamine.

*Synthesis of Compound **(5)*** – 1 equiv of lissamine rhodamine B sulfonyl chloride was mixed with 2 equiv of 3,6,9,12,15,18-hexaoxahenicos-20yn-1-amine and 5 equiv of Et_3N at a final concentration of 100 mM in DMF. **The mixture was reacted overnight at room temperature and purified via semi-preparative RP-HPLC.** The product eluted at 19.2 minutes and was characterized by LC-MS (*m/z* calculated: 860.35 observed: 860.20 $[M+H]^+$).

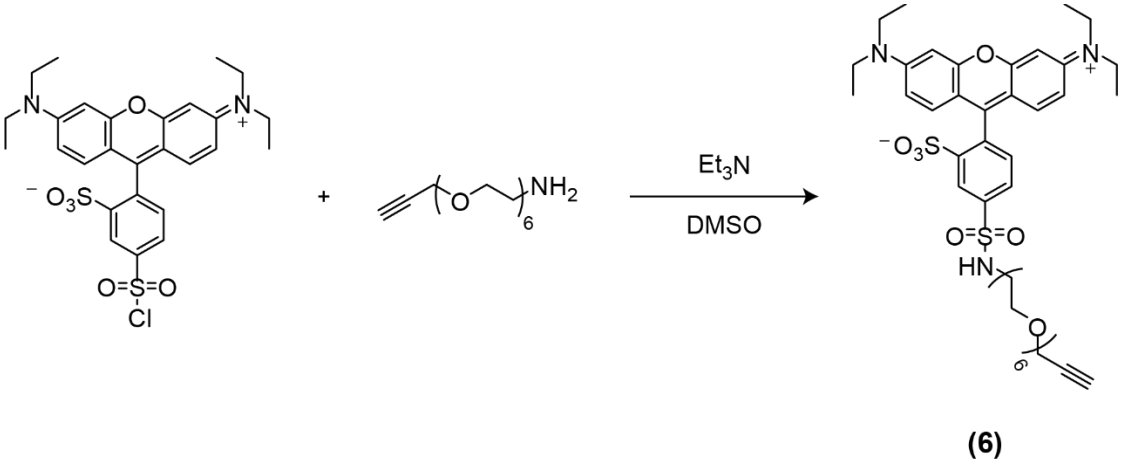

(6)

Figure A5.23. Scheme for synthesis of Compound **(6)**.

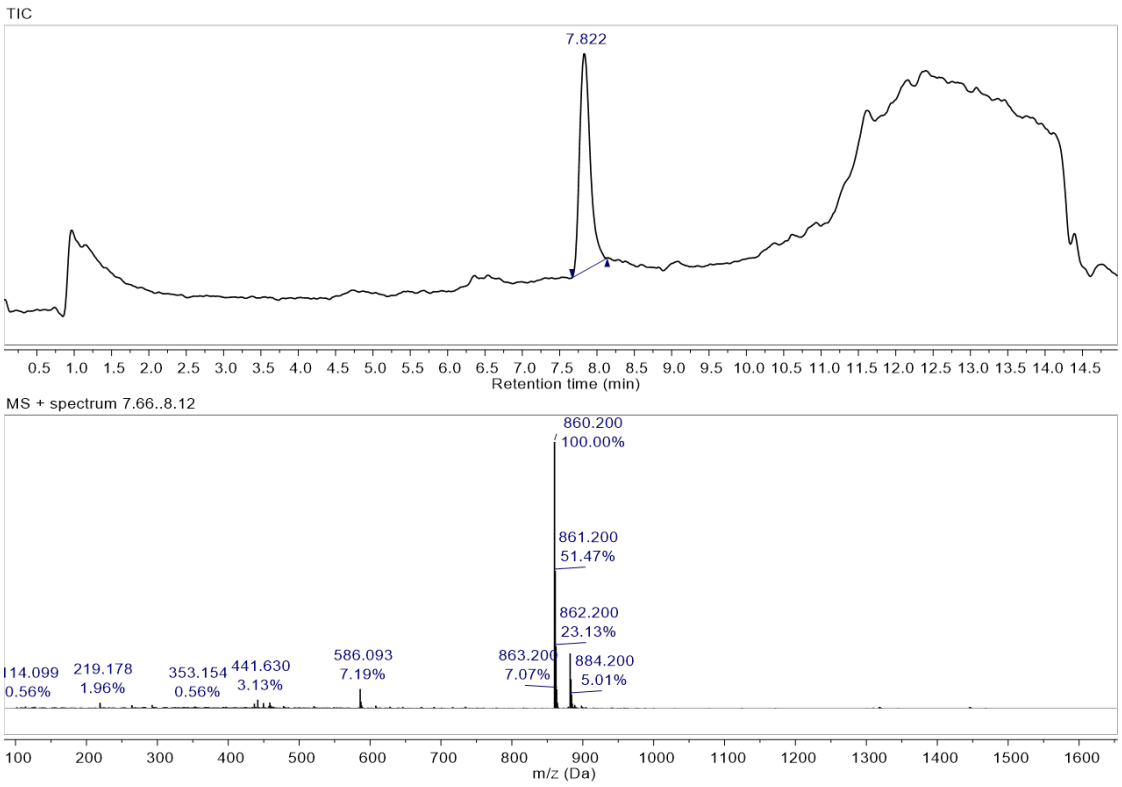

Figure A5.24. LC-MS of Compound **(6)**.

Synthesis of Compound ***(6)*** – 1 equiv of D-biotin *N*-succinimidyl ester was mixed with 2 equiv of 3,6,9,12,15,18-hexaoxahenicos-20yn-1-amine and 5 equiv of Et_3N at a final concentration of 100 mM in DMF. **The mixture was reacted overnight at room temperature and purified via semi-preparative RP-HPLC (mobile phase with TFA).** The product eluted at 11.5 minutes and was characterized by LC-MS (*m/z* calculated: 546.29 observed: 546.20 $[M+H]^+$).

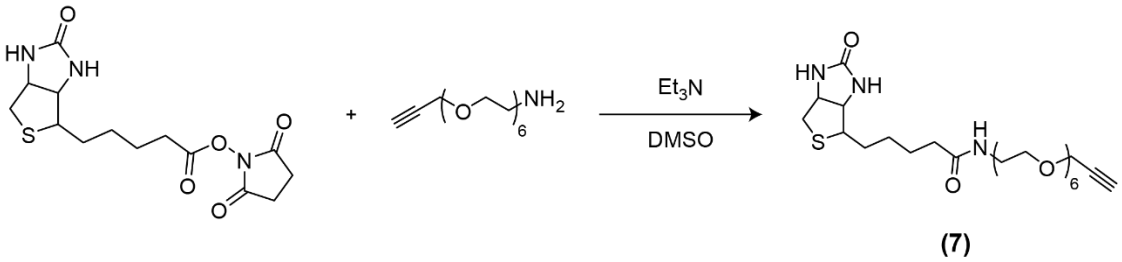

(7)

Figure A5.25. Scheme for synthesis of Compound **(7)**.

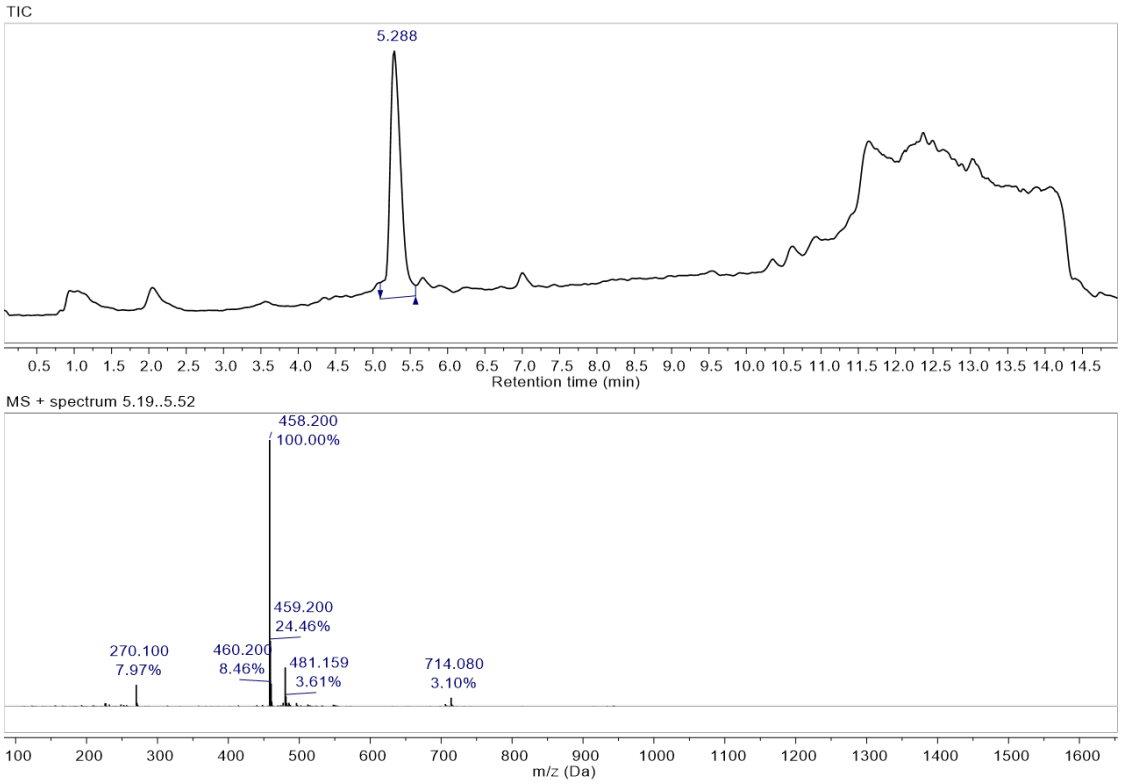

Figure A5.26. LC-MS of Compound **(7)**.

*Synthesis of Compound **(7)*** – 1 equiv of Atto 647N amine was mixed with 2 equiv of 2,5-dioxopyrrolidin-1-yl 4,7,10,13,16,19-hexaoxadocos-21-ynoate and 5 equiv of Et_3N at a final concentration of 100 mM in DMF. **The mixture was reacted overnight at room temperature and purified via semi-preparative RP-HPLC (mobile phase with TFA). The product eluted at 23.4 minutes and** was characterized by LC-MS (*m/z* calculated: 1018.63 observed: 1018.40 $[M]^+$).

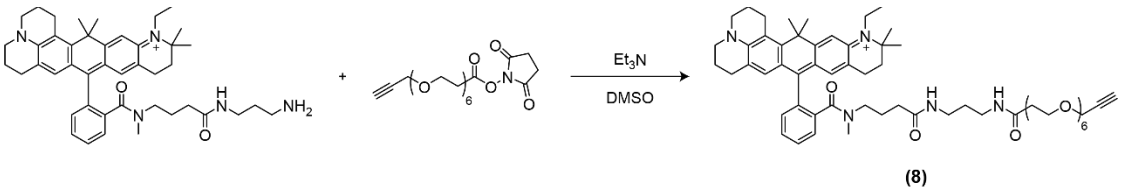

Figure A5.27. Scheme for synthesis of Compound **(8)**.

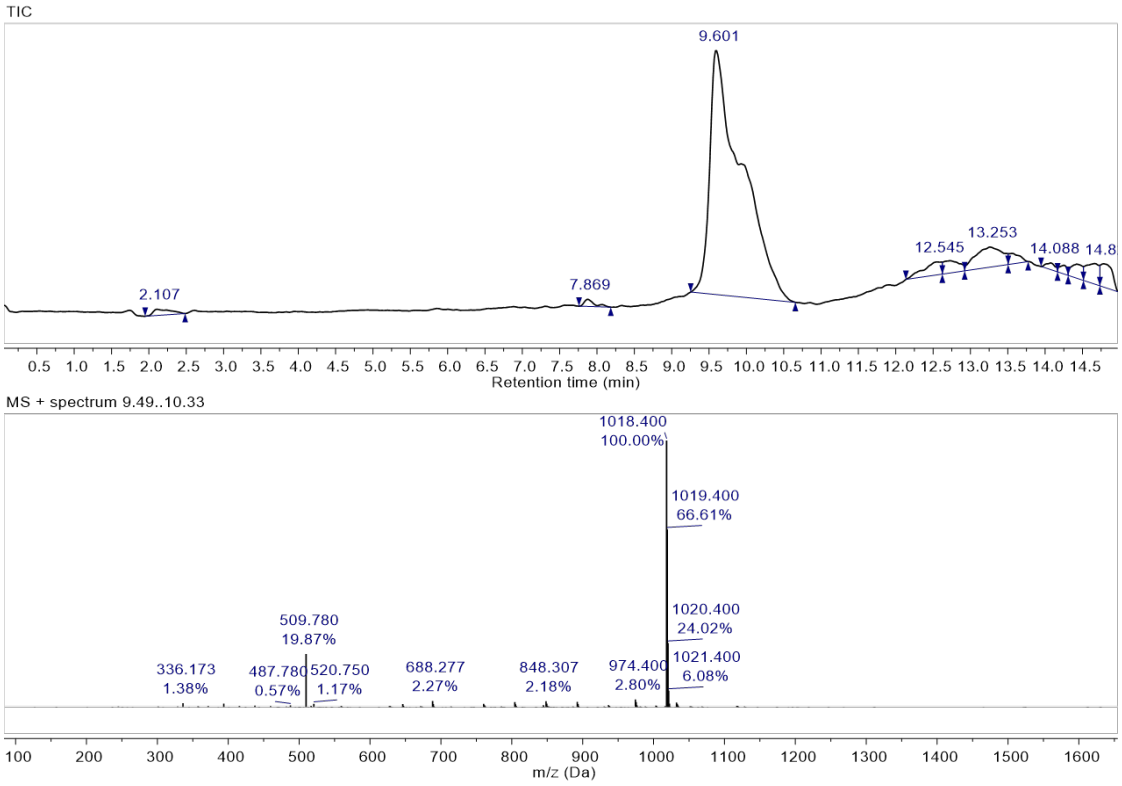

Figure A5.28. LC-MS of Compound **(8)**.

*Synthesis of Compounds **(9)**, **(10)**, and **(11)*** – 1 equiv of 4,7,10,13,16-pentaoxanonadec-18-ynoic acid *N*-succinimidyl ester (Alkyne-PEG4-NHS), 3-[2-[2-[2-[2-[2-[4-(6-methyl-1,2,4,5-tetrazin-3-yl)phenoxy]ethoxy]ethoxy]ethoxy]ethoxy]-, 2,5-dioxo-1-pyrrolidinyl ester (Methyltetrazine-PEG4-NHS), or 2,5-dioxo-1-pyrrolidinyl 20-(11,12-didehydrodibenz[b,f]azocin-5(6H)-yl)-17,20-dioxo-4,7,10,13-tetraoxa-16-azaeicosanoate (DBCO-PEG4-NHS) (50 mg/ml in DMSO) was mixed with 2 equiv of 2-(phenyldithio)-ethanamine (100 mg/ml in DMSO) and 3 equiv of Et_3N at a final concentration of 80 mM in DMSO. **The mixture was reacted overnight at room temperature and purified via semi-preparative RP-HPLC. Compound (9) eluted at 14 minutes. Compound (10) eluted at 18.3 minutes (mobile phase with TFA). Compound (11) eluted at 20 minutes (mobile phase without TFA).** The product was characterized by LC-MS (Compound **(9)** *m/z* calculated: 473.18 observed: 473.10 $[M+H]^+$; Compound **(10)** *m/z* calculated: 721.28 observed: 721.20 $[M+H]^+$; Compound **(11)** *m/z* calculated: 605.10 observed: 605.22 $[M+H]^+$).

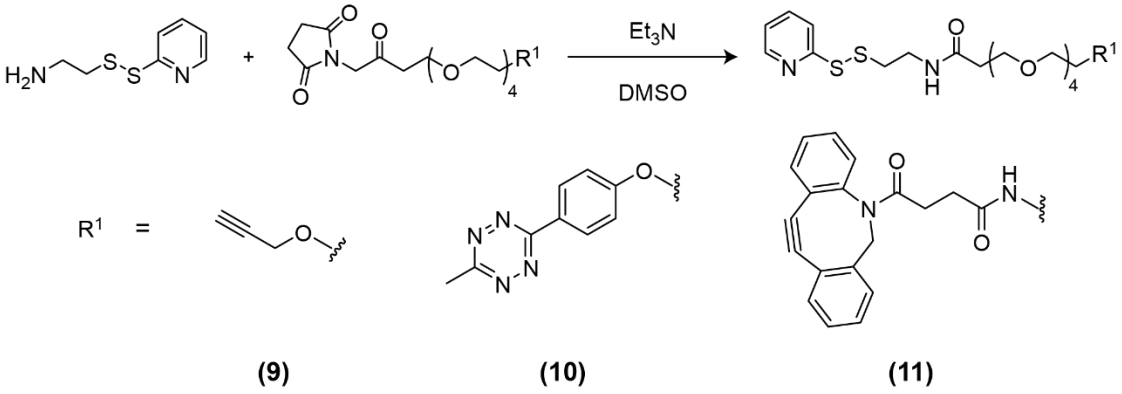

Figure A5.29. Scheme for synthesis of Compounds **(9)**, **(10)**, and **(11)**.

*Synthesis of Compounds **(12)**, **(13)**, and **(14)*** – 1 equiv of Compound **(5)** was dissolved at 15 mg/ml in DMSO. To this solution was added 1 equiv of Compound **(6)**, **(7)**, or **(8)** (160 mg/ml in DMSO), 0.25 equiv of copper sulfate (10 mg/ml in water), 0.5 equiv of tris[(1-benzyl-1*H*-1,2,3-triazol-4-yl)methyl]amine (TBTA) (50 mg/ml in DMSO), and 2.5 equiv of sodium ascorbate (30 mg/ml in water). The final concentration of Compound **(5)** was 8.5 mM in 20% water in DMSO. The mixture was reacted overnight at room temperature and purified via semi-preparative RP-HPLC (mobile phase with TFA). Compound **(12)** eluted at 19.1 minutes. Compound **(13)** eluted at 15 minutes. Compound **(14)** eluted at 22.2 minutes. The product was characterized by LC-MS (Compound **(12)** *m/z* calculated: 782.20 observed: 782.33 $[M+2H]^{2+}$; Compound **(13)** *m/z* calculated: 646.30 observed: 646.30 $[M+2H]^{2+}$; Compound **(14)** *m/z* calculated: 882.98 observed: 882.40 $[M+2H]^{2+}$).

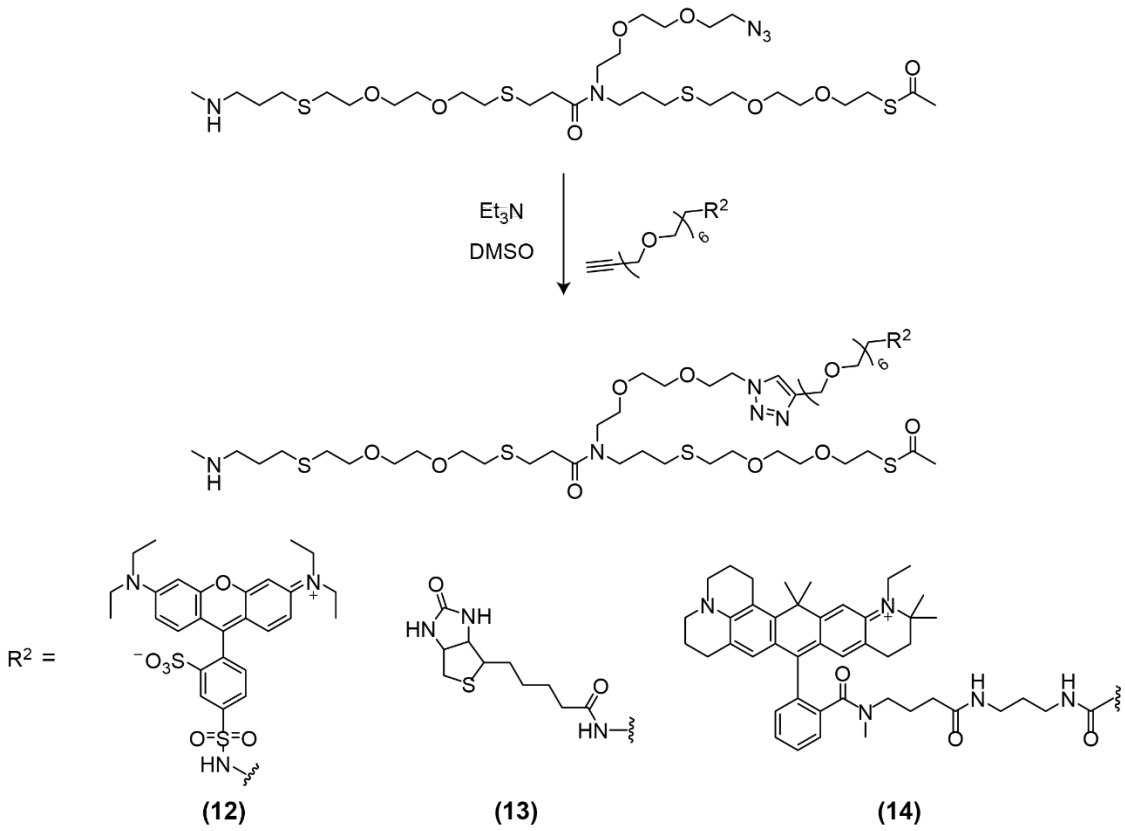

Figure A5.30. Scheme for synthesis of Compounds **(12)**, **(13)**, and **(14)**.

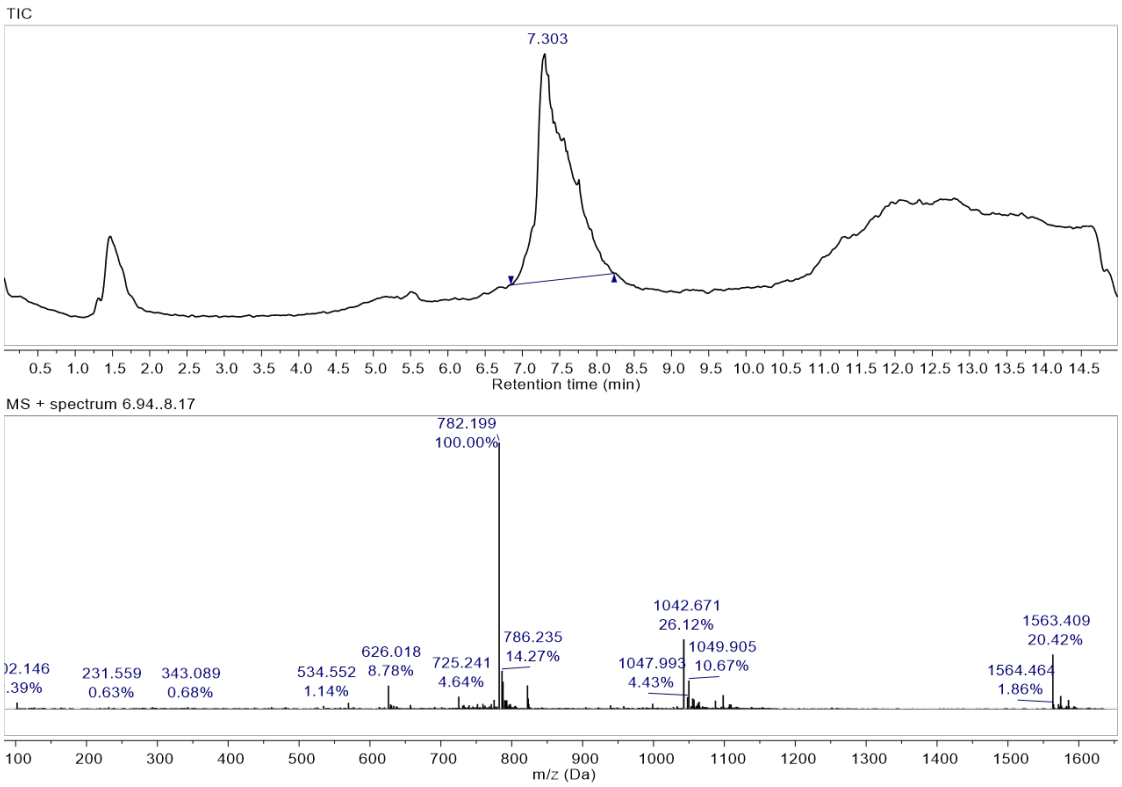

Figure A5.31. LC-MS of Compound **(12)**.

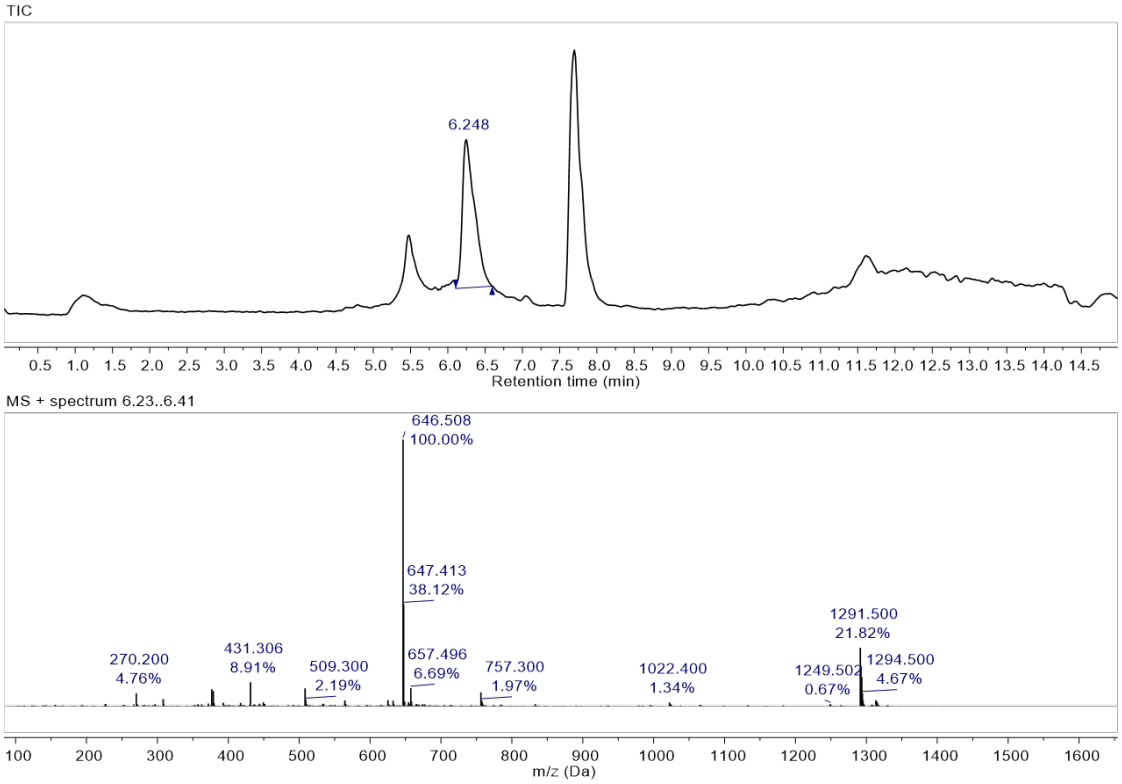

Figure A5.32. LC-MS of Compound **(13)**.

*Conjugation of Compounds **(12)**, **(13)**, or **(14)** to Compound **(9)**, **(10)**, or **(11)** [Synthesis of **"Click" Handle-modified Oligomers**]* – To 1 equiv of Compound **(12)**, **(13)**, or **(14)** was added 200 equiv of ammonia (7N in MeOH) to give a final concentration of 500 mM in MeOH. The mixture was reacted for 30 minutes at room temperature. Next, 1.2 equiv of Compound **(9)**, **(10)**, or **(11)** was added and reacted for 2 hours at room temperature. The reaction was then purified via semi-preparative RP-HPLC (mobile phase with TFA). Compound **(12-9)** eluted at 25.5 minutes. Compound **(12-10)** eluted at 26 minutes. Compound **(12-11)** eluted at 26.5 minutes. Compound **(13-9)** eluted at 15.8 minutes. Compound **(14-9)** eluted at 29 minutes. The product was characterized by LC-MS (Compound **(12-9)** *m/z* calculated: 962.91 observed 963.26 $[M+2H]^{2+}$; Compound **(12-10)** *m/z* calculated: 1028.93 observed: 1029.73 $[M+2H]^{2+}$; Compound **(12-11)** *m/z* calculated: 1086.95 observed 1087.30 $[M+2H]^{2+}$; Compound **(13-9)** calculated: 805.88 observed: 805.99 $[M+2H]^{2+}$; Compound **(14-9)** *m/z* calculated: 1042.44 observed: 1042.43 $[M+2H]^{2+}$).

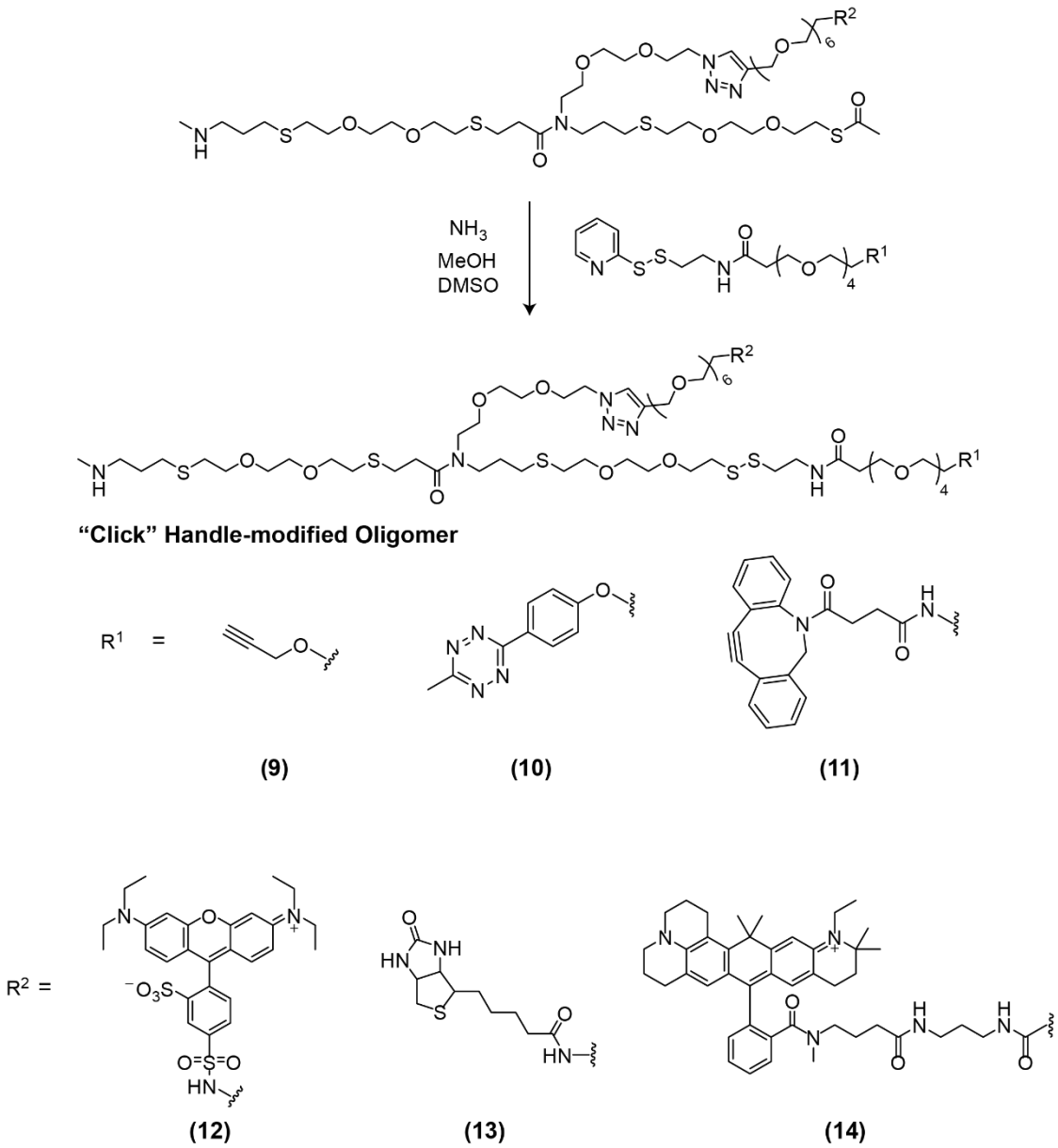

Figure A5.33. Scheme for conjugation of Compounds **(12)**, **(13)**, or **(14)** to Compound **(9)**, **(10)**, or **(11)**

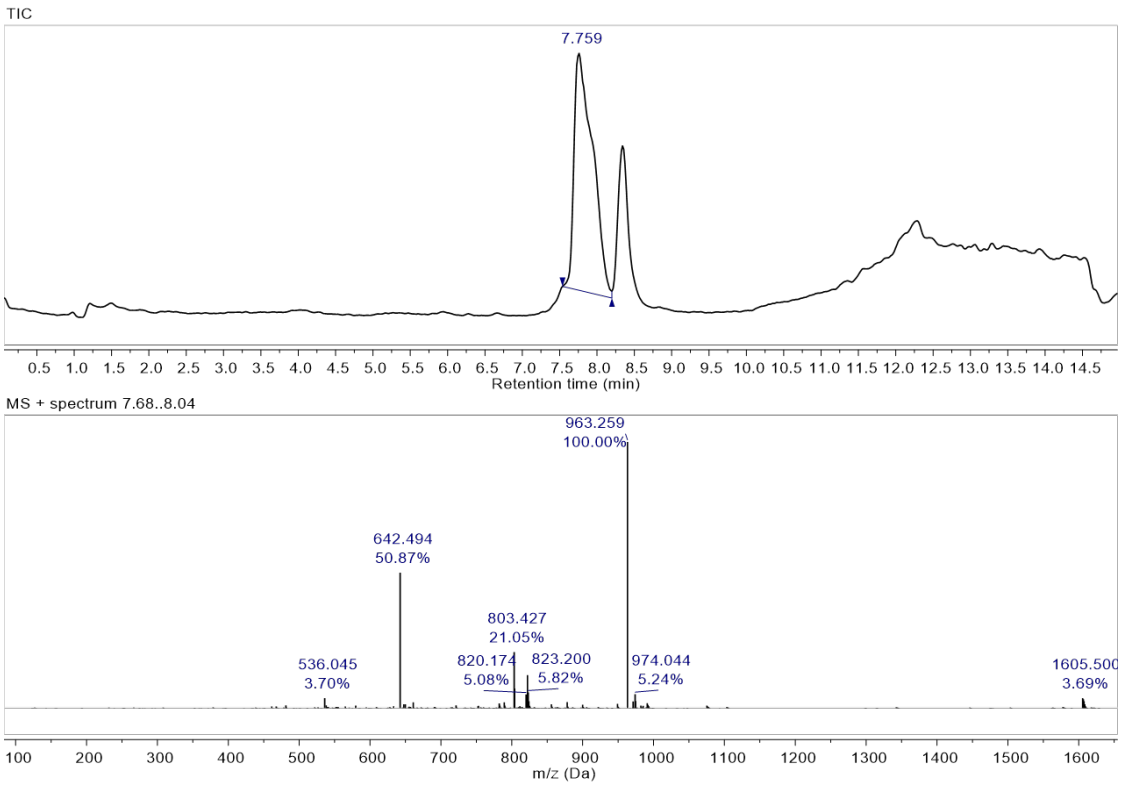

Figure A5.34. LC-MS of Compound **(12-9)**.

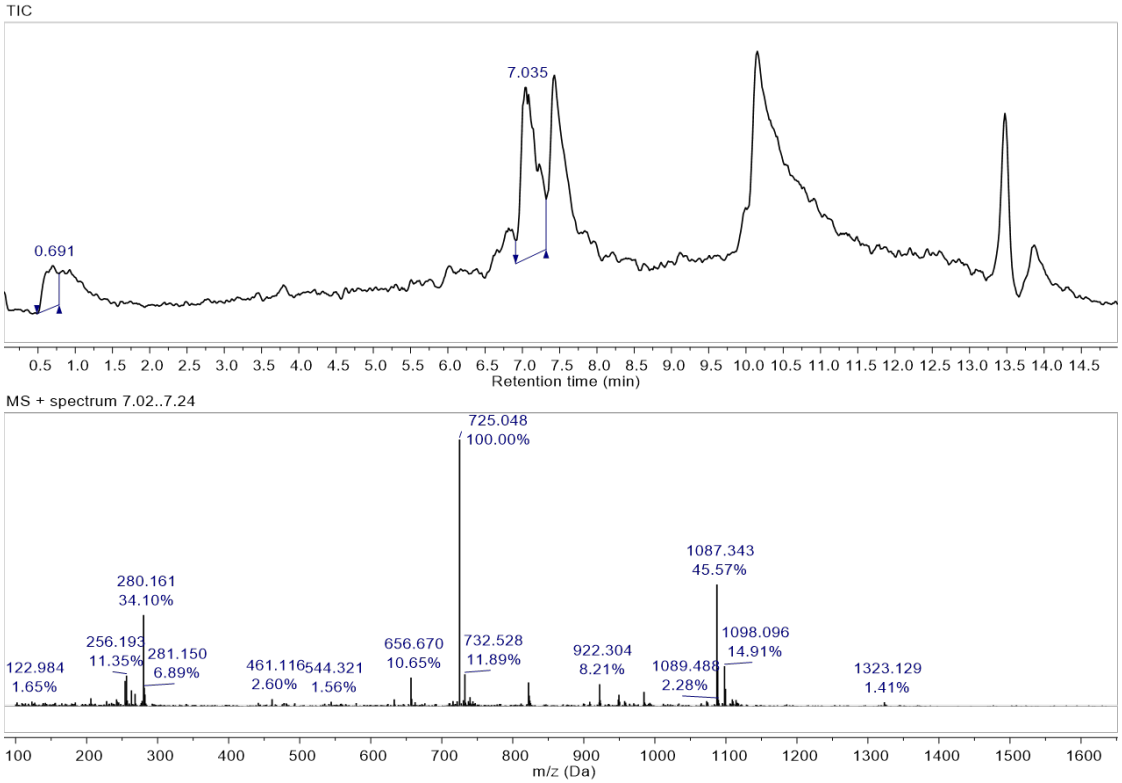

Figure A5.35. LC-MS of Compound **(12-11)**.

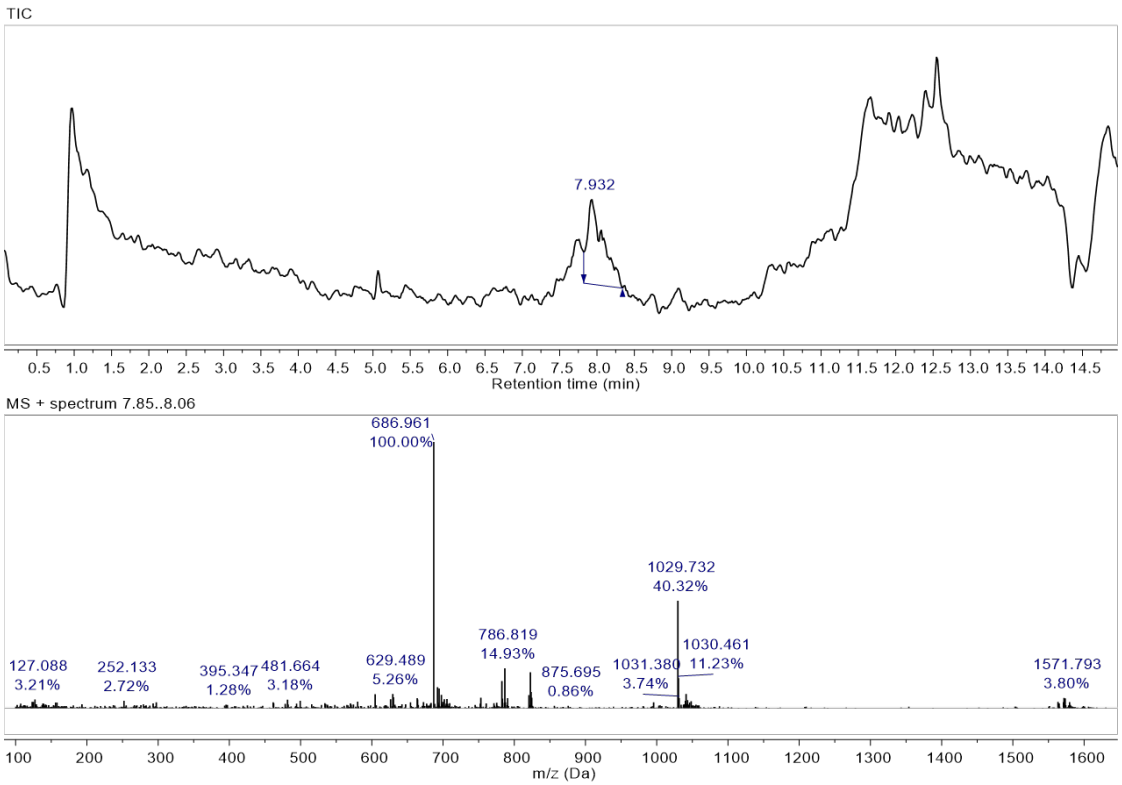

Figure A5.36. LC-MS of Compound **(12-10)**.

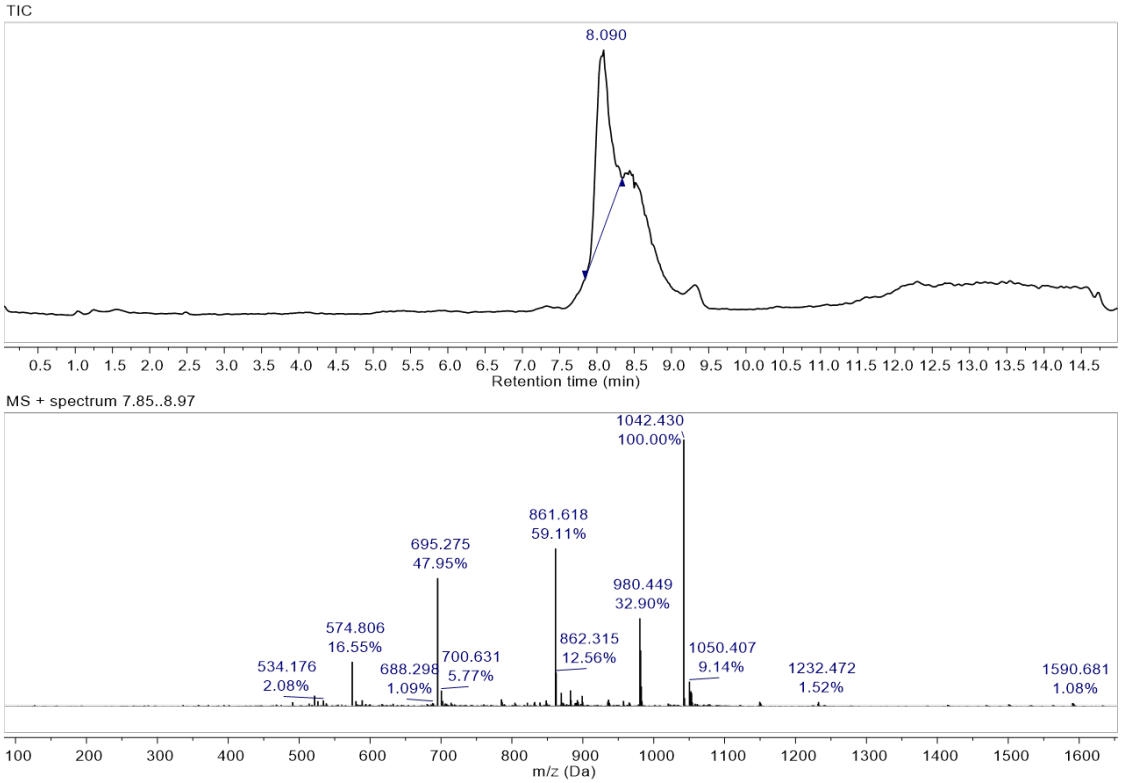

Figure A5.37. LC-MS of Compound **(14-9)**.

*Conjugation of fmoc-N-amido-dPEG$_{12}$-TFP ester to "Click" Handle-modified Oligomer [Synthesis of **PEG12-Modified Oligomer**]* – 1 equiv of "Click" Handle-modified Oligomer was dissolved at 15 mg/ml in DMSO. To this solution was added 2.2 equiv of fmoc-N-amido-dPEG$_{12}$-TFP ester and 5 equiv of Et_3N. The final concentration of "Click" Handle-modified Oligomer was 5 mM in DMSO. The mixture was reacted for 1 hour at room temperature and then purified via semi-preparative RP-HPLC (mobile phase with TFA). Using the standard RP-HPLC gradient, Compound **(PEG12-12-10)** eluted at 28.5 minutes. Compound **(PEG12-12-11)** eluted at 25.5 minutes. Compound **(PEG12-14-9)** eluted at 26 minutes. **The other** compounds were eluted at a flow rate of 4 mL/min with a linear gradient of 5% to 95% solvent B (0-45 minutes), then 95% solvent B (45-47.5 min) and equilibrated back to 5% solvent B (47.5-55 minutes). Compound **(PEG12-12-9)** eluted at 31.5 minutes. Compound **(PEG12-13-9)** eluted at 23.5 minutes. The product was characterized by LC-MS (Compound **(PEG12-12-9)** *m/z* calculated: 1373.62 observed: 1374.31 $[M+2H]^{2+}$; Compound **(PEG12-12-10)** *m/z* calculated: 1086.95 observed: 1087.34 $[M+2H]^{2+}$; Compound **(PEG-12-12-11)** *m/z* calculated: 1439.64 observed 1440.60 $[M+2H]^{2+}$; Compound **(PEG12-13-9)** calculated: 1216.59 observed: 1217.17 $[M+2H]^{2+}$; Compound **(PEG12-14-9)** *m/z* calculated: 1453.26 observed: 1453.50 $[M+2H]^{2+}$).

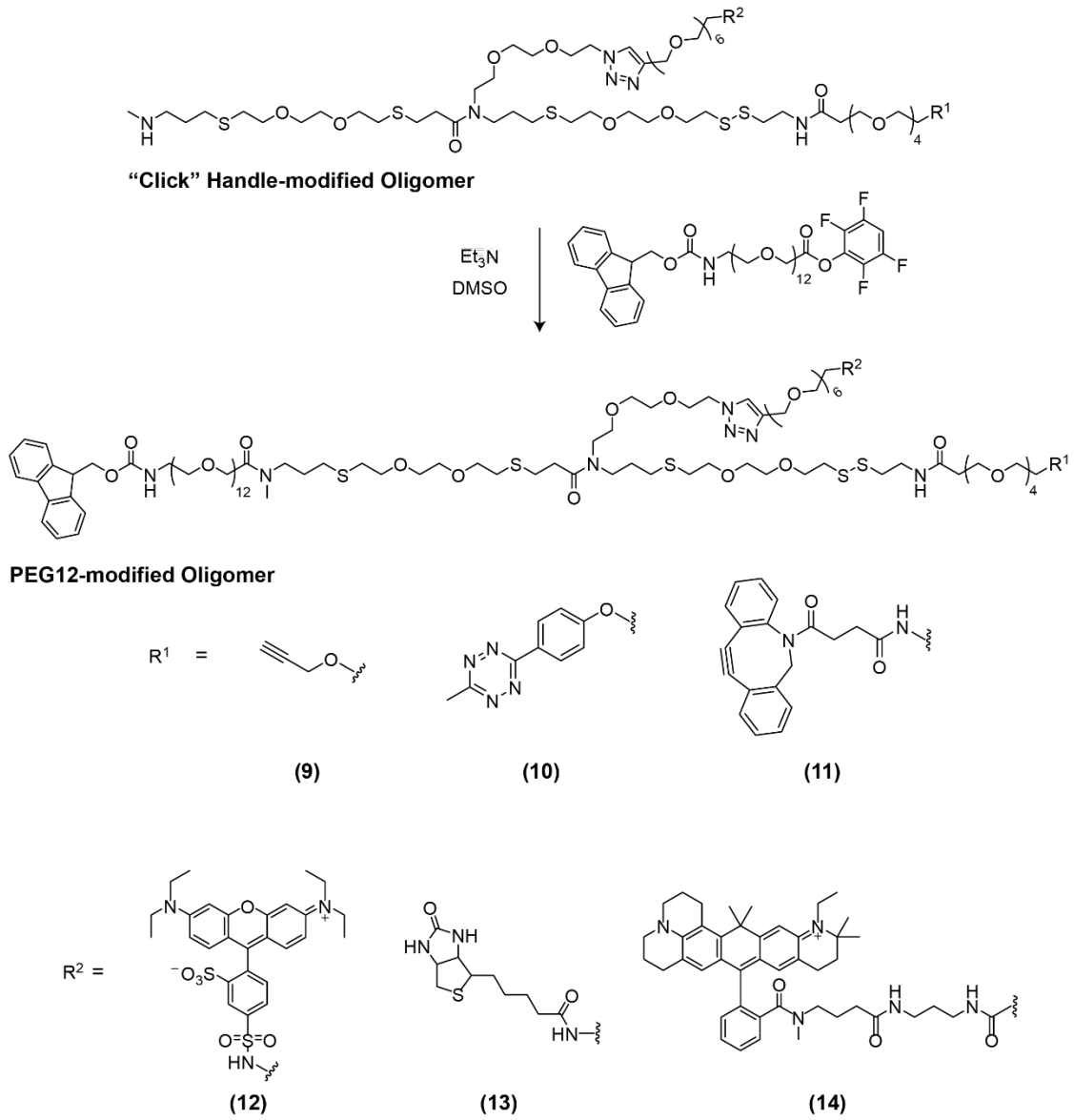

Figure A5.38. Scheme for conjugation of fmoc-N-amido-dPEG$_{12}$-TFP ester to "Click" Handle-modified Oligomer.

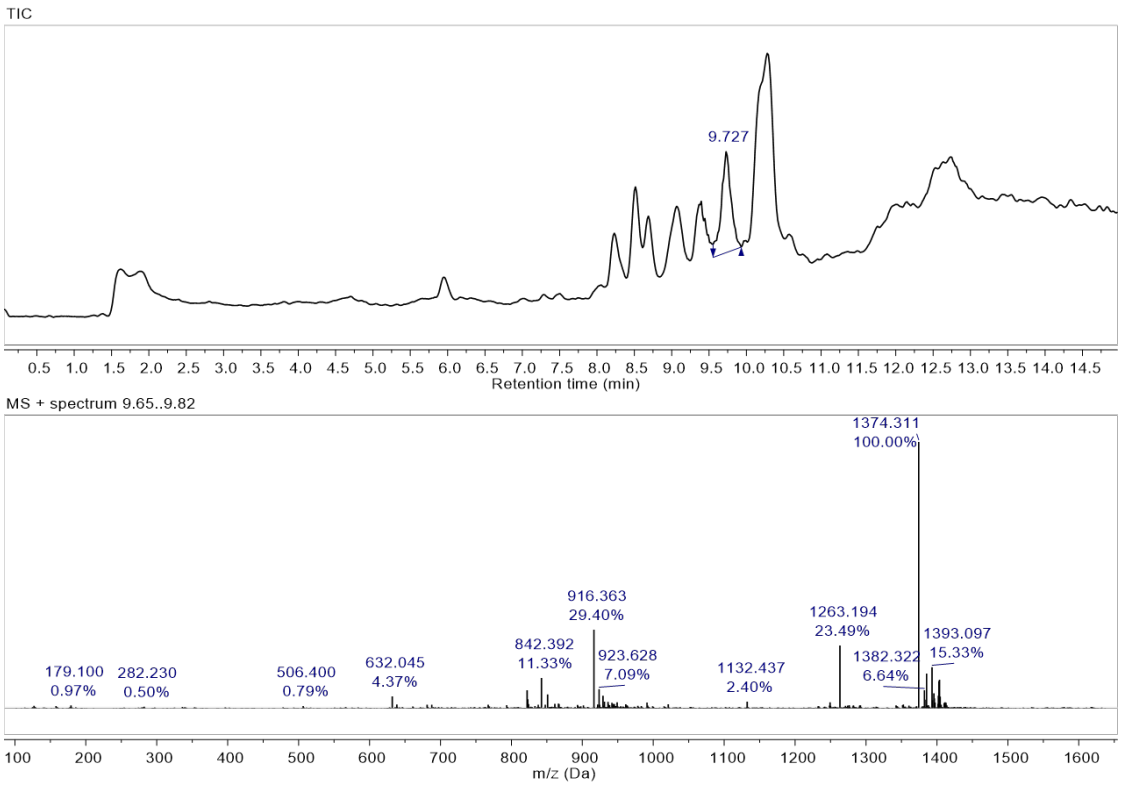

Figure A5.39. LC-MS of Compound **(PEG12-12-9)**.

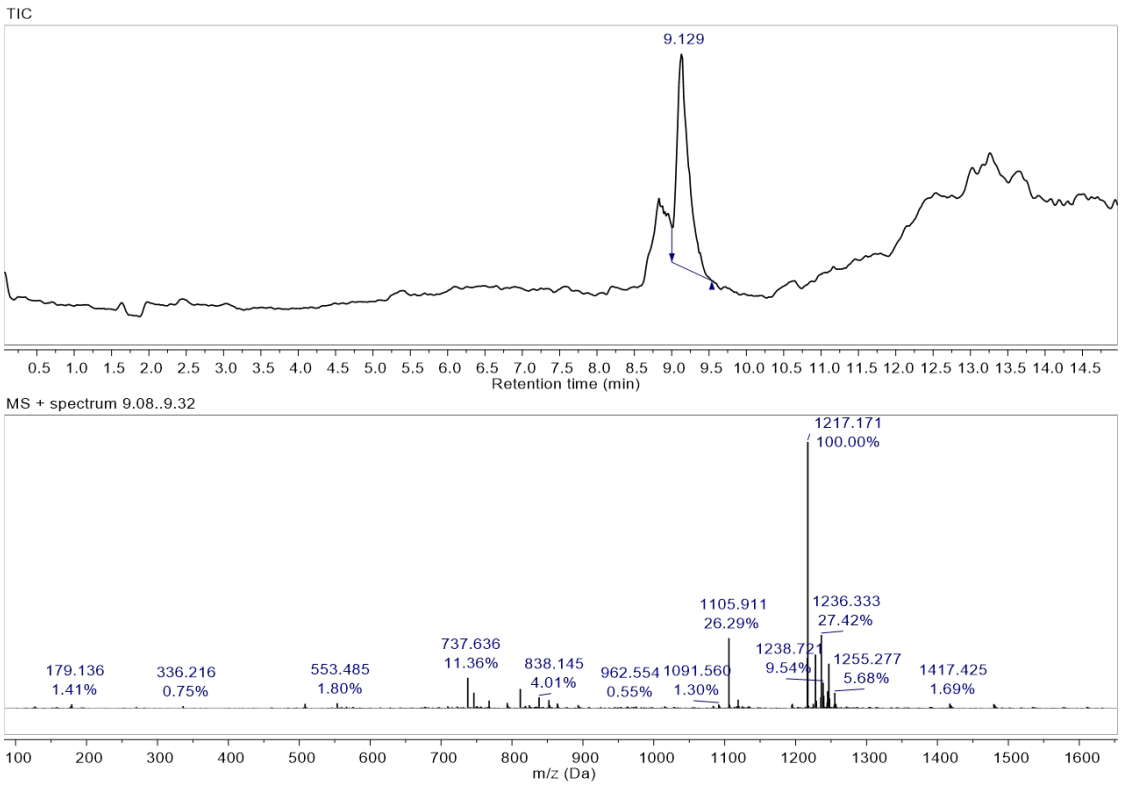

Figure 40. LC-MS of Compound **(PEG12-13-9)**.

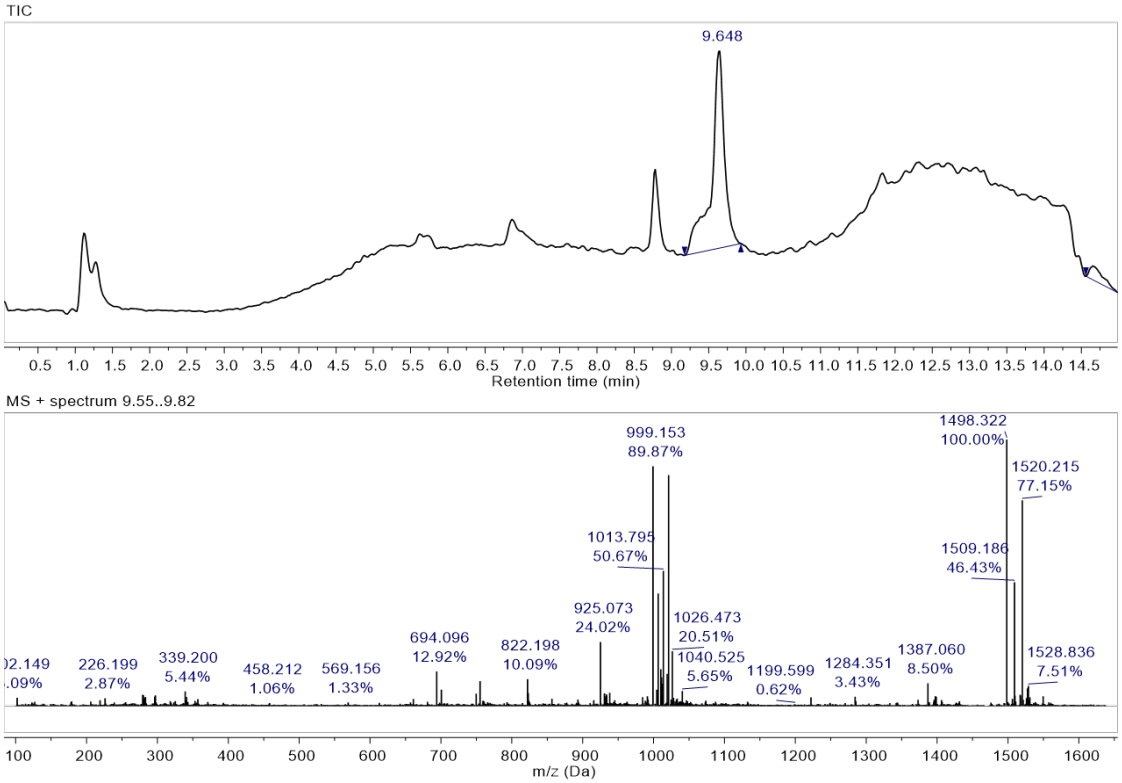

Figure A5.41. LC-MS of Compound **(PEG12-14-11)**.

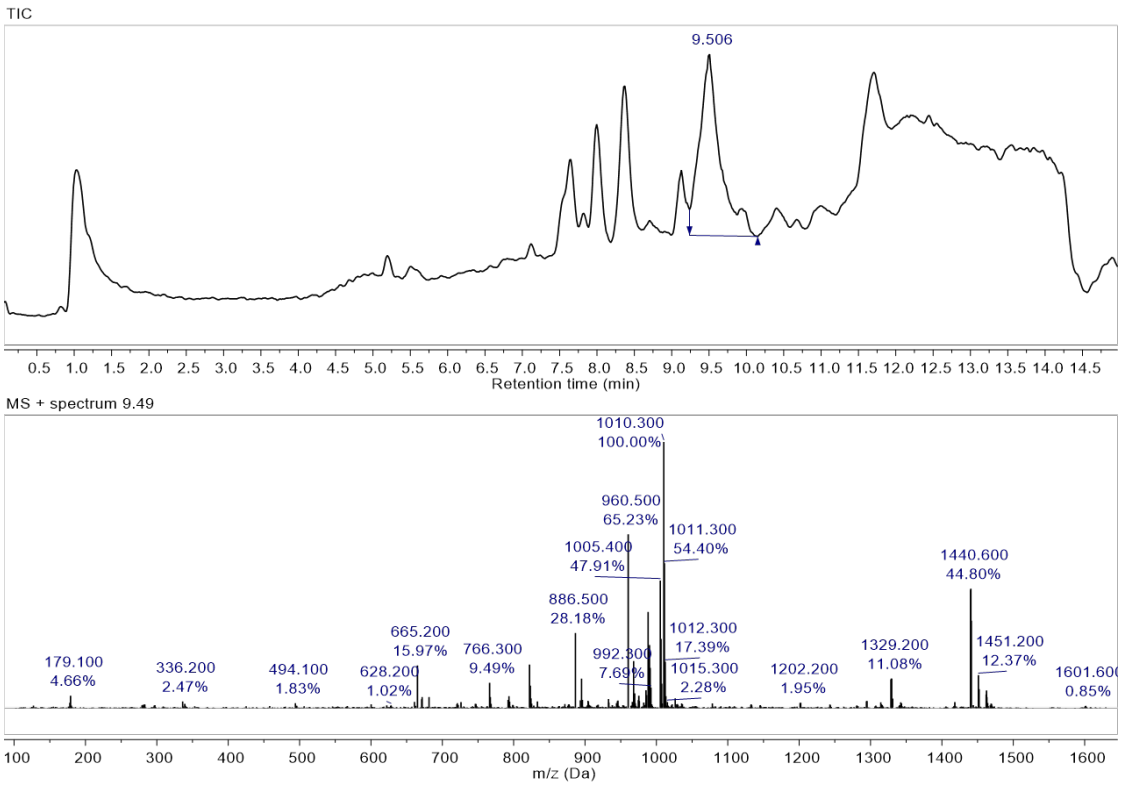

Figure A5.42. LC-MS of Compound **(PEG12-12-10)**.

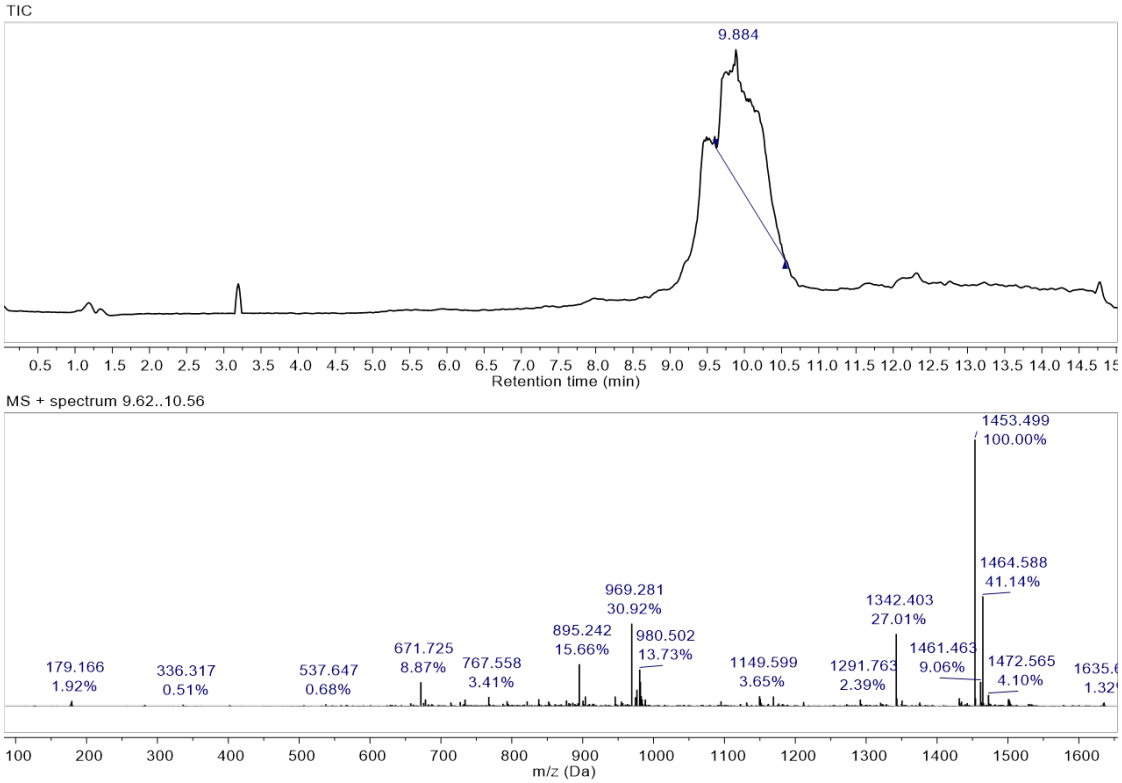

Figure A5.43. LC-MS of Compound **(PEG12-14-9)**.

*Conjugation of Methacrylic Acid NHS Ester to PEG12-modified Oligomer (Synthesis of **"Click" ExM Scaffolds**)* – 1 equiv of PEG12-modified oligomer was dissolved at 30 mg/ml in DMSO. To this solution was added 5 equiv of piperidine to give a final concentration of 69 mM in DMSO. After reacting for 1 hour at room temperature, 10 equiv of methacrylic acid NHS ester (100 mg/ml) and 15 equiv of Et_3N were added. The final concentration was 3 mM in DMSO. The mixture was reacted for 2 hours at room temperature and then purified via semi-preparative RP-HPLC (mobile phase with TFA). Compound **(Methac-PEG12-12-9)** eluted at 20.5 minutes. Compound **(Methac-PEG12-12-10)** eluted at 21.7 minutes. Compound **(Methac-PEG12-12-11)** eluted at 22.1 minutes. Compound **(Methac-PEG12-14-9)** eluted at 24 minutes. Compound **(Methac-PEG12-13-9)** co-purified with an undesired by-product using the standard RP-HPLC gradient and was re-purified with a linear gradient of 5% to 95% solvent B (0-90 minutes), then 95% solvent B (90-91 minutes) and equilibrated back to 5% solvent B (91-100 minutes). On this gradient, Compound **(Methac-PEG12-13-9)** eluted at 41 minutes. The product was characterized by LC-MS (Compound **(Methac-PEG12-12-9)** *m/z* calculated: 1296.60 observed: 1297.29 $[M+2H]^{2+}$; Compound **(Methac-PEG12-12-10)** *m/z* calculated: 1362.62 observed: 1363.35 $[M+2H]^{2+}$; Compound **(Methac-PEG12-12-11)** calculated: 1420.64 observed: 1421.22 $[M+2H]^{2+}$; Compound **(Methac-PEG12-13-9)** calculated: 1139.56 observed: 1139.89 $[M+2H]^{2+}$; Compound **(Methac-PEG12-14-9)** calculated: 1376.24 observed: 1376.42 $[M+2H]^{2+}$

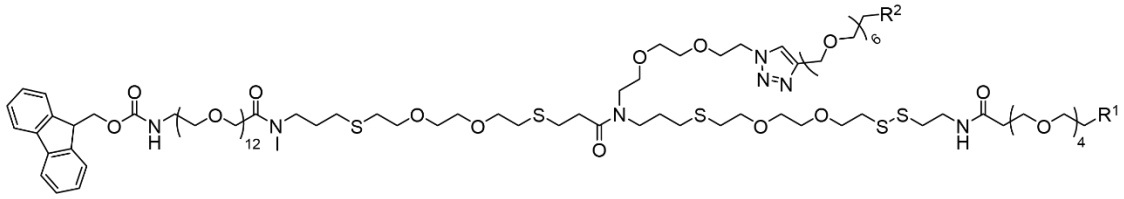

PEG12-modified Oligomer

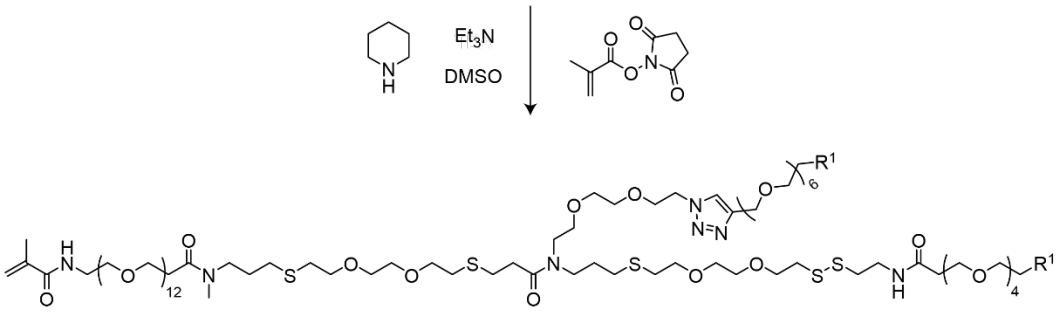

"Click" ExM Scaffold

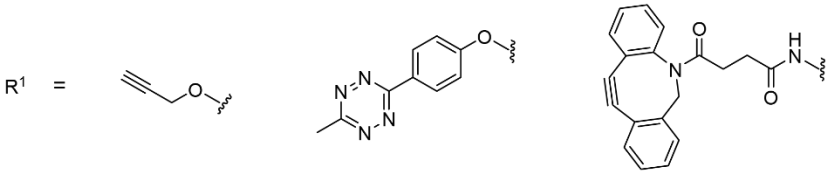

(9) **(10)** **(11)**

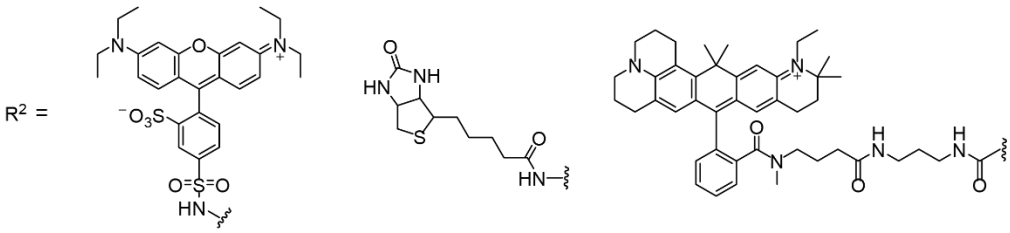

(12) **(13)** **(14)**

Figure A5.44. Scheme for conjugation of methacrylic acid NHS ester to PEG12-modified oligomer.

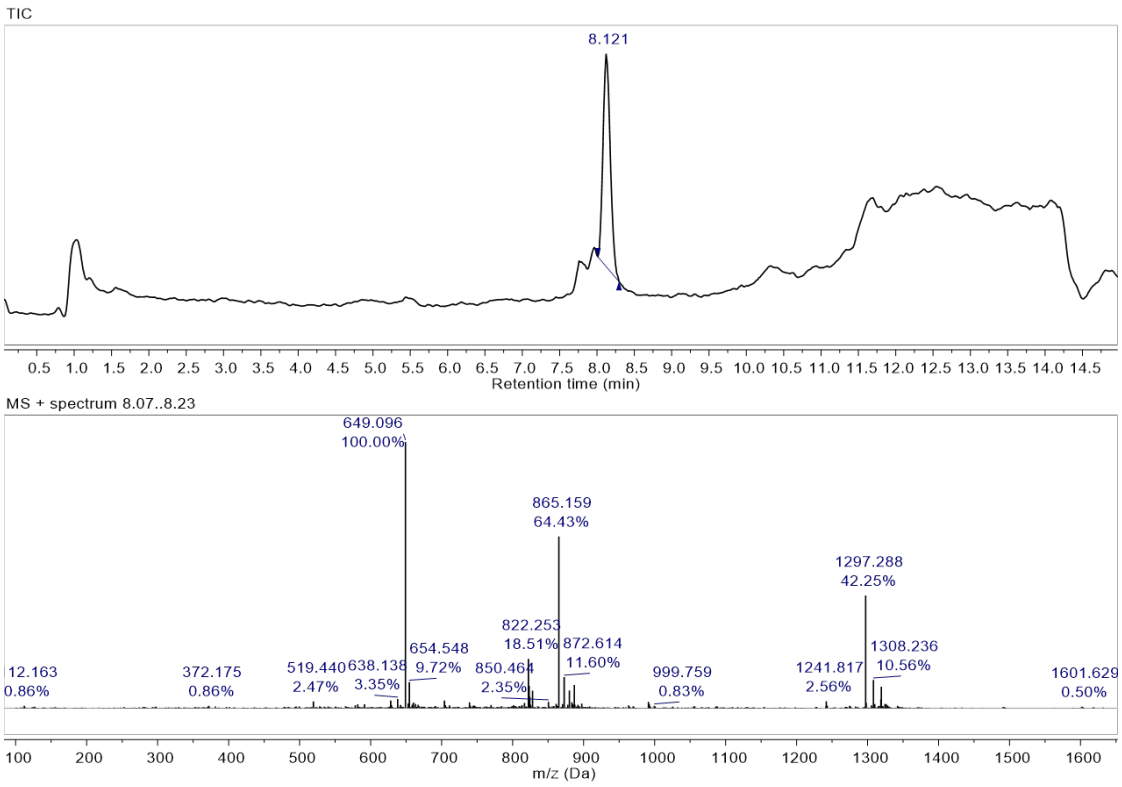

Figure A5.45. LC-MS of Compound **Methac-PEG12-12-9**.

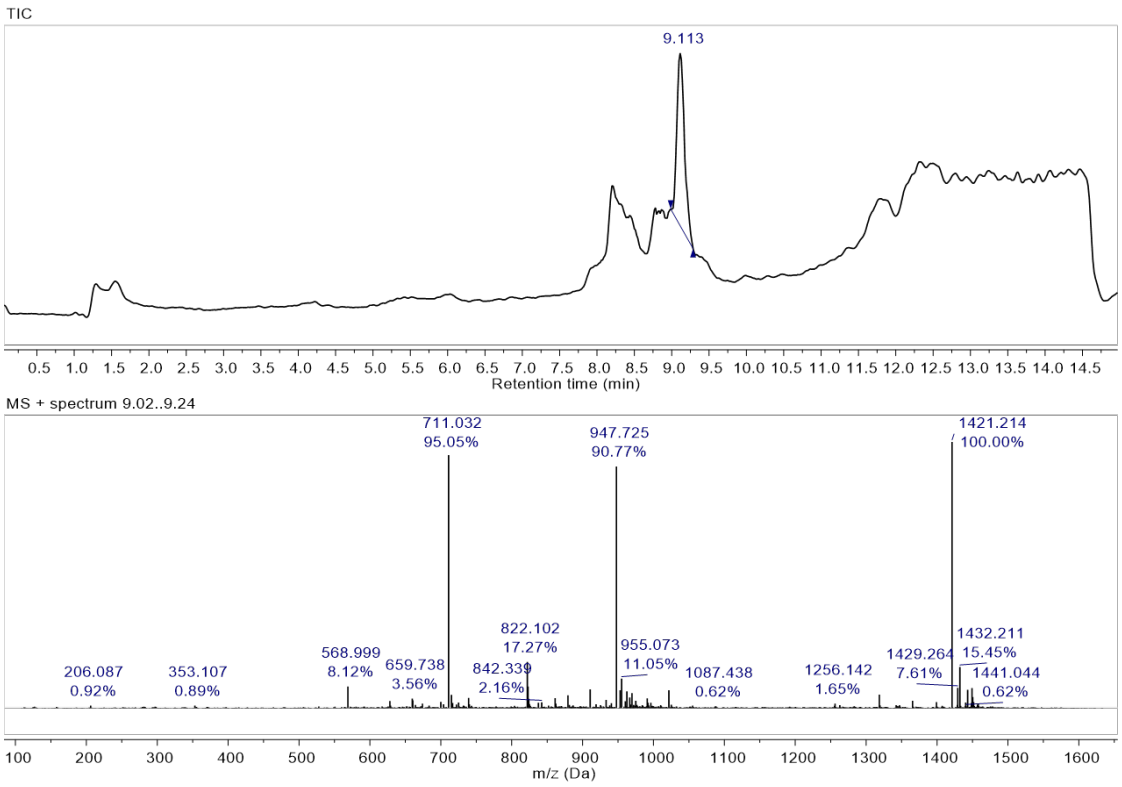

Figure A5.46. LC-MS of Compound **Methac-PEG12-12-11**.

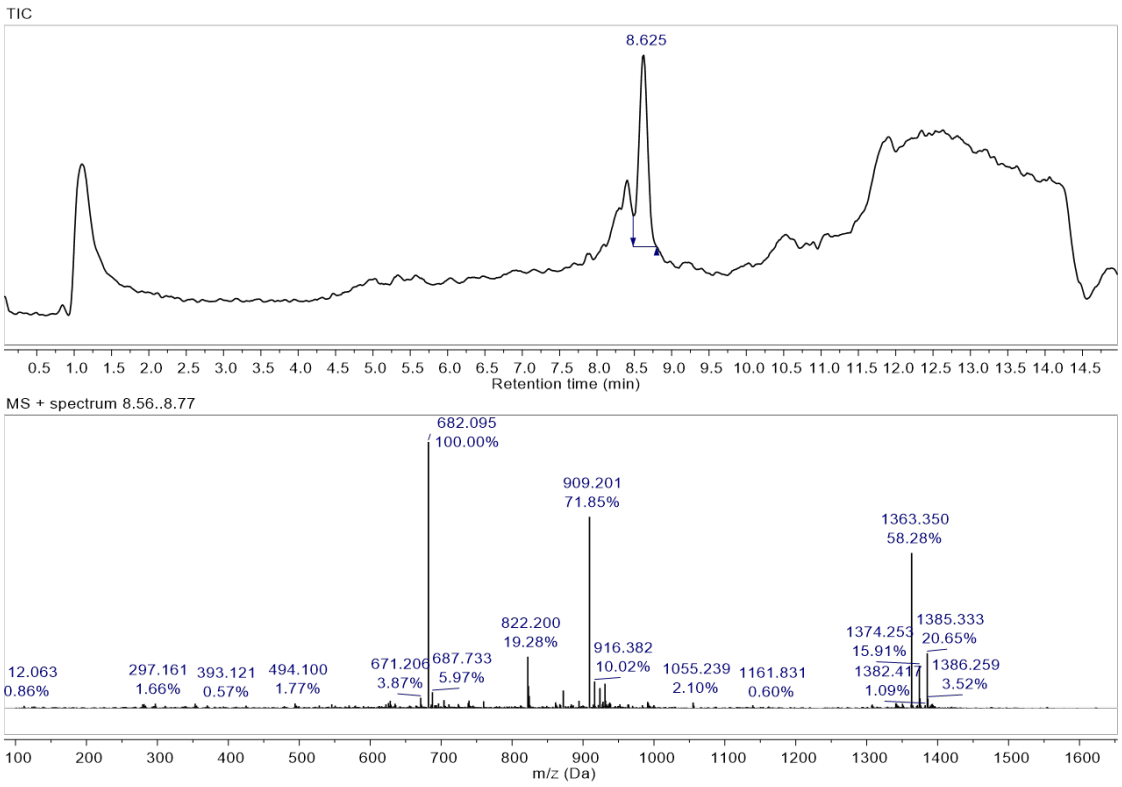

Figure A5.47. LC-MS of Compound **Methac-PEG12-12-10**.

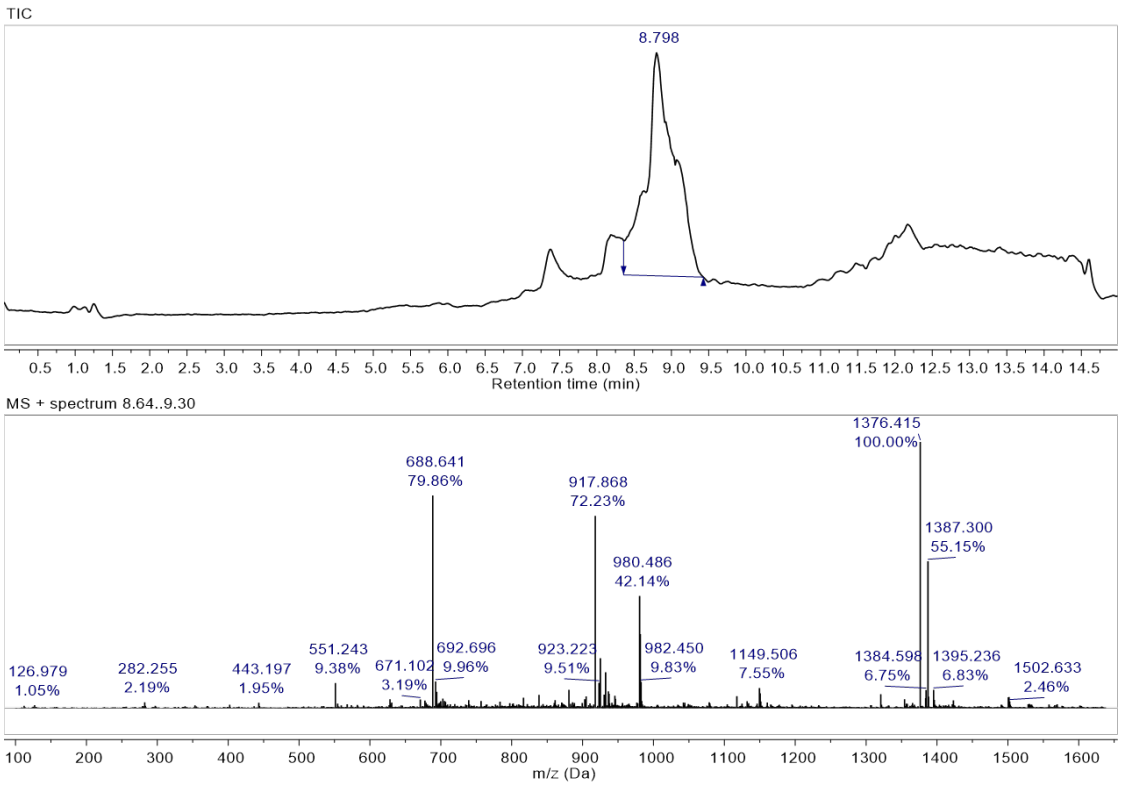

Figure A5.48. LC-MS of Compound **Methac-PEG12-14-9**.

Chapter 5 – REFERENCES

1.Chen, F. *et al.* Nanoscale imaging of RNA with expansion microscopy. *Nat Methods* **13,** 679–684 (2016).

2.Asano, S. M. *et al.* Expansion Microscopy: Protocols for Imaging Proteins and RNA in Cells and Tissues. *Curr Protoc Cell Biol* **80,** e56 (2018).

3.Chen, F., Tillberg, P. W. & Boyden, E. S. Optical imaging. Expansion microscopy. *Science* **347,** 543–548 (2015).

4.Chozinski, T. J. *et al.* Expansion microscopy with conventional antibodies and fluorescent proteins. *Nat Methods* **13,** 485 (2016).

5.Chang, J.-B. *et al.* Iterative expansion microscopy. *Nat Methods* **14,** 593–599 (2017).

6.Tillberg, P. W. *et al.* Protein-retention expansion microscopy of cells and tissues labeled using standard fluorescent proteins and antibodies. *Nat Biotechnol* **34,** 987–992 (2016).

7.Betzig, E., Trautman, J. K., Harris, T. D., Weiner, J. S. & Kostelak, R. L. Breaking the diffraction barrier: optical microscopy on a nanometric scale. *Science* **251,** 1468–1470 (1991).

8.Oh, Y. I., Sheng, G. J., Chang, S.-K. & Hsieh-Wilson, L. C. Tailored glycopolymers as anticoagulant heparin mimetics. *Angew Chem Int Ed Engl* **52,** 11796–11799 (2013).

9.van Berkel, P. H. C. *et al.* N-linked glycosylation is an important parameter for optimal selection of cell lines producing biopharmaceutical human IgG. *Biotechnol Prog* **25,** 244–251 (2009).

10.Maverakis, E. *et al.* Glycans in the immune system and The Altered Glycan Theory of Autoimmunity: a critical review. *J Autoimmun* **57,** 1–13 (2015).

11.Laughlin, S. T. & Bertozzi, C. R. Metabolic labeling of glycans with azido sugars and subsequent glycan-profiling and visualization via Staudinger ligation. *Nat Protoc* **2,** 2930–2944 (2007).

Chapter 6 – FUTURE DIRECTIONS

6.1. VERSATILE PLATFORM FOR THE SYNTHESIS OF ORTHOGONALLY CLEAVABLE, HETEROMULTIFUNCTIONAL CROSS-LINKERS

Cleavable and heteromultifunctional crosslinkers have proven critical in a wide range of biological applications. Traditional approaches for synthesizing these linkers suffer from various synthetic and functional limitations. In this work, an efficient sequence-defined synthetic methodology, developed for the assembly of oligothioetheramides, was used to address many of these limitations. Four heterotrifunctional crosslinkers with up to two orthogonal internal cleavage sites were synthesized. These linkers were conjugated to a pair of fluorophores that undergo Förster resonance energy transfer (FRET) and a model protein – human transferrin. Orthogonal bond cleavage was validated by mass spectrometry, fluorescent gel electrophoresis, and confocal microscopy. These studies demonstrate the versatility and biological utility of oligothioetheramides as a new class of multifunctional chemical crosslinkers and biologically relevant fluorescent probes.

From this work, we learned the difficulties of purifying hydrophilic oligoTEAs using the fluorous-tagged support. The recoveries were often poor when using the standard fluorophobic wash protocol when using hydrophilic dithiols such as DTT and hydrophilic monomers such as the azide allylacrylamide monomer. After this work, we started to use the support-free synthesis approach using monoacetylated dithiols. This greatly increased the recovery of these cross-linkers.

It would be interesting to try to incorporate additional functionalities into oligoTEA-based heteromultifunctional cross-linkers. Attempts were made at synthesizing an allylacrylamide monomer with a tetrazine functional group, but it was found to be incompatible with the monomer synthesis methodology. Another functional handle that may be more stable and interesting to incorporate would be an isonitrile

group which can react with tetrazines. It would also be worthwhile to explore other cleavable chemistries, such as dipeptide bonds and photocleavable groups.

6.2. RESPONSIVE ANTIBODY CONJUGATES ENABLE QUANTITATIVE DETERMINATION OF INTRACELLULAR BOND DEGRADATION RATE

Degradable cross-linkers that respond to intracellular biological stimuli are a critical component of many drug delivery systems. With numerous stimuli-responsive drug delivery systems in development, it is important to quantitatively study their intracellular processing. Herein we report a framework for quantifying the rate of intracellular bond degradation in the endocytic pathway. Towards this end, we devised and synthesized a reduction-sensitive FRET-based cross-linker that can be readily conjugated to a variety of targeting ligands. This cross-linker was conjugated to trastuzumab, a humanized monoclonal antibody against the HER2 receptor. We developed a model based on mass-action kinetics to describe the intracellular processing of this conjugate. The kinetic model was developed in conjunction with live-cell experiments to extract the rate constant for intracellular disulfide bond degradation. This framework can be applied to other endocytosis pathways, bond types, and cell types to quantify this fundamental degradation rate parameter.

Two out of the six FDA-approved antibody-drug conjugates employ a valine-citrulline dipeptide bond which has been shown to possess exceptional stability in plasma. Thus, it would be interesting to synthesize FRET-based cross-linkers containing this bond type, with a self-immolating spacer as used in ADCs, and measure bond cleavage intracellularly. This cleavage will be on a longer time scale (days), but the methods used in Chapter 3 involving flow cytometry and confocal microscopy can still be used. It would also be interesting to compare cleavage of the disulfide bond and the dipeptide bond in other cell types and pathways. The system we developed is

modular and thus it would be very feasible to explore other bond types, cell types, and pathways.

Another point to explore would be to try to determine the agent responsible for cleaving the disulfide bond in the endocytic pathway. The lysosomal thioreductase GILT is known to cleave disulfide bonds in lysosomes. It would be impactful to confirm that GILT is responsible for disulfide bond reduction of the antibody probe in the endocytic pathway. Some attempts were made to generate a GILT knock-out cell line with CRISPR, but it was difficult to identify and isolate a GILT knock-out clone. It may be best to try siRNA knockdown of the gene or perhaps try to overexpress GILT and measure the impact on bond degradation rate. For these modified cells, it would be best to quantify rate constants such as internalization and association/dissociation experimentally in-house as opposed to using literature values for the parent cell type in case these parameters are affected.

6.3. DEVELOPMENT OF ALTERNATIVE QUENCHED PROBES FOR MONITORING INTRACELLULAR BOND DEGRADATION

Static or contact quenching occurs when a fluorophore-quencher pair forms a ground state complex before excitation occurs. We previously developed a cross-linker that exhibited dynamic quenching, specifically FRET. We hypothesized that modifying the FRET system to a contact quenching system would be best in order to quantify bond degradation kinetically. This type of “turn on” system would offer reduced background and thus improved signal-to-noise. We synthesized variations of the cross-linker with different fluorophore-quencher pairs including BODIPY/DNP, BODIPY/Dabcyl, and Rhodamine/DNP. There were various issues with these systems, the biggest drawback being the loss of quenching upon conjugation to trastuzumab. From this result, it was determined that a FRET-based system is best.

This data indicated the structural effects on the efficiency of contact quenching. It would be interesting to explore whether this loss of quenching would occur if the cross-linker was conjugated to other parts of the antibody, perhaps starting with a nonspecific conjugation to lysine residues. We had not previously measured the quenching efficiency of our transferrin probes with the BODIPY/DNP cross-linkers but based on our flow cytometry data it seems that those probes were effectively quenched.

It would also be interesting to explore other cross-linker structures and fluorophores, as we found that the hydrophobicity of these structures impacted conjugation efficiency. Based on their structure, the fluorophores used were very hydrophilic, so perhaps there is some hydrophobicity in the oligoTEA even though it contains hydrophilic dithiols and a hydrophilic monomer. Perhaps a simpler PEG-based cross-linker rather than an oligoTEA-based cross-linker would aid in improving hydrophobicity.

Lastly, in Chapter 4, we explored the use of the IncuCyte technique for kinetic intracellular measurements. The technique appeared to work well for one cell type used but was inconsistent for other cell types. It would be interesting to revisit this technique and try to better understand the data processing that is required, as using this method would be useful for throughput. Confocal microscopy would still be used in conjunction with the IncuCyte technique to demonstrate intracellular localization.

6.4. SUPER-RESOLUTION IMAGING OF THE GLYCOCALYX VIA MODULAR "CLICK" PROBES

Expansion microscopy (ExM) is a powerful tool for super-resolution imaging of biological structures. Traditional ExM reagents are not compatible with the study of cell-surface glycans. In this work, we developed a modular chemical cross-linker that enables ExM imaging of the glycocalyx in metabolically labeled cells and tissues. To

visualize the cell surface glycocalyx, cells were fed azide-modified sugars and the azide functional handle were then used to attach the “click” ExM probe. The “click” ExM probe demonstrate enhanced resolution post-expansion as well as co-localization with glycoproteins. Additionally, the “click” ExM probe was shown to improve visualization over traditional ExM reagents due to its proteolytic stability.

There were many synthetic challenges that arose when developing the probes for this work. The thiol-disulfide reaction step proved to be very sensitive to reaction conditions, especially concentration. Further work must be undergone in order to determine the optimal conditions for reaction. In addition, it was found that occasionally when this thiol-disulfide exchange step was carried out, the linker would be capped with a pyridyl disulfide group. This was unexpected, as the pyridyl disulfide group is considered an excellent leaving group. For future work, it would be best to assess whether the disulfide bond within the probe is necessary. The synthesis of these cross-linkers would be greatly simplified if a cleavable bond was not needed. The oligoTEA could then be terminated in an Fmoc-protected amine instead of an acetylated thiol. The amine could be reacted with an NHS ester, which is a much less finnicky reaction. Additionally, it would allow for the “click” functionality to be added first before the more precious fluorophores. With the current scheme, the fluorophore must be added first in the copper-click reaction as the sodium ascorbate would reduce the disulfide bond. When the disulfide bond was added in the probe design, it was added along with the long PEG spacer to the methacrylamide group, so it is unclear what feature helped to diminish background more or if both features are indeed critical to the design.

Another synthetic difficulty involved the probe that incorporated a DBCO group. During some of the synthetic steps, the probe had to be purified via HPLC with 0.1% TFA. The DBCO group within these scaffolds was found to be very acid-sensitive and

solution-sensitive. When concentrated after HPLC, it was often found that the DBCO group was completely removed from the structure. To circumvent this issue, TEA was added to neutralize the TFA and the solution was immediately concentrated in the Speed-vac. It would be interesting to try to not add the TEA for neutralization and lyophilize the fractions to see if that might be an easier method that keeps the DBCO intact. The final step product was purified without TFA, dried immediately under nitrogen, and then placed in the Speed-vac to get completely dry. It is unclear whether lyophilization would be useful for the last step or if it may cause polymerization of the methacrylamide group.

6.5. CONCLUSION

In this work, we developed a methodology for synthesizing cleavable heteromultifunctional cross-linkers. These cross-linkers were synthesized used the oligothioetheramide synthesis approach. OligoTEAs are sequence-defined, structurally diverse, and particularly attractive for biological applications due to their stability to proteolytic degradation. We have taken oligoTEA-based multifunctional cross-linkers and used them to quantify the intracellular processing of stimuli-responsive drug carriers. We have also used our methodology to develop probes to visualize the glycocalyx via expansion microscopy. Taken together, these works highlight the utility of oligoTEAs as a platform to design heteromultifunctional cross-linkers for a range of biological applications.